Università degli Studi di Palermo

AREA QUALITÀ, PROGRAMMAZIONE E SUPPORTO STRATEGICO
SETTORE STRATEGIA PER LA RICERCA
U. O. DOTTORATI

Dottorato in Scienze della Terra e del Mare
Dipartimento di Scienze della Terra e del Mare (DiSTeM)
Settore Scientifico Disciplinare GEO/08

Earth Degassing in Tectonically Active Regions: New Evidences from Southern Italy and the Balkans

IL DOTTORE
PAOLO RANDAZZO

IL COORDINATORE
PROF. MARCO MILAZZO

IL TUTOR
PROF. ALESSANDRO AIUPPA

I CO TUTOR
DOTT. ANTONIO CARACAUSI
PROF. CARLO CARDELLINI

CICLO XXXIV
ANNO ACCADEMICO 2021/2022

...To all dreamers

thrown into the world

of "How" and "Why"...

TABLE OF CONTENTS

LIST OF FIGURES

LIST OF TABLES

Abstract

Carbon dioxide (CO_2) is released from the Earth's interior into the atmosphere in a variety of tectonic settings. A quantitative understanding of CO_2 outgassing fluxes is critical for decoding the link between the global carbon budget and climate evolution over geological timescales, and for a better characterization of natural processes (e.g., volcanism, earthquake nucleation). In addition to CO_2, noble gases are among the most powerful geochemical tools to probe geological processes, and are among the most valuable tracers of volatiles' origin and processing, and of magmatic/crustal dynamics. As such, the helium isotopic signature of natural fluids, when interpreted in tandem with He/CO_2 ratios and $\delta^{13}C$ compositions, is extremely suitable to resolve volatiles' source (i.e., mantle vs. crustal), sinks, and the processes that operate during storage and transfer through the crust.

This PhD dissertation aims to contribute to a better understanding of Earth degassing processes, by presenting novel information on the outgassing of deeply sourced volatiles (e.g., CO_2, He) in Southern Italy (Calabria) and the Balkans (Serbia and Croatia). The main objectives is to reveal that large fractions of deeply rising volatiles can be transported through the continental crust in areas away from any active/recent volcanic source, confirming the large potential role of continental degassing on the global natural carbon and helium cycles.

After a general introduction and background (*Chapter 1*), the dissertation is divided into three chapters, one for each of the studied areas.

Chapter 2 focusses on Calabria region, a collisional orogen representing one of the most active seismogenetic areas in Southern Italy, and being characterised by the presence of several hydrothermal springs, some of which representing low-enthalpy geothermal resources. The chemical and isotopic (He, C) composition of dissolved gas in groundwater allows to identify two different compositional domains, dominated by respectively (i) atmospheric and biogenic components and (ii) deep derived fluids. The Helium isotope composition reveals low mantle

contributions, and rather point to the addition of crustal radiogenic ^{4}He to the thermal groundwater. Using helium and carbon isotope data, the possible secondary processes (dissolution/precipitation) that act to modify the pristine chemistry of deeply rising volatiles are explored. One key result is that a large fraction of deep crustal (i.e metamorphic) carbon (CO_2) is outgassed in Calabria, being comparable with what seen in several active and dormant volcanic areas.

Chapter 3 reports on an extensive geochemical survey of fluids released in the Vardar zone (central-western Serbia), a mega-suture zone at the boundary between Eurasia and Africa plates, now characterized by active tectonics. The area exhibits high regional heat flow (up to 130 mW/m^2) and geothermal energy potential. Gas samples have been analyzed for their chemical and isotopic composition (e.g., CO_2, noble gases), revealing the presence of a mantle-derived He component at regional scale. The CO_2-He relationships highlight the occurrence of secondary processes occurring during the storage and/or the transfer of fluids in shallow crustal layers. Finally, the estimated mantle-derived He flux suggests a structural/tectonic control (i.e., through lithospheric faults) on the migration of deep-mantle fluids through the crust.

Finally, *Chapter* 4 illustrates the results of a geochemical investigation on natural gaseous manifestations in the Croatian Pannonian basin. This area is a back-arc basin formed due to diachronous extension linked to subduction roll-back in the Carpathians and Dinarides regions, and it affected by asthenospheric mantle flow combined with the lithospheric delamination. Gas compositions are very heterogeneous and identify three compositional groups. For the first time the He isotopic composition of gas sample from the Croatian Pannonian basin are analysed, allowing to identify a mantle component accounting for up to 40 % of the degassed He. A geochemical model is set in which crustal CO_2-rich fluids, characterized by organic/biogenic C signatures at places related to oil biodegradation processes, (i) mix with mantle-derived fluids and (ii) undergo chemical/isotopic fractionations during gas-water-rock interactions in shallow crustal acquifers. The average estimated mantle-derived He flux for the Pannonian basin system is one order of magnitude

greater than that defined by O'Nions & Oxburgh, (1988) ($4x10^9$ atoms m^{-2} s^{-1}), placing the Pannonian basin as one of the most actively degassing continental segments worldwide.

CHAPTER I

I.1. INTRODUCTION

Deep-derived fluids are continuously released from the Earth's interior into the atmosphere and oceans. Over the past few decades, the study of natural fluids in both volcanic (e.g., Bragagni et al., 2022; Kimani et al., 2021; Aiuppa et al. 2019; Werner et al. 2019; Caracausi et al. 2015; Chiodini et al. 2007) and seismically-active regions (e.g., Xu et al., 2022; Buttitta et al. 2020; Frondini et al. 2019; Caracausi and Paternoster, 2015; Chiodini et al.,2004) has received renewed impetus due to the need of refining present-day global deep Earth Carbon Dioxide (CO_2) fluxes, and its possible impact on paleo-climate (e.g., Longman et al., 2022; Kaiho et al., 2022; Retallack, 2022; Burton et al. 2013; Aiuppa et al. 2010; Mörner and Etiope 2002). CO_2 Earth degassing occurs in different tectonic settings (Lee et al., 2019), from both volcanic and non-volcanic sources, and it known to be globally associated with tectonically/seismically active zones (Tamburello et al., 2018; Chiodini et al., 2004; Barnes et al., 1978). Deep earth fluids are discharged in a variety of gas manifestation types (e.g., volcanic plumes, bubbling gas, soil degassing, mofettes, fumaroles, etc.), including as dissolved gases in subsurface water bodies. Regional scale degassing studies are not only crucial for understanding the evolution of the atmosphere, but also to understand the potential relationships between fluid storage/accumulation and seismogenetic processes. Despite continuous improvements in direct measurements and global extrapolations, the global CO_2 Earth degassing budget remains poorly constrained (Fischer and Aiuppa, 2020; Fischer et al., 2019,2013; Burton et al., 2013; Berner and Lagasa, 1989). One commonly accepted view is that the tectonic (e.g., non-volcanic) CO_2 contribution remains the least understood (Werner et al., 2019; Wong et al., 2019; Fischer and Aiuppa, 2020). Yet notwithstanding, quantitative estimates of CO_2 outgassing fluxes in different tectonic settings are critical for decoding the links between Earth degassing and climate change from a whole-Earth carbon cycling perspective (Zhang et al., 2021). In particular, several studies emphasize the important contribution to the earth carbon budget from CO_2 degassing in non volcanic areas (e.g Chiodini et al., 2020, 2004, Caracausi and Sulli, 2019; Rolfo et al., 2017;

Becker et al., 2008). In this way, volatile signatures can be utilized to understand volatile source features (i.e., mantle vs. crustal), sinks, and volatile pathways through the crust as well as connections to larger tectonic processes (Barry et al., 2021). In this context the noble gases and CO_2 carbon isotopes are powerful tracers of crustal fluid processes that act on subsurface CO_2 (Cathles et al., 2007; Ballentine et al., 2001). Noble gases are chemically inert elements that exist as extremely volatile gases at standard temperature and pressure. Their lack of reactivity results in no change in their isotopic compositions via chemical processes but allows them to be used as a tracer of physical processes, which can alter both their isotopic and relative elemental compositions (Holland & Gillfillan,2013). Comparing ^3He amounts with the concentration of ^4He (i.e. the $^3He/^4He$ ratio) can identify magmatic contributions to subsurface reservoirs (Ballentine, et al. 2002). Likewise, the ^3He amount can be compared to the concentration of CO_2 within a natural environments to determine the origin of the CO_2 (Marty, et al. 1992; Oxburgh, et al. 1986). Moreover additional insights into volatile sources and sinks, and into the processes occurring during the migration of fluids through the crust and their storage in shallow crustal layers can be derived from a joint analysis and interpretation of He and carbon isotopic signatures (e.g., Randazzo et al., 2021; Barry et al., 2020; Zhou et al., 2012).

This PhD dissertation aims to contribute new information relevant to understanding Earth degassing processes in tectonically/seismically active regions, by presenting the results of an extensive gas (CO_2, noble gases) and groundwater surveys carried out in Croatia and Serbia (South-Eastern Europe) and in the Calabrian-Peloritan orogen (Southern Italy).

Croatia and Serbia in South-Eastern Europe (SEE) represent segments of the Alpine–Himalayan collisional orogenic belt, consisting of several Phanerozoic mobile belts. The SEE region inherits its geology from the evolution of the Vardar Tethys ocean, which existed in-between the Eurasian (Europe) and Gondwana (Africa) continental plates and whose relicts presently outcrop along the Vardar–Tethyan mega-suture (Cvetkovic et al. 2016). The region is characterized by the presence of i) several hydrothermal basins, mineral waters and natural CO_2 emissions; ii) high heat flow, sign of high geothermal energy potential (< 150 mW/m^2; Horvath et al., 2015; Lenkey et al., 2002); iii)

active seismicity with earthquake magnitudes up to 6.5 (http://www.seismo.gov.rs/Seizmicnost/Katalog-zemljotresa.pdf; Markušić et al., 2020; ISC and USGS catalogue); and iv) active faulting (e.g., Basili et al., 2013). All these features make of Croatia and Serbia two suitable areas to investigate Earth degassing. Our objectives here are to (i) infer the sources of volatiles released in continental areas, thus contributing to assessing the natural degassing of C and noble gases far from active volcanic systems, and (ii) understand the processes that control the transit of fluids through the crust.

The Calabria-Peloritani Orogen (CPO) is an arcuate Alpine mountain belt connecting the southern Apennines and the Sicilian Maghrebides, in southern Italy (Tortorici, 1982 a,b;) and represent a tectonically complex region where a variety of processes such as orogenic accretion, subduction of a narrow slab, back-arc extension, regional uplift, basaltic magmatism, and intra-orogenic extension coexist in a restricted area. The driving force behind these processes is the interaction between the European and the African Plates that sutures the two tectonic plates in the central Mediterranean (e.g., Faccenna et al., 2010). The CPO is bounded by two main tectonic lineaments: the Sangineto line to the North, and the Taormina line, to the South (Tortorici, 1982a,b), and is classically subdivided into a northern and southern sector, separated in correspondence to the Catanzaro Strait Basin, a Neogene-Quaternary basin connecting the Ionian and Tyrrhenian sea (Chiarella et al., 2012, 2016; Longhitano et al., 2014; Brutto et al., 2016; Tortorici, 1982). The area is one of the most tectonically active zones of the central Mediterranean and has been struck by some of the most destructive seismic events ever seen in Europe (e.g., Messina in 1908 and Calabria in 1905 and 1783; Neri et al., 2020). The seismological and geodetic data depict two main crustal domains marked by different stress regimes: a compressive domain in the northern Sicilian offshore and an extensional domain in north-eastern Sicily and southern Calabria (Pondrelli et al., 2006; Neri et al., 2004; Cuffaro et al., 2011). The presence of thermal springs and bubbling waters is evidence for the close connection between the fluids' circulation pattern and the local tectonic structures and seismicity (Italiano et al., 2019).

In summary, the main aims of this research project are:

1. To highlight the pristine sources of gas emission in CPO, Serbia and Croatia, defining the role of secondary processes in controlling the chemical and isotopic composition of emitted fluids.
2. To emphasize the importance of the combined use of major volatiles (e.g., CO_2, N_2), noble gases (e.g., He, Ne) and their isotopic composition to assess the degassing history and geochemical evolution of fluids during storage in, and transit through, the crust.
3. To quantify the CO_2 earth degassing flux in these areas, investigating the hydrogeological systems of the areas.
4. To investigate the relationships between Earth degassing and geological features of the areas, with possible implications for seismogenesis and tectonic/geodynamic setting.

I.2. STATE OF ART

I.2.1. Earth degassing process

Earth degassing is a process in which gas species (CO_2, N_2, CH_4, noble gases, etc.) are transferred from the solid earth (i.e. crust and/or mantle) into the atmosphere. This process is notably more manifest at active volcanoes and hydrothermal systems via emissions through plumes and fumaroles, but also occurs in less evident form (e.g., regionally, in diffuse form) from tectonically active areas and geothermal areas not related to active volcanism (Condie, 2005). CO_2 is the second most abundant volcanic gas after water (Giggenbach, 1996), and dominates the natural gas diffuse emissions in tectonic areas (e.g., Li Vigni et al., 2022; Zhang et al., 2021; Chiodini et al., 2020; Tamburello et al., 2018, Italiano et al., 2008). CO_2 is known to have played a crucial role in controlling temperatures on the earth surface via the greenhouse effect (Royer et al., 2007; Royer, 2014). On geological timescales, the atmospheric CO_2 level is controlled by the balance between CO_2 consumed by chemical weathering and CO_2 form Earth degassing (Isson et al., 2020; Plankand

Manning, 2019; Wong et al., 2019; Foster et al., 2017; McKenzie et al., 2016; Royer et al., 2014, 2007; Berner, 2004; Kerrick & Caldeira 1993). Therefore, carbon exchanges between the Earth interior, atmosphere and hydrosphere play a fundamental role in planetary and atmospheric evolution. Active volcanoes are considered the biggest natural CO_2 sources, with emission forms including crater fumaroles and volcanic plumes from open vents (Aiuppa et al., 2019; Fischer et al., 2019) and diffuse degassing through soils, acquifers and springs (Werner et al., 2019; Fischer and Aiuppa, 2020). CO_2 emissions are also typically highest in thermal areas where gases are emitted through hydrothermal fumaroles, soils and fractures as diffuse degassing, and hot and cold springs (Werner et al., 2019 and reference therein).

One additional, perhaps overlooked form of CO_2 release to the atmosphere occurs through diffuse degassing through soils and aquifers in tectonically/seismically active area (e.g., Li Vigni et al., 2022; Xu et al., 2022; Rufino et al., 2021; Zhang et al., 2021;Cangemi et al., 2020; Chen et al., 2020; Chiodini et al., 2000,2004,2020; Caracausi & Sulli, 2019; Ascione et al., 2018; Italiano et al. 2009,2010,2019; Tamburello et al., 2018; Evans et al., 2008, Becker et al., 2008, Newell et al., 2008). Unfortunately however, this CO_2 contribution is less understood compared to the volcanic gas emissions, and the sources and controlling processes remain poorly constrained (Xu et al., 2022;.Chiodini et al., 2020; Fischer & Aiuppa, 2020). Several models have been used over the years to study and to define the long-term global carbon cycle (Fig.I.1). The BLAG (Berner-LAsaga_Garrels) model and subsequent GEOCARB models (Royer, 2014 and reference therein) derived the rate of CO_2 degassing over geological time assuming the present-day CO_2 output is balanced by CO_2 consumption by chemical weathering (Berner et al., 1983; Berner, 2006). Other models for long-term carbon cycle, track the mass abundance of carbon- and sulphur bearing rocks much like GEOCARB, but they do not incorporate isotopes and include fewer modifying parameters (e.g., Budyko et al. 1987). Tajika (1998) and Kashiwagi and Shikazono (2003) model CO_2 for the last 150 and 65 My, respectively, in a manner similar to GEOCARB except for expanded treatments of degassing while Wallmann (2001, 2004) developed a set of independent

GEOCARB-style models, with an additional focus on the submarine weathering of basalt. However, global estimates of present-day CO_2 degassing flux, based on the assumptions underlying these models, are inconsistent with those derived from volcanic degassing data (Burton et al. 2013), suggesting that the two flux contributions (chemical weathering and metamorphic-magmatic output) should be computed separately (Fresia & Frezzotti, 2015).

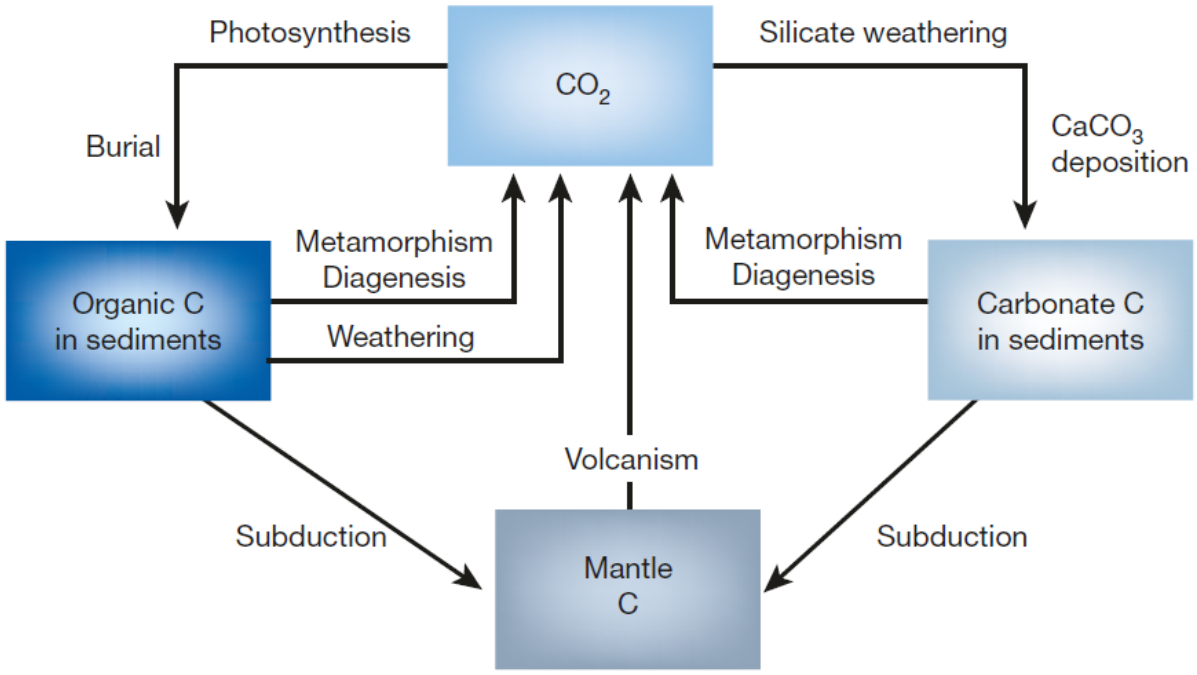

Figure I.1 | A model of the long-term carbon cycle.The deposition of carbonates derived from the weathering of carbonates is not shown because these processes essentially balance one another over the long term as far as carbon dioxide is concerned. However, carbonate deposition derived from carbonate weathering leads to additional degassing of carbon dioxide upon deep burial and thermal decomposition. Diagenesis, chemical changes at low temperatures during burial. The cycle can be subdivided into two subcycles involving organic matter (left side of figure) and silicate weathering and carbonate deposition (right side of figure) (from Berner, 2003; modified).

In the last two decades, attempts have been made to refine estimates of the global volcanic CO_2 flux. Burton et al., (2013) separately quantified CO_2 emissions from plumes, diffuse degassing from historically active volcanoes, hydrothermal and inactive areas, volcanic lakes, and middle ocean ridge (MOR). They estimated that ~150 volcanoes are today passively degassing, or 10% of the ~1500 volcanoes active in the Holocene (Siebert et al., 2002). By extrapolation, they then calculated

a CO_2 volcanic flux of about 12×10^{12} mol·yr^{-1} and a total flux including mid-ocean ridges degassing of about 14×10^{12} mol·yr^{-1}. These values are higher than previous estimates (Gerlach,1991; Brantley & Koepenick,1995; Marty & Tolstikhin 1998; Mörner & Etiope 2002) but are still affected by large uncertainties mainly caused by the limited information available for the diffuse CO_2 degassing from inactive/quiescent volcanoes and hydrothermal systems. Moreover, most of the measurements used by Burton et al. (2013) for their extrapolation represented spot measurements often collected during periods of heightened activity that might span several decades (Werner et al., 2019). More recently, the Deep Earth CArbon DEgassing (DECADE) research initiative of the Deep Carbon Observatory (Fischer, 2013) has allowed a better global coverage of subaerial volcanic CO_2 emissions (Werner et al., 2019; Fischer et al., 2019). Synthesis of the DECADE results has allowed to fix the CO_2 flux at 51.3 ± 5.7 Tg CO_2/y (11.7×10^{11} mol CO_2/y) for non-eruptive degassing and 1.8 ± 0.9 Tg/y for eruptive degassing during the period from 2005 to 2015 (Fischer et al., 2019) and 83 Tg CO_2/year from the known (e.g., measured) diffuse degassing (Werner et al. 2019).

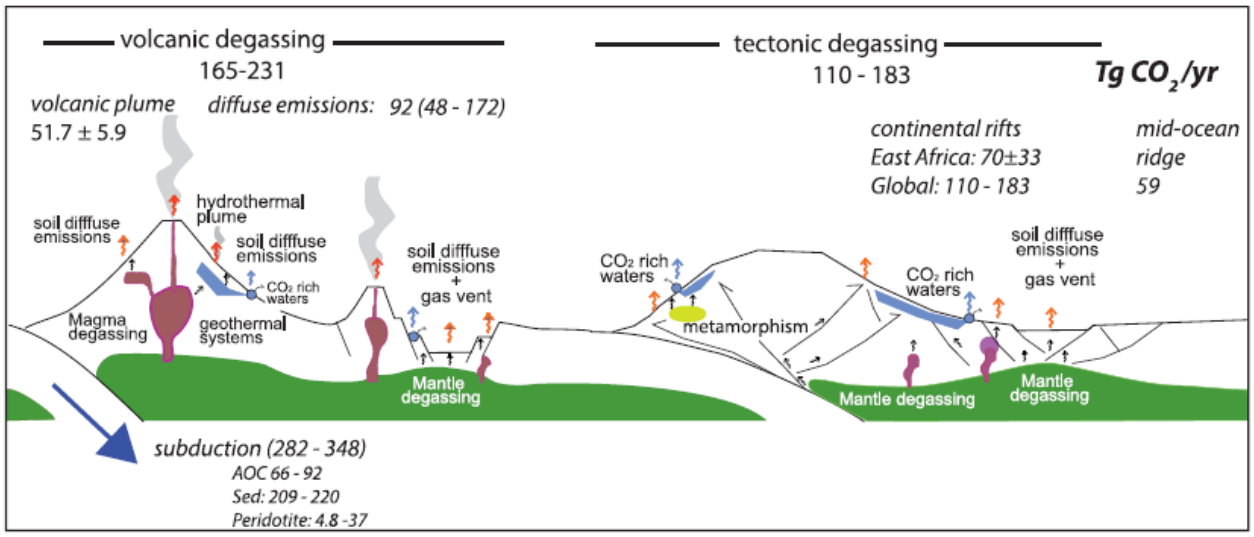

Figure I.2| Global volcanic and tectonic CO_2 degassing in teragrams of CO_2 per year. From Fischer and Aiuppa, 2020.

Tectonic/seismic active regions worldwide, including orogenic belts, continental rifts and geothermal areas, are often characterized by widespread regional CO_2 degassing (Fig. I.2; Barnes et. al., 1978; Irwin and Barnes, 1980). Recent work demonstrated the presence of a spatial

correlation between CO_2 discharges and active fault systems, in particular with those characterized by a normal slip type (Tamburello et al., 2018), demonstrating that an active tectonic regime plays a key role in fluid transport and discharge. Such tectonic CO_2 emissions, whose surface manifestation include gas vents, diffuse soil degassing, gases dissolved in lakes, cold and hot springs (i.e., CO_2 dissolved in groundwaters), have complicated source processes, as they can derive from a combination of mantle degassing and metamorphic reactions in the crust (Frezzotti et al., 2010).

In this way, the noble gases are powerful tracers of crustal fluid processes that act on subsurface CO_2 (Cathles et al., 2007; Ballentine et al., 2001) and they can be combined with major volatiles such to investigate their sources (Sano & Fischer, 2013). In fact, noble gases are chemically inert elements that exist as extremely volatile gases at standard temperature and pressure. Their lack of reactivity results in no change in their isotopic compositions via chemical processes but allows them to be used as a tracer of physical processes, which can alter both their isotopic and relative elemental compositions (Holland & Gillfillan,2013). Noble gases in the Earth are broadly derived from two sources: noble gases trapped during the accretionary process ('primordial' noble gases, e.g., ^{3}He) and those generated by radioactive processes (e.g., ^{4}He; Ballentine and Burnard 2002; Table I.1). Differentiation of the Earth into mantle and continental crust, degassing and early processes of atmosphere loss has resulted in the formation of reservoirs in which the abundance pattern and isotopic compositions of primitive noble gases have been variably altered. Combined with their different radioelement concentrations (U, Th, K) producing radiogenic noble gases, the mantle, crust and atmosphere are now distinct in both their noble gas isotopic composition and relative elemental abundance pattern (Ballentine et al., 2002).

Nuclide	Half-life	Daughter	Yield	Comments
^{3}H	12.26 a	^{3}He	1	Continuously produced in atmosphere
^{238}U	4.468 Ga	^{4}He	8	
		^{136}Xe	3.6×10^{-8}	Spontaneous Fission
^{235}U	0.704 Ga	^{4}He	7	$^{238}U/^{235}U = 137.88$
^{232}Th	14.01 Ga	^{4}He	6	Th/U = 3.8 in bulk Earth
		^{136}Xe	$<4.2 \times 10^{-11}$	No significant production in Earth
^{40}K	1.251 Ga	^{40}Ar	0.1048	$^{40}K = 0.01167\%$ total K
^{244}Pu	80 Ma	^{136}Xe	7.0×10^{-5}	$^{244}Pu/^{238}U = 6.8 \times 10^{-3}$ at 4.56 Ga
^{235}U	0.704 Ga	^{4}He	1	$^{129}I/^{127}I = 1.1 \times 10^{-4}$ at 4.56 Ga

Table I.1| Radiogenic nuclides and their half-life for noble gases (from Holland & Gillfillan, 2002 and reference therein)

The present-day radiogenic production of ^{4}He is governed by the α-decay of $^{235,238}U$ and ^{232}Th and the crustal output produced in 1 g of rock per year is given by:

$$^{4}He \text{ atoms } g^{-1} \text{ } yr^{-1} = (3.115 \times 10^{6} + 1.272 \times 10^{5})\,[U] + 7.710 \times 10^{5}\,[Th]$$

where [U] and [Th] are the concentrations of $^{235,238}U$, ^{232}Th in weight fraction or parts per million (ppm) (Ballentine and Burnard 2002). Crustal production of ^{3}He is governed by thermal neutron capture by ^{6}Li and other reactions described in Mamyrin and Tolstikhin 1984. For average crustal compositions, ^{3}He produced within the crust yields orders of magnitude lower than ^{6}Li and can, thus, be considered negligible. Fluids that originate from these different sources will contain noble gases that are therefore isotopically distinct and resolvable (Holland & Gillfillan, 2013, Fig I.3). In particular noble gases volatile signatures can be utilized to understand volatile source features (i.e., mantle vs. crustal), sinks, and volatile pathways through the crust as well as connections to larger tectonic processes (Barry et al., 2021). The elemental and isotopic make-up of noble gases provides insight into the source of CO_2 in continental settings (Sherwood Lollar & Ballentine, 2009). Comparing ^{3}He amounts with the concentration of ^{4}He (i.e. the $^{3}He/^{4}He$ ratio) can identify magmatic contributions to subsurface reservoirs (Kennedy & van Soest, 2007; Ballentine, et al. 2002; Oxburgh et al., 1986). Likewise, the ^{3}He amount can be compared to the concentration of

CO_2 within a natural environments to determine the origin of the CO_2 (Marty, et al. 1992; Oxburgh, et al. 1986). This is because magmatic $CO_2/^3He$ ratios fall in a very tight range compared with many crustal fluids (Marty et al., 2020; Griesshaber et al., 1992), hence this characteristic 'fingerprint' can be used to identify mantle-derived CO_2 from other CO_2 sources, such as carbonate minerals in the crust. ^3He is most notably linked to volcanic carbon dioxide and has long been used to quantify volatile fluxes at mid-ocean ridges (e.g., Marty & Tolstikhin, 1998), arcs (e.g., Barry et al., 2021, Sano & Marty, 1995), subduction zones (De Leeuw et al., 2007; Sano et al 1998) .

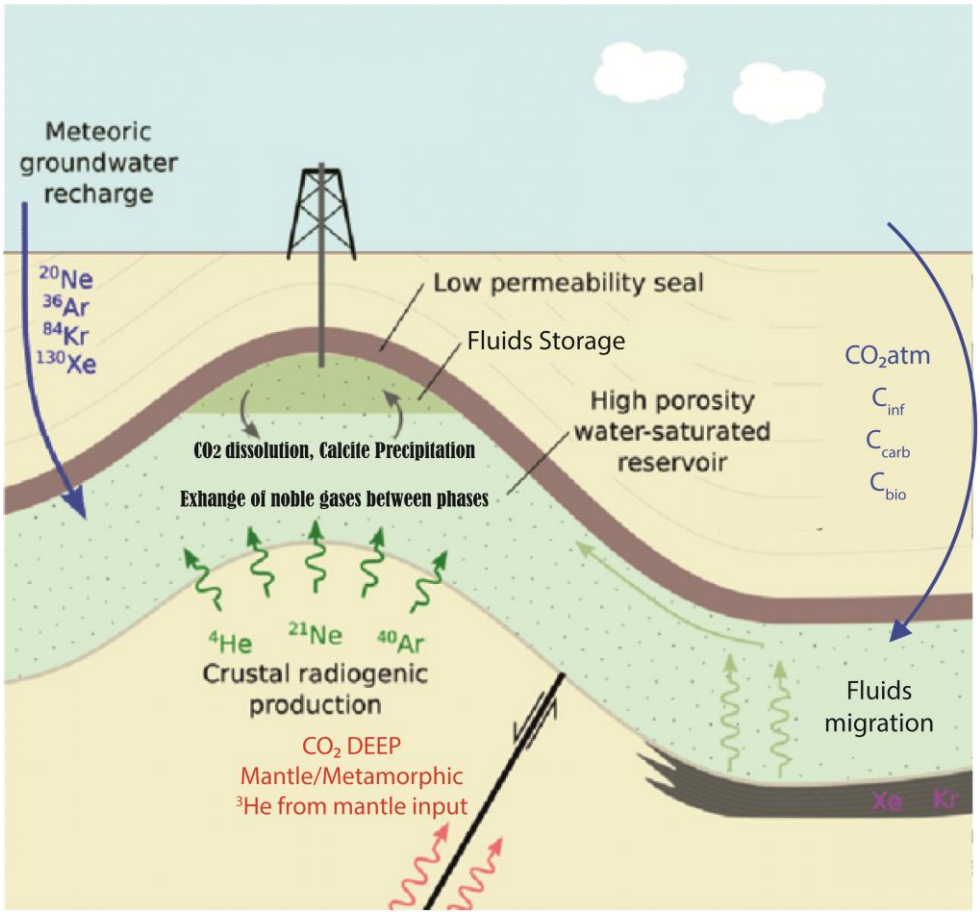

Figure I.3 | Noble gases source/s in crustal environments. Simplified sketch showing the three sources of noble gases in any subsurface fluid: the atmosphere, crust and mantle. Each noble gas source has a unique isotopic composition and elemental abundance pattern. Hence noble gas tracers allow quantification of the contribution of differently sourced fluids, independent of subsequent chemical or biological reactions. After Ballentine et al., 2002. Modified.

Noble gases and stable isotopes (C) have long been used to characterize sources, fluxes and pathways of carbon through volcanic groundwater systems (Barry et al., 2019a,2019b,2021; Bergfeld et al., 2017; Werner et al., 2013; Saar et al., 2005; Allard et al., 1997; Davisson and Rose,

1997) and more recently to identify magmatic carbon dioxide in continental settings far from any volcanism (Xu et al., 2022; Randazzo et al., 2021; Caracausi & Sulli, 2019; Ballentine et al., 2001; Sherwood Lollar et al., 1997). Measurements of $^{3}He/^{4}He$ and $CO_2/^{3}He$ were used to identify a magmatic CO_2 input in a series of gas reservoirs (e.g., Gilfillan et al., 2008), to monitor the fate of geologically sequestered CO_2 (Gilfillan et al., 2009) and, addition with carbon isotopic composition and others noble gases (e.g. ^{20}Ne), to define the role of secondary processes in the CO_2 removal processes (Barry et al., 2020; Brauer et al., 2016; Gilfillan et al., 2009; Ballentine et al., 1991). In the subsurface, water occupying rock pore-space (groundwater) has often equilibrated with the atmosphere. The atmospheric-derived noble gases (^{20}Ne, ^{36}Ar, ^{84}Kr; Fig. I.3) in groundwaters then preserve a record of the physical conditions (such as surface temperature) when that equilibration last occurred (Sherwood Lollar & Ballentine, 2009). Natural gas phases (e.g., CO_2) that contact the pore water result in transfer of the noble gases between phases, with distinct fractionation patterns that can then be used to quantify the role of groundwater in these systems (Zhou et al., 2012; Gilfillan et al., 2009; Zhou et al., 2005; Ballentine et al., 2002; Ballentine & Sherwood Lollar, 2002; Ballentine et al., 1991; Torgersen & Kennedy, 1992)

The transport of the noble gases from the proximity of their production to near surface systems and, ultimately, the atmosphere, is dependant on the driving force. This must be in the form of either a concentration gradient driving diffusion, or a pressure gradient resulting in advective fluid flow (Ballentine & Burnard, 2002). The most well studied mechanisms for deep (i.e., mantle- and subduction-derived) volatile transport to shallow groundwater is tectonic activity and transport along active faults (e.g., Lupton, 1983; Oxburgh et al., 1986; Oxburgh and O'Nions, 1987; Kennedy et al., 1997; Kulongoski et al., 2005, 2013; Crossey et al., 2016). A quantitative He flux estimate can provide insights into the transfer of volatiles through the crust. Among the first studies to define the mantle helium flux from continental region were Sano et al., (1986) and O'Nions & Oxburgh, (1988). While the first derived the flux from $^{3}He/^{4}He$ ratio gradients in Taiwan gas wells the second based flux calculation on the principle that if the degassing of helium in a particular segment of

crust occurs at steady state, then the mantle helium flux may be estimated from the average helium isotope composition of the system. The results from this study have been showed that areas under tectonic extension have He flux values two order of magnitude higher than that of continental stable areas allowed to identify an advective transport which occur though the faults. Noble gases can therefore furnish valuable information about source of CO_2 (e.g., Brauer et al., 2016), secondary processes that act during the up rise of fluids (e.g., Randazzo et al., 2021, Barry et al., 2020; Sherwood Lollar & Ballentine, 2009) and on transfer modality (e.g., Cacausi et al., 2005, O'nions & Oxburgh, 1988) to better understand and quantify CO_2 degassing processes in active tectonic environments. However, the contribution of such tectonic/metamorphic degassing sources to the global carbon cycle is even less characterised due to the limited observational dataset available (Evans et al. 2008; Girault et al. 2016). CO_2 flux measurements in non-volcanic environments are in fact limited to a relatively few well-studied areas (Chiodini et al,. 2000; 2004; 2011; 2020; Lee et al., 2016; Hunt et al., 2017). The catalogue of Italian CO_2-rich gas emissions (www.magadb.net and googas.ov.ingv.it) and the regional map of CO_2 degassing in Central Italy, (Chiodini et al. 2000; 2004; 2011) represent the first studies, at a regional scale, of CO_2 earth degassing in non-volcanic areas. More recent studies on diffuse soil CO_2 degassing from extensional areas suggest that globally relevant amounts of CO_2 are currently being released by the East African Rift system (Lee et al., 2016; Hunt et al., 2017).

Studying Earth degassing is not only relevant to understanding the global CO_2 flux, but also find important application in a variety of field and topics, such as i) to demonstrate the role of fluids in fault movements, earthquake nucleation and triggering (Rice, 1992; Cox, 1995; Sibson, 2000, 2007; Cappa et al., 2009; Umeda et al., 2011; Waldhauser et al., 2012; Di Luccio et al., 2018); ii) to define the primary role of fluids on past movement of exhumed faults, as the case of Italian Apennines (Collettini et al., 2008); iii) to investigate the gas hazard related to gas emissions, as documented in Italy and in other regions of the world, where atmospheric and topographic conditions can determine CO_2-rich gas accumulation at ground, eventually being lethal for animals and also

humans (Annunziatellis et al., 2003; Carapezza et al., 2003), and iv) for geothermal exploration purpose as made for example in "VIGOR" project, (http://www.vigor-geotermia.it, 2011-2014) and "Geothermal Atlas of Southern Italy" (http://atlante.igg.cnr.it, 2013-2015) where analytical and technical data have been used to locate and categorize the geothermal resources (Minissale et al., 2016; 2019). In the last 3 years, a new large-scale project on CO_2 degassing entitled "Improving the estimation of the tectonic carbon flux" has been supported by the Deep Carbon Observatory (DCO Grant n. 10881-TDB "Improving the estimation of tectonic carbon flux", http://deepcarbon.science/). This project coordinates and supports different research groups currently active in the study of the earth degassing process. The project is focused on the detection, quantification and fingerprinting of carbon degassing by studying groundwaters, and it is aimed to study different tectonically active areas of Europe, such as Slovenia, Croatia, Serbia, Romania, Macedonia, Alps and Southern Italy. This PhD project is part of this general study of the Earth degassing process.

I.3. The study areas: previous studies

This PhD dissertation is centred on two studied areas: i) south-eastern Europe, more specifically Croatia and Serbia, and ii) the Calabrian-Peloritan orogen in southern Italy. This site selection is motivated by the peculiar geodynamic, geological, tectonic, seismic and geochemical contexts, as examined below.

I.3.1. South eastern Europe: Croatia and Serbia

South-Eastern Europe (SEE) occupies a segment of the Alpine–Himalayan collisional orogenic belt and consists of several Phanerozoic mobile belts. The SEE region has inherited its present geological setting from the evolution of the Vardar Tethys ocean (Fig.I.4), which existed in between the Eurasian (Europe) and Gondwana (Africa) continental plates and whose relicts presently occur along the Vardar–Tethyan mega-suture (Cvetkovic et al. 2016).

During the last four decades several studies have been carried out in south-eastern Europe, in the attempt i) to understand natural earth degassing in active tectonic regions (e.g., Etiope et al., 2003, 2004; Frunzeti, 2013; Ionescu et al., 2017; Italiano et al., 2017; Kis et al., 2017; Sarbu et al., 2018; Vaselli et al., 2002), ii) to investigate the possible presence of magma at depth below "quiescent" volcanoes (e.g., Kis et al., 2019), and iii) to assess the role of fluids in seismogenetic processes (e.g., Baciu et al., 2007; Bräuer et al., 2004, 2005, 2008). A large-scale outgassing of mantle-derived fluids has been recognized in different regions of Europe, where volcanism has manifested as recently as thousands of years ago (e.g., Eger rift, Czech Republic; Eifel, Germany; Carpathians, Romania; Pannonian basin; Aeschbach-Hertig et al., 1996; Ballentine et al., 1991; Bräuer et al., 2013, 2016; Kis et al., 2017, 2019; Palcsu et al., 2014; Sherwood Lollar et al., 1997; Szöcs et al., 2013). Numerous mineral and thermal water springs, with free gas manifestation, are known in Serbia, and 230 mineral and thermal springs have been thoroughly studied (Filipović 2003). Exploitation of thermal and mineral waters in Serbia has a much longer history than scientific research. Hot spring have been used since Roman times for bathing and rehabilitation (Joksimović and Pavlović 2014). Geothermal resources in Serbia concentrate in the Pannonian basin (e.g. Mrazovac & Basic, 2009) and in the neighbouring areas (e.g., the Mačva geothermal system; Martinović & Milivojević, 2000), as well as in central and south-eastern Serbia (Joksimović et al., 2014). In global geothermal catalogues (Nuhovic & Djokic, 2013), Serbia is indicated as a country in which thermal and mineral waters are mainly used for balneological purposes, and for recreation and bottling. They are also used in agriculture, aquaculture, industry and technology (Hurter & Schellschmidt, 2003). For these reasons previous investigations have mainly been focused on hydrogeochemical characterization (e.g., Todorovic et al., 2016; Lyons et al., 1995), on geothermal potential and utilization of geothermal resources (e.g. Alimpic, 1985; Basic et al., 1988) and on ground water quality (e.g., Mrazovac & Basic, 2009).

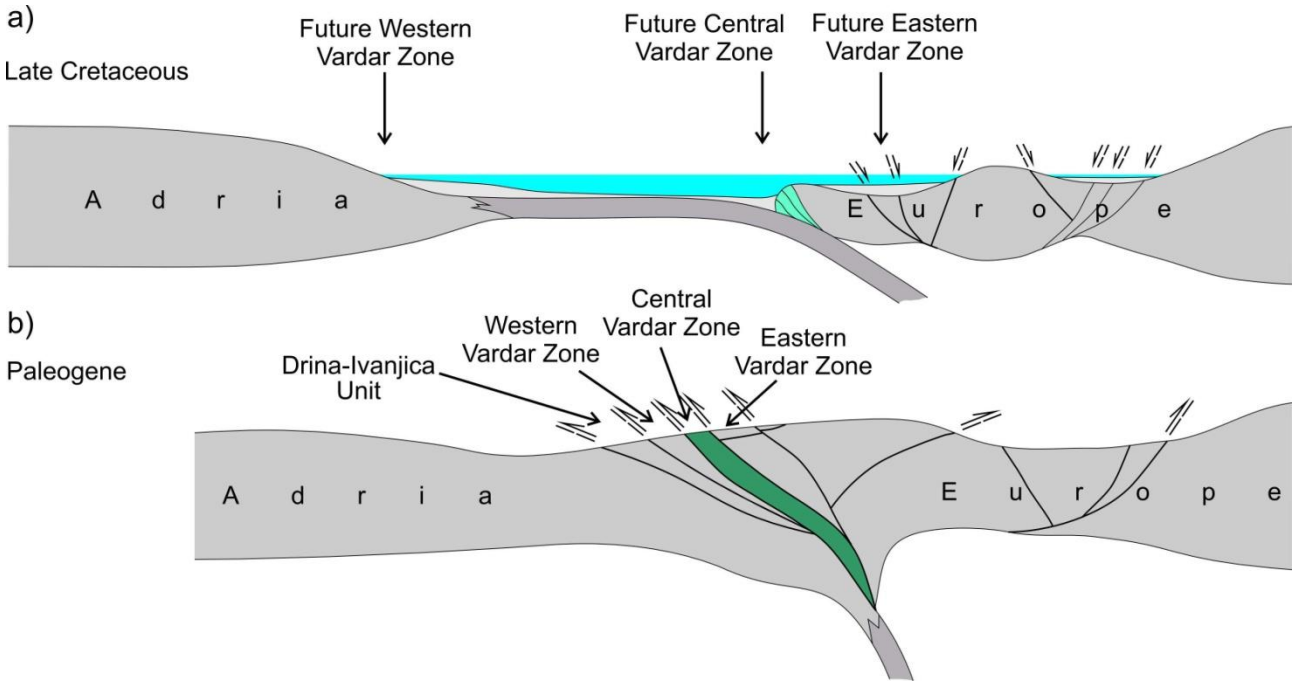

Figure I.4| Evolution of Dinarides-Carpatho-Balkanides during Cretaceous–Paleogene times. Conceptual sketch of the evolution of the subduction-fore-arc-back-arc system during Cretaceous–Paleogene times in the Dinarides-Carpatho-Balkanides. a) Late Cretaceous times: low-angle subduction, b) Paleogene times: continental collision associated with contraction and thrusting (from Marton et al., 2022).

In Croatia, mineral and thermal water springs have been known to exist since before the Roman Empire, with some localities and springs being utilized even in prehistoric time (Šimunić 2008). Given the use of these waters in such a vast period of time, the first geochemical analyses date back to the last decades of the 18th century (Crantz 1777). Comprehensive geological research started at the end of the 19th century (Pilar 1884; Koch 1889; Voyt 1890), but reached its peak during the 1970s with results summarized in the monograph "*Geothermal and mineral waters of the Republic of Croatia*" (Šimunić 2008). So far, the geothermal waters have been mainly exploited for medicinal and recreational purposes. Available literature data on the geochemistry of Croatian thermal waters includes studies on natural radioisotope abundance (Bituh *et al.*, 2009; Radolić *et al.*, 2005), on the related exposure (Marović and Senčar, 2001) and health risks (Marović *et al.*, 1996). Recent study first report on major and trace elements in groundwaters (e.g., Fiket et al., 2015) and on the high CO_2 concentrations in mineral waters (e.g. Borovic et al., 2016).

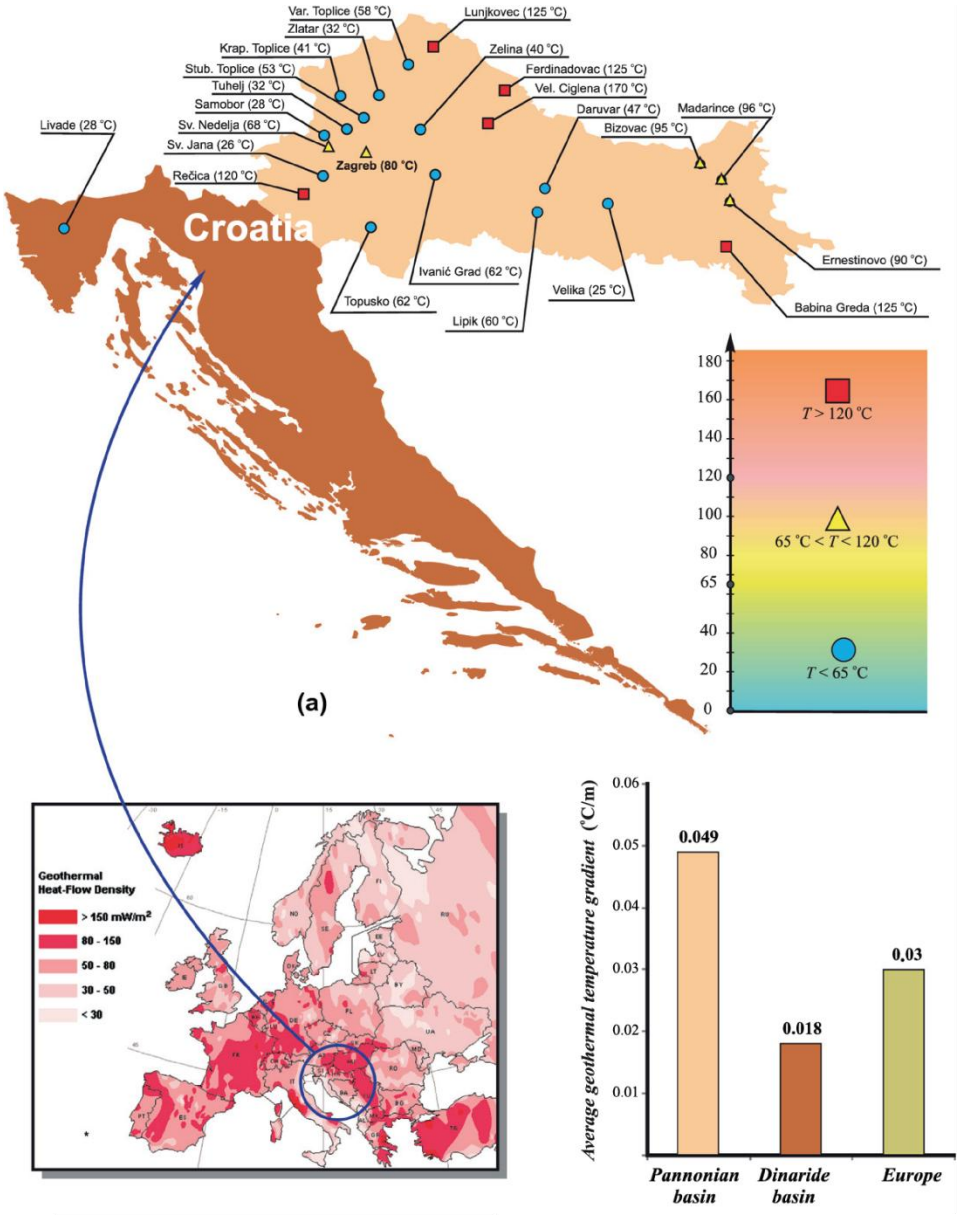

Figure I.5| Croatia Geothermal data: (a) geothermal sources in the Republic of Croatia, (b) geothermal heat-flow density in Europe and (c) average geothermal temperature gradient in the Republic of Croatia. (Source:http://www.geni.org/globalenergy/library/renewable-energy-resources/world/Europe/geo-europe/index.shtml) (Modified after Guzovic et al., 2012).

In conclusion, i) the presence of several hydrothermal basins, mineral waters and natural CO_2 emissions; ii) the high heat flow (< 150 mW/m^2; Horvath et al., 2015; Lenkey et al., 2002) and geothermal energy potential; iii) the active seismicity, with earthquakes of magnitudes up to 6.5 (http://www.seismo.gov.rs/Seizmicnost/Katalog-zemljotresa.pdf; Markušić et al., 2020; ISC and USGS catalogue) and iv) the active faulting regime (e.g., Basili et al., 2013) make of Croatia and

Serbia two suitable areas to investigate Earth degassing processes. We seek to understand the processes that control the transfer of fluids through the crust, and the source of fluids in such a complicated continental area.

I.3.2 Earth Degassing process in Italy

The geological evolution of Italy, and of the entire Western-Central Mediterranean area, is the result of the Oligocene to Present convergence between the African and Eurasian plates (van Hinsbergen et al., 2014). This led to the opening of the Ligurian-Provençal, Algerian, and Valencia and Tyrrhenian basins (Jolivet et al., 2021), the formation of the Apennine chain (Faccenna et al., 2018) and the emplacement of a wide variety of both orogenic and anorogenic magmas (Frezzotti et al., 2010 and reference therein).

Earth degassing has extensively been studied in Italy, and many of the techniques now in use globally to estimate non-volcanic CO_2 degassing at regional scale were originally developed in the Italian territory (Chiodini et al., 1999, 2002, 2004; Frondini et al., 2019). In Italy, CO_2 is trasported in dissolved form in regional groundwater systems (Chiodini et al., 2004; Frezzotti et al., 2010) and several anomalous soil CO_2 degassing zones have been discovered in Tuscany, Latium, Campania, in the Apennines, Sicily and Sardinia, along with numerous cold, CO_2-rich gas emissions (Fig. I.6; e.g., Chiodini *et al.*, 1999, 2000, 2004b, 2011; Rogie *et al.*, 2000; Chiodini and Frondini, 2001; Minissale 2004). The measured gas flow rates in some of these cold emissions are very high, as, for example, at Mefite d'Ansanto, the largest cold CO_2 emission ever measured on Earth (CO_2 flux of 1.7×10^{10} mol yr^{-1}; Chiodini et al. 2010). Earth degassing in Italy, including the volcanic contribution, may emit as much as 35-60 Mt CO_2/year (Mörner and Etiope, 2002, and references therein), or 7–12 % of the national anthropogenic CO_2 emissions (e.g., 457 Mt CO_2/year in 2004; Bassani *et al.*, 2009). Non-volcanic CO_2 emissions, including diffuse soil emissions, focused gas vents, and regional (Chiodini et al., 1998; 1999; 2000; 2004; Etiope, 1999; Italiano et al., 2000; Rogie et al., 2000; Gambardella et al., 2004; Caracausi et al., 2015) may contribute 4 to 30 Mt/yr

(Mörner and Etiope, 2002), or in the same order of magnitude of volcanic degassing. A direct link between deeply sourced CO_2 emissions and the structural tectonic setting (location of extensional faults and fractures), has been brought to light in different Italian sectors (e.g., the Appennines, Chiodini et al., 2004, 2020; in Irpinia, Italiano et al., 2000; Rogie et al., 2000; in the Campidano graben, Sandinia, Minissale et al., 1999; and in eastern Sicily, De Gregorio et al., 2002).

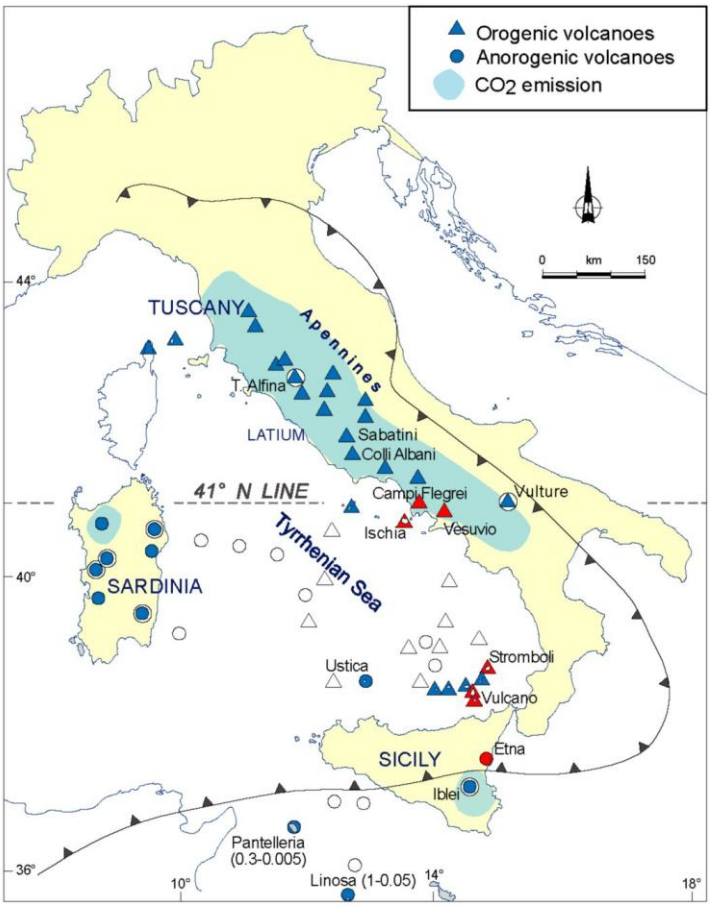

Figure I.6| Earth's CO_2 emission in Italy. Data derived from the online catalogue of Italian gas emissions (blue area; http://googas.ov.ingv.it; Chiodini and Valenza, 2007), and from the distribution of the main Plio-Quaternary volcanoes (Peccerillo, 2005). Active volcanoes in red. Open symbols refer to outcrops below the sea level). Volcanic centers marked by white circle bear peridotite xenoliths.(from Frezzoti et al., 2010)

The elevated CO_2 emissions sustained by Erath degassing in Italy reflect the complex geodynamic, geologic and hydrogeologic setting of the region, characterised by two different crustal domains: 1) the western Tyrrhenian sector and 2) the eastern Apenninic domain (Tavani et al., 2021; Binda et al., 2020; Chiodini et al., 2020,2004; Girolami et al., 2014; Barchi et al., 2010;2006; Cosentino et

al., 2010; Piana Agostinetti et al., 2002). The Tyrrhenian sector is characterized by crustal thinning, high thermal flow, ascent of mantle-derived fluids, Miocene-Quaternary volcanism, and seismicity along its eastern margin as due to extensional tectonic regime (Tavani et al., 2021; Loreto et al., 2020; Zitellini et al., 2020; Moeller et al., 2014; Mattei et al., 2010; Collettini et al., 2006). Furthermore, this sector is characterized by outcropping of relatively low permeability lithologies (e.g., volcanic and continental/marine shales) that do not favour the development of large aquifers. Due to these features, the deeply derived fluids can rise through the crust, accumulate in relatively shallow reservoirs, and further migrate upwards through a mature network of extensional faults and fractures to feed localized CO_2-rich gas emissions, CO_2-rich springs (volcanic/low permeability aquifers) and diffuse soil degassing (e.g., Chiodini et al., 1995, Chiodini et al., 2007). In contrast, the Apenninic domain is characterized by higher crustal thickness (average value of 35 km), low conductive heat flux, strong seismicity (Amato et al., 1998; Chiarabba et al., 2009; Chiaraluce et al., 2017), limited or no active surface degassing, and abundant groundwater transport through from carbonate rocks. This last peculiarity explains the lack of surface gas emissions, as rising fluids (e.g., CO_2) get dissolved into these regional aquifers upon ascent (Chiodini et al., 2004, 2020).

It is generally agreed that the bulk of the CO_2 degassing in Italy should reflect deep mantle processes, with shallow crustal contributions being significant only at a few active or recent volcanoes (Allard *et al.*, 1997; Chiodini *et al.*, 2000; Minissale, 2004; Gaeta *et al.*, 2009; Iacono Marziano *et al.*, 2009). Recent studies show that deeply derived CO_2 dissolved in Apenninic aquifers is characterized by a carbon isotopic composition ($\delta^{13}C$) in a range compatible with that of CO_2 emitted by geothermal systems and active Italian volcanoes (from -5‰ to 1‰; Chiodini et al., 2004 and reference therein), suggesting a regional degassing process. In general, the most important geological processes producing CO_2 are thermo-metamorphic reactions (Kerrick and Caldeira, 1998; Italiano et al., 2009,2008), hydrolysis of carbonates (Kissing & Parkhonov, 1969), degassing of shallow magma bodies (Edmonds et al., 2020) and mantle degassing (Hauri et al. 2018, 2019;

Lee et al., 2016; Hirschmann and Dasgupta 2009;). Metamorphic processes can produce CO_2 through chemical reactions involving carbonate minerals and/or silicate rocks in a wide temperatures range. Possible reactions include (Groppo et al., 2017,2020,2022):

$$5CaMg(CO_3)_2 + 8SiO_2 + H_2O = Ca_2Mg5(H_2O)_2Si_2O_{22}\ (tremolite) + 3CaCO_3 + 7CO_2$$

$$2CaMg(CO_3) + SiO_2 = MgSiO_4\ (fosterite) + 2CaCO_3 + CO_2$$

$$CaCO_3 + SiO_2 = CaSiO_3\ (wallostonite) + CO_2$$

These reactions produce CO_2 in a temperatures range between 200°C (hydrate conditions) and 600-700°C (anhydrous conditions). Giannelli (1985) suggested as source of fluids a metamorphosed crustal source, but this is not in agreement with other evidence. The isotopic composition of the CO_2 produced by metamorphic decarbonation processes depends on several factors but, as shown by Marini and Chiodini (1994), is generally more positive than the carbon isotopic composition of the protolites. The CO_2-calcite fractionation factor at relevant temperature (400–600°C) ranges from +2.59‰ to +2.77‰ (Ohmoto and Rye, 1979); considering that $\delta^{13}C$ of the possible protolites (i.e., Trias to Mesozoic marine limestones) generally lies between 0 and +2‰ (Chiodini et al., 2000, 2004, 2011) the carbon isotopic composition of metamorphic CO_2 is expected to be in the range from +2.5‰ to +5‰ (Chiodini et al., 2007). Another process able to produce carbon dioxide is mineral carbonates hydrolysis. Following reaction is one of the many possible:

$$CaCO_{3\,(s)} + 2H^+ = Ca^{2+} + H_2CO_3$$

This process requires a temperatures range between 100°C and 300°C and cannot explain the large anomalous degassing in Italy as it requires very acid environment that is uncommon in the Apennines (Marini & Chiodini, 1994). Different authors propose the degassing of the metasomatized mantle wedge in the Tyrrhenian side of Italy (Chiodini et al., 2004; 2011; Frondini et al., 2019) as the most probable source of regional CO_2 Earth degassing. In support to this hypothesis, it is found that the Tuscan-Roman and Campanian volcanic provinces are characterized

by potassic and ultrapotassic magmas rich in fluids with high CO_2/H_2O ratio (Foley 1992), in which magma geochemistry is consistent with melting of a mantle source metasomatized by the addition of subducted crustal materials of carbonate composition (Peccerillo et al., 1999; Frezzotti et al., 2009).

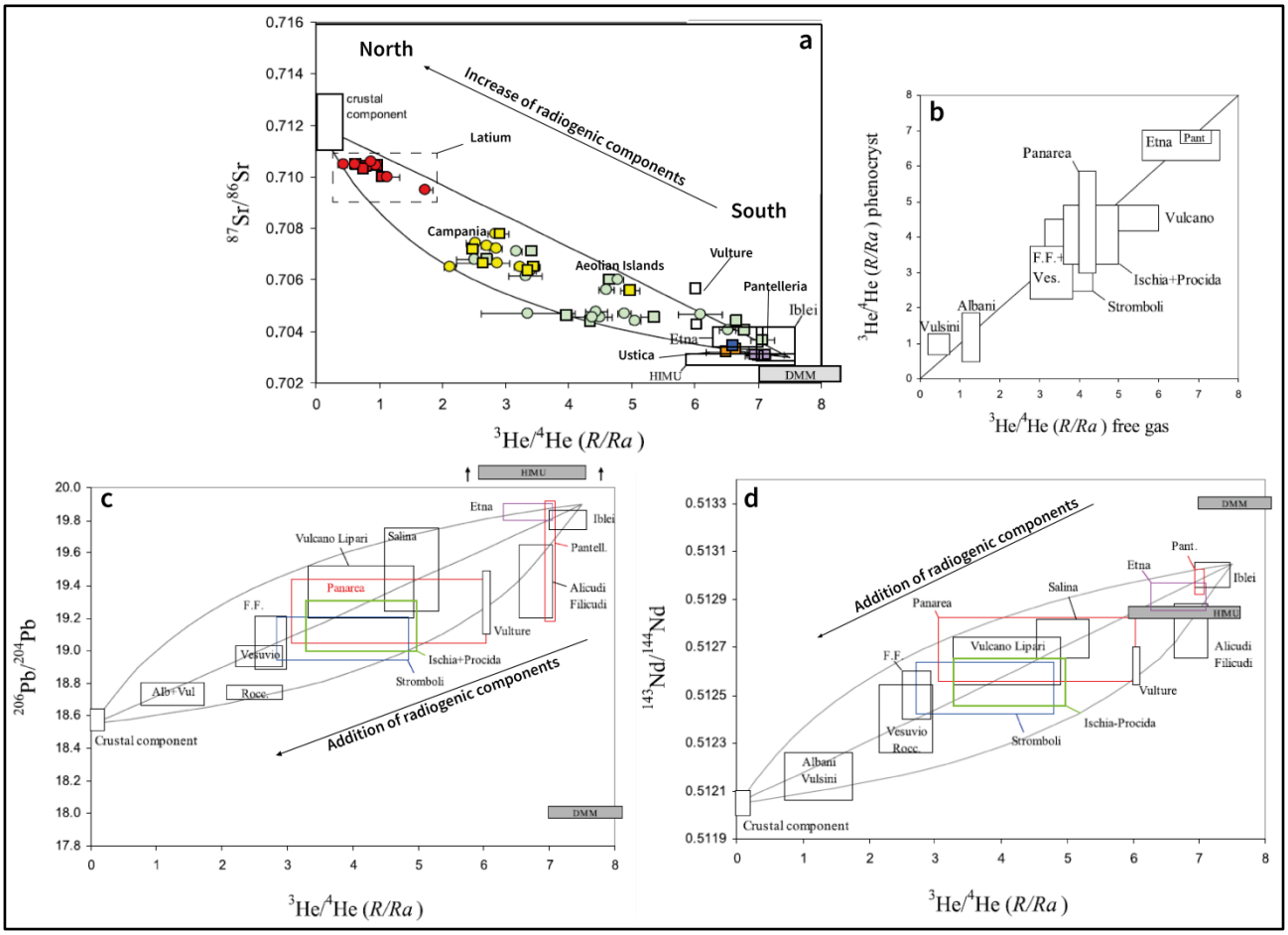

Figure I.7 | He, Sr, Pb and Nd relationships for Italian Plio-Quaternary volcanism. **a**) Values of $^{87}Sr/^{86}Sr$ versus $^{3}He/^{4}He$; **b**) a comparison of the $^{3}He/^{4}He$ of phenocryst hosted fluid inclusions with $^{3}He/^{4}He$ of free gases from the same volcanic district; **c**) $^{3}He/^{4}He$ versus $^{143}Nd/^{144}Nd$ and and **d**) $^{3}He/^{4}He$ versus $^{206}Pb/^{204}Pb$ (for more details see Martelli et al., 2008) (Modified after Martelli et al., 2008).

Others works have been studied olivine and/or pyroxene phenocryst-bearing basaltic lavas or pyroclastic deposits from different areas of Italy identifying a correlation trend in He-Sr isotope space interpreted as a binary mix between a high-$^{3}He/^{4}He$ low$^{87}Sr/^{86}Sr$ (Gasperini et al., 2002) asthenospheric mantle source and a low-$^{3}He/^{4}He$ high-$^{87}Sr/^{86}Sr$ component consistent with

metasomatically altered mantle (Martelli et al., 2004; Fig. I.7). The authors argued that the general northward increase in radiogenic He, Sr and Pb and unradiogenic Nd reflects the progressive contamination of the mantle wedge by metasomatic fluids released by the subducting Ionian-Adriatic plate (Martelli et al., 2008). He isotope ratio in the volcanic areas of peninsular Italy displays same values for free gas and fluid inclusion in recent lavas (Italiano et al., 2001; Martelli et al., 2008; Fig. I.7b). The general $^{3}He/^{4}He$ distribution in the peninsular Italy clearly show that mantle fluid contribution is greatest in perityrrhenian regions and decrease towards the periadriatic regions in agreement with recent and active volcanism (Italiano et al., 2001), crustal thickness (Panza et al., 2008), heat flow density (Cataldi et al., 1995) and seismic waves attenuation (Chiarabba et al., 2005). Despite this, an additional contribution from shallower (i.e., at crustal depth) metamorphic processes, at local scale, cannot be excluded, especially for gas emissions related to some higher temperature geothermal systems (e.g., Larderello, Amiata, Latera; Chiodini et al., 2007, Collettini et al., 2008). In addition, several studies have demonstrated, using geochemical and geophysical data, the possible presence of melt intrusions into faults along the axial direction of the Italian Apennines (e.g., Improta et al., 2014; Di Luccio et al., 2018). Intrusions of melts would be promoted by an uprising of the asthenosphere in correspondence of slab tear faults, as revealed by seismic tomography (Lucente et al., 1999). Slab tear faults along the margin of the peri-Tyrrhenian sector have been identified by Rosenbaum et al., (2008). These structures have determined lithospheric gaps that allow asthenosphere upwelling and decompression melting. The release of magmatic/mantle volatiles (including CO_2 and noble gases) from these intruding bodies may feed the degassing process in the Apennines deep crust, with upward fluid migration favoured by the interconnected systems of faults and fractures (Di Luccio et al., 2018). Active mantle/magmatic degassing has been recognized in many areas of the southern Apennines, including beneath the Matese mountains (Di Luccio et al., 2018), along the Vulture line (Caracausi et al., 2013; 2015), at Mefite d'Ansanto (Chiodini et al., 2010), and in other widespread gas emissions located in Campania and Basilicata region (Italiano et al., 2000).

I.3.2.1 Earth degassing process and seismicity in Italy

The Italian peninsula is one of the most seismically active regions of the world (Amato et al., 1998). The Apennine area, from north to south, is characterized by an upper crustal seismicity that shows a rotation from NW-trending alignments in the north to NNE-trending in Calabria, paralleling the rotation of the Apenninic and Calabrian arcs (Fig. I.8a; Chiarabba et al., 2005). In the northern and southern Apennines, the NW-striking segments are confined within the upper 6–8 and 12–15 km of depth, respectively. The largest events show normal faulting mechanisms (Fig. I.8b), consistent with the regional NE-trending extension (Westaway, 1992; Montone et al., 1999). Recent studies highlight a strong correlation between the Apennines seismicity and the presence of over-pressurized gas pockets at different crustal depths, which may facilitate seismic swarms and/or the nucleation of strong earthquakes (Miller et al., 2004; Chiodini et al., 2011; Di Luccio et al., 2018). Earthquake's epicentres concentrate in a belt that separates two distinct crustal domains: the Tyrrhenian hinterland, where two different CO_2 degassing structures are located (Tuscan-Roman Degassing Structure – TRDS - and Campanian Degassing Structure – CDS -; Chiodini et al., 2004; Frondini et al., 2019) and the Adriatic foreland where deeply derived CO_2 is virtually absent. From geological and geophysical data (e.g., the CROP project; Collettini, 2002) a conceptual model to explain this relation has been proposed. A marked mantle upwelling exists in the Tyrrhenian hinterland (Fig. I.9). In this zone, mantle fluids may enter the ductile lower crust at near lithostatic pressure (Kennedy et al., 1997), infiltrate upwards through the interconnected network of extensional fractures and normal faults, and generate the high CO_2 domains observed at the surface (Chiodini et al., 2004).

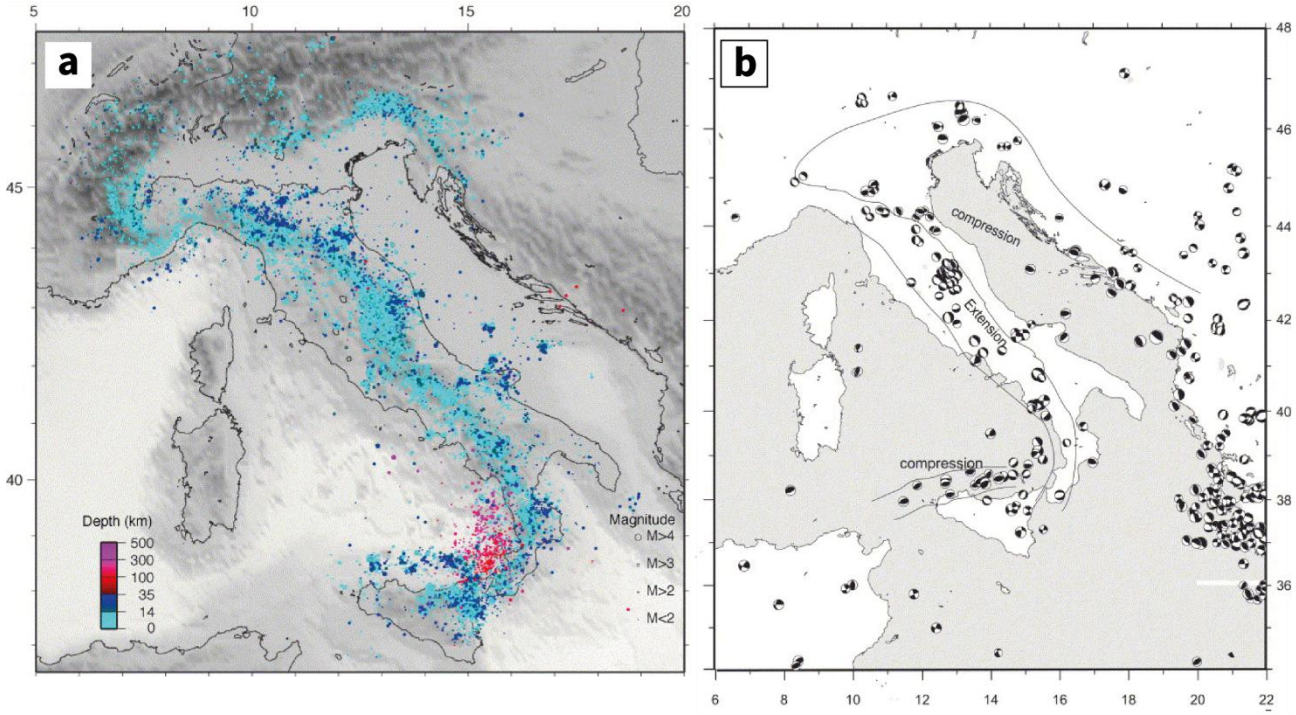

Figure I.8 | Italian Seismicity. **a**) Hypocentral distribution of the about 45,000 selected events. Colour scale, continuously varying, indicates the depth of events (blue colours for the crustal seismicity and red colours for the mantle seismicity). The different size of circles is given by the magnitude scale indicated on the lower right corner; **b**) CMT (Harvard) and RCMT (Pondrelli et al., 2002) solutions for the M>4.5 seismicity since 1976. The extension along the Apennines belt and the compression around the Adria lithosphere and in the northern Sicily offshore are evident.(Modified after Chiarabba et al., 2005)

The extensional processes started several million years ago in the peri-Tyrrhenian domain, allowing the development of a mature set of faults and fractures. In contrast, earthquake focal mechanisms suggest that the Apennine belt is also undergoing extension, but only since very recent times (Frepoli and Amato, 1997; Mariucci et al., 1999). This explains the lack of a well-developed system of interconnected fractures, and of clear degassing at the surface. In the Apenninic domain, at depths ranging from 5 to about 15 km b.s.l., the thrusts are dislocated by seismogenetic low-angle normal faults, where seismicity is concentrated. These faults can move at depth only in response to high fluid pressure (Kennedy et al., 1997; Collettini, 2002; Ghisetti and Vezzani, 2002) and their arrangements describe outward verging structures that could act as traps (structural seal) in which CO_2 can accumulate and generate over-pressurized reservoirs.

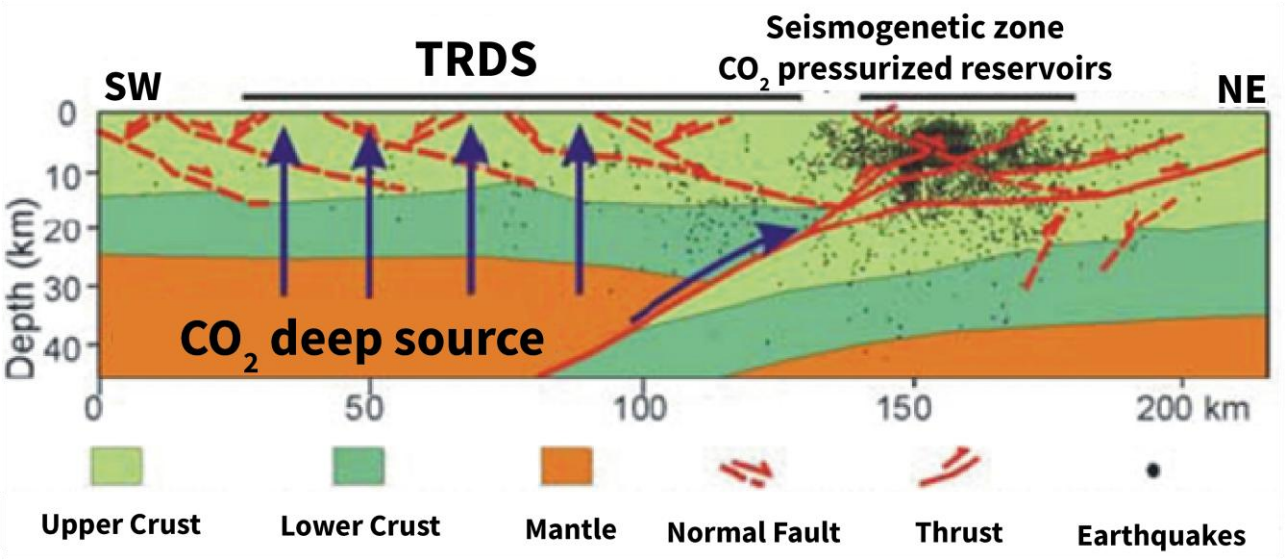

Figure I.9 | Earth degassing-seismicity relation in Appenine. Crustal section modified by Collettini et al. (2002) and conceptual model of the Earth degassing process in relation with the seismic activity in the appenninic domain (from Chiodini et al. 2004. Modified).

Over-pressurized reservoirs have been recognized in deep well exploration in central Italy on the boundary of the Tyrrhenian domain (S. Donato and Pieve S. Stefano wells; Chiodini et al., 2004 and reference therein). Such high-pressure fluids are likely to play a key role in fault failure and seismogenesis, as inferred by different authors (Miller et al., 2004 for the 1997 Colfiorito earthquake; Di Luccio et al., 2010, Terakawa et al. 2010 Lucente et al. 2010). Recently Di Luccio et al. (2018) analysed a deep seismic sequence (M_w of 5) occurred in 2013 beneath the Matese mountains in southern Apennines. In particular they showed seismic evidence of fluids involvement in the earthquake nucleation processes, identifying a thermal anomaly in aquifers dissolving CO_2 of magmatic origin. They highlighted that the intrusion of dyke-like bodies in mountain chains may trigger earthquakes of relevant magnitude. More recently, Chiodini et al. (2020) revealed the strong time-correlation of deep CO_2 flux in the Apennines (Italy) during intense seismicity analyzing the results of a 10-year record (2009–2018) of the deep CO_2 dissolved in large springs of central Italy discharging the groundwater circulating above the epicentral areas of the Abruzzo 2009 and Central Italy 2016-17 seismic crisis. They showed the gas emission, i.e. the input of CO_2 in to the aquifers,

strongly correlates with the evolution of the seismic sequences (Fig. I.9) with peak occuring concurrently with the main shocks followed by a CO_2 emission decrease following the seismicity decay in terms of magnitude and rate. Chiodini et al. (2020) concluded that the ascent of huge amount of deeply-derived CO_2 that continually accumulates at depth, possibly in crustal traps, significantly contribute to earthquake occurrence in the Apennine.

In conclusion, all these studies converge to indicate the Italian peninsula is affected by an active anomalous earth degassing process, with possible strong correlation with seismicity. Consensus exists for that CO_2 fluxes cannot be reliably quantified without the investigation of groundwaters. In tectonically young and permeable orogens, the majority of deep rising CO_2 may in fact dissolve into regional aquifers, ultimately preventing direct emission of CO_2-rich gases at the surface. Current estimates of deep CO_2 output in Italy must be considered as lower bounds, because several CO_2-rich cold gas vents, soil degassing areas, and regional groundwater systems (especially in the western sector of Italy) are still unstudied (Chiodini et al., 2008).

References

Allard, P., Carbonnelle, J., Dajlevic, D., Le Bronec, J., Morel, P., Robe, M.C., Maurenas, J.M., Faivre-Pierret, R., Martin, D., Sabroux, J.C., Zettwoog, P., 1991. Eruptive and diffuse emissions of CO2 from Mount Etna. Nature 351, 387-391.

Allard, P., Jean-Baptiste, P., D'Alessandro, W., Parello, F., Parisi, B., Flehoc, C., 1997. Mantle-derived helium and carbon in groundwaters and gases of Mount Etna, Italy. Earth and Planetary Science Letters 148, 501-16.

Amato, A. et al. 1998. The 1997 Umbria–Marche, Italy, Earthquake Sequence: A first look at the main shocks and aftershocks. Geophysical Research Letters, 25, 1861–1864.

Annunziatellis A., Ciotoli G., Lombardi S., Nolasco F., Short- and long-term gas hazard: the release of toxic gases in the Alban Hills volcanic area (central Italy), Journal of Geochemical Exploration, Volume 77, Issues 2–3, 2003, Pages 93-108, ISSN 0375-6742, https://doi.org/10.1016/S0375-6742(02)00272-8.

Ascione A., Ciotoli G., Bigi S., Buscher J., Mazzoli S., Ruggiero L., Sciarra A., Tartarello MC., Valente E; Assessing mantle versus crustal sources for non-volcanic degassing along fault zones in the actively extending southern Apennines mountain belt (Italy). *GSA Bulletin* 2018;; 130 (9-10): 1697–1722. doi: https://doi.org/10.1130/B31869.1

Ballentine, C. J., & Burnard, P. (2002). Production, release and transport of noble gases in the continental crust. *Reviews in Mineralogy and Geochemistry*, *47*(1), 481–538. https://doi.org/10.2138/rmg.2002.47.12

Barchi M., Pauselli C., Chiarabba C., Di Stefano R., Federico C & Minelli G., 2006: Crustal structure, tectonic evolution and seismogenesis in the Northern Apennines (Italy). Bollettino di Geofisica Teorica e Applicata. Bollettino di Geofisica Teorica e Applicata. Vol.47, n.2, 249-270.

Barchi, M. (2010), The Neogene-Quaternary evolution of the Northern Apennines: Crustal structure, style of deformation and seismicity [online], J. Virtual Explor., 36, paper 11.

Barnes, I., Irwin, W.P. & White, D.E. 1978. Global distribution of carbondioxide discharges, and major zones of seismicity, scale 1:40,000,000. US Geological Survey, Water Resources Investigation Report, WRI 78-39

Barry, P.H., de Moor, J.M., Giovannelli, D., Schrenk, M.O., Hummer, D.R., Lopez, T., Pratt, C.A., Alpízar Segura, Y., Battaglia, A., Beaudry, P., Bini, G., Cascante, M., D'errico, G., Di Carlo, M., Fattorini, D., Fullerton, K., Gazel, E., Gonz´alez, G., Halld´orsson, S.A., Iacovino, K., Kulongoski, J.T., Manini, E., Martínez, M., Miller, H., Nakagawa, M., Ono, S., Patwardhan, S., Ramírez, C.J., Regoli, F., Smedile, F., Turner, S., Vetriani, C., Yücel, M., Ballentine, C.J., Fischer, T.P., Hilton, D.R., Lloyd, K.G., 2019a. Forearc carbon sink reduces long-term volatile recycling into the mantle. Nature 568 (7753), 487–492.

Barry, P.H., Nakagawa, M., Giovannelli, D., de Momor, J.M., Schrenk, M., Seltzer, A.M., Manini, E., Fattorini, D., di Carlo, M., Regoli, F., Fullerton, and K., Lloyd, K.G., 2019b. Helium, inorganic and organic carbon isotopes of fluids and gases across the Costa Rica convergent margin. Sci. Data 6 (1), 1–8.

Barry, P. H., Negrete-Aranda, R., Spelz, R. M., Seltzer, A. M., Bekaert, D. V., Virrueta, C., & Kulongoski, J. T. (2020). Volatile sources, sinks and pathways: A helium-carbon isotope study of Baja California fluids and gases. *Chemical Geology*, *550*(2020), 119722. https://doi. org/10.1016/j.chemgeo.2020.119722

Barry P. H., Bekaer D. V. t, Krantz J. A., Halldórsson S. A., de Moor J.M., Fischer T. P., Werner C., Kelly P. J., Seltzer A. M., Franz B. P., Kulongoski J. T., Helium-carbon systematics of groundwaters in the Lassen Peak Region, Chemical Geology, Volume 584, 2021, 120535, ISSN 0009-2541, https://doi.org/10.1016/j.chemgeo.2021.120535

Basili R., Kastelic V., Demircioglu M. B., Garcia Moreno D., Nemser E. S., Petricca P., Sboras S. P., Besana-Ostman G. M., Cabral J., Camelbeeck T., Caputo R., Danciu L., Domac H., Fonseca J., García-Mayordomo J., Giardini D., Glavatovic B., Gulen L., Ince Y., Pavlides S., Sesetyan K., Tarabusi G., Tiberti M. M., Utkucu M., Valensise G., Vanneste K., Vilanova S., Wössner J. (2013). The European Database of Seismogenic Faults (EDSF) compiled in the framework of the Project SHARE. Istituto Nazionale di Geofisica e Vulcanologia (INGV). https://doi.org/10.6092/ingv.it-share-edsf

Bassani, G.-F., Bianucci, M., Carra`, S., Cifarelli, L., De Sanctis, E., Mariotti, G., Masi, M., Menna, P., Monti, S., Renieri, A., Ricci R. A., Ricco, G., Romano, U., Ronchi, E., Rostagni, G., Silvestrini, G. Tocci, W. 2009. Energy in Italy: Problems and perspectives (1990-2020). IL NUOVO CIMENTO, 124 B, DOI 10.1393/ncb/i2010-10829-y

Baubron, J.C., Allard, P., Toutain, J.P., 1990. Diffuse volcanic emissions of carbon dioxide from Volcano Island, Italy. Nature 344, 51-53.

Becker, J. A., Bickle, M. J., Galy, A. & Holland, T. J. B. Himalayan metamorphic CO_2 fluxes: quantitative constraints from hydrothermal springs. Earth Planet. Sci. Lett. 265, 616–629 (2008).

Bergfeld, D., Evans, W.C., Spicer, K.R., Hunt, A.G., Kelly, P.J., 2017. Evidence for degassing of fresh magma during the 2004–2008 eruption of Mount St. Helens: Subtle signals from the hydrothermal system. J. Volcanol. Geotherm. Res. 343, 109–121.

Berner, R.A., Lasaga, A.C. & Garrels, R.M. 1983. The carbonate–silicate geochemical cycle and its effect on atmospheric carbon dioxide over the past 100 million years. American Journal of Science, 283, 641–683, https://doi.org/10.2475/ajs.2 83.7.641

Berner, R.A. 1993. Weathering and its effect on atmospheric CO_2 over Phanerozoic time. Chemical Geology, 107, 373–374, https://doi.org/10. 1016/0009-2541(93)90212-2

Berner, R. The long-term carbon cycle, fossil fuels and atmospheric composition. *Nature* **426,** 323–326 (2003). https://doi.org/10.1038/nature02131

Berner, R.A. 2004. The Phanerozoic Carbon Cycle: CO_2 and O_2. Oxford University Press, Oxford

Berner, R.A. 2006. GEOCARBSULF: A combined model for Phanerozoic atmospheric O_2 and CO_2. Geochimica et Cosmochimica Acta, 70, 5653–5664, https://doi.org/10.1016/j.gca.2005.11.032

Binda G, Pozzi A, Michetti AM, Noble PJ, Rosen MR. Towards the Understanding of Hydrogeochemical Seismic Responses in Karst Aquifers: A Retrospective Meta-Analysis Focused on the Apennines (Italy). *Minerals*. 2020; 10(12):1058. https://doi.org/10.3390/min10121058

Bragagni A., Mastroianni F., Münker C., Conticelli S., Avanzinelli R.; A carbon-rich lithospheric mantle as a source for the large CO_2 emissions of Etna volcano (Italy). *Geology* 2022; doi: https://doi.org/10.1130/G49510.1

Brantley, S. L. & Koepenick, K. W. Measured carbon dioxide emissions from Oldoinyo Lengai and the skewed distribution of passive volcanic fluxes. Geology 23, 933–936 (1995)

Brutto, F., Muto, F., Loreto, M.F., De Paola, N., Tripodi, V., Critelli, S., Facchin, L., 2016. The Neogene-Quaternary geodynamic evolution of the central Calabrian Arc: a case study from the western Catanzaro Trough basin. J. Geodyn. 102, 95–114.

Budyko MI, Ronov AB, and Yanshin AL (1987) History of the Earth's Atmosphere. Berlin: Springer.

Burton, M.R., Sawyer, G.M. & Granieri, D. 2013. Deep carbon emissions from volcanoes. In: Hazen, R.M., Jones, A.P. & Baross, J.A. (eds) Carbon in Earth. Mineralogical Society of America and Geochemical Society, Reviews in Mineralogy and Geochemistry, 75, 323–354, https://doi.org/10.2138/rmg. 2013.75.11

Cangemi M, Di Figlia MG, Favara R, Liotta M. CO_2 Degassing in Sicily (Central Mediterranean) as Inferred from Groundwater Composition. *Water*. 2020; 12(7):1959. https://doi.org/10.3390/w12071959

Cappa F., Rutqvist J., Yamamoto K., Modeling crustal deformation and rupture processes related to upwelling of deep CO2-rich fluids during the 1965–1967 Matsushiro earthquake swarm in Japan. J. Geophys. Res. 114, B10304 (2009).

Caracausi, A., Favara, R., Italiano, F., Nuccio, P. M., Paonita, A., & Rizzo, A. (2005). Active geodynamics of the central mediterranean sea: Tensional tectonic evidences in western Sicily

from mantle‐derived helium. Geophysical Research Letter, 32, L04312. https://doi.org/10.1029/2004GL021608

Caracausi, A., Martelli, M., Nuccio, P.M., Paternoster, M., Stuart, F.M., 2013 - Active degassing of mantle-derived fluid: a geochemical study along the Vulture line southern Apennines (Italy). J. Volcanol. Geotherm. Res. 253, 65–74.

Caracausi A., Paternoster M., Nuccio P. M. 2015 – Mantle CO_2 degassing at Mt. Vulture volcano (Italy): relationship between CO_2 outgassing of volcanoes and the time of their last eruption. Earth and Planetary Science Letters 411 (2015) 268–280. http://dx.doi.org/10.1016/j.epsl.2014.11.049.

Caracausi, A., & Sulli, A. (2019). Outgassing of mantle volatiles in compressional tectonic regime away from volcanism: The role of continental delamination. *Geochemistry, Geophysics, Geosystems*, *20*, 2007–2020. https://doi.org/10.1029/2018GC008046

Carapezza, M.L., Federico, C., 2000. The contribution of fluid geochemistry to the volcano monitoring of Stromboli. Journal of Volcanology and Geothermal Research 95, 227-245.

Carapezza M.L., Badalamenti B., Cavarra L., Scalzo A., Gas hazard assessment in a densely inhabited area of Colli Albani Volcano (Cava dei Selci, Roma), Journal of Volcanology and Geothermal Research, Volume 123, Issues 1–2, 2003, Pages 81-94, ISSN 0377-0273, https://doi.org/10.1016/S0377-0273(03)00029-5.

Cathles, L. M. & Schoell, M. Modeling CO_2 generation, migration and titration in sedimentary basins. Geofluids 7, 441–450 (2007).

Chen Z., Li Y., Martinelli G., Liu Z., Lu C., Zhao Y., Spatial and temporal variations of CO_2 emissions from the active fault zones in the capital area of China, Applied Geochemistry, Volume 112, 2020, 104489, ISSN 0883-2927, https://doi.org/10.1016/j.apgeochem.2019.104489.

Chiarabba C., Jovane L., DiStefano R., A new view of Italian seismicity using 20 years of instrumental recordings, Tectonophysics, Volume 395, Issues 3–4, 2005, Pages 251-268, ISSN 0040-1951, https://doi.org/10.1016/j.tecto.2004.09.013.

Chiarabba, C. et al. 2009. The 2009 L'Aquila (central Italy) MW 6.3 earthquake: Main shock and aftershocks. Geophysical Research Letters, 36, L18308, https://doi.org/10.1029/2009GL0396.

Chiaraluce, L., Di Stefano, R. et al. 2017. The 2016 Central Italy Seismic Sequence: A First Look at the Mainshocks, Aftershocks, and Source Models. Seismological Research Letters, 88, 757–771, https://doi.org/10.1785/0220160221.

Chiarella, D., Longhitano, S.G., Muto, F., 2012. Sedimentary features of the Lower Pleistocene mixed siliciclastic- bioclastic tidal deposits of the Catanzaro Strait (Calabrian Arc, south Italy). Rend. Online Soc. Geol. Ital. 21, 919–920.

Chiarella, D., Moretti, M., Longhitano, S.G., Muto, F., 2016. Deformed cross-stratified deposits in the Early Pleistocene tidally-dominated Catanzaro strait-fill succession, Calabrian Arc (Southern Italy): triggering mechanisms and environmental significance. Sediment. Geol. 344, 277–289.

Chiodini, G., Cioni, R., Guidi, M., Raco, B., Marini, L., 1998. Soil CO_2 flux measurements in volcanic and geothermal areas. Applied Geochemistry 13, 543-552.

Chiodini, G., Frondini, F., Kerrick, D.M., Rogie, J.D., Parello, F., Peruzzi, L., Zanzari, A.R., 1999. Quantification of deep CO_2 fluxes from central Italy. Examples of carbon balance for regional aquifers and of soil diffuse degassing. Chemical Geology 159, 205-222.

Chiodini, G., Frondini, F., Cardellini, C., Parello, F., Peruzzi, L. (2000), Rate of diffuse carbon dioxide Earth degassing estimated from carbon balance of regional aquifers: The case of central Apennine, Italy. JGR., 105, 8423-8434

Chiodini, G., Frondini, F., Cardellini, C., Granieri, D., Marini, L., Ventura, G., 2001. CO_2 degassing and energy release at Solfatara volcano, Campi Flegrei, Italy. Journal Geophysical Research 106, 16, 213-16, 10.1029/2001JB000246

Chiodini, G., Frondini, F., 2001. Carbon dioxide degassing from the Albani Hills volcanic region, central Italy. Chemical Geology 177, 67-83.

Chiodini, G., Cardellini, C., Amato, A., Boschi, E., Caliro, S., Frondini, F., Ventura, G., 2004. Carbon dioxide Earth degassing and seismogenesis in central and southern Italy. Geophys. Res. Lett., 31

Chiodini, G., Baldini, A., Barberi, F., Carapezza, M.L., Cardellini, C., Frondini, F., Granirei, D., Ranaldi, M., 2007. Carbon dioxide degassing at Latera caldera (Italy): evidence of geothermal reservoir and evaluation of its potential energy. J. Geophys. Res. 112, B12204. doi:10.1029/2006JB004896.

Chiodini G., Valenza M., Cardellini C. & Frigeri A. (2008) - A new web-based catalogue of Earth degassing sites in Italy. Eos, Vol. 89, N. 37, 341342.

Chiodini G., Granieri D., Avino R., Caliro S., Costa A., Minopoli C., and Vilardo G., (2010) Non-volcanic CO_2 Earth degassing: case of Mefite d'Ansanto (southern Apennines), Italy. - GEOPHYSICAL RESEARCH LETTERS, VOL. 37, L11303, doi:10.1029/2010GL042858,

Chiodini, G., Caliro, A., Cardellini, C., Frondini, F., Inguaggiato, S., Matteucci, F. (2011). Geochemical evidence for and characterization of CO_2 rich gas sources in the epicentral area of the Abruzzo 2009 earthquakes. EPSL, 304, 389-398.

Chiodini G., Cardellini C., Di Luccio F., Selva J., Frondini F., Caliro S., Rosiello A., Beddini G., Ventura G., Correlation between tectonic CO_2 Earth degassing and seismicity is revealed by a 10-year record in the Apennines, Italy. *Sci. Adv.* **6**, eabc2938 (2020).

Condie K. C., High field strength element ratios in Archean basalts: a window to evolving sources of mantle plumes?, Lithos, Volume 79, Issues 3–4, 2005, Pages 491-504, ISSN 0024-4937, https://doi.org/10.1016/j.lithos.2004.09.014.

Collettini, C. (2002), Hypothesis for the mechanics and seismic behaviour of low-angle normal faults: The example of the altotiberina fault northern Apennines., Ann. Geophys., 45, 683–698

Collettini, C., Cardellini, C., Chiodini, G., De Paola, N., Holdsworth, R.E., Smith, S.A.F., 2008. Fault weakening due to CO2 degassing in the Northern Apennines: short- and long-term processes. In: Wiberley, C.A.J., Kurz, W., Imber, J., Holddsworth, R.E., Collettini, C. (Eds.), The Internal Structure of Fault Zones: Implications for Mechanical and Fluid-Flow Properties. Geological Society, London, pp. 175–194

Domenico Cosentino, Paola Cipollari, Pietro Marsili, Davide Scrocca Journal of the Virtual Explorer, Electronic Edition, ISSN 1441-8142, volume 36, paper 12 In: (Eds.) Marco Beltrando, Angelo Peccerillo, Massimo Mattei, Sandro Conticelli, and Carlo Doglioni, The Geology of Italy: tectonics and life along plate margins, 2010.

Cox, S.F., 1995. Faulting processes at high fluid pressures: an example of fault valve behavior from the Wattle Gully Fault, Victoria, Australia. J. Geophys. Res. 100, 12841–12859.

Cuffaro M., Riguzzi F., Scrocca D., and Doglioni C., "Coexisting tectonic settings: the example of the southern Tyrrhenian Sea," International Journal of Earth Sciences, vol. 100, no. 8, pp. 1915–1924, 2011.

Davisson, M.L., Rose, T.P., 1997. Comparative isotope hydrology study of groundwater sources and transport in the three cascade volcanoes of northern California (no. UCRL-ID-128423). Lawrence Livermore National Lab.(LLNL), Livermore, CA (United States).

De Gregorio, S., Diliberto, I.S., Giammanco, S., Gurrieri, S., Valenza, M., 2002. Tectonic control over large-scale diffuse degassing in eastern Sicily (Italy). Geofluids 2, 273-284.

De Leeuw, G. A. M., Hilton, D. R., Fischer, T. P. & Walker, J. A. The He-CO_2 isotope and relative abundance characteristics of geothermal fluids in El Salvador and Honduras: New constraints on volatile mass balance of the Central American Volcanic Arc. *Earth Planet. Sci. Lett.* **258,** 132–146 (2007).

Di Luccio, F., Chiodini, G., Caliro, S., Cardellini, C., Convertito, V., Pino, N.A., Tolomei, C. & Ventura, G. 2018. Seismic signature of active intrusions in mountain chains. Science Advances, 4, e1701825, https://doi.org/10.1126/sciadv.1701825.

Edmonds M., Tutolo B., Iacovino K., Moussallam Y.; Magmatic carbon outgassing and uptake of CO_2 by alkaline waters. *American Mineralogist* 2020;; 105 (1): 28–34. doi: https://doi.org/10.2138/am-2020-6986CCBY

Etiope, G., 1999. Subsoil CO_2 and CH_4, and their advective transfer from faulted grassland to the atmosphere. Journal Geophysical Research.

Evans, M.J., Derry, L.A. & France-Lanord, C. 2008. Degassing of metamorphic carbon dioxide from the Nepal Himalaya. Geochemistry, Geophysics, Geosystems, 9, Q04021, https://doi.org/10.1029/2007GC001796

Favara, R., Giammanco S., Inguaggiato, S., Pecoraino, G., 2001. Preliminary estimate of CO_2 output from Pantelleria Island volcano (Sicily, Italy): evidence of active mantle degassing. Applied Geochemistry 16, 883-894.

Fischer, T. P. (2013). DEep CArbon DEgassing: The Deep Carbon Observatory DECADE initiative. Mineralogical Magazine, 77(5), 1089.

Fischer, T. P., & Aiuppa, A. (2020). AGU Centennial Grand Challenge: Volcanoes and deep carbon global CO_2 emissions from subaerial volcanism— Recent progress and future challenges. Geochemistry, Geophysics, Geosystems, 21, e2019GC008690. https://doi.org/ 10.1029/2019GC008690

Foley, S.F. 1992. Petrological characterization of the source components of potassic magmas: Geochemical and experimental constraints. Lithos, 28, 187–204

Foster, G., Royer, D. & Lunt, D. Future climate forcing potentially without precedent in the last 420 million years. *Nat Commun* **8,** 14845 (2017). https://doi.org/10.1038/ncomms14845

Frepoli, A., Amato, A., 2000. Spatial variation in stresses in Peninsular Italy and Sicily from background seismicity. Tectonophysics 317, 109–124.

Fresia, C. & Frezzotti, M.L. 2015. The dilemma of the dwarf Earth's CO_2 degassing: Irrelevant or crucial? Journal of Geochemical Exploration, 152, 118–122, https://doi.org/10.1016/j.gexplo.2015.02.006

Frezzotti, M.L., Peccerillo, A. & Panza, G. 2009. Carbonate metasomatism and CO_2 lithosphere–asthenosphere degassing beneath the Western Mediterranean: An integrated model arising from petrological and geophysical data. Chemical Geology, 262, 108–120.

Frezzotti M.L., Peccerillo A., Panza G.,2010. Earth's CO_2 degassing in Italy. In: (Eds.) Marco Beltrando, Angelo Peccerillo, Massimo Mattei, Sandro Conticelli, and Carlo Doglioni, *Journal of the Virtual Explorer*, volume **36**, paper 21, doi: 10.3809/jvirtex.2010.00227

Frondini, F., Chiodini, G., Caliro, S., Cardellini, C., Granieri, D. Ventura, G., 2004. Diffuse CO_2 degassing at Vesuvio, Italy. Bulletin of Volcanology 66, 642-651.

Frondini F., Cardellini C., Caliro S., Beddini G., Rosiello A., & Chiodini G., 2019 – Measuring and interpretino CO_2 fluxes at regional scale: the case of the Apennines, Italy. Journal of Geological Society – vol. 176; 408-416.

Gaeta, M., Di Rocco, T., Freda, C., 2009. Carbonate assimilation in open magmatic systems: the role of meltbearing skarns and cumulate-forming processes. Journal of Petrology 50, 361-385.

Gambardella, B., Marini, L., Ottonello, G., Vetuschi, M., Zuccolini, R., Cardellini, C., Chiodini, G., Frondini, F., 2004. Fluxes of deep CO_2 in the volcanic areas of centralsouthern Italy. Journal of Volcanology and Geothermal Research 136, 31-52.

Giannelli G. 1985 - On the origin of geothermal CO_2 by metamorphic processes. Boll. Soc. Geol. Ital. 104, 575-584.

Gerlach, T. M. Present-day carbon dioxide emissions from volcanos. Earth in Space 4, 5 (1991)

Gerlach, T.M., 1991b. Etna's greenhouse pump. Nature 31, 352-353.

Ghisetti, F., and L. Vezzani (2002), Normal faulting, transcrustal permeability and seismogenesis in the Apennines (Italy), Tectonophysics, 348, 155– 168.

Giggenbach, W. F. (1996). Chemical composition of volcanic gases. In R. Scarpa & R. Tilling (Eds.), *IAVCEI-UNESCO: Monitoring and mitigation of volcano hazards* (pp. 221–256). Berlin: Springer.

Girault, F., Koirala, B.P., Bhattarai, M. & Perrier, F. 2016. Radon and carbon dioxide around remote Himalayan thermal springs. In: Gillmore, G.K., Perrier, F.E. & Crockett, R.G.M. (eds) Radon, Health and Natural Hazards. Geological Society, London, Special Publications, 451, 155–181, https:// doi.org/10.1144/SP451.6

Griesshaber, E., O'Nions, R. K. & Oxburgh, E. R. Helium and carbon isotope systematics in crustal fluids from the Eifel, the Rhine Graben and Black Forest, F. R. G. *Chem. Geol.* **99,** 213–235 (1992).

Groppo C., Rolfo F., Mosca P. & Castelli D. (2017) - *Metamorphic CO_2 production in collisional orogens: petrologic constraints from phase diagram modeling of Himalayan, scapolite-bearing, calc-silicate rocks in the NKC(F)MAS(T)-HC system.* Journal of Petrology. doi: 10.1093/petrology/egx005

Groppo C., Rapa G., Frezzotti M. L. and Rolfo F. (2020) The fate of calcareous pelites in collisional orogens. J. Metamorph. Geol.. https://doi.org/10.1111/jmg.12568.

Groppo, C., Rolfo, F. & Frezzotti, M.L. CO_2 outgassing during collisional orogeny is facilitated by the generation of immiscible fluids. *Commun Earth Environ* **3,** 13 (2022). https://doi.org/10.1038/s43247-022-00340-w

Guzović, Z., Majcen, B., & Cvetković, S. (2012). Possibilities of electricity generation in the Republic of Croatia from medium-temperature geothermal sources. *Applied Energy, 98*, 404-414.

Hauri, E.H., Maclennan, J., McKenzie, D., Gronvold, K., Oskarsson, N., and Shimizu, N. (2018) CO_2 content beneath northern Iceland and the variability of mantle carbon. Geology, 46(1), 55–58.

Hauri, E.H., Cottrell, E., Kelley, K.A., Tucker, J.M., Shimizu, K., Le Voyer, M., Marske, J., and Saal, A.E. (2019) Carbon in the Convecting Mantle. Earth's Deep Carbon: past to present. Cambridge.

Hirschmann, M.M., and Dasgupta, R. (2009) The H/C ratios of Earth's near-surface and deep reservoirs, and consequences for deep Earth volatile cycles. Chemical Geology, 262(1-2), 4–16.

Holland G., Gilfillan S. (2013) Application of Noble Gases to the Viability of CO_2 Storage. In: Burnard P. (eds) The Noble Gases as Geochemical Tracers. Advances in Isotope Geochemistry. Springer, Berlin, Heidelberg. https://doi.org/10.1007/978-3-642-28836-4_8

Hunt, J. A., Zafu, A., Mather, T. A., Pyle, D. M., & Barry, P. H. (2017). Spatially variable CO_2 degassing in the Main Ethiopian Rift: Implications for magma storage, volatile transport, and rift-related emissions. Geochemistry, Geophysics, Geosystems., 18, 3714– 3737, https://doi.org/10.1002/2017GC006975.

Iacono Marziano, G., Gaillard, F., Scaillet, B., Pichavant, M., Chiodini, G., 2009. Role of non-mantle CO_2 in the dynamics of volcano degassing: The Mount Vesuvius example. Geology 37, 319-322.

Improta, L., De Gori, P., and Chiarabba, C. (2014), New insights into crustal structure, Cenozoic magmatism, CO_2 degassing, and seismogenesis in the southern Apennines and Irpinia region from local earthquake tomography, *J. Geophys. Res. Solid Earth*, 119, 8283– 8311, doi:10.1002/2013JB010890.

Irwin, W.P. & Barnes, I. 1980. Tectonic relations of carbon dioxide discharges and earthquakes. Journal of Geophysical Research, 85, 2156–2202, https:// doi.org/10.1029/JB085iB06p03115.

Italiano, F., Nuccio, M., Pecoraino, G., 1998. Steam output from fumaroles of an active volcano: tectonic and magmatic hydrothermal controls on the degassing system at Vulcano (Aeolian arc). Journal Geophysical Research 103, 29829-29841.

Italiano, F., Martelli, M., Martinelli, G., Nuccio, P.M., 2000. Geochemical evidence of melt intrusions along lithospheric faults of the Southern Apennines, Italy: geodynamic and seismogenic implications. Journal of Geophysical Research 105 (B6), 13569-13578.

Italiano, F., Martinelli, G., Plescia, P., 2008. CO_2 degassing over seismic areas: the role of mechanochemical production at the study case of Central Apennines. Pageoph 165 (1), 75–94. doi:10.1007/s00024-007-0291-7.

Italiano F., Bonfanti P., Ditta M., Petrini R., Slejko F.; Helium and carbon isotopes in the dissolved gases of Friuli Region (NE Italy): Geochemical evidence of CO_2 production and degassing over a seismically active area, Chemical Geology, Volume 266, Issues 1–2, 2009, Pages 76-85, ISSN 0009-2541, https://doi.org/10.1016/j.chemgeo.2009.05.022.

Italiano, F., Bonfanti, P., Pizzino, L., Quattrocchi, F., 2010. Geochemistry of fluids discharged over the seismic area of the Southern Apennines (Calabria region, Southern Italy): implications for fluid-fault relationships. Appl. Geochem. 25, 540–554.

Italiano F., Bonfanti P. ,and Maugeri S.R.(2019)- Evidence of Tectonic Control on the Geochemical Features of the Volatiles Vented along the Nebrodi-Peloritani Mts (Southern Apennine Chain, Italy). Hindawi, Geofluids, Volume 2019, Article ID 6250393, 17 pages https://doi.org/10.1155/2019/6250393

Jolivet L., Baudin T., Calassou S., Chevrot S., Ford M., Issautier B., Lasseur E., Masini E., Manatschal G., Mouthereau F., Thinon I., Vidal O.; Geodynamic evolution of a wide plate boundary in the Western Mediterranean, near-field *versus* far-field interactions. *Bulletin de la Société Géologique de France* 2021;; 192 (1): 48. doi: https://doi.org/10.1051/bsgf/2021043

Lee, H., Muirhead, J.D., Fischer, T.P., Ebinger, C.J., Kattenhorn, S.A., Sharp, Z.D., and Kianji, G. (2016) Massive and prolonged deep carbon emissions associated with continental rifting. Nature Geoscience, 9(2), 145.

Li Vigni, L., Cardellini, C., Temovski, M., Ionescu, A., Molnár, K., Palcsu, L., et al. (2022). Duvalo "Volcano" (North Macedonia): A Purely Tectonic-related CO_2 Degassing

System. *Geochemistry, Geophysics, Geosystems*, 23, e2021GC010198. https://doi.org/10.1029/2021GC010198

Loreto, MF, Zitellini, N, Ranero, CR, Palmiotto, C, Prada, M. Extensional tectonics during the Tyrrhenian back-arc basin formation and a new morpho-tectonic map. *Basin Res*. 2021; 33: 138– 158. https://doi.org/10.1111/bre.12458

Kaiho K., Tanaka D., Richoz S., Jones D. S., Saito R., Kameyama D., Ikeda M., Takahashi S., Aftabuzzaman Md., Fujibayashi M.- Volcanic temperature changes modulated volatile release and climate fluctuations at the end-Triassic mass extinction, Earth and Planetary Science Letters, Volume 579, 2022, 117364, ISSN 0012-821X, https://doi.org/10.1016/j.epsl.2021.117364.

Kashiwagi H and Shikazono N (2003) Climate change during Cenozoic inferred from global carbon cycle model including igneous and hydrothermal activities. Palaeogeography, Palaeoclimatology, Palaeoecology 199: 167–185.

Kennedy, B. M., Y. K. Kharaka, W. C. Evans, A. Ellwood, D. J. De Paolo, J. Thordsen, G. Ambats, and R. H. Mariner (1997), Mantle fluids in the San Andreas fault system, California, Science, 278, 1278– 1281

Kerrick, D.M. & Caldeira, K. 1993. Paleoatmospheric consequences of CO_2 released during early Cenozoic regional metamorphism in the Tethyan orogen. Chemical Geology, 108, 201–230, https://doi.org/10.1016/0009-2541(93) 90325-D

Kerrick, D.M., and Caldeira, K. (1998) Metamorphic CO_2 degassing from orogenic belts. Chemical Geology, 145(3-4), 213–232

Kimani C.N., Kasanzu C.H., Tyne R.L., Mtili K.M., Byrne D.J., Kazimoto E.O., Hillegonds D.J., Ballentine C.J., Barry P.H., He, Ne, Ar and CO_2 systematics of the Rungwe Volcanic Province, Tanzania: Implications for fluid source and dynamics, Chemical Geology, Volume 586, 2021, 120584, ISSN 0009-2541, https://doi.org/10.1016/j.chemgeo.2021.120584

Kissin, I.G., Pakhomov, S.I., 1969. Geochemistry of Carbon Dioxide in Deep Zones of the Underground Hydrosphere. Geokhimiya, 1969, no. 4, pp. 460–471.

Lee H., Muirhead J. D., Fischer T. P., Ebinger C. J., Kattenhorn S. A., Sharp Z. S. & Kianji G. (2016) – Massive and prolonged deep carbon emissions associated with continental rifting. Nature Geosciences 3, 145-149 (2016).

Longhitano, S.G., Chiarella, D., Muto, F., 2014. Three-dimensional to two-dimensional cross-strata transition in the lower Pleistocene Catanzaro tidal strait trasgressive succession (southern Italy). Sedimentology 61, 2136–2171.

Longman, J., Mills, B. J. W., Donnadieu, Y., & Goddéris, Y. (2022). Assessing volcanic controls on Miocene climate change. Geophysical Research Letters, 49, e2021GL096519. https://doi.org/10.1029/2021GL096519

Lucente, F.P., Chiarabba, C., Cimini, D., Giardini, G.B., 1999. Tomographic constraints on the geodynamic evolution of the Italian region. Journal of Geophysical Research 104, 20307–20327.

Lucente F.P., De Gori P., Margheriti L., Piccinini D., Di Bona M., Chiarabba C., Agostinetti N.P., 2010. Temporal variation of seismic velocity and anisotropy before the 2009 M-W 6.3 L'Aquila earthquake, Italy. Geology 38, 1015–1018.

Marini L. & Chiodini G. (1994) The role of carbon dioxide in the carbonate-evaporite geothermal system of Tuscany and Latium (Italy). Acta Vulcanologica, 5, 95-104.

Mariucci, M.T., Amato, A. & Montone, P., 1999. Recent tectonic evolution and present stress in the northern Apennines, Tectonics, 18, 108–118.

Marty, B., O'Nions, R.K., Oxburgh, E.R., Martel, D., Lombardi, S., 1992. Helium isotopes in alpine regions. Tectonophysics 206, 71-78.

Marty, B. & Tolstikhin, I.N. 1998. CO_2 fluxes from mid-ocean ridges, arcs and plumes. Chemical Geology, 145, 233–248, https://doi.org/10.1016/S0009- 2541(97)00145-9

Mattei M., Conticelli S., Giordano G., 2010. "The Tyrrhenian margin geological setting: from the Apennine orogeny to the K-rich volcanism", The Colli Albani Volcano, R. Funiciello, G. Giordano

McKenzie N R, Horton B K, Loomis S E, Stockli D F, Planavsky N J, Lee C T A. 2016. Continental arc volcanism as the principal driver of icehouse-greenhouse variability. Science, 352: 444−447

Miller, S.A., Collettini, C., Chiaraluce, L., Cocco, M., Barchi, M., Kaus, B.J.P., 2004. Aftershocks driven by a high-pressure CO2 source at depth. Nature 427, 724–727.

Minissale, A., Magro, G., Tassi, F., Frau, F., Vaselli, O., 1999. The origin of natural gas emissions from Sardinia island, Italy. Geochemical Journal 33, 1-12.

Minissale, A., 2004. Origin, transport and discharge of CO_2 in central Italy. Earth Science Review 66, 89-141

Minissale A., Donato A., Procesi M., Giammanco S., Pizzino L., (2016) – Dati e Carte geochimiche del Mezzogiorno d'Italia. Progetto Atlante Geotermico del Mezzogiorno, CNR per il Mezzogiorno, CNR-IGG.

Minissale A., Donato A., Procesi M., Pizzino L., Giammanco S. - (2019) - Systematic review of geochemical data from thermal springs, gas vents and fumaroles of Southern Italy for geothermal favourability mapping. Earth-Science Reviews 188 (2019) 514–535.

Moeller, S., Grevemeyer, I., Ranero, C. R., Berndt, C., Klaeschen, D., Sallares, V., Zitellini, N., and de Franco, R. (2014), Crustal thinning in the northern Tyrrhenian Rift: Insights from multichannel and wide-angle seismic data across the basin, *J. Geophys. Res. Solid Earth*, 119, 1655– 1677, doi:10.1002/2013JB010431.

Montone, P.& Mariucci, M.T., 1999. Active stress in the NE external margin of the Apennines: the Ferrara arc, northern Italy, J. Geodyn., 28(2–3), 251–265.

Mörner, N.A. & Etiope, G. 2002. Carbon degassing from the lithosphere. Global and Planetary Change, 33, 185–203, https://doi.org/10.1016/S0921-8181(02) 00070-X

Neri G., Barberi G., Oliva G., and Orecchio B., "Tectonic stress and seismogenic faulting in the area of the 1908 Messina earthquake, South Italy," Geophysical Research Letters, vol. 31, no. 10, 2004.

Neri G., Orecchio B., Scolaro S. and Totaro C. (2020) Major Earthquakes of Southern Calabria, Italy, Into the Regional Geodynamic Context. Front. Earth Sci. 8:579846. doi: 10.3389/feart.2020.579846

Newell, D. L., M. J. Jessup, J. M. Cottle, D. R. Hilton, Z. D. Sharp, and T. P. Fischer (2008), Aqueous and isotope geochemistry of mineral springs along the southern margin of the Tibetan plateau: Implications for fluid sources and regional degassing of CO_2, Geochem. Geophys. Geosyst., 9, Q08014, doi:10.1029/2008GC002021.

Nuhovic, S ., Djokic, I . (2013): Geothermal energy use, country update for Serbia - Abstracts, European Geothermal Congress 2013, Pisa, Italy, 3-7 June 2013

Ohmoto, H., and R. A. Rye (1979), Isotopes of sulfur and carbon, in Geochemistry of hydrothermal ore deposits 2d Ed., edited by H. L. Barnes, pp. 517-612, John Wiley, New York.

Oxburgh, E.R., O'Nions, R.K., Hill, R.I., 1986. Helium isotopes in sedimentary basins. Nature 324, 632-635.

Piana Agostinetti N., Lucente F.P., Selvaggi G., Di Bona M., 2002: Crustal structure and Moho geometry beneath the Northern Apennines (Italy). Geophys. Res. Lett. 29, 60-63.

Plank T, Manning C E. 2019. Subducting carbon. Nature, 574: 343−352

Pondrelli, S., Morelli, A., Ekstrfm, G., Mazza, S., Boschi, E., Dziewonski, A.M., 2002. European–Mediterranean regional centroid-moment tensors: 1997–2000. Phys. Earth Planet. Inter. 130, 71–101.

Pondrelli S., Salimbeni S., Ekstrom G., Morelli A., Gasperini P., and Vannucci G., "The Italian CMT dataset from 1977 to the present," Physics of the Earth and Planetary Interiors, vol. 159, no. 3-4, pp. 286–303, 2006.

Retallack G. J.- Soil Carbon Dioxide Planetary Thermostat Astrobiology 2022 22:1, 116-123

Rice, J.R., 1992. Fault stress states, pore pressure redistributions, and the weakness of the San Andreas fault. In: Evans, B., Wong, T.F. (Eds.), Fault Mechanics and Transport Properties of Rock. Academic Press Ltd., San Diego, pp. 476–503

Rogie, J.D., Kerrick, D.M., Chiodini, G., Frondini, F., 2000. Flux measurements of non-volcanic CO_2 emission from some vents in central Italy. Journal of Geophysical Research 105 (B4), 8435-8446.

Royer, D., Berner, R. & Park, J. Climate sensitivity constrained by CO_2 concentrations over the past 420 million years. *Nature* **446,** 530–532 (2007). https://doi.org/10.1038/nature05699

Royer D.L., 6.11 - Atmospheric CO_2 and O_2 During the Phanerozoic: Tools, Patterns, and Impacts, Editor(s): Heinrich D. Holland, Karl K. Turekian, Treatise on Geochemistry (Second Edition), Elsevier, 2014, Pages 251-267, ISBN 9780080983004, https://doi.org/10.1016/B978-0-08-095975-7.01311-5.

Rosenbaum, G., Gasparon, M., Lucente, F.P., Peccerillo, A., Miller, M.S., 2008. Kinematics of slab tear faults during subduction segmentation and implications for Italian magmatism. Tectonics 27 http://dx.doi.org/10.1029/2007TC002143.

Rufino, F., Cuoco, E., Busico, G. *et al.* Deep carbon degassing in the Matese massif chain (Southern Italy) inferred by geochemical and isotopic data. *Environ Sci Pollut Res* **28,** 46614–46626 (2021). https://doi.org/10.1007/s11356-020-11107-1

Saar, M.O., Castro, M.C., Hall, C.M., Manga, M., Rose, T.P., 2005. Quantifying magmatic, crustal, and atmospheric helium contributions to volcanic aquifers using all stable noble gases: Implications for magmatism and groundwater flow. Geochem. Geophys. Geosyst. 6 (3).

Sano Y., Fischer T.P. (2013) The Analysis and Interpretation of Noble Gases in Modern Hydrothermal Systems. In: Burnard P. (eds) The Noble Gases as Geochemical Tracers. Advances in Isotope Geochemistry. Springer, Berlin, Heidelberg. https://doi.org/10.1007/978-3-642-28836-4_10

Shinohara, H. Composition of volcanic gases emitted during repeating Vulcanian eruption stage of Shinmoedake, Kirishima volcano, Japan. Earth Planets and Space 65, 667–675 (2013)

Sibson R. H., 1992. Implications of fault-valve behaviour for rupture nucleation and recurrence. Tectonophysics, 211, 283–293.

Sibson, R.H., 2000. Fluid involvement in normal faulting. J. Geodyn. 29, 449–469

Sibson R. H., An episode of fault-valve behaviour during compressional inversion? — The 2004 MJ6.8 Mid-Niigata Prefecture, Japan, earthquake sequence, Earth and Planetary Science Letters, Volume 257, Issues 1 2, 2007, Pages 188-199, ISSN 0012-821X, https://doi.org/10.1016/j.epsl.2007.02.031

Siebert, L., & Simkin, T. (2002). Volcanoes of the world: An illustrated catalogue of Holocene volcanoes and their eruptions. Smithsonian Institution, Global Volcanism Program Digital Information Series, GVP-3. Tucson, AZ: Geoscience Press. http://www.volcano.si.edu/world/

Tajika E (1998) Climate change during the last 150 million years: Reconstruction from a carbon cycle model. Earth and Planetary Science Letters 160: 695–707.

Tamburello G., Pondrelli S., Chiodini G. & Rouwet D. (2019) – Global-sclae control of extensional tectonics on CO_2 earth degassing. NATURE COMMUNICATIONS | (2018) 9:4608 | DOI: 10.1038/s41467-018-07087-z

Tavani, S., Cardello, G. L., Vignaroli, G., Balsamo, F., Parente, M., Sabbatino, M., et al. (2021). Segmentation of the Apenninic margin of the Tyrrhenian back-arc basin forced by the subduction of an inherited transform system. *Tectonics*, 40, e2021TC006770. https://doi.org/10.1029/2021TC006770

Terakawa, T., Zoporowski, A., Galvan, B., Miller, S.A., 2010. High-pressure fluid at hypocentral depths in the L'Aquila region inferred from earthquake focal mechanisms. Geology. doi:10.1130/G31457.1

Tortorici L. (1982a) -Analisi delle deformazioni fragili dei sedimenti postorogeni della calabria Settentrionale.Boll. Soc. Geol.It., 100(3), 291-380.

Tortorici L. (1982b) - Lineamenti geologico strutturalidell'Arco Calabro-Peloritano. Rend. Soc. It. Mineral. e Petrol., 38(3), 927-940.

Umeda K., Asamori K., Negi T., Kusano T., A large intraplate earthquake triggered by latent magmatism. *J. Geophys. Res.* **116**, B01207 (2011).

van Hinsbergen DJJ, Vissers RLM, Spakman W. 2014. Origin and consequences of western Mediterranean subduction, rollback, and slab segmentation. *Tectonics* 33: 393–419. https://doi.org/10.1002/tect.20125.

Waldhauser F., Schaff D. P., Diehl T., Engdahl E. R., Splay faults imaged by fluid-driven aftershocks of the 2004 M-w 9.2 Sumatra-Andaman earthquake. *Geology* **40**, 243–246 (2012).

Walker, J.C.G., Hays, P.B. & Kasting, J.F. 1981. A negative feedback mechanism for the long-term stabilization of Earth's surface temperature. Journal of Geophysical Research, 86, 9776–9782, https://doi.org/10.1029/ JC086iC10p09776.

Wallmann K (2001) Controls on the Cretaceous and Cenozoic evolution of seawater composition, atmospheric CO2 and climate. Geochimica et Cosmochimica Acta 65: 3005–3025.

Wallmann K (2004) Impact of atmospheric CO_2 and galactic cosmic radiation on Phanerozoic climate change and the marine $\delta^{18}O$ record. Geochemistry, Geophysics, Geosystems 5: Q06004. http://dx.doi.org/10.1029/2003GC000683.

Werner, C., Fischer, T., Aiuppa, A., Edmonds, M., Cardellini, C., Carn, S., . . . Allard, P. (2019). Carbon Dioxide Emissions from Subaerial Volcanic Regions: Two Decades in Review. In B. Orcutt, I. Daniel, & R. Dasgupta (Eds.), *Deep Carbon: Past to Present* (pp. 188-236). Cambridge: Cambridge University Press.

Westaway, R., 1992. Seismic moment summation for historical earthquakes in Italy: tectonic implications. J. Geophys. Res. 97, 15437–15464.

Wong K., Mason E., Brune S., East M., Edmonds M., Zahirovic S.- Deep Carbon Cycling Over the Past 200 Million Years: A Review of Fluxes in Different Tectonic Settings. Frontiers in Earth Science, Vol.7, 2019, https://doi.org/10.3389/feart.2019.00263, ISSN2296-6463

Xu, S., Guan, L., Zhang, M. *et al.* Degassing of deep-sourced CO_2 from Xianshuihe-Anninghe fault zones in the eastern Tibetan Plateau. *Sci. China Earth Sci.* **65,** 139–155 (2022). https://doi.org/10.1007/s11430-021-9810-x

Zitellini N., Ranero C. R., Loreto M. F., Ligi M., Pastore M., D'Oriano F., Sallares V., Grevemeyer I., Moeller S., Prada M.; Recent inversion of the Tyrrhenian Basin. *Geology* 2019;; 48 (2): 123–127. doi: https://doi.org/10.1130/G46774.1

Zhang, M., Guo, Z., Xu, S. *et al.* Linking deeply-sourced volatile emissions to plateau growth dynamics in southeastern Tibetan Plateau. *Nat Commun* **12,** 4157 (2021). https://doi.org/10.1038/s41467-021-24415-y

Zhou Z., Ballentine C. J., Schoell M., Stevens S. H.- Identifying and quantifying natural CO_2 sequestration processes over geological timescales: The Jackson Dome CO_2 Deposit, USA, Geochimica et Cosmochimica Acta, Volume 86, 2012, Pages 257-275, ISSN 0016-7037, https://doi.org/10.1016/j.gca.2012.02.028.

CHAPTER II

Active degassing of crustal CO_2 in tectonic collision areas: a case study from the Pollino and Calabria sectors (Southern Italy)

II.1. Introduction

The current rise in atmospheric CO_2, and its link with the global climate change, provides a strong motivation to understand the natural processes that control the nature and magnitude of geological CO_2 cycling (Evans et al., 2011). The release of carbon dioxide into the atmosphere via Earth degassing has played a crucial role in controlling global planetary temperature over geological time via the greenhouse effect (Foster et al., 2017). The modes and rates of geological CO_2 release are thus crucial to understanding the compositional evolution of the atmosphere through geological time, life on Earth and climate changes (Guo et al., 2021; Fischer and Aiuppa, 2020; Aiuppa et al., 2019; Dasgupta, 2013; Kerrick, 2001; Berner & Lasaga, 1983). Despite continuous improvements via direct measurements, models and global extrapolations, the CO_2 Earth degassing output remains poorly constrained, hampering full understanding of the geological carbon cycle (Fischer and Aiuppa, 2020; Fischer et al., 2019, 2013; Burton et al., 2013; Berner and Lagasa, 1989). The release of CO_2 from Earth's interior to the atmosphere occurs in different tectonic settings (Lee et al., 2019), from volcanic and non-volcanic sources, and on a global scale it is known that CO_2 discharges are associated to tectonically/seismically active zones (Tamburello et al., 2018; Chiodini et al., 2004; Barnes et al., 1978). Quantitative estimates of CO_2 outgassing fluxes in different tectonic settings are thus critical for decoding the link between the global carbon budget and climate evolution from a whole-Earth carbon cycling perspective (Zhang et al., 2021). In the last decades, the number of studies on CO_2 degassing in non-volcanic areas has risen exponentially, emphasizing the important contribution of these areas to the earth carbon budget (e.g., Chiodini et al., 2020, 2004, Caracausi and Sulli, 2019; Rolfo et al., 2017; Becker et al., 2008; Groppo et al. 2022, 2017, 2013; Tamburello et al., 2018; Lee et al., 2016; Minissale, 2004; Italiano et al., 2008). The first regional-scale CO_2 Earth degassing studies led to the catalogue of Italian CO_2-rich gas emissions (googas.ov.ingv.it and www.magadb.net), and to the regional map of deeply derived CO_2 degassing in Central Italy that uses the quantification of carbon dissolved in regional

groundwater systems (e.g., Chiodini et al,. 2000; 2004; 2011). Some studies (Chiodini et al., 2004, 2020; Miller et al., 2004) also demonstrated a relation between CO_2 degassing and seismogenesis in the Italian Apennines. They proposed that CO_2 degassing drastically decreases in correspondence of the main seismogenetic sectors, pointing to gas accumulation in crustal traps and the role of over-pressurized CO_2 reservoirs along the faults in triggering earthquakes. The Mt. Pollino region, at the southern end of the Apennines (southern Italy), has been historically recognized as one of the most hazardous seismic gaps in the intra-Appenine seismogenic belt (Napolitano et al., 2021) but it has recently been affected by seismic sequence occurred between 2010 and 2014 and characterized by about 10,000 earthquakes with highly variable rate (strongest events ML 4.3 and ML 5.0; De Matteis et al., 2021; Pastori et al., 2021) . Moreover recent studies identified fluid related dynamics responsible for historical and recent seismicity of the area (Sketsiou et al., 2021).The Calabrian arc further to the south, is one of the most active seismogenetic areas in Italy (Neri et al., 2021; Italiano et al., 2010) which has been repeatedly affected by catastrophic seismic events with $5.9 < M < 7.2$ during the last centuries (18 times from 1626 to 1908; Gruppo di Lavoro CPTI, 2004; Boschi et al., 2000). The two areas are characterized by the presence of several springs, some representing low-enthalpy geothermal resources (e.g., Zarlenga, 2011; Apollaro et al. 2015, 2016, 2020). The geochemical and isotopic composition of Calabrian and Pollino waters have previously been investigated to define their geochemical features and geothermal potential (e.g., Bencini and Ciracò, 1982; Duchi et al. 1991), to investigate a link with seismicity and implications for fluid-fault relationship (Gurrieri et al. 1984; Calcara and Quattrocchi, 1993; Italiano et al. 2010; Apollaro et al., 2020), and to evaluate potential natural metal contamination of spring waters (Paternoster et al., 2021; Margiotta et al., 2012, 2014). However, no attempt has been made so far to model water-gas interaction processes, and to quantify the regional scale budget of CO_2 sequestrated/transported by aquifers at depths, and released to the atmosphere upon spring discharge.

In this chapter, we present the results of a geochemical study of cold and thermal springs from both the Calabrian arc and the Pollino region. Our goals are to 1) investigate the relationships

between Earth degassing and geological features in the two areas; 2) assess the presence and eventual origin of deep volatiles released in the hydrothermal basins and the surrounding areas; 3) model the processes at depth that can modify the pristine chemistry of deeply rising volatiles, potentially affecting the deep carbon budget; 4) estimate the total deeply derived CO_2 output. To this aim, we combine helium isotopes ($^3He/^4He$), Dissolved Inorganic Carbon (DIC) and carbon isotopes ($\delta^{13}C_{DIC}$) in groundwaters to explore the origin of carbon, and to develop a model of water-gas-rock interaction. The results are then compared with the CO_2 output from some active tectonic regions and volcanic areas worldwide.

II.2. Geological and hydrogeochemical background

The Calabrian-Peloritan orogen (CPO) is a well-developed, arc-shaped segment of the circum-Mediterranean orogenic belt between the southern Apennines and the Sicilian Maghrebides, bounded by two main tectonic lineaments: the Sangineto line to the North and the Taormina line to the South (Tortorici, 1982a,b; Fig. II.1). Incorporation of the Calabria terranes into the Apennine–Maghrebian chain is related to the processes responsible for the formation of the Tyrrhenian Basin since the late Miocene (Alterberger et al., 2011 and reference therein). In this context, the Calabrian arc represents an accretionary wedge, caused by the collision of Eurasian and African plates (Amodio Morelli et al., 1976; Tortorici, 1981), consisting of a series of ophiolite bearing tectonic units (Liguride Complex; Ogniben, 1969) and overlying basement nappes (Calabride Complex; Ogniben, 1969), with Paleozoic metamorphic and plutonic terranes that represent the remnants of Caledonian, Hercynian and Alpine orogens (e.g., Amodio Morelli et al., 1976; Schenk, 1981; Zanettin Lorenzoni, 1982; Atzori et al., 1984; Del Moro et al., 1986; Zeck, 1990; Messina et al., 1994).

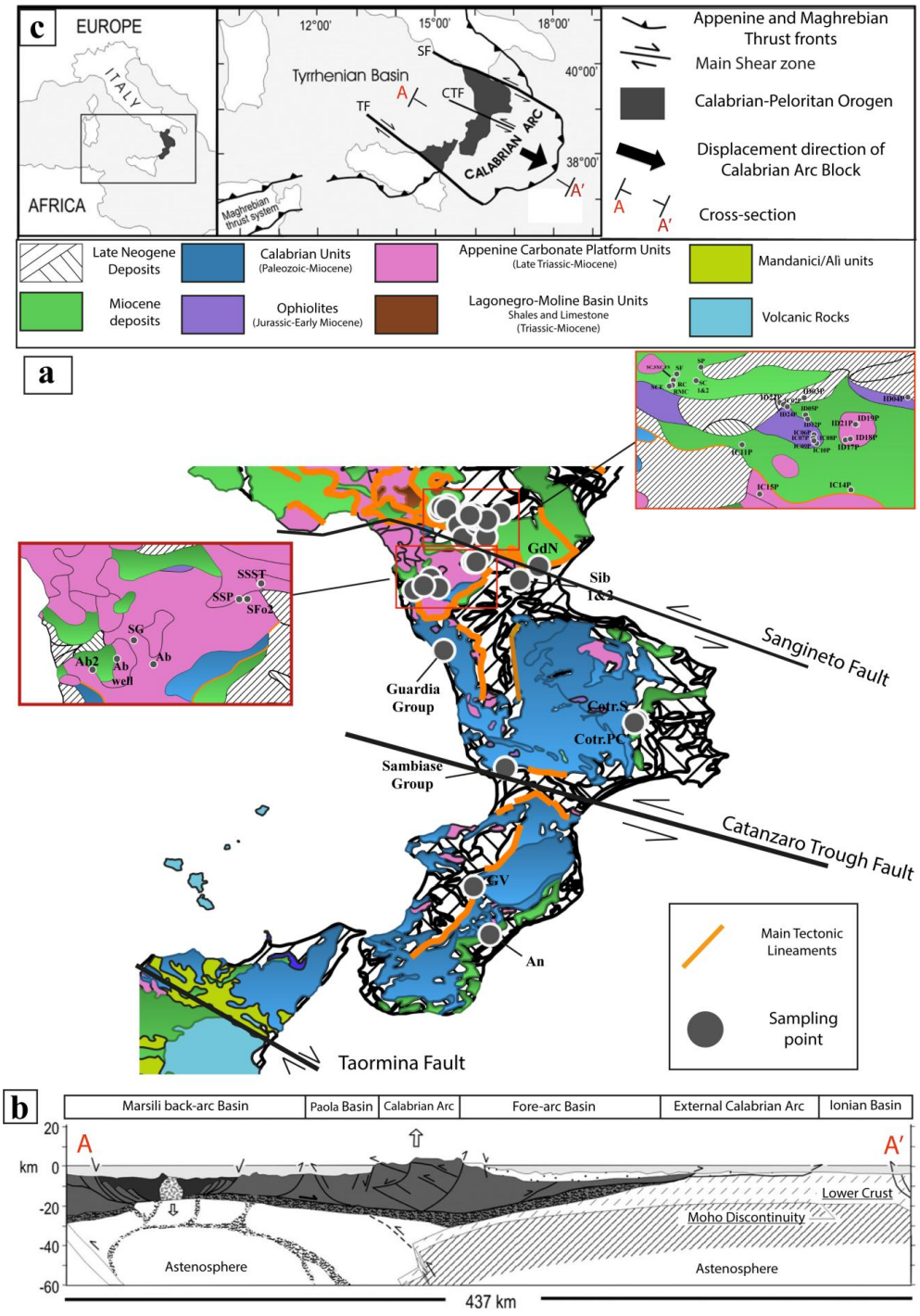

Figure II.1| Calabria Geology and sampling location. **a**) Simplified geological map of Calabrian arc and surrounding region (modified after Amodio-Morelli et al., 1976 and Bonardi et al., 1988b) with **b**) geological section on bottom (after Van Dijk and Scheepers, 1995, and Van Dijk et al., 2000, modified) and on top **c**) the location of the study area and tectonic simplified sketch of the Calabrian Arc (after Tansi et al., 2007, modified). TF=Taormina Fault; CTF=Catanzaro Trough Fault; SF=Sangineto Fault. For a detailed overview of the individual springs see Paternoster et al., 2021; Apollaro et al., 2020; Apollaro et al., 2019;Apollaro et al., 2012; Vespasiano et al., 2021.

The CPO is classically subdivided into a northern and southern sector, separated in correspondence to the Catanzaro Strait Basin, a Neogene-Quaternary basin connecting the Ionian and Tyrrhenian seas (Chiarella et al., 2012, 2016; Longhitano et al., 2014; Brutto et al., 2016; Tortorici, 1982). The two sectors differ for structural style and assemblage of the chain. The northern block exhibits overthrust of alpine and pre-alpine crystalline units on carbonatic tectono-stratigraphic units. In the southern block, the chain is made up of alpine and pre-alpine crystalline units, while the Apennine carbonate rocks are not present beneath the crystalline-metamorphic units (Apolllaro et al., 2019 and reference therein). In particular, the Calabria arc terrane consists of three main groups of stacked tectonic units (Tursi et al., 2021) that can be summarized, from bottom to top, as: (i) the Lower Complex, characterized by Apennine units with Meso-Cenozoic phyllites and partly metamorphosed carbonate rocks exhibiting high pressure (~1.4 GPa) and low temperature (~390°C) metamorphic imprint (Iannace et al., 2007); (b) the Intermediate Complex, composed of ophiolite units of the Ligurian Tethys' oceanic lithosphere (Liberi et al., 2006), that records *HP/LT* Eocene metamorphism with peak conditions at ~2.0–2.1 GPa and 470–490° C (Tursi et al., 2020); (c) the Upper Complex, which consists of Hercynian continental crust, showing a local Alpine metamorphic overprint at 0.3–0.7 GPa and 200–450° C in the Sila Massif and Catena Costiera (Acquafredda et al., 1994; Graessner & Schenk, 2001; Liberi et al., 2011; Ortolano et al., 2020; Piccarreta, 1981) and up to 1.1–1.2 GPa and 540–570° C in the Aspromonte Massif (Cirrincione et al., 2008). According to the current geodynamic models, the evolution of the Calabrian Arc was driven by the south-eastward retreat of the Ionian slab (Faccenna et al., 2001; Jolivet and Faccenna, 2000; Malinverno and Ryan, 1986). During the Eocene, subduction of the Ligurian Tethys oceanic crust underneath the continental margin, represented by the Calabria terrane, (Rossetti et al., 2004; Stampfli & Borel, 2002; Vitale et al., 2019), is thought to have occurred at 47-20 Ma (Shimabukuro et al., 2012; Rossetti et al., 2001,2004; Thomson, 1994, 1998; Beccaluva et al., 1981; Schenk, 1980; Borsi and Dubois, 1968). Currently, active subduction residue of the ancient, 200 km wide, subducting slab dipping 70° towards NE is found beneath the Calabrian arc with the presence of

deep seismicity (150-300 km) (Neri et al., 2012; Neri et al., 2009; Chiarabba et al., 2008; Spakman & Wortel, 2004; Lucente et al., 1999). Different studies show a rapid deepening of the Ionian Moho beneath Calabria, illustrating the geometry of the subduction zone (Scarfì et al., 2018; Piana Agostinetti et al., 2009). The estimated current plate convergence velocity between the two plates is 3–5 mm/yr (Neri et al.,2020; Mattei et al., 2007) and the rollback of the subducting slab occurs at about 2 mm/yr rate (Nocquet, 2012; Devoti et al., 2008; Hollenstein et al., 2003).

The Calabrian arc in one of the strongest seismic areas in Italy (Neri et al., 2020), and experienced several destructive earthquakes with estimated magnitudes of about 7 or higher (Scarfì et al. 2018). After the destructive 1908 earthquake (Rovida et al., 2016), a few events with M > 4 and about 200 shocks with magnitude between 3 and 4 (out of a total of 3800 events) have occurred between 1980 and 2005 (Castello et al., 2006; Gruppo di Lavoro CPTI, 2004). Crustal thickness reaches value of about 35–38 km in correspondence of the highest portion of the chain (Di Stefano et al., 2009) and the recorded seismicity is marked by focal depths <30 km (i.e. crustal depths; Neri et al., 2020; Boschi et al., 2000). Since the Middle Pleistocene, an intense WNW–ESE oriented regional extensional phase occurred, resulting in a longitudinal faults system with NNE−SSW strikes and parallel to the mountain system (Fig II.1a), consisting of a 10–50 km-long distinct normal fault segments running along the western side of the Calabrian arc (Catalano et al., 2008; Tansi et al., 2005). The development of the rift-zone, coupled with contrasting vertical movements, such as mountain chain uplifting of 0.5–1.2 mm/yr in the last 1–0.7 Myr (Faccenna et al., 2011; Ferranti et al., 2008; Monaco et al., 1996), are still active processes (Dumas et al., 2004) and probably represents the response to the isostatic rebound due to detachment of the Ionian subducted slab (Tortorici et al.,2003, 1995; Westaway, 1993). GPS data show differential motion of the Calabrian arc relative to both the Nubia and Eurasia plates, which causes active extension on the region with the developments of the aforementioned extensive faults (Fig.II.2; Maesano et al., 2017; Mattei et al., 2007 and reference therein). These normal faults are considered to be major

seismogenetic faults (Neri et al., 2006; Monaco et al., 1996), with the NE trending fault systems of the Messina Straits, Gioia Basin and Mesima Valley believed to have generated the major earthquakes of the area (Rovida et al., 2019, 2020; Neri et al., 2020).

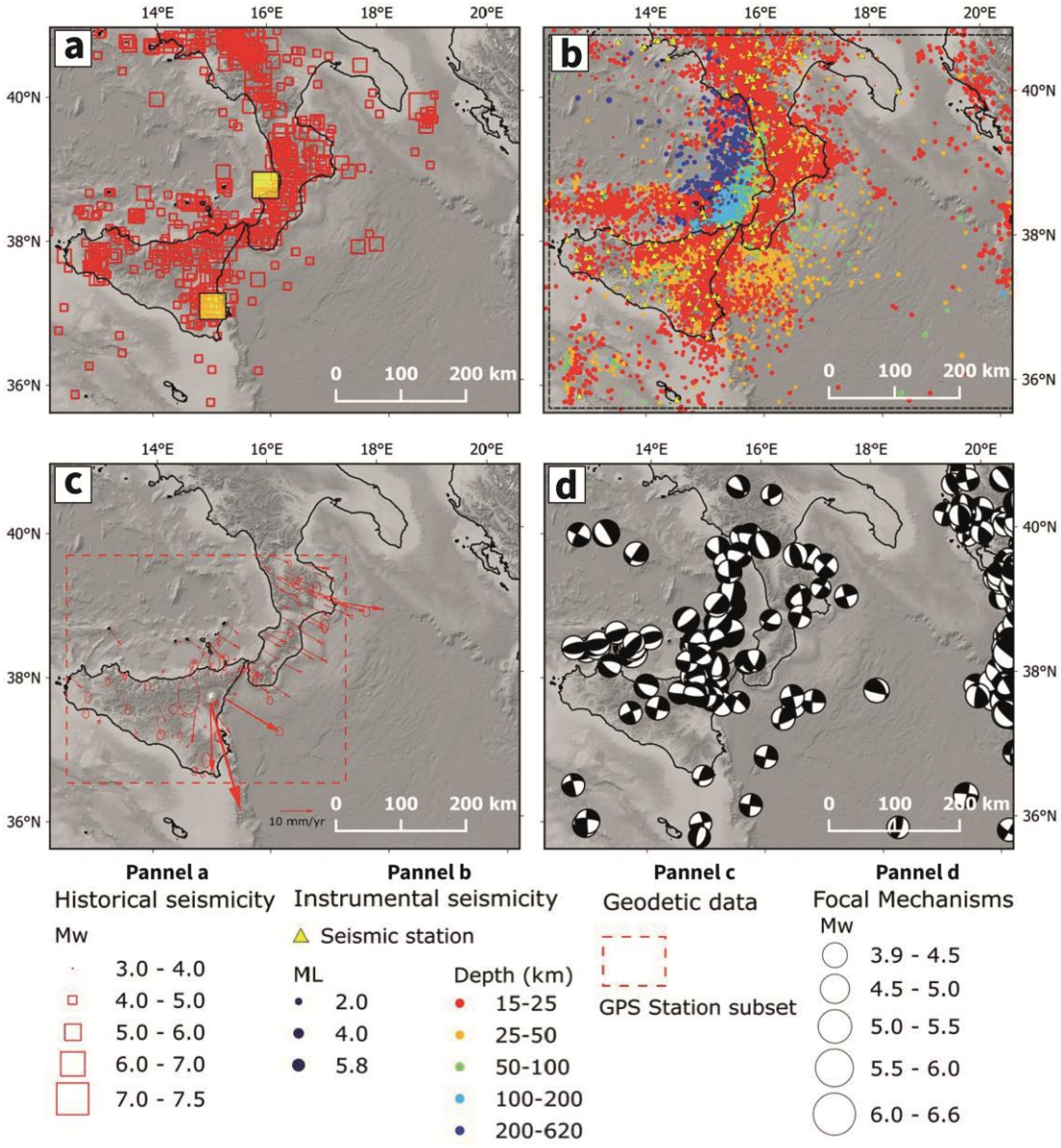

Figure II.2 | Calabria Seismicity. Panel **a**) Historical seismicity from CPTI1569; Panel **b**) Instrumental seismicity from the Italian Seismological Instrumental and Parametric Database68, earthquake plotted are recorded in the time period 2005–2016; Panel **c**) Velocity field from continuous GPS station in the 1998–2009 time span for Sicily and Calabria plotted with a fixed Africa (Devoti et al., 2011). Velocity ellipses represent 1-sigma confidence errors. Panel d) Regional Centroid Moment Tensor solution. After Maesano et al., 2017 (modified).

The first comprehensive geochemical data-set for fluids circulating over the Calabrian arc has been presented by Italiano et al., (2010). The authors used the chemical and isotopic (C and He) composition of groundwater and dissolved gas to show the aquifers contain deeply derived CO_2-rich gas with radiogenic He signature, consequence of long residence in the crust. Clear fault-fluid relationships have been found in some of the investigated sites, with the thermal character of the investigated waters being linked with deeper hydrological circuits and normal geothermal gradients (30 °C/km). Recent studies have reconstructed the conceptual geothermal model of some Calabrian sites using a "site-specific" (Vespasiano et al., 2021), multidisciplinary approach, involving geological, hydrogeological and geochemical data. These studies highlighted different features between thermal waters from north to south, related to complex geologic and tectonic settings of the region (e.g., Apollaro et al. 2012, 2016, 2019a, 2019b, 2019c, 2020, 2021; Vespasiano et al., 2012, 2014, 2015a, b). Moreover, a deep component for dissolved gases of Pollino water have been identified from Apollaro et al., (2020) on the base of their C and He isotopic compositions.

II.3. Materials and Methods

II.3.1. Sampling and analytical methods

In total, 55 water samples were collected (see Fig. II.1) during two field campaigns in February and July 2019 (Table II.1). Water temperature, pH, Eh, and electrical conductivity (EC) were measured in-situ by means of high-resolution multi-parametric probes (Hanna Instruments HI-9828). Total alkalinity was measured in-situ by acidimetric titration with 0.05 N HCl using methyl-orange as indicator. Water samples were filtered in situ through a 0.45 μm pore-size membrane and acidified with supra-pure HNO_3. Different sample aliquots (1 filtered and 2 filtered and acidified) were collected. All samples were stored in high-density polyethylene bottles for laboratory analysis. Major elements were determined by High Performance Liquid Chromatography (HPLC) by using a Thermo Scientific Dionex™ ICS-1100 equipped with Dionex IOnPac AS23 and Dionex IonPac CS12A columns for the determination of anionic (F^-, Cl^-, SO_4^{2-} and NO_3^-) and cationic (K^+, Na^+,

Ca^{2+} and Mg^{2+}) species, respectively. The computed charge balance resulted <5% in all water analysis. Chromatographic and spectrophotometric analysis were performed at the Department of Biology, Ecology and Earth Sciences laboratories of the University of Calabria (Cosenza, Italy). Total Dissolved Inorganic Carbon (TDIC) was computed modelling the equilibrium carbonate speciation at measured pH, HCO_3^- and T values. TDIC and saturation index (SI) with respect to the mineral phases (calcite, dolomite, gypsum), were calculated using the PHREEQC Interactive computer code (Parkhurst & Appelo, 1999)

The water samples used for the analysis of dissolved gases, $\delta^{13}C$ and He and Ne isotopes (^3He, ^4He, ^{20}Ne) were sampled in glass bottles according to Capasso and Inguaggiato (1998), and analysed in a few days from their collection in order to prevent any contamination and/or loss of volatiles. The chemical composition of the dissolved gases were analysed by using the method described in Capasso and Inguaggiato (1998), which is based on the equilibrium partition of gas species between a liquid and a gas phase. The analysis were performed utilizing a Perkin Elmer Clarus 500 gaschromatograph equipped with 3 meters packed column (100/120 Shincarbon, Ar gas carrier) and two detectors (a thermal conductivity detector [TCD] and a flame ionization detector [FID]), and using Ar as the carrier gas. H_2, O_2, N_2 and CO_2 were measured by means of the TCD detector, while CH_4 and CO were determined through a FID detector coupled with a methanizer. Analytical errors for CO_2, N_2, H_2, CO, CH_4, O_2 is within 3%.

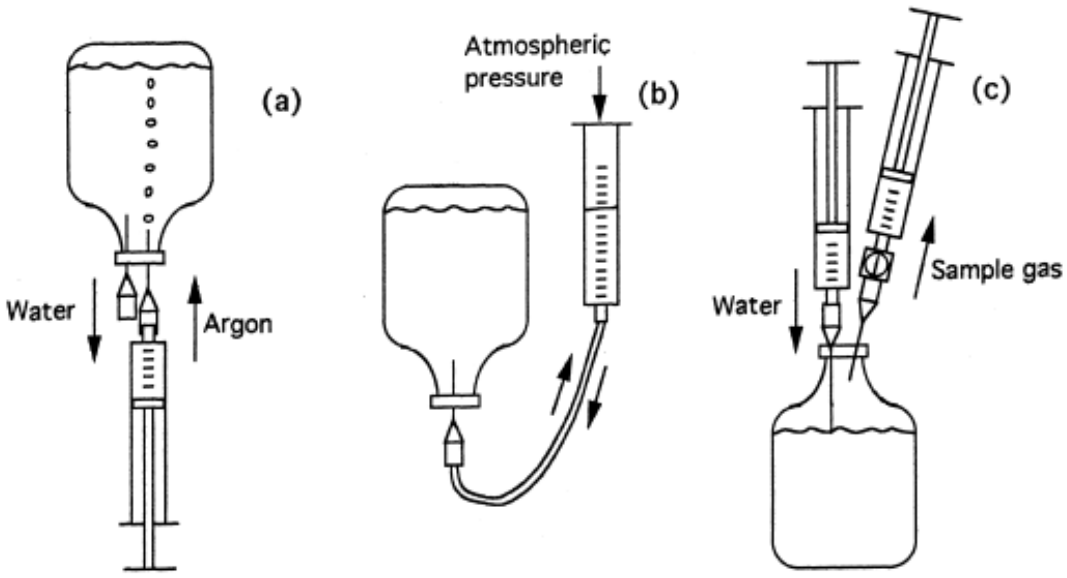

Figure II.3 | Scheme of analytical treatment for dissolved gases. Sampling apparatus and analytical treatment of the sample as proposed from Capasso & Inguaggiato, 1998. **(a)** introduction of the host-gas into the flask; **(b)** restoring the atmospheric pressure in the flask; **(c)** extraction of the gas phase after equilibration.

Analyses of the dissolved noble gases (He and Ne) and He isotopic composition ($^3He/^4He$) were performed by using the methodology proposed by Inguaggiato and Rizzo (2004), which is based on isotope equilibrium between liquid and a host gas phases (e.g., N_2). The extracted gases from waters are purified in high-vacuum purification line that is directly connected to the mass spectrometers (Rizzo et al., 2019 and references therein). He and Ne isotopes are analysed using a static vacuum mass spectrometer (GVI Helix SFT) with a double collector in order to detect ^3He and ^4He ion beams simultaneously with a multi-collector Thermo-Helix MC Plus mass spectrometer (isotopic ratio precision within ±0.5%.). The $^3He/^4He$ ratio was determined by measuring ^3He in an electron multiplier detector and ^4He in an axial Faraday detector. The isotopic composition of TDIC ($\delta^{13}C_{TDIC}$) is measured by using the method proposed by Capasso et al., (2005), using a Thermo Scientific Delta V Advantage continuous flow isotope ratio mass spectrometer. All $\delta^{13}C_{TDIC}$ values were reported relative to Vienna Pee Dee Belemnite (VPDB) international reference standard, and the analytical precision is ±0.15‰. All sampling and analytical devices are provided by the Istituto Nazionale di Geofisica e Vulcanologia, Sezione di Palermo.

II.3.2. Carbon mass balance and C flux

Following the method developed by Chiodini et al. (2004;2020) is possible to deconvolve DIC in groundwater into distinct carbon pools. The external C contribution, C_{ext}, (i.e without carbonates contribution) and its isotopic composition $\delta^{13}C_{ext}$ for each sample have been calculated by following carbon mass balance equations:

$$TDIC = C_{ext} + C_{carb} \quad (1)$$

$$\delta^{13}C_{ext} \times C_{ext} + \delta^{13}C_{carb} \times C_{carb} = \delta^{13}C_{TDIC} \times TDIC \quad (2)$$

where TDIC and $\delta^{13}C_{TDIC}$ are analytically determined, C_{carb} is computed as (Ca + Mg) − SO_4 considering the dissolution of carbonate minerals (i.e., calcite and dolomite) and the possible presence of gypsum/anhydrite and $\delta^{13}C_{carb}$ is assumed to be constant and equal to the average $\delta^{13}C$ of numerous samples of carbonate rocks from southern Appennines investigated aquifers (+1.8‰; Chiodini et al., 2020 and references therein).

To apply the C_{carb} correction some conditions have to occur. In fact, if the C_{carb} is, for definition, the carbon from dissolution of carbonate then the first condition to calculate it is the presence of carbonate rocks in the studied areas. In our case this condition is true only for some samples (Table II.2) located on the Calabria-Basilicata border. Here the aquifers that feed the sampled springs are hosted by carbonate rocks (Apollaro et al., 2020,2012). For these samples we applied the C_{carb} correction. Other samples from Basilicata region are located in correspondence of terrains of the ophiolite-bearing Ligurian Complex tectono-stratigraphic unit where crustal and ultramafic rocks as Gneiss and Serpentinite are dominant (Sansone et al., 2011). Margiotta et al. (2014), have been studied the interaction between these water and the surrounding rocks defining with R-mode factor analysis the relationships between trace elements, Ca^{2+}, Mg^{2+}, and HCO_3^- present the in waters. The results show a correlation between Ca and HCO_3, but not between Mg and HCO_3, demonstrating that calcium comes from the dissolution of carbonate compounds. In light of this, the correction of

C_{carb} cannot be carried out with the typical method (i.e computation from Ca+Mg-SO_4, also considering the absence of gypsum/anhydrite), but considering only the Ca concentration.

The other samples are located over the entire Calabria region at the base of the three main mountain chain: Catena Costiera, Sila massif and Aspromonte where metamorphic lithologies are dominant (Fig.II.1, Table II.2; Tursi et al., 2021, Apollaro et al. 2019,2009; Vespasiano et al., 2021), thus no significant carbonate dissolution should occur because silicate host rock should be carbonate free (Barry et al., 2021).

Moreover comparing dolomite saturation index (SI_{dol}) with calcite saturation index (SI_{calc}) all samples for which is possible to define C_{carb} are in equilibrium with calcite and dolomite ($-0.1 \leq SI \leq 0.1$). Other samples show $SI < -0.1$ (i.e undersaturated) with only two samples (Cotr.PC and An) with $SI > 0.1$ (i.e oversaturated) (Fig.II.4 and Table II.2).

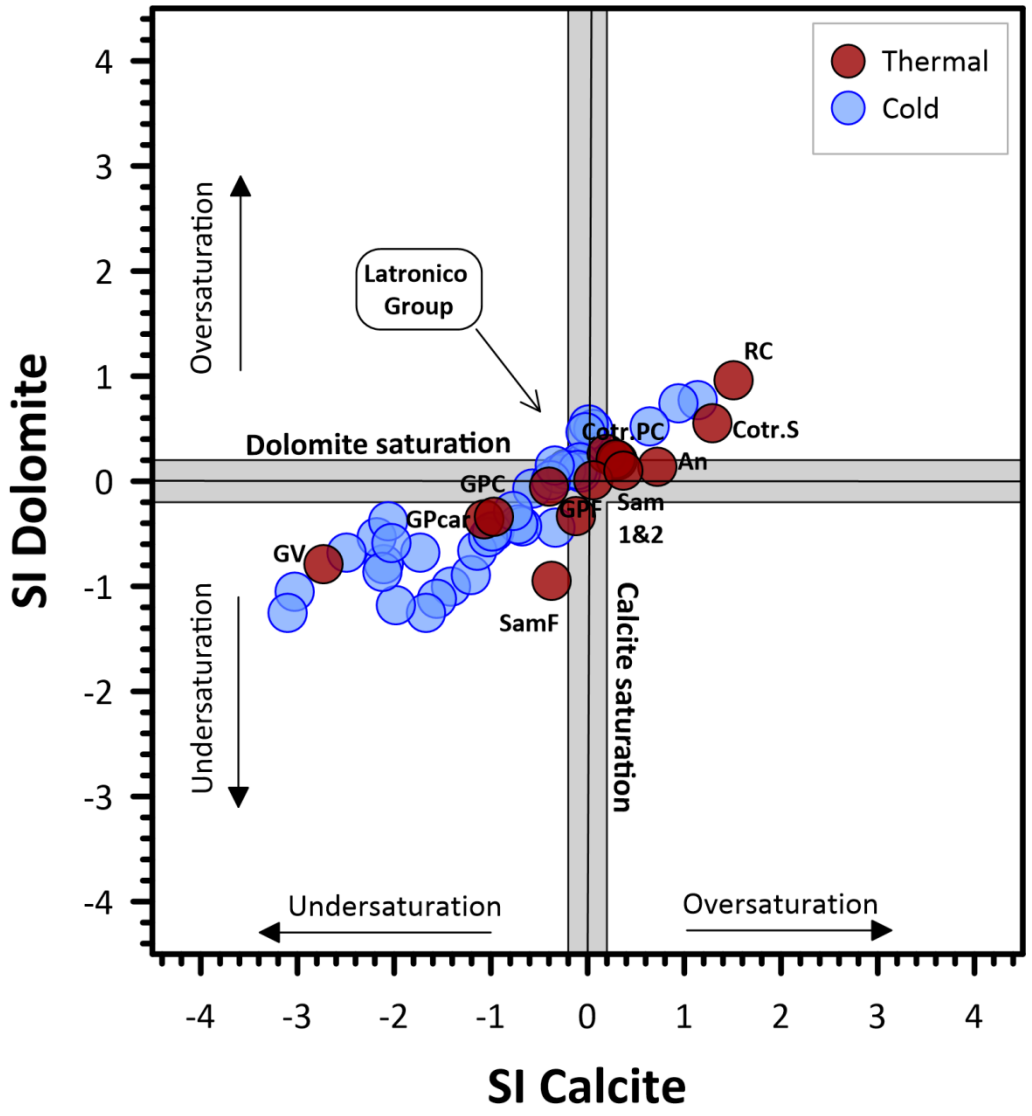

Figure II.4 | Dolomite Saturation Index vs Calcite Saturation Index

We need to clarify that the elements (Ca, Mg, HCO_3) needed for calcite and dolomite precipitation in acquifers hosts in non-carbonate lithologies could come from the dissolution, by CO_2 and H_2SO_4, of silicate minerals, as shown, for example, by the following reactions (Ulloa-Cedamanos et al., 2021):

$$2NaAlSi_3O_{8\,(s)}\ (\text{Albite}) + 2CO_{2\,(g)} + 11H_2O_{(l)} \rightarrow Al_2Si_2O_5(OH)_{4}\ (\text{Kaolinite}) + 2Na^{+}_{(aq)} + 2HCO_3^{-}{}_{(aq)} + 4H_4SiO_{4\,(aq)}$$

$$2KAlSi_3O_{8\,(s)\ (rthoclase)} + 2CO_{2\,(g)} + 6H_2O_{(l)} \rightarrow Al_2Si_4O_{10}(OH)_{2\ (montmorillonite)} + 2K^+_{(aq)} + 2HCO_3^-{}_{(aq)} + 2H_4SiO_{4\ (aq)}$$

$$CaAl_2Si_2O_{8(s)\ (Anorthite)} + 2CO_{2(g)} + 2H_2O_{(l)} \rightarrow Al_2Si_2O_5(OH)_{4\ (Kaolinite)} + Ca^{2+}_{(aq)} + 2HCO_3^-{}_{(aq)}$$

$$Ca_{2-x}Mg_x(SiO_3)_{2\,(s)\ (Ca\text{-}Mg\ silicate)} + 2H_2SO_4 + 2H_2O_{(l)} \rightarrow (2-x)Ca^{2+}_{(aq)} + xMg^{2+}_{(aq)} + 2SO_4^{2-} + 2H_4SiO_{4(aq)}$$

In figure II.5 a and b the major element ratios, as HCO_3^-/Na^+, Ca^{2+}/Na^+ and Mg^{2+}/Na^+ have been used to define possible correlations between the elements in water and their origin from the host rocks. In fact these ratios in water can reflect the elemental ratios in different local bedrock and solubility of corresponding elements during chemical weathering (Liu et al., 2021). Cold water significantly approach to a carbonate end-member, suggesting that carbonate weathering is dominant. Thermal samples show lower elemental ratios, even than a silicate end member (see Liu & Han, 2020), indicating weathering processes dominant on silicate rocks. The lowest values can due to other processes as Halite dissolution. In any case the calculated fraction of major elements come from carbonate dissolution results negligible for these samples (<0.05%).

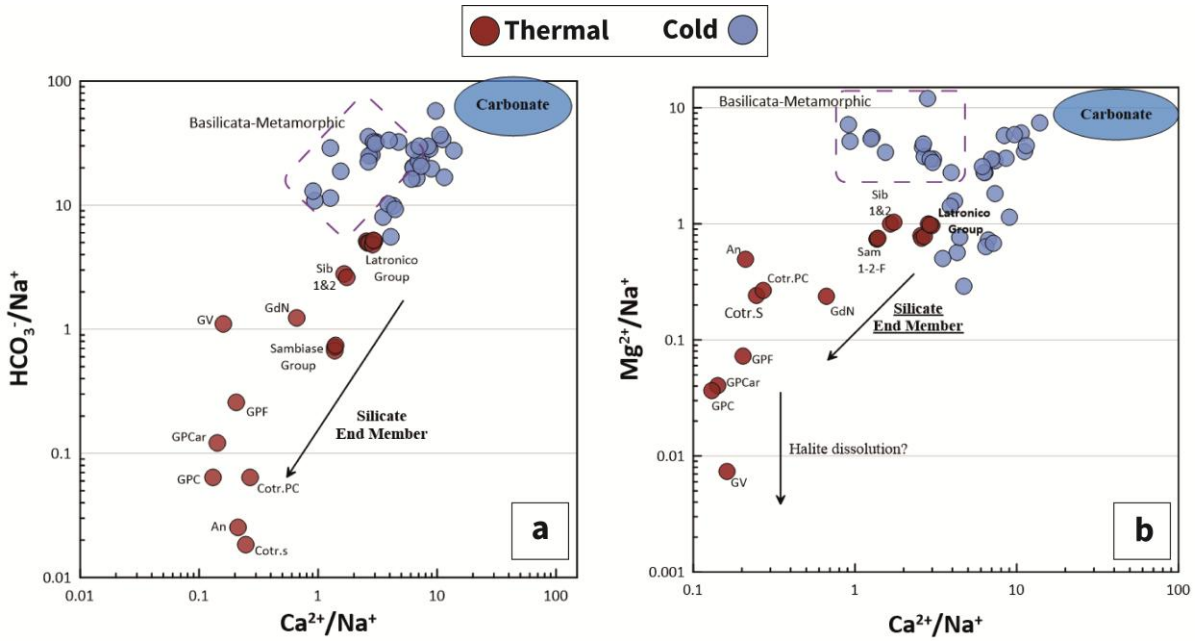

Figure II.5 | Mixing diagrams (a) Ca^{2+}/Mg^{2+} versus HCO^{3-}/Na^{+}; (b)Ca^{2+}/Mg^{2+} versus Mg^{2+}/Na^{+} molar ratios in thermal and cold spring of Calabria region. End-members values from Liu & Hann, 2020. Basilicata-Metamorphic are water hosted in serpentinites and Gneiss acquifer.

These evidence demonstrate that C_{carb} contribution cannot be calculated for thermal water, but it should not weight on the total carbon balance allow us to approximate that all the C present in thermal waters come from external sources (i.e. C_{deep} and C_{inf}) and we can write:

$$TDIC = C_{ext} \quad (1)$$

$$\delta^{13}C_{TDIC} = \delta^{13}C_{ext} \quad (2)$$

Hence the total amount of C_{ext} can be divided into two different contributions: i) C_{inf}, i.e. soil carbon from biogenic source and ii) C_{deep}, i.e carbon from deep (mantle/crustal) source.

The C_{inf}, C_{deep} and the relative isotopic compositions, $\delta^{13}C_{inf}$ and $\delta^{13}C_{deep}$ are computed by considering the following carbon balance:

$$C_{inf} + C_{deep} = C_{ext} \quad (3)$$

$$\delta^{13}C_{inf} \times C_{inf} + \delta^{13}C_{deep} \times C_{deep} = \delta^{13}C_{ext} \times C_{ext} \quad (4)$$

To solve this system of two equations and four unknown variables we use the binary plot $\delta^{13}C_{ext}$ versus $1/C_{ext}$ where mixtures among different sources show a linear trend (Fig. II.6).

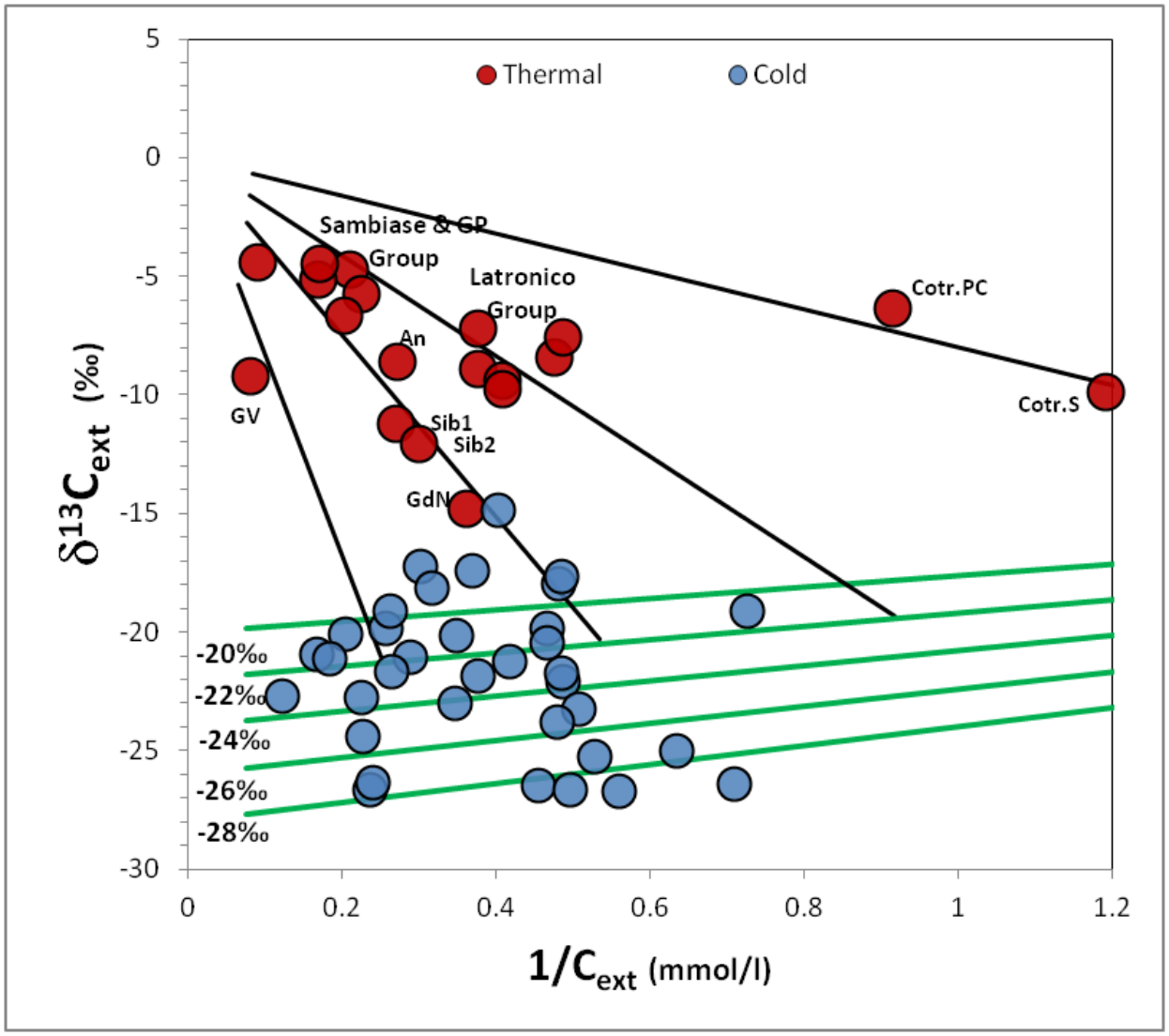

Figure II.6 | $1/C_{ext}$ versus $\delta^{13}C_{ext}$ diagram. The diagram allows the estimation of the infiltrating water end members with C_{inf} that is determined for different group of samples at the interception of the mixing lines connecting a defined deep end-member ($1/C_{ext}$=0 and $\delta^{13}C_{deep}$= 0.13 mean value for metamorphic CO_2; Dai et al.,1996; Hunt, 1996; Clark and Fritz, 1997; Evans et al., 2008) with the infiltrating water line computed at $\delta^{13}C$= -22‰ (green line). This computations gives different C_{inf} values from 0.55 to 3.5 mmol on the base of hypothetical trend lines (black lines).

In detail, (i) the isotopic composition of soil-derived CO_2 ($\delta^{13}C_{inf}$ = -22‰) is considered unique and derived from $\delta^{13}C_{ext}$ average value of the infiltrating water samples; (ii) C_{inf} is determined for different group of samples at the interception of the mixing lines connecting a defined deep end-

member ($1/C_{ext}$=0 and $\delta^{13}C_{deep}$= 0.3 mean value for metamorphic CO_2; Dai et al.,1996; Hunt, 1996; Clark and Fritz, 1997; Evans et al., 2008) with the infiltrating water line computed at $\delta^{13}C$= -22‰ (green line). This computations gives different C_{inf} values from 0.55 to 3.5 mmol on the base of hypothetical trend lines (black lines); iii) the carbon concentration from deeply derived CO_2 (C_{deep}) of each sample is given by inserting the computed C_{inf} in Eq. 3. We would like to clarify that carbon budget estimates represent a maximum values due to the assumptions made to estimate C_{ext}. If indeed there has been appreciable carbonate dissolution for all samples, our estimates would be an overestimation.

The influx rate of deep sourced CO_2 (FC_{deep} in $mol \cdot km^{-2} \cdot yr^{-1}$) was calculated for each spring by following equation:

$$FC_{deep} = C_{deep} \cdot \rho_{H_2O} \cdot (Q/S) \quad (5)$$

where C_{deep} is deep sourced CO_2 expressed in $mol \cdot kg^{-1}$, ρ_{H_2O} is density of water in $kg \cdot m^{-3}$, Q is the spring flow rate in $m^3 \cdot yr^{-1}$ and S is the spring catchment area in km^2.

Table II.3 report for each spring the needed data to calculate the deep carbon flux. For thermal water in the northern part of the region it was possible to calculate for each spring the specific flows (hydrogeological data from Allocca et al., 2007 and De Vita et al.,2018). For all the other thermal springs distributed throughout the Calabrian territory, the existing hydrogeological data do not allow an equally precise calculation to be made. The only available data for these samples are the areas of the aquifers to which the single spring belong (http://www.ildistrettoidrograficodellappenninomeridionale.it). The total water discharge of these aquifers is not known and therefore it was not possible to calculate the specific surface for each spring and consequently its carbon flux. However, in order to have a minimum value, the deep carbon fluxes for each spring were calculated considering the total area of the belonging aquifer. In this case for the springs belonging to the same aquifer, the C_{deep} contributions were added together

and divided by the total area of the aquifer. The flow values (FC_{deep}) for these springs could therefore be an underestimation of those actually present in the area.

II.4. Results

The physico-chemical parameters of the collected waters are reported in Table II.1 together with the computed TDIC values, chemical and isotopic compositions (He and C) of dissolved gases. Major ions water chemistry is presented in Table II.2. The 55 samples have been subdivided in two categories on the base of their discharge temperature following the classification of Apollaro et al., (2020) and Italiano et al., (2010): cold (T<20 °C) and thermal (T≥20 °C). The cold waters show compositions typical of shallow air-saturated waters (ASW) with N_2 concentrations ranging between 10.3 and 17.6 ccSTP/l and CO_2 from 1.5 to 24.4 ccSTP/l. O_2 concentrations are between 2.6 and 8.6 ccSTP, while CH_4, CO and H_2 concentrations are very low ($CH_4 \leq 5.5x10^{-04}$ ccSTP/l; $CO \leq 3.5x10^{-4}$ ccSTP/l; $H_2 \leq 1.6x10^{-3}$ ccSTP/l). Both He and Ne are present in trace amounts (up to $9.4x10^{-5}$ ccSTP/l and $2.9x10^{-4}$ ccSTP/l). In thermal waters the measured He amounts are much higher (up to 0.11 ccSTP/l) than in cold samples, while Ne range between $1.4x10^{-4}$ and $4.3x10^{-4}$ ccSTP/l (Table II.1).

In the ternary diagram CO_2-N_2-O_2 of Figure II.2, thermal samples cluster along the CO_2-N_2 axis, as implied by their low to negligible O_2 contents (≤1.4 ccSTP/l). These samples have CO_2 concentrations from 0.1 to 36.6 ccSTP/l and N_2 from 0.004 to 22.6 ccSTP/l . Sample RC is the unique thermal sample falling close the ASW field (Fig. II.7).

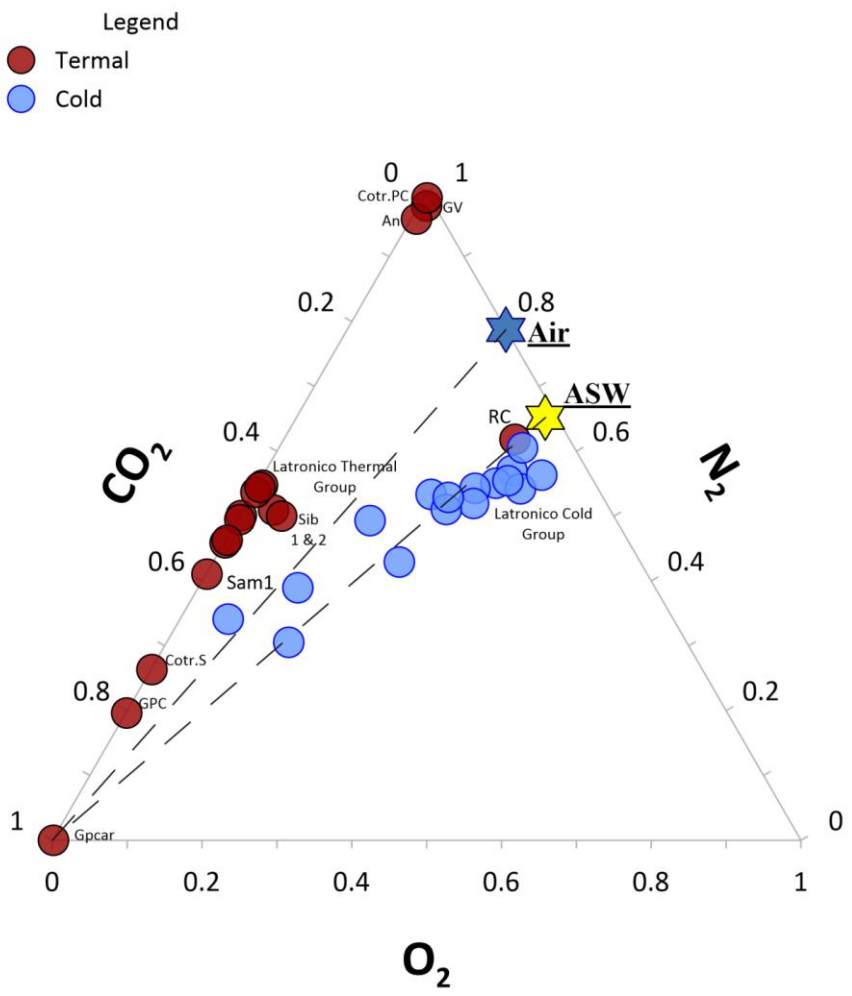

Figure II.7 | CO_2-O_2-N_2 ternary diagram. Thermal samples (red) fall along the axis between CO_2 and N_2 , as implied by their being the two dominant gas species, showing low O_2 values. The cold waters (blue circles) show compositions typical of shallow water falling on mixing line between Air Saturated Water (ASW) and CO_2-rich end member.

The measured C-isotope compositions of TDIC ($\delta^{13}C_{TDIC}$) range from -14.8‰ to −5‰ (vs V-PDB) in cold samples and from -9.9‰ to -4.4‰ in thermal samples (Table II.1). The $^{3}He/^{4}He$ isotopic ratio (R) of each sample is normalized to the same ratio in air (R_a=1.386·10^{-6}; Ozima & Podosek, 2002). The R/R_a ratios range from 0.8 to 1.1, and from 0.03 to 0.5 R_a, for cold and thermal waters, respectively. The $^{4}He/^{20}Ne$ ratios are up to 659 for thermal samples, well above the ASW ratio (0.295 at 25°C; Ozima & Podosek, 2002), indicating a negligible atmospheric contamination. On the contrary, the $^{4}He/^{20}Ne$ ratios of the cold waters, ranging between 0.26 and 0.35, indicate a dominant atmospheric derivation (Fig. II.8).

Table II.1 | Chemical and isotopic composition of Calabria and Pollino springs.

T-Thermal; C-Cold; <d.l- below detection limits; - not measured

Name	ID	Type	Coordinates		pH	T	Cond	Eh	Q	TDIC	δ13CTDIC	He	O_2	N_2	CH_4	CO_2	Ne	$^4He/^{20}Ne$	R/R_a
			X	Y		°C	uS/cm	mV	l/s	mmol/l	‰ vs PDB	ccSTP/l	ccSTP/l	ccSTP/l	ccSTP/l	ccSTP/l	ccSTP/l		
Fontana Solfurea	FS	T	583623.0	4438112.0	7.5	21.8	698	-207	0.41	4.4	-4.7	2.17E-03	0.17	13.12	2.9E-02	10.68	2.15E-04	10.1	0.10
Solfurea Cupola	SC	T	583619.0	4438165.0	7.5	21.8	710	-101	11	4.1	-4.8	1.38E-03	1.02	12.61	6.2E-03	11.12	2.29E-04	6.0	0.14
Sinistra Cupola	SXC	T	583644.0	4438165.0	7.4	21.5	689	-14	10	4.1	-5.1	1.25E-03	1.38	12.35	5.2E-03	10.94	2.06E-04	6.1	0.13
Ruscello Caldo	RC	T	583623.1	4437576.5	8.3	20.3	713	76	78	3.6	-4.2	<d.l.	5.37	10.76	1.0E-04	1.27	-	-	-
Ruscello meno caldo	RMC	T	583576.1	4437538.5	8.2	20.0	699	97	135	3.4	-3.84	<d.l.	5.94	10.30	9.6E-05	1.82	-	-	-
Sorgente Pargo	SP	C	586220.2	4439782.9	7.4	11.8	627	265	0.60	7.0	-15.5	5.66E-05	6.59	11.46	3.5E-05	2.75	1.98E-04	0.3	0.90
Sorgente Celano	SCE	T	583263.5	4437427.6	7.6	18.4	735	228	20	4.1	-4.02	0.00E+00	6.09	11.40	0.0E+00	19.82	-	-	-
Sorgente Fraccia	SF	C	583951.0	4438936.6	8.0	12.0	396	162	0.10	3.4	-13.2	7.06E-05	7.55	14.05	9.4E-05	1.60	2.25E-04	0.3	0.92
S. Latronico Centro 1	SC1	C	585776.6	4438117.9	8.1	10.1	368	220	0.10	3.5	-12.1	<d.l.	6.41	11.87	5.5E-04	3.58	-	-	-

S. Latronico Centro 2	SC2	C	585776.6	4438117.9	7.9	10.7	460	240	0.07	3.9	-14.1	<d.l.	5.04	11.27	5.5E-05	4.80	-	-	-
Sorgente Serra	SS	C	598892.8	4415866.0	8.4	8.3	377	192	50	3.8	-9.1	<d.l.	8.39	12.86	7.9E-05	2.45	-	-	-
sorgente tufarazzo	ST	C	599003.9	4415898.8	8.3	6.7	366	202	90	3.7	-11.3	<d.l.	8.64	13.09	9.0E-05	1.50	-	-	-
sorgente san paolo	SSP	C	595778.0	4412859.0	7.9	10.4	347	245	15	3.6	-11.0	<d.l.	7.61	13.04	4.2E-05	4.46	-	-	-
sogente foce	SFo	C	596945.0	4412912.0	7.6	10.5	350	265	101	3.6	-11.3	6.81E-05	6.87	12.90	0.0E+00	5.53	2.49E-04	0.3	1.09
sogente foce 2	SFo2	C	597003.0	4412912.0	7.7	11.1	352	260	101	3.6	-9.4	<d.l.	6.73	13.47	5.8E-05	5.25	-	-	-
sorgente Guaglianone	SG	C	580341.4	4404915.4	7.6	11.2	456	258	20	4.7	-9.3	<d.l.	6.37	10.96	0.0E+00	8.22	-	-	-
abatemarco 2	Ab2	C	574291.6	4399292.9	7.4	12.1	804	258	50	4.2	-11.3	<d.l.	4.70	13.00	0.0E+00	8.68	-	-	-
solfurea abatemarco	AbS	C	582183.9	4399373.5	7.3	12.5	880	64	1.50	6.0	-12.2	9.45E-05	2.65	14.02	1.2E-04	24.42	2.69E-04	0.4	0.75
sorgente Abatermarco	Ab	C	583278.7	4400412.0	7.9	8.5	295	227	634	2.8	-13.4	<d.l.	7.93	13.29	5.2E-05	2.73	-	-	-
pozzo abatemarco	Ab well	C	577884.1	4401371.0	7.4	13.2	512	277	10	5.6	-12.4	7.53E-05	6.00	17.62	0.0E+00	21.57	2.86E-04	0.3	0.99

Grotta delle Ninfe	GdN	T	620010.3	4411051.4	7.4	26.2	1103	-255	70	4.4	-8.6	1.15E-03	0.04	11.31	1.9E-01	13.30	1.95E-04	5.9	0.05
Sibarite 1	Sib1	T	613100.1	4404494.9	7.3	24.2	1086	-253	0.70	4.8	-8.3	1.79E-03	0.05	11.55	3.5E-02	11.47	1.90E-04	9.4	0.17
Sibarite 2	Sib2	T	613100.1	4404494.9	7.4	23.7	1088	-266	10	4.6	-8.3	2.23E-03	0.08	14.26	4.2E-02	12.22	2.33E-04	9.6	0.17
Tarantola Nuova	IC02P	C	594115.7	4435291.2	6.7	11.2	488	429	22.5	7.0	-14.9	-	-	-	-	-	-	-	-
Fosso S. Arcangelo	ICP06P	C	596944.0	4431641.7	7.1	11.1	701	552	0.45	9.1	-20.6	-	-	-	-	-	-	-	-
Fontana Pagnotella	ICP07P	C	596873.8	4431199.8	6.8	12.4	548	591	0.39	6.5	-19.3	-	-	-	-	-	-	-	-
Fontna di Mezzo	IC09P	C	596983.4	4430781.8	6.9	12.3	434	516	0.25	5.2	-18.8	-	-	-	-	-	-	-	-
Fontana Giudea	IC10P	C	597201.6	4430587.3	6.9	11.8	479	550	0.27	5.8	-20.0	-	-	-	-	-	-	-	-
Sorgente Montagna Pastoroso	IC11P	C	590186.8	4430325.1	6.7	9.9	289	356	0.23	4.2	-15.4	-	-	-	-	-	-	-	-
Frida	IC14P	C	600498.7	4424909.8	6.8	6.0	320	457	525	2.4	-10.2	-	-	-	-	-	-	-	-
Mercure	IC15P	C	591921.7	4424289.0	6,8	10.7	357	571	2050	5.0	-10.9	-	-	-	-	-	-	-	-

Tarantola Nuova 2	ID02P	C	594115.7	4435291.2	7.0	11.5	494	353	5.5	3.6	-14.1	-	-	-	-	-	-	-	-
Acqua Ficavozza	ID03P	C	595955.3	4436159.1	6.8	13.2	278	337	2.7	3.2	-	-	-	-	-	-	-	-	-
Sorgente Altosano	ID04P	C	605692.6	4436356.2	6.9	12.3	683	321	0.06	4.7	-15.7	-	-	-	-	-	-	-	-
Sorgente Bosco Magnano	ID05P	C	596121.7	4434058.1	7.0	12.3	509	330	0.14	4.7	-17.5	-	-	-	-	-	-	-	-
Fontana Matarazzo	ID08P	C	596936.9	4430898.4	7.0	12.5	441	328	0.36	3.5	-16.5	-	-	-	-	-	-	-	-
Sorgente Timpa della Gatta (Cropani)	ID12P	C	596315.5	4433533.3	6.9	10.3	416	300	0.24	5.3	-19.3	-	-	-	-	-	-	-	-
Fontana Camauli - Sorgente Costa Cirasa	ID17P	C	599896.5	4431020.0	7.0	9.3	298	603	2	3.2	-13.9	-	-	-	-	-	-	-	-
Fontana Mancini - Sorgente Mancini	ID18P	C	600366.6	4431152.6	6.8	8.8	315	355	1.5	4.2	-13.3	-	-	-	-	-	-	-	-
Sorgente Murge Muretto	ID19P	C	600942.4	4432958.0	7.1	9.7	397	340	2	2.4	-15.0	-	-	-	-	-	-	-	-
Frida Alta	ID20P	C	600498.7	4424909.8	6.8	5.9	322	344	100	3.8	-9.1	-	-	-	-	-	-	-	-
Fontana Fosso del Pantano	ID21P	C	600816.9	4432950.2	6.7	11.3	270	229	0.03	6.6	-16.0	-	-	-	-	-	-	-	-
Miretta	ID22P	C	593688.7	4435523.3	7.0	11.2	483	341	2.2	3.4	-13.2	-	-	-	-	-	-	-	-

Tarantola Vecchia	ID23P	C	594030.3	4435302.4	7.0	11.2	493	348	0.50	3.7	-12.8	-	-	-	-	-	-	-	-
Curcio	ID24P	C	594386.7	4435026.2	7.1	11.8	496	338	1.2	3.6	-16.1	-	-	-	-	-	-	-	-
Galatro Vecchia	GV	T	597973.8	4257944.8	6.4	35.6	5370	-96	3	12.5	-9.2	1.02E-02	0.18	16.74	2.2E-01	0.19	3.21E-04	31.8	0.12
Antonimina	An	T	604399.2	4235058.8	7.0	20.0	1226	-41	0.5	3.7	-8.6	1.09E-01	0.11	14.20	1.7E-03	0.51	1.66E-04	658.7	0.03
Guardia Caronte	Gpcar	T	585607.7	4370563.8	6.3	35.9	5157	-67	5	11.2	-4.4	2.67E-03	0.04	0.00	2.5E+00	36.43	1.41E-04	18.9	0.11
Guardia Calda	GPC	T	585597.1	4370566.2	6.7	37.2	2405	26	5	4.8	-4.7	2.55E-03	0.04	8.11	2.4E+00	33.08	1.67E-04	15.2	0.11
Guardia Fredda	GPF	T	585589.1	4370565.2	6.9	37.4	2413	37	100	4.4	-5.8	6.24E-04	0.07	11.76	4.6E-01	11.96	1.97E-04	3.2	0.13
Sambiase 1	Sam1	T	609125.3	4314733.7	6.6	36.8	2292	42		6.0	-5.1	2.59E-03	0.03	9.95	1.2E-01	14.27	1.93E-04	13.4	0.14
Sambiase 2	Sam2	T	609074.3	4314786.3	6.8	35.9	2520	87	60	4.9	-6.7	1.12E-03	0.12	12.65	8.1E-02	10.46	1.63E-04	6.9	0.13
Sambiase fiume	SamF	T	609053.0	4314732.1	6.6	20.3	1690	49		5.9	-4.5	2.69E-03	0.05	11.14	1.2E-01	12.88	1.86E-04	14.5	0.15
Sulfurea Cotronei	Cotr.S	T	657615.3	4338191.2	8.0	36.6	1995	118	0.6	0.8	-9.9	7.69E-05	0.08	13.09	2.0E-01	36.57	1.89E-04	0.4	0.51

Cotronei P. Coniglio	Cotr.PC	T	656593.0	4337113.0	7.7	35.2	15350	-7	1	1.1	-6.4	5.02E-02	0.11	22.60	4.5E-01	0.10	4.35E-04	115.3	0.08

Table II.2 | Chemical composition of Calabrian waters. Major ion water chemistry, Index Saturation for Calcite, Dolomite and Gypsum and lithology of host rocks acquifer

ID	Ca2+	Mg2+	Na+	K+	HCO3	F-	Cl-	NO3-	SO4 2-	SI	SI	SI	Host Rocks
	mmol/l	mmol/l	mmol/l	mmol/l	mmol/l	mmol/l	mmol/l	mmol/l	mmol/l	Calcite	Dolomite	Gypsum	Type
FS	2.07	0.64	0.81	0.18	4.15	0.06	0.94	0.003	0.99	0.3	0.2	-1.9	Limestone
SC	2.03	0.58	0.78	0.17	3.90	0.06	0.86	<d.l.	0.94	0.1	0.3	-1.9	Limestone
SXC	2.04	0.59	0.76	0.16	3.80	0.06	0.85	<d.l.	0.97	-0.2	0.1	-1.9	Limestone
RC	2.11	0.69	0.71	0.14	3.63	0.07	0.78	0.01	1.33	1.5	1.0	-1.8	Limestone
RMC	2.03	0.71	0.71	0.14	3.43	0.07	0.79	0.01	1.38	1.1	0.8	-1.8	Limestone
SP	1.92	0.91	0.26	0.04	6.28	<d.l.	0.26	0.08	0.10	-0.1	0.2	-3.0	Limestone
SCE	2.16	0.73	0.74	0.15	3.88	0.07	0.82	0.004	1.45	0.1	0.3	-1.8	Limestone
SF	1.54	0.20	0.17	0.01	3.35	<d.l.	0.17	0.002	0.13	0.1	0.5	-2.9	Limestone
SC1	1.42	0.15	0.21	0.02	3.50	0.01	0.20	0.04	0.10	0.0	0.5	-3.1	Limestone
SC2	1.64	0.22	0.39	0.03	3.83	0.01	0.42	0.02	0.15	0.0	0.5	-2.8	Limestone
SS	1.24	0.47	0.11	0.01	3.78	<d.l.	0.10	0.004	0.03	0.9	0.7	-3.7	Limestone
ST	1.07	0.61	0.10	0.01	3.70	<d.l.	0.10	0.01	0.03	0.6	0.5	-3.7	Limestone
SSP	1.06	0.45	0.12	0.01	3.53	<d.l.	0.13	0.02	0.02	-0.1	0.2	-3.7	Limestone
SFo	1.06	0.47	0.17	0.01	3.43	<d.l.	0.19	0.03	0.03	-0.6	-0.1	-3.7	Limestone
SFo2	1.08	0.47	0.17	0.01	3.43	<d.l.	0.20	0.03	0.04	-0.3	0.1	-3.6	Limestone
				0.00									
SG	1.23	0.86	0.15	0.01	4.43	0.02	0.11	0.02	0.12	-0.1	0.1	-3.1	Limestone
Ab2	2.64	1.08	0.23	0.01	3.88	0.01	0.17	0.02	1.91	-0.2	0.1	-1.7	Limestone
AbS	2.69	1.45	0.19	0.01	5.38	0.05	0.19	0.02	2.03	-0.1	0.1	-1.7	Limestone

Ab	0.83	0.43	0.12	0.01	2.70	0.01	0.12	0.03	0.07	-0.4	0.0	-3.4	Limestone
Ab well	1.81	0.45	0.25	0.02	5.13	0.01	0.23	0.02	0.15	-0.3	0.2	-2.8	Limestone
GdN	2.23	0.79	3.36	0.13	4.15	0.10	3.51	<d.l.	1.37	0.2	0.3	-1.8	Limestone
Sib1	2.64	1.60	1.59	0.09	4.43	0.10	0.94	<d.l.	3.15	0.3	0.2	-1.4	Limestone
Sib2	2.81	1.65	1.61	0.09	4.25	0.10	0.95	<d.l.	3.21	0.3	0.2	-1.4	Limestone
IC02P	1.70	0.87	0.28	0.03	4.52	0.00	0.22	0.02	0.05	-1.7	-0.7	-3.3	Limestone
ICP06P	0.84	3.57	0.30	0.07	7.52	<d.l.	0.26	0.02	0.53	-0.3	-0.4	-2.7	Serpentinites
ICP07P	0.51	2.25	0.40	0.28	4.61	<d.l.	0.42	0.50	0.19	-1.4	-1.0	-3.3	Serpentinites
IC09P	0.34	1.86	0.36	0.25	3.93	<d.l.	0.32	0.14	0.13	-1.6	-1.1	-3.6	Serpentinites
IC10P	0.30	2.39	0.33	0.06	4.33	<d.l.	0.31	0.12	0.14	-1.7	-1.3	-3.7	Serpentinites
IC11P	1.17	0.17	0.33	0.17	2.67	<d.l.	0.24	0.08	0.06	-3.0	-1.1	-3.3	Limestone
IC14P	1.19	0.45	0.29	0.08	1.61	<d.l.	0.33	0.03	0.62	-3.1	-1.3	-2.4	Limestone
IC15P	1.32	0.48	0.34	0.04	3.46	<d.l.	0.14	0.01	0.15	-2.1	-0.8	-2.9	Limestone
ID02P	0.76	0.91	0.25	0.02	8.10	<d.l.	0.24	0.02	0.07	-1.0	-0.5	-3.5	Limestone-conglomerate
ID03P	0.37	0.99	0.24	0.01	4.56	0.004	0.17	0.09	0.10	-2.0	-1.2	-3.6	Serpentinites
ID04P	0.83	1.43	0.32	0.01	11.19	<d.l.	0.55	0.29	0.11	-0.7	-0.4	-3.3	Gneiss
ID05P	0.89	1.26	0.33	0.02	8.34	<d.l.	0.30	0.00	0.11	-0.7	-0.4	-3.3	Gneiss
ID08P	0.32	1.35	0.25	0.08	7.23	<d.l.	0.25	0.12	0.13	-1.2	-0.9	-3.6	Serpentinites
ID12P	0.80	1.48	0.30	0.02	6.82	<d.l.	0.32	0.01	0.08	-1.1	-0.7	-3.5	Gneisses
ID17P	1.13	0.11	0.18	0.03	4.88	<d.l.	0.18	0.07	0.06	-2.2	-0.5	-3.4	Limestone
ID18P	1.24	0.12	0.17	0.01	5.16	0.003	0.18	0.02	0.06	-2.5	-0.7	-3.3	Limestone
ID19P	0.95	0.06	0.20	0.01	6.51	<d.l.	0.21	0.16	0.05	-2.1	-0.4	-3.5	Limestone

ID20P	0.89	0.53	0.09	0.01	5.28	0.003	0.10	0.01	0.12	-2.1	-0.9	-3.2	Limestone
ID21P	2.13	0.36	0.48	0.04	4.42	<d.l.	0.51	<d.l.	0.07	-2.0	-0.6	-3.1	Limestone
ID22P	0.71	0.88	0.24	0.02	7.92	<d.l.	0.25	0.02	0.07	-1.0	-0.5	-3.5	Limestone-conglomerate
ID23P	0.78	0.86	0.26	0.02	8.08	<d.l.	0.22	0.02	0.06	-1.0	-0.5	-3.6	Limestone-conglomerate
ID24P	0.96	0.68	0.24	0.02	8.13	<d.l.	0.25	0.02	0.08	-0.8	-0.3	-3.4	Gneiss
GV	1.08	0.05	6.70	0.08	7.35	0.00	3.57	<d.l.	3.59	-2.7	-0.8	-1.6	Plutonic rocks(acid)
An	27.55	64.38	130.45	0.75	3.30	0.00	98.20	<d.l.	47.20	0.7	0.1	-0.2	Plutonic rocks(acid)
Gpcar	7.45	2.12	52.47	1.94	6.40	0.00	41.61	<d.l.	12.90	-1.1	-0.4	-0.7	Gneisses
GPC	7.47	2.08	57.32	1.79	3.70	0.00	41.91	<d.l.	0.17	-0.4	-0.1	-2.4	Gneisses
GPF	2.94	1.04	14.39	0.46	3.70	0.00	10.30	<d.l.	14.15	-1.0	-0.3	-0.9	Gneisses
Sam1	8.22	4.40	6.00	0.28	4.30	0.00	3.39	<d.l.	14.76	-0.1	-0.3	-0.3	Gneisses
Sam2	8.22	4.38	5.97	0.25	4.00	0.00	3.37	<d.l.	14.93	0.1	0.0	-0.3	Gneisses
SamF	7.59	4.08	5.46	0.25	4.05	0.00	3.05	<d.l.	13.69	-0.4	-1.0	-0.3	Gneisses
Cotr.S	11.78	11.65	47.94	0.30	0.88	0.00	49.50	<d.l.	25.05	1.3	0.6	-0.4	Granites/Granodiorites
Cotr.PC	4.57	4.52	16.95	16.90	1.08	0.00	23.18	<d.l.	11.73	0.4	0.1	-0.9	Granites/Granodiorites

Table II.3 | Hydrogeological data for Calabria and Pollino Thermal water. CO_2 lost is the amount of CO_2 removed by secondary processes

FCdeep cor is the deep carbon flux corrected for the amount of CO_2 lost by secondary processes.

**Q is total value from the three spring; 1 data from Allocca et al., 2007 and De Vita et al., 2018; 2 data from http://www.ildistrettoidrograficodellappenninomeridionale.it

ID	Acquifer	Total Area	Q total	Unit Area	Q spring	FC_{deep}	CO_2 lost	FC_{deep} Cor
	Name	Km^2	m^3/s	km^2	m^3/s	mol yr^{-1} km^{-2}	%	mol yr^{-1} km^{-2}
FS	Mt.Alpi[1]	14.55	0.26	0.02	4.1E-04	8.1E+05	98.0	4.0E+07
SC				0.63	1.1E-02	6.9E+05	98.0	3.4E+07
SXC				0.57	1.0E-02	6.9E+05	97.6	2.9E+07
RMC				4.45	7.8E-02	5.0E+05	-	-
SCE				1.14	2.0E-02	8.1E+05	-	-
GdN	Mt.Pollino[1]	275	7.69	2.50	7.0E-02	7.6E+05	92.2	9.7E+06
Sib1				0.03	7.0E-04	1.6E+06	98.0	8.0E+07
Sib2				0.36	1.0E-02	1.3E+06	98.6	9.0E+07
GV	Le Serre[2]	1100	-	-	3.0E-03	8.0E+02	98.3	5.8E+04
An				-	5.0E-04		99.8	
GPCar	Catena Costiera[2]	765	-	-	5.0E-03	1.6E+04	93.6	2.0E+05
GPCar				-	5.0E-03		97.3	
GPF				-	1.0E-01		90.9	
Sam1**	Sila Piccola[2]	697	-	-	6.0E-02	1.0E+04	97.3	3.4E+05
Sam2**				-			94.7	
SamF**				-			97.6	
Cotr.PC	P.di Crotone[2]	316	-	-	1.00E-03	7.7E+01	99.9	1.9E+05
Total						7.1E+06		2.8E+08
Average						6.0E+05		2.8E+07

II.5. Discussion

In the following sections, we discuss the sources of fluids (both CO_2 and He) in the studied areas, and the secondary processes that affect the groundwater He–CO_2 signature during circulation and storage in the aquifers.

II.5.1. Helium

In natural fluids, He is typically fed by three distinct sources: the mantle, the crust and the atmosphere (e.g., Sano et al., 1997). Each of these sources has distinct He isotopic signature and $^{4}He/^{20}Ne$ ratio (>1,000 for crust and mantle, 0.295 for Air Saturated Water at 25°C; Sano et al., 1985; Ozima & Podosek, 2002). Therefore, the contributions of these three different sources can be solved by using binary mixing equations. Applying the approach of Sano et al., (1997), and assuming that all ^{20}Ne is of atmospheric origin, we estimate low atmospheric contributions (< 10%) for the thermal samples, along with small percentages (up to 2-3%) of mantle He contribution, in agreement with the data reported by Italiano et al., 2010 (Fig. II.8).

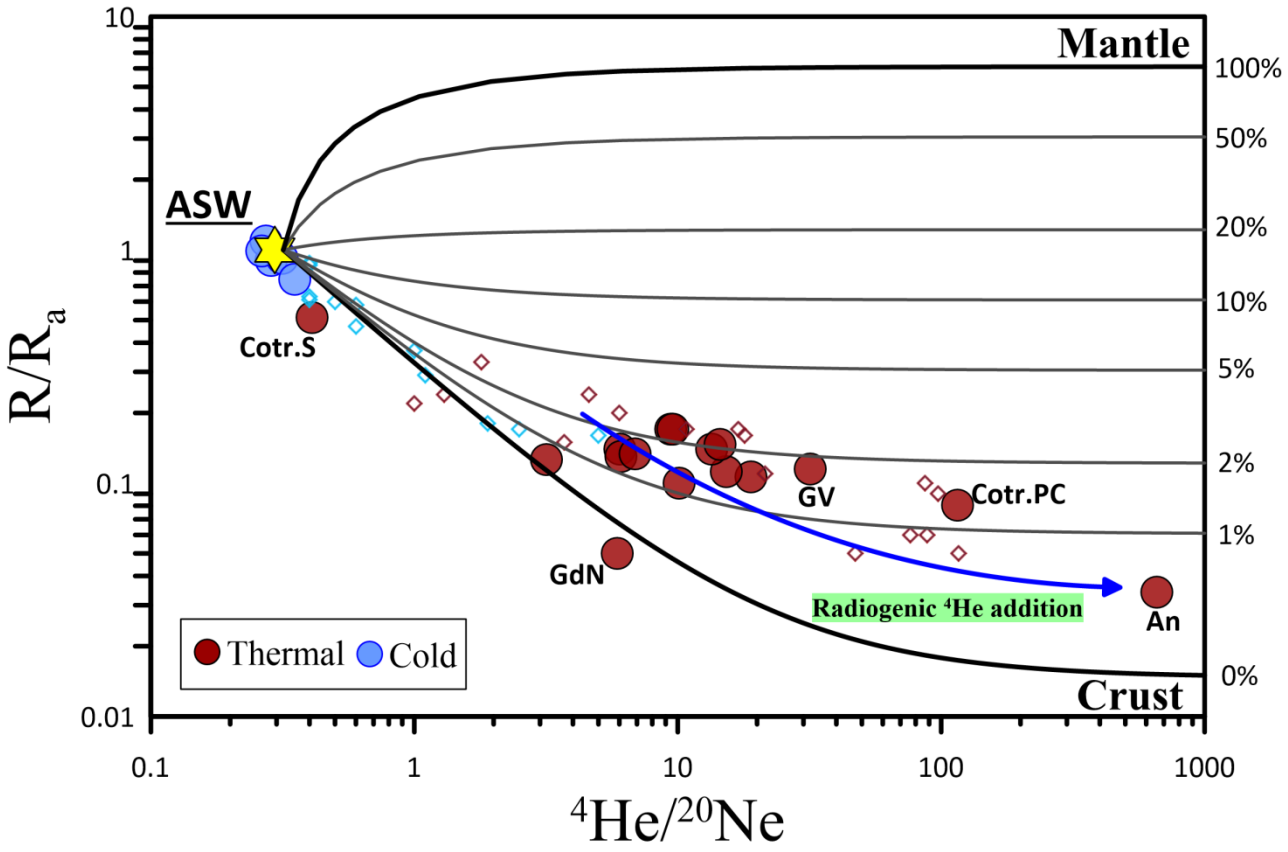

Figure II.8 | $^{3}He/^{4}He$ ratios (expressed as R/R_a) versus $^{4}He/^{20}Ne$ ratios. All samples fall along mixing lines between three possible end-members characterized by distinct He isotopic signatures: 1 Ra, for Air saturated water (ASW; Ozima & Podosek, 2002), 0.01–0.02 Ra, for pure crustal fluids dominated by radiogenic ^{4}He produced by U and Th decay (Ballentine & Burnard, 2002) and 6.1 ± 0.9 Ra, for the European Subcontinental Lithospheric Mantle, ESCLM (Gautheron & Moreira, 2002) and $^{4}He/^{20}Ne$ values ($^{4}He/^{20}Ne$ ratios >1,000 for crust and mantle and 0.295 for ASW respectively ;Sano et al., 1985; Ozima & Posek, 2002). Thermal samples show helium isotopic composition near the crustal value of 0.02 R_a with small percentages of mantle contribution (2-3%) and negligible atmospheric contamination while cold waters and only one thermal sample show ASW-like composition. Data for comparison (small diamonds) from Italiano et al., 2010.

Dissolved gases from the cold waters and one thermal sample (Cotr.S) have an ASW-like composition, which indicates an high atmospheric contamination probably due to a shallow hydrological circuit. We find a statistically significant (R^2=0.91) positive correlation between He isotopic composition with 1/He concentration (Fig. II.9). The lower (relative to cold waters) R/Ra values of the He-rich thermal waters is thus explained by the addition of crustal He, rich in radiogenic ^{4}He produced by U and Th decay (Ballentine & Burnard, 2002), during deep/prolonged

circulation in the crust. It is noteworthy that the He enriched samples have been collected in areas geologically-dominated by metamorphic rocks characterized by high U and Th concentrations (e.g., 3.3 ppm of U and 19.4 ppm of Th for the "Sila" gneiss; Micheletti et al., 2007; 297 ppm of U and 155 ppm of Th for zircons from the "Catena costiera" gabbros; Liberi et al., 2011). Hence, it is reasonable that these low He isotopic ratios reflect, in addition to possible long residence times, also the high radiogenic ^{4}He production in such U-Th-rich lithologies.

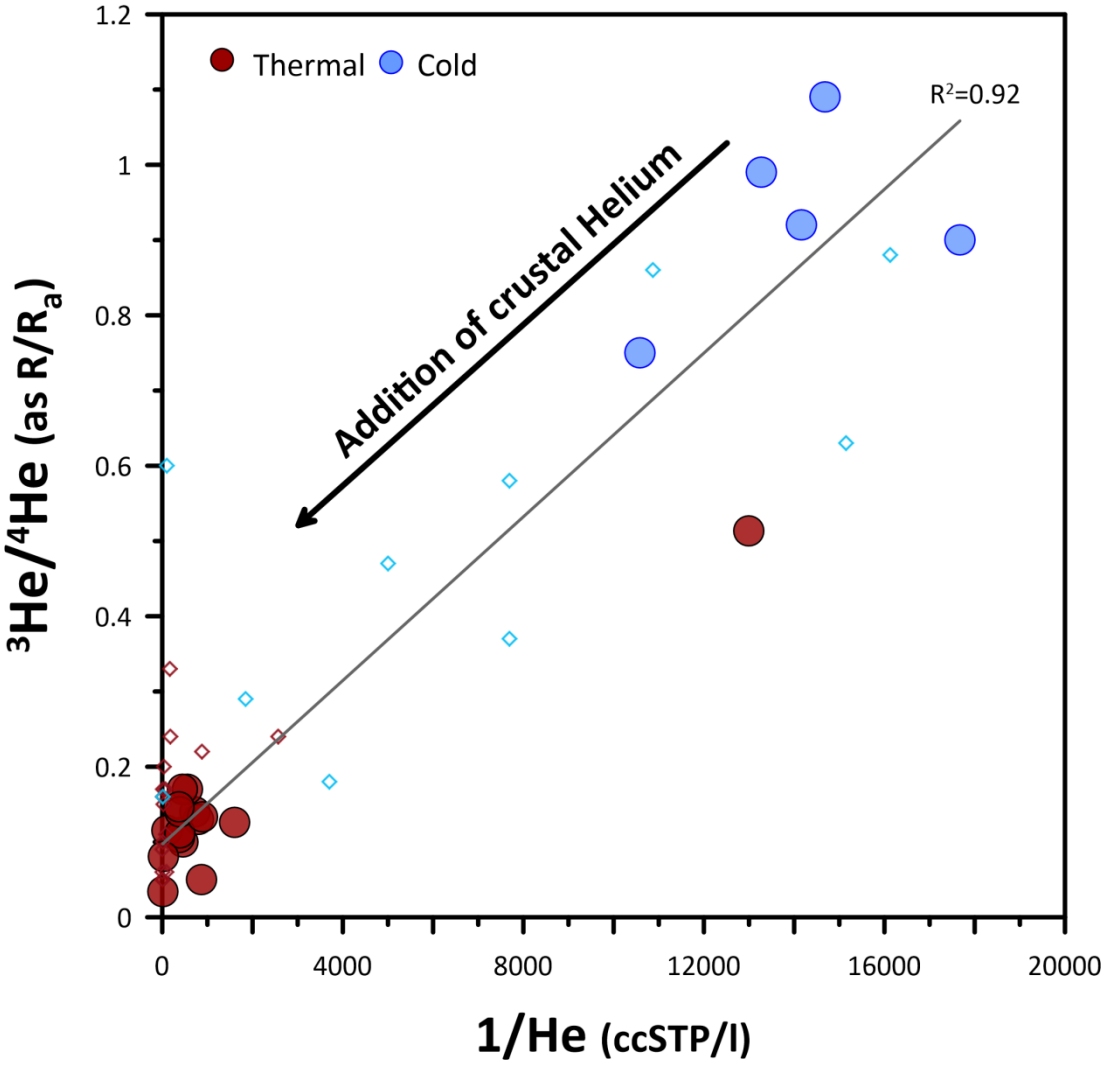

Figure II.9 | ^{3}He/^{4}He vs 1/He. A good correlation between Helium isotopic composition and Helium concentrations (R^2=0.91) is found. The lower R/R_a values can be explained by an addition of crustal radiogenic ^{4}He to the thermal waters that also shifts the He isotopic ratio from the ASW-like values (1Ra; 1/He=24000) towards the crustal radiogenic end-member (0.01-0.02Ra). In this scenario, the samples which show higher He values and lower ^{3}He/^{4}He could be interested by longer residence periods in the crust. Small blue and red diamonds are data from Italiano et al., 2010.

II.5.2. Carbon

The relationship between the total dissolved carbon (TDIC) and its isotopic composition ($\delta^{13}C_{TDIC}$) can provide additional constraints on the sources of fluids. Indeed, deeply rising fluids ascending through the crust interact with rocks and groundwaters that cause changes in carbon abundance and its isotopic composition (e.g., Randazzo et al., 2021). From the carbon mass balance approach developed by Chiodini et al. (2000, 2020), we estimate, for each sample, the external carbon contribution, C_{ext}, (i.e., the C fractions not resulting from carbonate rock dissolution) and its isotopic composition $\delta^{13}C_{ext}$ (see paragraph II.3.2). The relationship between C_{ext} and $\delta^{13}C_{ext}$ suggests the presence of three distinct carbon sources in the studied groundwaters (Fig. II.10). The cold waters fall along the mixing lines (green lines in Fig. II.10) between a meteoric component (C_{ext}= 0.03 mmol/l; $\delta^{13}C_{ext}$= -7 to -5.5‰; Apollaro et al., 2020; Chiodini et al., 2011) and a set of end members whose isotopic compositions are in the range of biogenic CO_2 (i.e., $\delta^{13}C$ from -20‰ to -28‰; Deines et al., 1974; Hoefs, 2018; Valley and Cole, 2019). We ascribe this component to biogenic (soil) CO_2 dissolving into groundwaters during their infiltration. Conversely, the samples characterized by more positive $\delta^{13}C_{ext}$ values (thermal waters) imply the addition to the shallow CO_2 component with heavier isotopic signature ($\delta^{13}C$ of ~-1‰). This heavy C signature matches well that of deep (crustal/mantle) CO_2 released along the Apennine (Chiodini et al., 2020,2004). However, also in light of the He isotope evidence above (Fig.II.8), a major mantle C contribution is very unlikely, and we conclude, therefore, that the thermal water are dominated by a crustal CO_2 component.

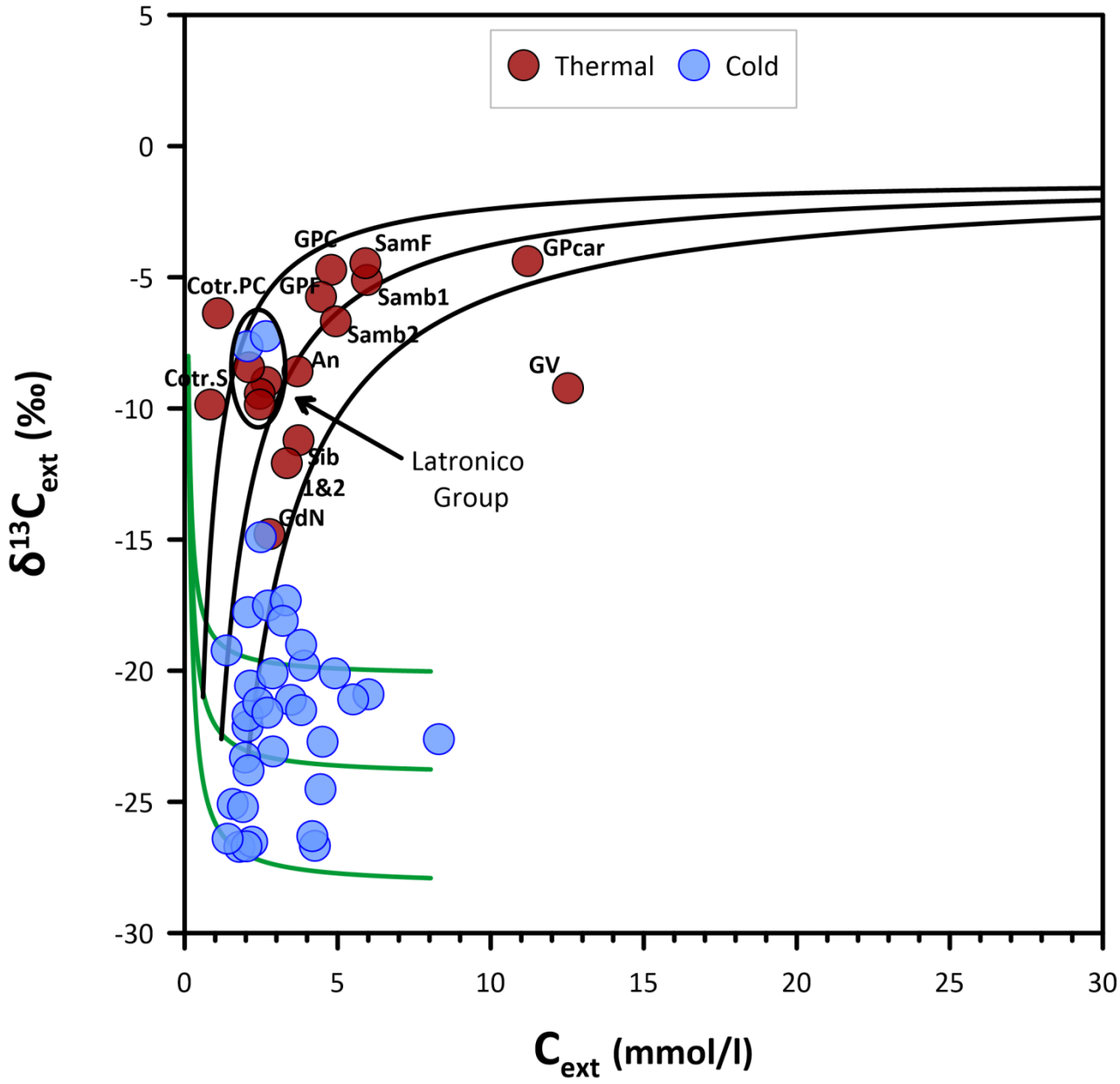

Figure II.10 | C_{ext} vs. $\delta^{13}C_{ext}$ diagram. Cold waters show the lowest C_{ext} and $\delta^{13}C_{ext}$ values with a negative correlation between the two variables due to the dissolution of isotopically "light" biogenic CO_2 falling along the mixing lines (green) between the infiltration water and the biogenic CO_2 end members ($\delta^{13}C$ of -20‰, -24 ‰ and -28 ‰) while thermal waters are characterized by higher $\delta^{13}C_{ext}$ values linked to the presence of deep CO_2 source end member. The theoretical curves have been computed considering C_{inf} (carbon linked to infiltration processes) contents of 1, 2 and 3 mmol/l and carbon isotopic composition for deep end member of -1‰ (black lines).

In collisional contexts, large crustal CO_2 fluxes (Guo et al., 2021; Girault et al., 2014; Menzies et al., 2018; Evans, 2011; Skelton, 2011; Perrier et al., 2009; Becker et al., 2008; Gaillardet & Galy, 2008) can be sustained by either regional metamorphism (e.g. Groppo et al.,2013; Eberhard & Pettke, 2021) or mechano-chemical CO_2 production (e.g. Italiano et al., 2009). Metamorphic processes can operate via either i) decarbonation reactions at relatively high temperatures within calc-silicate rocks (Groppo et al.,2013, 2017,2020), or ii) dehydration reactions of mineral phases (Eberhard & Pettke, 2021), in which CO_2 degassing is triggered by prograde heating arising from conductive heating triggered by slab breakoff (von Blanckenburg and Davies, 1995), slab rollback (Sizova et al., 2019), or by thermal relaxation of the crust following tectonic thickening upon continent–continent collision. These processes may operate in combination and have certainly interested the past evolution of Calabrian arc. Notably, metamorphic reactions can have large CO_2 yield not only where calc-silicate minerals in high grade rocks and/or limestones are abundant, but also in contexts with relatively few carbonate rocks and/or where siliciclastic metasediments with low carbon contents (<2 wt.% C, Pitcairn et al., 2006) prevail. As mentioned, the entire study area is made up of important metamorphic complexes (e.g., Tursi et asl., 2021) that include metabasic rocks, felsic granulites, metapelites and metacarbonate rocks (Schenk, 1984). The conditions for metamorphic CO_2 production are thus certainly met in the study area. Because such metamorphism occurs at very slow rates, amagmatic CO_2 mobilisation along convergent plate boundaries can endure over millions of years (Eberhard & Pettke, 2021). Considering that the sampled springs fall on major active tectonic discontinuities, responsible for the regional crustal seismicity (Rovida et al., 2019, 2020; Neri et al.,2006, 2020) and for the circulation and discharge of the thermal waters themselves (Vespasiano et al., 2021,2015,2012; Apollaro et al., 2020,2019,2012; Tiberti et al., 2017; Italiano et al., 2010), it is likewise possible that mechano-chemical CO_2 production is an additional source for crustal CO_2, as already proposed for other active seismic areas as Central Apennines (Italiano et al., 2008), eastern Alps (Italiano et al., 2009) and Japan (Nojima fault; Famin et al., 2008).

II.5.3. C/^{3}He relationship

During their migration and storage in the crust, fluids can undergo different processes that modify their chemical and isotopic composition. Insights into these processes, and into volatile sources and sinks, can be derived from a joint analysis and interpretation of He and C isotopic signatures (e.g., Randazzo et al., 2021; Barry et al.,2020; Holland & Gilfillan, 2013). In order to reconstruct the original signature of deeply sourced fluids, the samples that are dominated by the atmosphere sourced volatiles (e.g., the cold water) are initially filtered out. Biogenic carbon can derive from soil or from deep source as thermal decarboxylation and pyrolysis of organic matter into metapeliti ($\delta^{13}C$ from -30 to -20‰, Evans et al., 2008). In light of the He isotope evidence it is reasonable to think that the carbon present in cold waters come from shallow environments (i.e., soil). In fact, carbon from thermal decarboxylation and pyrolysis should be linked to high He concentrations and crustal isotopic signature while the cold water are characterized by atmosphere derived He. Then, we analyse the remaining sample in a $\delta^{13}C_{ext}$ vs $C_{ext}/^3He$ ratio space (Fig. II.11), in which the potential C-He sources typically plot in distinct compositional fields: mantle, and two crustal sources (biogenic vs crustal-metamorphic) (modified by Sano & Marty, 1995).

We find our samples have $C_{ext}/^3He$ ratios of $4.4x10^9$ to $9.1x10^{11}$ that, coupled with $\delta^{13}C_{ext}$ values, would be consistent with a mixing between crustal-metamorphic ($C_{ext}/^3He$= $1x10^{13}$ and δ^{13}Cext=-3‰ to +3‰; Evans et al., 2008; Becker et al., 2008; Dai et al., 1996; Sano & Marty, 1995) and mantle ($CO_2/^3He$= $2\text{-}4x10^9$ and $\delta^{13}C$=-4‰; Marty et al., 2020) fluids in proportions of 88% and 12% (average values; biogenic component would account for 0.8%). However, mantle component fractions (up to 91%) are much higher than calculated above from helium isotopes (2-3%, Fig. II.8). This discrepancy can be reconciled taking into account the impact of secondary processes on both $C_{ext}/^3He$ ratios and $\delta^{13}C_{ext}$.

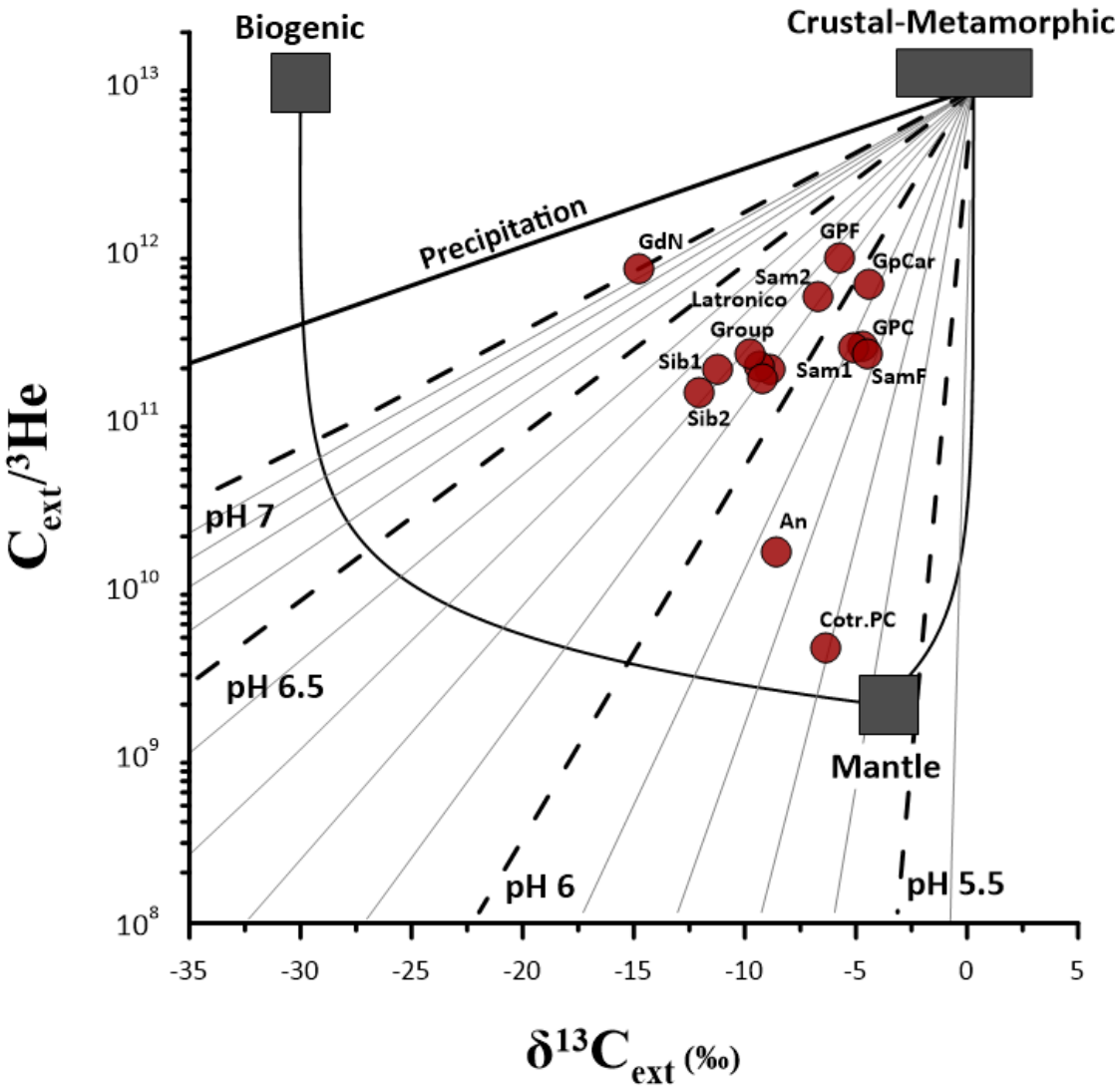

Figure II.11 | $\delta^{13}C_{ext}$ versus $C_{ext}/^3He$ plot. Changes in $\delta^{13}C$ are calculated following the method from Gillfillan et al. (2009) using the Rayleigh fractionation equation either for precipitation or for dissolution. In the case of precipitation there is zero ^3He loss from the CO_2 phase and $CO_2/^3He$ changes in proportion to the fraction of the remaining CO_2 phase while for CO_2 dissolution, the change in $CO_2/^3He$ ratio is calculated following the Rayleigh equation. The gradual loss of CO_2, with a decrease in the $C_{ext}/^3He$ ratio and the $\delta^{13}C$ according with Rayleigh-type gas dissolution at different pHs is showed from broken lines and slim solid lines while the predicted trend for carbonate mineral precipitation from the black solid line. Deep end member with $C_{ext}/^3He=1x10^{13}$ (crustal range; Sano & Marty, 1995; O'Nions and Oxburgh, 1988) and $\delta^{13}C_{ext}$ from -3 to 3‰ (mean value of $\delta^{13}C$ for metamorphic CO_2 is 0.3‰; Dai et al.,1996; Hunt, 1996; Clark and Fritz, 1997; Evans et al., 2008). The computed model fit nicely the entire dataset with the samples most affected by secondary processes that have also the highest He concentrations and the lowest values of R/Ra.

II.5.4 Secondary processes

CO_2 and He have contrasting solubilities in water (e.g., Ellis and Golding, 1963; Vogel et al., 1970). As such, the two elements undergo selective gas/water partitioning as deeply rising fluids interact with aquifer(s), ultimately altering the $C_{ext}/^3He$ ratio. Carbon isotopes are likewise fractionated during gas-water interactions (e.g., Randazzo et al., 2021 and references therein). Thus, both elemental ratios and $\delta^{13}C$ can be severely modified by secondary processes such as gas dissolution in water, and solid phase (carbonate) precipitation (e.g., Barry et al., 2021; Randazzo et al., 2021; Gilfillan et al., 2009). We investigate the possible role of secondary processes (e.g., partial gas dissolution in water and calcite precipitation) during fluid transfer trough the crust by modelling (see Gillfillan et al., 2009) their impact on $C_{ext}/^3He$ ratios and $\delta^{13}C_{ext}$ (Figure II.11). The process can be modelled as (i) an open-system degassing (Rayleigh type) at isotopic equilibrium (between phases) and (ii) calcite precipitation (Gillfilan et al., 2009). We want to clarify that for a thick crustal sector as Calabrian orogen (thickness up to 38 km; Di Stefano et al., 2009) our model is evidently a simplified approach. He isotopes indicate a negligible mantle component in thermal waters (up to 2%), hence the mantle component computed by the C-He relationships (up to 91%) in a simple approach based on mixing between mantle and crustal end members could be an artefact. Assuming a crustal-metamorphic deep end-member ($C_{ext}/^3He$ of $1x10^{13}$; Sano & Marty, 1995; O'Nions and Oxburgh, 1988 and $\delta^{13}C_{ext}$ of 0.3‰, i.e. mean value for metamorphic CO_2; Becker et al., 2008; Evans et al., 2008; Dai et al.,1996; Fig. II.11) as pristine gas composition, in order to explain the variability of the $C_{ext}/^3He$ ratio and $\delta^{13}C_{ext}$ in the samples we used a 2 steps model : 1) the partial dissolution of He and CO_2 in groundwater and the progressive variation of the $C_{ext}/^3He$ ratio and $\delta^{13}C_{ext}$ in the residual gas (Fig. II.11) and 2) total dissolution of the residual gas (step 1) into a shallow groundwater. The computed model curves show increasing extents of gas dissolution, over a range of pH values at fixed temperature (30°C mean sample temperature). Noteworthy that even using different temperatures (from 10 to 40 °C), the models do not show significant

differences. The results of the modelling well fit the $C_{ext}/^3He$ ratio and $\delta^{13}C_{ext}$ of the thermal waters suggesting that processes of partial gas dissolution occur at depth. Despite this, we cannot exclude the lowest $\delta^{13}C$ values are not at least partially reflecting a biogenic origin (e.g. sample *GdN*), and carbonate precipitation (together with CO_2 dissolution at a lower pH than 5.7–7; Gillfillan et al., 2009) has not taken a role. In light of this, it is plausible to think that the amount of carbon (i.e. CO_2) present below the study area is much more than what we can measure on the surface and that it can be distributed along a multilayer aquifer of which we can only sample the final member. Our model in addition to highlights the role played by gas-water interaction in determining the composition of fluid released in the studied area also identifies a metamorphic CO_2 as a potential source of fluid.

II.5.5. Carbon fluxes

We here use the estimated external carbon contributions (C_{ext}) from thermal and cold waters (Fig. II.10) to constrain the external carbon outflow through the investigated Calabrian groundwater systems. For each site we combined the spring flow rates with computed C_{ext}. The so-calculated total C_{ext} flux is ~ $3.63x10^8$ mol yr^{-1} of which ~ $4.19x10^7$ mol yr^{-1} and ~ $3.21x10^8$ mol yr^{-1} from thermal and cold waters respectively. For the cold water we assume that all the C_{ext} is from a shallow biogenic source (i.e. $C_{ext}=C_{inf}$). This evidence is also supported by the presence of atmospheric He dissolved in the cold water, in contrast the thermal water are crustal-He rich (Fig. II.8 and Fig. II.10). Including the biogenic C contribution deconvolved from total C_{ext} (see paragraph II.3.2) for the thermal waters (C_{inf}= 8.78 x 10^6 mol yr^{-1}) the total C flux from biogenic source is $3.3x10^8$ mol yr^{-1}. This value, considering the difference in the flow rates, fits those computed for the groundwaters of the central Apennines, where a C from biogenic shallow source has been identified ($C_{inf}=5x10^9$ mol $yr^{-1;}$ Chiodini et al., 2020).

As $C_{deep} = C_{ext} - C_{inf}$, assuming that also for the thermal waters the biogenic component (C_{inf}) is shallow (i.e., soil carbon from biogenic source) the deep carbon budget is obtained by multiplying the dissolved C_{deep} content by the relative water flow rate (see paragraph II.3.2). The total deep-derived CO_2 output associated to the investigated waters is $\sim 2.6\times10^{7}$ mol yr^{-1}. However, this value is not representative of the flux from the entire Calabrian orogen and is closely related to the flow rates of the investigated springs as shown by Figure II.12a. Therefore, in order to better compare the contribution of deep carbon released from different areas, we also computed for each spring the specific flux, i.e. the deep carbon outputs normalized for the catchment areas (see paragraph II.3.2). We estimate a value of $2.6x10^{7}$ mol yr^{-1} of deep carbon for the thermal water. Including the percentage of carbon lost due to secondary processes (section II.5.4) we estimate a value of $6.1x10^{8}$ mol yr^{-1} (Fig. II.12 b) of deeply derived carbon that for an area of 2880 km^2 (Table II.3) produce a specific flux of $2.1x10^{5}$ mol km^{-2} yr^{-1}.

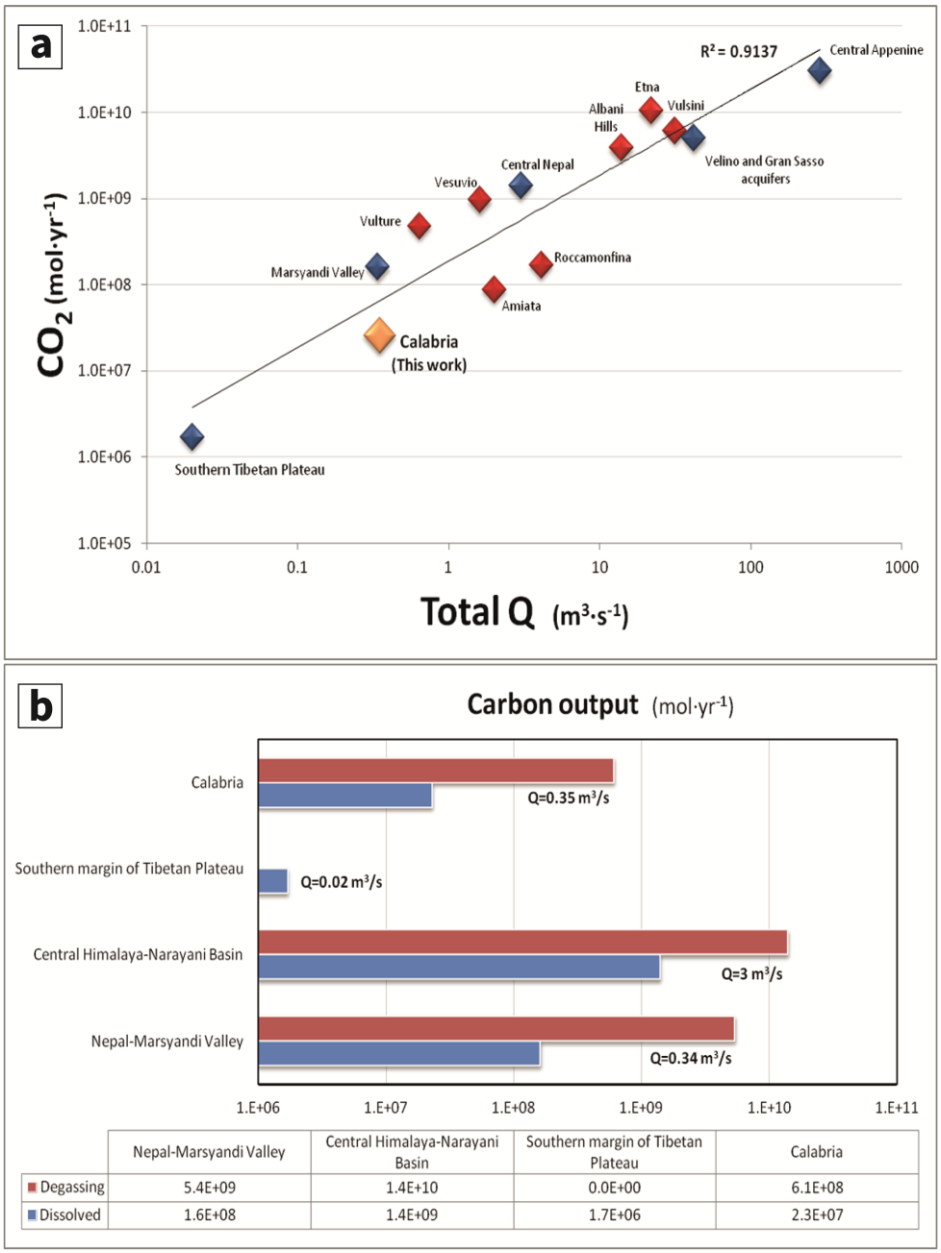

	Nepal-Marsyandi Valley	Central Himalaya-Narayani Basin	Southern margin of Tibetan Plateau	Calabria
Degassing	5.4E+09	1.4E+10	0.0E+00	6.1E+08
Dissolved	1.6E+08	1.4E+09	1.7E+06	2.3E+07

Figure II.12 | CO_2 budget for thermal water. **a**) CO_2 budget vs total flow rate for different volcanic and non-volcanic acquifers. The CO_2 budgets are closely related to the flow rates of the investigated springs. The values for CO_2 lost for secondary processes are not included in this budgets. Blue diamonds= Non Volcanic Area; Red Diamonds= Volcanic Area. Data from Caracausi et al., 2015, Becker et al., 2008, Evans et al., 2008, Newell et al., 2008 and Chiodini et al., 2004); **b**) Differnce in carbon output with and without considering loss of CO_2 due to secondary processes. The difference between values is one order of magnitude and is in line with the difference range defined by others studies from collisional orogen (Becker et al., 2008, Evans et al., 2008, Newell et al., 2008). While for the Calabrian orogen the carbon output refers to C_{deep} (i.e without C from biogenic origin) other values refers to Total carbon. Therefore considering only the carbon from deep origin (i.e metamorphic) the values could be lower.

This value range from two order of magnitude lower to the same order of CO_2 fluxes defined for some volcanic acquifers (dissolved in Fig. II.13; e.g., Etna $5.7x10^6$ mol $km^{-2}yr^{-1}$, Vulcano $3.4x10^6$ mol km^{-2} yr^{-1}, Mammoth Mountain $1.7x10^7$ mol km^{-2} yr^{-1}, Mt. Amiata $1.1x10^6$ mol km^{-2} yr^{-1}, Roccamonfina $4.8x10^5$ mol km^{-2} yr^{-1}; Caracausi et al., 2015 and reference therein). Compared with a values from active tectonic region and collisional orogen (violet gradient background in Fig. II.13) our result is one order of magnitude lower than deep CO_2 flux estimated for the Central Appenine ($2.4x10^6$ mol km^{-2} yr^{-1}; Chiodini et al., 2000) and well fitted the range of values estimated for some Himalayan areas. In the latter case, our values are higher than those calculated for the Southern margin of Tibetan Plateau ($9.9x10^3$ mol km^{-2} yr^{-1}; Newell et al., 2008), of the same order for the Narayani Basin ($4.4x10^5$ mol km^{-2} yr^{-1}; Evans et al., 2008) and one order of magnitude lower than flux values estimated by Becker et al. (2008) for the Marsyandi Valley area ($1.1x10^6$ mol km^{-2} yr^{-1}). For the Marsynadi Valley and Narayani basin the values estimated included the CO_2 lost for degassing processes, but no correction relating to the carbon content link to carbonate dissolution or to biogenic source was made. Therefore is probable that the values relating to the deep CO_2 are slightly lower. In any case, the values calculated for the Calabria region are comparable to those of areas in which a strong outgassing of CO_2 from metamorphic source has been identified. We want to clarify that our estimate has many assumptions, and thus an unknown uncertainty, but our intent here is to present a possible limits on CO_2 fluxes for the Calabria region. However, if accurate, our values suggest that the Calabrian orogen is an important contributor to the global carbon budget today.

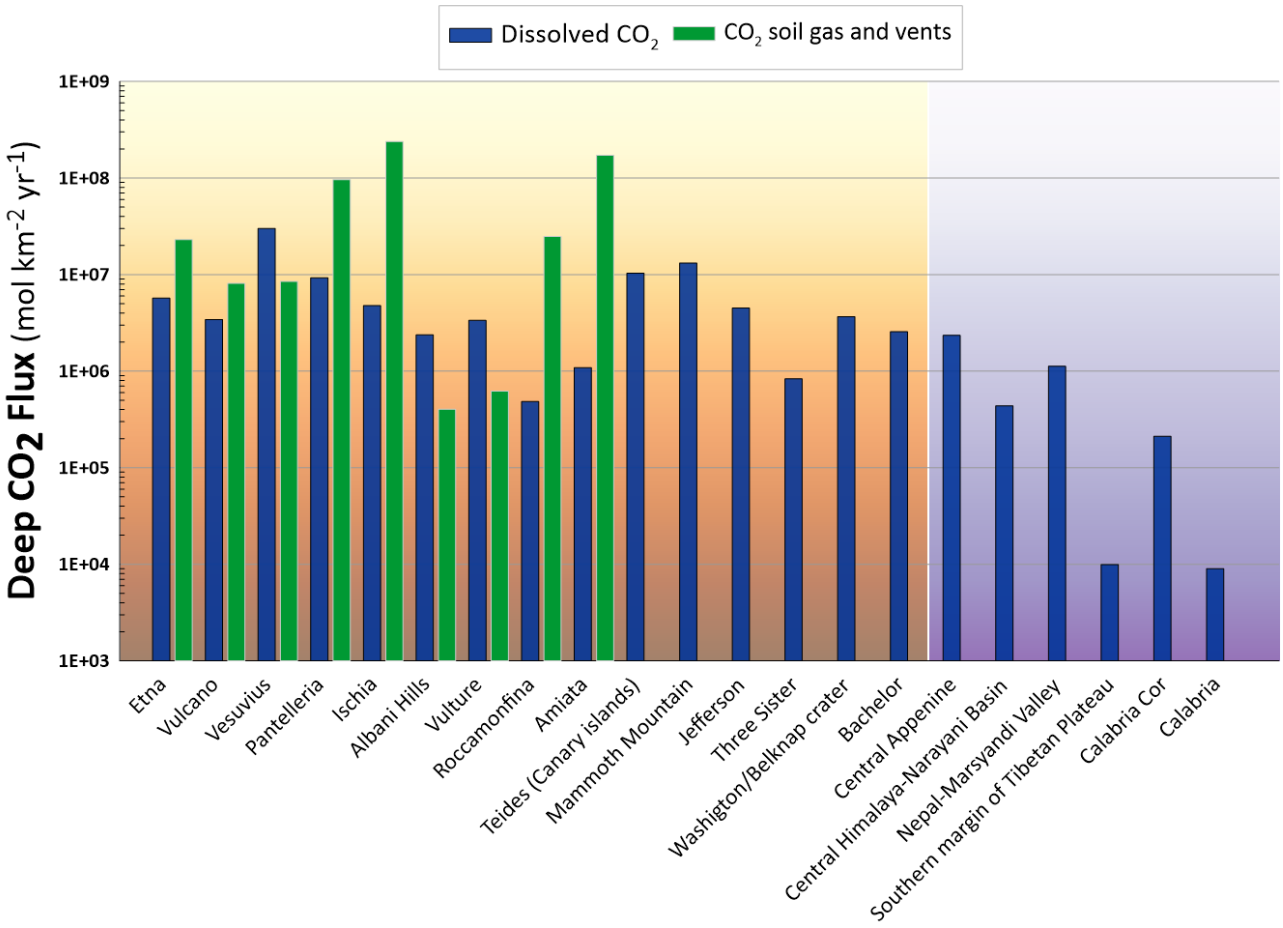

Figure II.13 | Deep CO_2 flux from volcanic and non-volcanic areas. *Calabria Cor* include the percentage of deep CO_2 lost for secondary processes (section 5.4). Marsyandi Valley and Narayani Basin values refers to Total C without extrapolation for biogenic and deep component and included CO_2 lost for degassing processes (Becker et al., 2008, Evans et al., 2008). Orange-yellow background for volcanic areas; Purple background for Non-Volcanic areas. Southern Tibetan Plateau from Newell et al., 2008. Modified after Caracausi et al., 2015.

6. Summary

Understanding carbon isotopic signatures and the processes that affect them are critical to make accurate CO_2 flux estimates and identify the origin of carbon. In this work, we investigate sources and sinks of fluid dissolved in groundwaters from Pollino and Calabria region. Chemical and isotopic composition (He and C) of sampled waters allowed to identify two different domains: (i) a shallow system dominated by gas components of atmospheric signature (He) and biogenic origin (C), and (ii) a deeper system in which crustal/deep fluids (CO_2, He) are dominant.

The external carbon contributions have been calculated following the mass balance approach and coupled with helium data allowed to identify a deep CO_2 (i.e. crustal/metamorphic) associated to the fluids released in the hydrothermal basins and to detect secondary process (dissolution/precipitation) which modify the pristine chemical and isotopic composition of fluids, affecting the deep carbon budget. Samples with highest He concentrations and lowest $^3He/^4He$ ratios also result the most affected by carbon removal processes. This could indicate longer residence time in the crust and/or more complex circulation system (multy-layer) of which the sampled water are only the last member. We also proposed metamorphic processes as a source of CO_2, but on this way more studies are required.

For the investigated springs a total deep-derived CO_2 output of $\sim 2.6\times10^7$ mol yr^{-1} was computed, but the value strongly depends on the flow rates and not represent the flux from the entire Calabrian orogen. Extrapolating from our model, the percentage of CO_2 lost due to secondary processes we estimated a maximum value of $6.1x10^8$ mol yr^{-1} for the deeply derived carbon. Scaling our estimate of deep CO_2 flux to the whole study area (2880 km^2) a value of $2.1x10^5$ mol km^{-2} yr^{-1}. The value compares to other globally significant carbon fluxes as that define for the Himalaya orogen and Central Appenine in Italy and despite the considerable uncertainties, represents the first estimate of CO_2 flux for the Calabria region based on field sampling and modelling of secondary processes facilitating a comparisons with estimates from other collisional orogens. Given the extent of flux values extrapolated, we emphasize that more studies should be conducted to implement knowledge on possible sources, circulation systems and deep CO_2 release by defining the contribution that a collision area such as Calabrian arc can provide to the global carbon budget.

References

Allocca, V., Celico, F., Celico, P., De Vita, P., Fabbrocino, S., Mattia, S., Tranfaglia, G. (2007). Note illustrative della Carta idrogeologica dell'Italia meridionale. [Illustrative notes of the Hydrogeological map of southern Italy]. Istituto Poligrafico e Zecca dello Stato, ISBN 88-448-0215-5 (p. 211), ISBN 88-448-0223-6 (3 maps included).

Acquafredda, P., Lorenzoni, S., & Zanettin Lorenzoni, E. (1994). Paleozoic sequences and evolution of the Calabrian Peloritani Arc (Southern Italy). Terra Nova, 6, 582–594.

Aiuppa, A., Fischer, T. P., Plank, T., & Bani, P. (2019). CO_2 flux emissions from the Earth's most actively degassing volcanoes, 2005–2015. Scientific Reports, 9, 5442. https://doi.org/10.1038/s41598-019-41901-y

Amodio Morelli, L., Bonardi, G., Colonna, V., Dietrich, D., Giunta, G., Ippolito, F., Liguori, V., Lorenzoni, S., Paglionico, A., Perrone, V., Picarretta, G., Russo, M., Scandone, P., Zanettin-Lorenzoni, E., Zappetta, A., 1976. L'arco calabropeloritano nell'orogene appenninico-magrebide. Mem. Soc. Geol. It. 17, 1–60.

Apollaro, C., Dotsika, E., Marini, L., Barca, D., Bloise, A., De Rosa, R., Doveri, M., Lelli, M., Muto, F., 2012. Chemical and isotopic characterization of the thermo mineral water of Terme Sibarite springs (Northern Calabria, Italy). Geochem. J. 46, 117–129.

Apollaro, C., Vespasiano, G., De Rosa, R., Marini, L., 2015. Use of mean residence time and flowrate of thermal waters to evaluate the volume of reservoir water contributing to the natural discharge and the related geothermal reservoir volume. Application to Northern Thailand hot springs. Geothermics 58, 62–74, 2015.

Apollaro, C., Vespasiano, G., Muto, F., De Rosa, R., Barca, D., Marini, L., 2016. Use of mean residence time of water, flowrate, and equilibrium temperature indicated by water geothermometers to rank geothermal resources. Application to the thermal water circuits of Northern Calabria. J. Volcanol. Geotherm. Res. 328, 147–158.

Apollaro, C., Buccianti, A., Vespasiano, G., Vard`e, M., Fuoco, I., Barca, D., Bloise, A., Miriello, D., Cofone, F., Servidio, A., De Rosa, R., 2019a. Comparative geochemical study between the tap waters and the bottled mineral waters in Calabria (southern Italy) by compositional data analysis (CoDA) developments. Appl. Geochem. 107, 19–33. https://doi.org/10.1016/j.apgeochem.2019.05.011.

Apollaro, C., Tripodi, V., Vespasiano, G., De Rosa, R., Dotsika, E., Fuoco, I., Critelli, S., Muto, F., 2019b. Chemical, isotopic and geotectonic relations of the warm and cold waters of the Galatro and Antonimina thermal areas, southern Calabria, Italy. Mar. Pet. Geol. 109, 469–483. https://doi.org/10.1016/j.marpetgeo.2019.06.020.

Apollaro, C., Fuoco, I., Brozzo, G., De Rosa, R., 2019c. Release and fate of Cr (VI) in the ophiolitic aquifers of Italy: the role of Fe (III) as a potential oxidant of Cr (III) supported by reaction path modelling. Sci. Total Environ. 660, 1459–1471.

Apollaro C., Caracausi A., Paternoster M., Randazzo P., Aiuppa A., De Rosa R., Fuoco I., Mongelli G., Muto F., Vanni E., Vespasiano G., Fluid geochemistry in a low-enthalpy geothermal field along a sector of southern Apennines chain (Italy), Journal of Geochemical Exploration, Volume 219, 2020, 106618, ISSN 0375-6742, https://doi.org/10.1016/j.gexplo.2020.106618.

Apollaro, C., Fuoco, I., Bloise, L., Calabrese, E., Marini, L., Vespasiano, G., Muto, F., 2021. Geochemical modeling of water-rock interaction processes in the Pollino National Park. Geofluids 17. https://doi.org/10.1155/2021/6655711.

Atzori P., Ferla P., Paglionico A., Piccarreta G., Rottura A., 1984. Remnants of the Hercynian orogen along the “Calabrian-Peloritan arc”, southern Italy: a review. *J. Geol. Soc.* London, 141: 137-145.

Ballentine, C. J., & Burnard, P. (2002). Production, release and transport of noble gases in the continental crust. *Reviews in Mineralogy and Geochemistry*, *47*(1), 481–538. https://doi.org/10.2138/rmg.2002.47.12

Barnes, I., Irwin, P. W. & White, D. E. Global Distribution of Carbon Dioxide Discharges, and Major Zones of Seismicity. Water Resour. Invest. WRI 78-39 (U.S. Geol. Surv., Washington, DC, 1978).

Barry, P.H., Nakagawa, M., Giovannelli, D., de Momor, J.M., Schrenk, M., Seltzer, A.M., Manini, E., Fattorini, D., di Carlo, M., Regoli, F., Fullerton, and K., Lloyd, K.G., 2019b. Helium, inorganic and organic carbon isotopes of fluids and gases across the Costa Rica convergent margin. Sci. Data 6 (1), 1–8.

Barry, P.H., Negrete-Aranda, R., Spelz, R.M., Seltzer, A.M., Bekaert, D.V., Virrueta, C., Kulongoski, J.T., 2020. Volatile sources, sinks and pathways: A helium-carbon isotope study of Baja California fluids and gases. Chem. Geol. 550, 119722.

Barry P. H., Bekaer D. V. t, Krantz J. A., Halldórsson S. A., de Moor J.M., Fischer T. P., Werner C., Kelly P. J., Seltzer A. M., Franz B. P., Kulongoski J. T., Helium-carbon systematics of groundwaters in the Lassen Peak Region, Chemical Geology, Volume 584, 2021, 120535, ISSN 0009-2541, https://doi.org/10.1016/j.chemgeo.2021.120535

Beccaluva, L., S. Chiesa, and M. Delaloye (1981), K/Ar age determinations on some Tethyan ophiolites, Rend. Soc. Ital. Mineral. Petrol., 37, 869 – 880.

Becker, J. A., Bickle, M. J., Galy, A. & Holland, T. J. B. Himalayan metamorphic CO_2 fluxes: quantitative constraints from hydrothermal springs. Earth Planet. Sci. Lett. 265, 616–629 (2008).

Bencini, A., Ciraco, G., 1982. Caratteristiche geochimiche di alcune acque termali della provincia di Catanzaro. Rendiconti SIMP 38, 1189–1195.

Berner, R.A., Lagasa, A.C., 1989. Modelling the geochemical carbon cycle. Sci. Am.260, 74–81.

Borsi, S., and R. Dubois (1968), Données géochronologiques sur l'histoire hercynienne et Alpine de la Calabre Centrale, C. R. Acad. Sci., Ser. D, 266, 72 – 75.

Boschi, E., Guidoboni, E., Ferrari, G., Mariotti, D., Valensise, G., and Gasperini, P. (2000). Catalogue of strong Italian earthquakes, 461 B.C. to 1997. Ann. Geofisc. 43, 609–868 (with database on CD-ROM). doi:10.4401/ag-3668

Brutto, F., Muto, F., Loreto, M.F., De Paola, N., Tripodi, V., Critelli, S., Facchin, L., 2016. The Neogene-Quaternary geodynamic evolution of the central Calabrian Arc: a case study from the western Catanzaro Trough basin. J. Geodyn. 102, 95–114.

Burton, M.R., Sawyer, G.M., Granieri, D., 2013. Deep carbon emissions from volca-noes. Rev. Mineral. Geochem.75, 323–354.

Calcara, M., Quattrocchi, F., 1993. Sulla Scelta di Siti Idonei al Monitoraggio Geochimico ai Fini Della Sorveglianza Sisimica Della Calabria Settentrionale: Valle Crati⁄ Piana di Sibari. Atti convegno nazionale GNGTS.

Castello, B., Selvaggi, G., Chiarabba, C., Amato, A., 2006. CSI, Catalogo della sismicità italiana 1981–2002, versione 1.1, INGV-CNT Roma. <http://www.ingv.it/CSI/>.

Catalano, S., De Guidi, G., Monaco, C., Tortorici, G., Tortorici, L., 2008. Active faulting and seismicity along the Siculo-Calabrian Rift Zone (Southern Italy). Tectonophysics 453, 177–192.

Capasso, G., and S. Inguaggiato (1998), A simple method for the determination of dissolved gases in natural waters: An application to the thermal waters from Volcano Island, Appl. Geochem., 13, 631– 642.

Capasso, G., Favara, R., Grassa, F., Inguaggiato, S., Longo, M., 2005. On-line technique for preparing and measuring stable carbon isotope of total dissolved inorganic carbon in water samples (δ 13CTDIC). Ann. Geophys. 48, 159–166. https://doi.org/10.4401/ag-3190.

Caracausi, A., Paternoster, M., Nuccio, P.M., 2015. Mantle CO_2 degassing at Mt. Vulture volcano (Italy): relationship between CO2 outgassing of volcanoes and the time of their last eruption. Earth Planet. Sci. Lett. 411, 268–280. https://doi.org/10.1016/j.epsl.2014.11.049

Caracausi, A., & Sulli, A. (2019). Outgassing of mantle volatiles in compressional tectonic regime away from volcanism: The role of continental delamination. *Geochemistry, Geophysics, Geosystems*, *20*, 2007–2020. https://doi.org/10.1029/2018GC008046

Cataldi, R., Mongelli, F., Squarci, P., Taffi, L., Zito, G., Calore, C. - 1995 - Geothermal ranking of Italian territory. Geothermics, 24 (1), 115-129

Chiarabba C., De Gpri P. & Speranza F. (2008)- The southern Tyrrhenian subduction zone. Deep geometry, magmatism and Plio-Pleistocenen evolution, Earth Planet. Sci. Lett., 268,408-423, doi:10.1016/j.epsl.2008.01.036.

Chiarella, D., Longhitano, S.G., Muto, F., 2012. Sedimentary features of the Lower Pleistocene mixed siliciclastic- bioclastic tidal deposits of the Catanzaro Strait (Calabrian Arc, south Italy). Rend. Online Soc. Geol. Ital. 21, 919–920.

Chiarella, D., Moretti, M., Longhitano, S.G., Muto, F., 2016. Deformed cross-stratified deposits in the Early Pleistocene tidally-dominated Catanzaro strait-fill succession, Calabrian Arc (Southern Italy): triggering mechanisms and environmental significance. Sediment. Geol. 344, 277–289.

Chiodini, G., Frondini, F., Cardellini, C., Parello, F., Peruzzi, L., 2000. Rate of diffuse carbon dioxide Earth degassing estimated from carbon balance of regional aquifers: the case of central Apennine, Italy. J. Geophys. Res. 105, 8423–8434.

Chiodini G., Cardellini C., Amato A., Bosc hi E., Caliro S., Frondini F. & Ventura G. (2004) - *Carbon dioxide Earth degassing and seismogenesis in central and southern Italy*. Geophys. Res. Lett., **31**, L07615.

Chiodini G., Caliro A., Cardellini C., Frondini F., Inguagg iato S. & Matteucc i F. (2011) - Geochemical evidence for and characterization of CO_2 rich gas sources in the epicentral area of the Abruzzo 2009 earthquakes. Earth Planet. Sci. Lett., **304**, 389-398.

Chiodini G., Cardellini C., Di Luccio F., Selva J., Frondini F., Caliro S., Rosiello A., Beddini G., Ventura G., Correlation between tectonic CO2 Earth degassing and seismicity is revealed by a 10-year record in the Apennines, Italy. *Sci. Adv.* **6**, eabc2938 (2020).

Cirrincione, R., Ortolano, G., Pezzino, A., & Punturo, R. (2008). Poly-orogenic multi-stage metamorphic evolution inferred via P-T pseudosections: An example from Aspromonte Massif basement rocks (Southern Calabria, Italy). *Lithos*, *103*(3–4), 466–502. https://doi.org/10.1016/j.lithos.2007.11.001

Clark I.D. , Fritz P. - Environmental Isotopes in Hydrogeology CRC Press/Lewis Publishers, Boca Raton (1997) 328 pp

Dai J., Song Y., Dai C., Wang D.; Geochemistry and Accumulation of Carbon Dioxide Gases in China. *AAPG Bulletin* 1996;; 80 (10): 1615–1625. doi: https://doi.org/10.1306/64EDA0D2-1724-11D7-8645000102C1865D

Dasgupta, R. (2013). Ingassing, storage, and outgassing of terrestrial carbon through geologic time. Reviews in Mineralogy and Geochemistry, 75(1), 183–229.

Deines P., Langmuir D., Harmon R. S., Stable carbon isotope ratios and the existence of a gas phase in the evolution of carbonate ground waters, Geochimica et Cosmochimica Acta, Volume 38, Issue 7, 1974, Pages 1147-1164, ISSN 0016-7037, https://doi.org/10.1016/0016-7037(74)90010-6.

Del Moro A., Paglionico A., Piccarreta G., Rottura A., 1986. Tectonic structure and post-Hercynian evolution of the Serre, Calabrian Arc, southern Italy: geological, petrological and radiometric evidences. *Tectonophysics*, 124: 223-238.

De Matteis, R., Convertito, V., Napolitano, F., Amoroso, O., Terakawa, T., & Capuano, P. (2021). Pore fluid pressure imaging of the Mt. Pollino region (southern Italy) from earthquake focal mechanisms. *Geophysical Research Letters*, 48, e2021GL094552. https://doi.org/10.1029/2021GL094552

De Vita P., Allocca V., Celico F., Fabbrocino S., Mattia C., Monacelli G., Musilli I., Piscopo V., Scalise Anna Rosa, Summa Gianpietro, Tranfaglia Giuseppe & Celico Pietro (2018) Hydrogeology of continental southern Italy, Journal of Maps, 14:2, 230-241, DOI: 10.1080/17445647.2018.1454352

Devoti, R., Riguzzi, F., Cuffaro, M., and Doglioni, C. (2008). New GPS constraints on the kinematics of the Apennines subduction. Earth Planet Sci. Lett. 273, 163–174. doi:10.1016/j.epsl.2008.06.031

Devoti, R., Esposito, A., Pietrantonio, G., Pisani, A. R. & Riguzzi, F. Evidence of large scale deformation patterns from GPS data in the Italian subduction boundary. *Earth and Planetary Science Letters* **311**, 230−241, doi:10.1016/j.epsl.2011.09.034 (2011).

Di Stefano, R., Kissling, E., Chiarabba, C., Amato, A., and Giardini, D. (2009), Shallow subduction beneath Italy: Three-dimensional images of the Adriatic-European-Tyrrhenian lithosphere system based on high-quality *P* wave arrival times, *J. Geophys. Res.*, 114, B05305, doi:10.1029/2008JB005641.

Duchi, V., Bencini, A., Cortese, G., Minissale, A., 1991. Caratteristiche geochimiche dei fluidi della Calabria centro settentrionale e loro potenzialit`a geotermiche. Boll. Soc. Geol. It. 110, 273–280.

Dumas, B., Raffy, J., 2004. Late Pleistocene tectonic activity deduced from uplifted marine terraces in Calabria, facing the Strait of Messina. Quaternaria nuova VIII, 79–99.

Eberhard L., Pettke T., Antigorite dehydration fluids boost carbonate mobilisation and crustal CO_2 outgassing in collisional orogens, Geochimica et Cosmochimica Acta, Volume 300, 2021, Pages 192-214, ISSN 0016-7037, https://doi.org/10.1016/j.gca.2021.02.030.

Ellis, A.J., Golding, R.M., 1963. The solubility of carbon dioxide above 100°C in water and sodium chloride solutions. Am. J. Sci. 261, 47–60

Evans, M. J., L. A. Derry, and C. France-Lanord (2008), Degassing of metamorphic carbon dioxide from the Nepal Himalaya, Geochem. Geophys. Geosyst., 9, Q04021, doi:10.1029/2007GC001796.

Evans K.; Metamorphic carbon fluxes: how much and how fast?. *Geology* 2011;; 39 (1): 95–96. doi: https://doi.org/10.1130/focus012011.1

Faccenna, C., Molin, P., Orecchio, B., Olivetti, V., Bellier, O., Funiciello, F., et al. (2011). Topography of the Calabria subduction zone (southern Italy): clues for the origin of Mt. Etna. Tectonics 30, TC1003. doi:10.1029/2010TC002694

Faccenna, C., Becker, T.W., Lucente, F.P., Jolivet, L., Rossetti, F., 2001. History of subduction and back-arc extension in the central Mediterranean. Geophys. J. Int. 145, 809–820.

Famin V., Nakashima S., Boullier A., Fujimoto K., Hirono T., Earthquakes produce carbon dioxide in crustal faults, Earth and Planetary Science Letters, Volume 265, Issues 3–4, 2008, Pages 487-497, ISSN 0012-821X, https://doi.org/10.1016/j.epsl.2007.10.041.

Ferranti, L., Monaco, C., Morelli, D., Antonioli, F., Maschio, L., 2008. Holocene activity of the Scilla fault, southern Calabria: insights from coastal morphological and structural investigations. Tectonophysics 453, 74–93.

Fischer, T. P. (2013). DEep CArbon DEgassing: The Deep Carbon Observatory DECADE initiative. Mineralogical Magazine, 77(5), 1089.

Fischer, T. P., Arellano, S., Carn, S., Aiuppa, A., Galle, B., Allard, P., et al. (2019). The emissions of CO2 and other volatiles from the world's subaerial volcanoes. Scientific Reports, 9(1), 18716. https://doi.org/10.1038/s41598-41019-54682-41591

Fischer, T. P., & Aiuppa, A. (2020). AGU Centennial Grand Challenge: Volcanoes and deep carbon global CO_2 emissions from subaerial volcanism— Recent progress and future challenges. Geochemistry, Geophysics, Geosystems, 21, e2019GC008690. https://doi.org/ 10.1029/2019GC008690

Foster, G., Royer, D. & Lunt, D. Future climate forcing potentially without precedent in the last 420 million years. *Nat Commun* **8,** 14845 (2017). https://doi.org/10.1038/ncomms14845

Gaillardet, J., and Galy, A., 2008, Atmospheric science -Himalaya-carbon sink or source?: Science, v. 320, p. 1727–1728, doi:10.1126/science.1159279.

Gilfillan, S. M. V., Lollar, B. S., Holland, G., Blagburn, D., Stevens, S., Schoell, M., et al. (2009). Solubility trapping in formation water as dominant CO_2 sink in natural gas fields. *Nature*, *458*(7238), 614–618. https://doi.org/10.1038/nature07852

Girault, F., Perrier, F., Crockett, R., Bhattarai, M., Koirala, B. P., France-Lanord, C., Agrinier, P., Ader, M., Fluteau, F., Gre´ au, C. & Moreira, M. (2014). The Syabru–Bensi hydrothermal system in central Nepal: 1. Characterization of carbon dioxide and radon fluxes. Journal of Geophysical Research: Solid Earth 119, 4017–4055.

Graessner, T., & Schenk, V. (2001). An exposed Hercynian deep crustal section in the Sila Massif of Northern Calabria: Mineral chemistry, petrology and a P-T path of granulite-facies metapelitic migmatites and metabasites. *Journal of Petrology*, *42*(5), 931–961. https://doi.org/10.1093/petro logy/42.5.931

Groppo C., Rolfo F., Castelli D. & Connolly J.A.D. (2013) - *Metamorphic CO_2 production from calc-silicate rocks via garnet-forming reactions in the CFAS-H_2O-CO_2 system,* Contrib. Mineral. Petrol., **166**, 1655–1675.

Groppo C., Rolfo F., Mosca P. & Castelli D. (2017) - *Metamorphic CO2 production in collisional orogens: petrologic constraints from phase diagram modeling of Himalayan, scapolite-bearing, calc-silicate rocks in the NKC(F)MAS(T)-HC system.* Journal of Petrology. doi: 10.1093/petrology/egx005

Groppo C., Rapa G., Frezzotti M. L. and Rolfo F. (2020) The fate of calcareous pelites in collisional orogens. J. Metamorph. Geol.. https://doi.org/10.1111/jmg.12568.

Groppo, C., Rolfo, F. & Frezzotti, M.L. CO_2 outgassing during collisional orogeny is facilitated by the generation of immiscible fluids. *Commun Earth Environ* **3,** 13 (2022). https://doi.org/10.1038/s43247-022-00340-w

Gruppo di lavoro CPTI, 2004. Catalogo parametrico dei terremoti italiani, versione 2004 (CPTI04), INGV, Bologna. http://emidius.mi.ingv.it/CPTI04.

Gulec, N., Hilton, D.R., 2016. Turkish geothermal fields as natural analogues of CO_2 storage sites: Gas geochemistry and implications for CO2 trapping mechanisms. Geothermics 64, 96–110.

Guo, Z., Wilson, M., Dingwell, D.B. *et al.* India-Asia collision as a driver of atmospheric CO_2 in the Cenozoic. *Nat Commun* **12,** 3891 (2021). https://doi.org/10.1038/s41467-021-23772-y

Gurrieri, S., Hauser, S., Valenza, M., 1984. Indagine preliminare su alcune sorgenti termali della Calabria per una futura sorveglianza geochimica dell'attivit`a sismica. Miner. Petrog. Acta 28, 101–122.

Hoefs, J. (2018) Variations of stable isotope ratios in nature. In J. Hoefs, Ed., Stable Isotope Geochemistry, p. 229–432. Springer.

Hollenstein, C., Kahle, H. G., Geiger, A., Jenny, S., Goes, S., and Giardini, D. (2003). New GPS constraints on the Africa-Eurasia plate boundary zone in southern Italy. Geophys. Res. Lett. 30 (18), 1935. doi:10.1029/2003gl017554

Holland, G., & Gilfillan, S. (2013). Application of noble gases to the viability of CO_2 storage. In P. Burnard (Ed.), *The noble gases as geochemical tracers. Advances in isotope geochemistry* (pp. 177–223). Springer. https://doi.org/10.1007/978-3-642-28836-4_8

Hunt, H.W., Elliott, E.T., Detling, J.K., Morgan, J.A. and Chen, D.-X. (1996), Responses of a C_3 and a C_4 perennial grass to elevated CO_2 and temperature under different water regimes. Global Change Biology, 2: 35-47. https://doi.org/10.1111/j.1365-2486.1996.tb00047.x

Kerrick, D. M. (2001). Present and past nonanthropogenic CO_2 degassing from the solid earth. Reviews of Geophysics, 39, 565–585.

Iannace, A., Vitale, S., D'errico, M., Mazzoli, S., Di staso, A., Macaione, E., Messina A., Reddy S.M., Somma R., Zamparelli V., Zattin M. and Bonardi, G. (2007). The carbonate tectonic units of northern Calabria (Italy): A record of Apulian palaeomargin evolution and Miocene convergence, continental crust subduction, and exhumation of HP–LT rocks. *Journal of the Geological Society, 164*(6), 1165–1186. https://doi.org/10.1144/0016-76492 007-017

Inguaggiato, S., and A. Rizzo (2004), Dissolved helium isotope ratios in ground-waters: A new technique based on gas-water re-equilibration and its application to a volcanic area, Appl Geochem., 19, 665–673.

Italiano, F., Martinelli, G. & Plescia, P. CO_2 degassing over seismic areas: the role of mechanochemical production at the study case of central apennines. Pure Appl. Geophys. 165, 75–94 (2008).

Italiano F., Bonfanti P., Ditta M., Petrini R., Slejko F.; Helium and carbon isotopes in the dissolved gases of Friuli Region (NE Italy): Geochemical evidence of CO_2 production and degassing over a seismically active area, Chemical Geology, Volume 266, Issues 1–2, 2009, Pages 76-85, ISSN 0009-2541, https://doi.org/10.1016/j.chemgeo.2009.05.022.

Italiano, F., Bonfanti, P., Pizzino, L., Quattrocchi, F., 2010. Geochemistry of fluids discharged over the seismic area of the Southern Apennines (Calabria region, Southern Italy): implications for fluid-fault relationships. Appl. Geochem. 25, 540–554.

Jolivet, L., and Faccenna, C. (2000), Mediterranean extension and the Africa-Eurasia collision, *Tectonics*, 19(6), 1095– 1106, doi:10.1029/2000TC900018.

Lee, H. et al. Massive and prolonged deep carbon emissions associated with continental rifting. Nat. Geosci. 9, 145 (2016).

Lee, C.-T., Jiang, H., Dasgupta, R., Torres, M., 2019. A framework for understanding whole-Earth carbon cycling. In: Orcutt, B.N., Daniel, I., Dasgupta, R. (Eds.), Deep Carbon: Past to Present. Cambridge University Press, Cambridge, pp. 313–357.

Liberi, F., Morten, L., & Piluso, E. (2006). Geodynamic significance of ophiolites within the Calabrian Arc. *Island Arc*, *15*(1), 26–43. https://doi.org/10.1111/j.1440-1738.2006.00520.x

Liberi, F., Piluso, E., & Langone, A. (2011). Permo-Triassic thermal events in the lower Variscan continental crust section of the Northern Calabrian Arc, Southern Italy: Insights from petrological data and in situ U-Pb zircon geochronology on gabbros. *Lithos*, *124*(3–4), 291–307. https://doi.org/10.1016/j.lithos.2011.02.016

Longhitano, S.G., Chiarella, D., Muto, F., 2014. Three-dimensional to two-dimensional cross-strata transition in the lower Pleistocene Catanzaro tidal strait trasgressive succession (southern Italy). Sedimentology 61, 2136–2171.

Lucente, F. P., Chiarabba, C., Cimini, G. B., and Giardini, D. (1999). Tomographic constraints on the geodynamic evolution of the Italian region. J. Geophys. Res. 104 (B9), 20307–20327. doi:10.1029/1999JB900147

Maesano, F.E., Tiberti, M.M. & Basili, R. The Calabrian Arc: three-dimensional modelling of the subduction interface. *Sci Rep* **7,** 8887 (2017). https://doi.org/10.1038/s41598-017-09074-8

Malinverno, A., Ryan, W.B.F., 1986. Extension in the Tyrrhenian Sea and shortening in the Apennines as result of arc migration driven by sinking of the lithosphere. Tectonics 5, 227–245.

Margiotta S, Mongelli G, Paternoster M, Sinisi R, Summa V (2014) Seasonal groundwater monitoring for trace-elements distribution and Cr(VI) pollution in an area affected by negligible anthropogenic effects. Fresen Environ Bull 23:1–15

Marty, B., Almayrac, M., Barry, P. H., Bekaert, D. V., Broadley, M. W., Byrne, D. J., et al. (2020). An evaluation of the C/N ratio of the mantle from natural CO2-rich gas analysis: Geochemical and cosmochemical implications. *Earth and Planetary Science Letters*, *551*(2020), 116574. https://doi.org/10.1016/j.epsl.2020.116574

Mattei M., Cifelli F. and D'Agostino N. (2007): The evolution of the Calabrian arc: evidence from paleomagnetic and GPS observations, Earth and Planetary Science Letters doi: 10.1016/j.epsl.2007.08.034.

Messina A., Russo S., Borghi A., Colonna V., Compagnoni R., Caggianelli A., Fornelli A., Piccarreta G., 1994. Il Massiccio della Sila Settore settentrionale dell'Arco Calabro-Peloritano. *Boll. Soc. Geol. It*., 113: 539-586.

Menzies C. D., Wright S. L., Craw D., James R. H., Alt J. C., Cox S. C., Pitcairn I. K., Teagle D. A.H., Carbon dioxide generation and drawdown during active orogenesis of siliciclastic rocks in the Southern Alps, New Zealand, Earth and Planetary Science Letters, Volume 481, 2018, Pages 305-315, ISSN 0012-821X, https://doi.org/10.1016/j.epsl.2017.10.010.

Minissale, A. Origin, transport and discharge of CO_2 in central Italy. Earth-Sci. Rev. 66, 89–141 (2004).

Micheletti, F., Barbey, P., Fornelli, A. *et al.* Latest Precambrian to Early Cambrian U–Pb zircon ages of augen gneisses from Calabria (Italy), with inference to the Alboran microplate in the evolution of the peri-Gondwana terranes. *Int J Earth Sci (Geol Rundsch)* **96,** 843–860 (2007). https://doi.org/10.1007/s00531-006-0136-0

Monaco, C., Tortorici, L., Nicolich, R., Cernobori, L., and Costa, M. (1996). From collisional to rifted basins: an example from the southern Calabrian arc (Italy). Tectonophysics 266 (1–4), 233–249. doi:10.1016/S0040-1951(96)00192-8

Napolitano F., Galluzzo D., Gervasi A., Scarpa R., La Rocca M., Fault imaging at Mt Pollino (Italy) from relative location of microearthquakes, *Geophysical Journal International*, Volume 224, Issue 1, January 2021, Pages 637–648, https://doi.org/10.1093/gji/ggaa407

Neri G., Barberi G., Oliva G., Orecchio B. and Presti D.; 2006: A possible seismic gap within a highly seismogenic belt crossing Calabria and eastern Sicily, Italy. Bull. Seism. Soc. Am., 96, 1321–1331, doi: 10.1785/0120050170.

Neri, G., Orecchio, B., Totaro, C., Falcone, G., and Presti, D. (2009). Subduction beneath southern Italy close the ending: results from seismic tomography. Seismol. Res. Lett. 80 (1), 63–70. doi:10.1785/gssrl.80.1.63

Neri, G., Marotta, A. M., Orecchio, B., Presti, D., Totaro, C., Barzaghi, R., et al. (2012). How lithospheric subduction changes along the Calabrian Arc in southern Italy: geophysical evidences. Int. J. Earth Sci. 101, 1949–1969. doi:10.1007/s00531-012-0762-7

Neri G., Orecchio B., Scolaro S. and Totaro C. (2020) Major Earthquakes of Southern Calabria, Italy, Into the Regional Geodynamic Context. Front. Earth Sci. 8:579846. doi: 10.3389/feart.2020.579846

Newell, D. L., M. J. Jessup, J. M. Cottle, D. R. Hilton, Z. D. Sharp, and T. P. Fischer (2008), Aqueous and isotope geochemistry of mineral springs along the southern margin of the Tibetan plateau: Implications for fluid sources and regional degassing of CO2, Geochem. Geophys. Geosyst., 9, Q08014, doi:10.1029/2008GC002021.

Nocquet, J.-M. (2012). Present-day kinematics of the Mediterranean: a comprehensive overview of GPS results. Tectonophysics 579, 220–242. doi:10.1016/j.tecto.2012.03.037

Ogniben, L., 1969. Schema introduttivo alla geologia del confine Calabro-lucano. Mem. Soc. Geol. It. 8, 453–763.

O'Nions, R. K., & Oxburgh, E. R. (1988). Helium, volatile fluxes and the development of continental crust. *Earth and Planetary Science Letters*, *90*(3), 331–334. https://doi.org/10.1016/0012-821X(88)90134-3

Ortolano, G., Visalli, R., Fazio, E., Fiannacca, P., Godard, G., Pezzino, A., Punturo, R., Sacco, V., & Cirrincione, R. (2020). Tectono-metamorphic evolution of the Calabria continental lower crust: The case of the Sila Piccola Massif. *International Journal of Earth Sciences*, 1–25. https://doi.org/10.1007/s0053 1-020-01873-1

Ozima, M., & Podosek, F. A. (2002). *Noble gas geochemistry* (p. 286). Cambridge University Press.

Panza, G.F. and Raykova, R.B. (2008), Structure and rheology of lithosphere in Italy and surrounding. Terra Nova, 20: 194-199. https://doi.org/10.1111/j.1365-3121.2008.00805.x

Parkhurst, D.L., Appelo, C.A.J., 1999. User's guide to PHREEQC a computer program for speciation, reaction-path, 1D-transport, and inverse geochemical calculations (Version 2). Technical Report 99-4259. U. S. Geological Survey, USA.

Pastori M, Margheriti L, De Gori P, Govoni A, Lucente FP, Moretti M, Marchetti A, Di Giovambattista R, Anselmi M, De Luca P, Nardi A, Agostinetti NP, Latorre D, Piccinini D, Passarelli L and Chiarabba C (2021) The 2011–2014 Pollino Seismic Swarm: Complex Fault Systems Imaged by 1D Refined Location and Shear Wave Splitting Analysis at the Apennines–Calabrian Arc Boundary. *Front. Earth Sci.* 9:618293. doi: 10.3389/feart.2021.618293

Paternoster, M., Rizzo, G., Sinisi, R. *et al.* Natural Hexavalent Chromium in the Pollino Massif Groundwater (Southern Apennines, Italy): Occurrence, Geochemistry and Preliminary Remediation Tests by Means of Innovative Adsorbent Nanomaterials. *Bull Environ Contam Toxicol* **106,** 421–427 (2021). https://doi.org/10.1007/s00128-020-02898-7

Perrier, F., Richon, P., Byrdina, S., France-Lanord, C., Rajaure, S., Koirala, B. P., Shrestha, P. L., Gautam, U. P., Tiwari, D. R., Revil, A., Bollinger, L., Contraires, S., Bureau, S. & Sapkota, S. N. (2009). A direct evidence for high carbon dioxide and radon-222 discharge in Central Nepal. Earth and Planetary Science Letters 278, 198–207.

Piana Agostinetti, N., Steckler, M. S., and Lucente, F. P. (2009). Imaging the subducted slab under the Calabrian Arc, Italy, from receiver function analysis. Lithosphere 1 (3), 131–138. doi:10.1130/L49.1

Piccarreta, G. (1981). Deep-rooted overthrusting and blueschistic metamorphism in compressive continental margins. An example from Calabria (Southern Italy). *Geological Magazine, 118*(5), 539–544. https://doi.org/10.1017/S0016 75680 0032908

Pitcairn, I.K., Teagle, D.A.H., Craw, D., Olivio, G.R., Kerrich, R., Brewer, T.S., 2006. Sources of metals and fluids in orogenic gold deposits: insights from the Otago and Alpine Schists, New Zealand. Econ. Geol.101, 1525–1546.

Randazzo, P., Caracausi, A., Aiuppa, A., Cardellini, C., Chiodini, G., D'Alessandro, W., et al. (2021). Active degassing of deeply sourced fluids in central Europe: New evidences from a geochemical study in Serbia. *Geochemistry, Geophysics, Geosystems*, *22*, e2021GC010017. https://doi.org/10.1029/2021GC010017

Rizzo, A. L., Pelorosso, B., Coltorti, M., Ntaflos, T., Bonadiman, C., Matusiak-Małek, M., et al. (2018). Geochemistry of noble gases and CO2 in fluid inclusions from lithospheric mantle beneath Wilcza Góra (Lower Silesia, Southwest Poland). *Frontiers in Earth Science*, *6*, 215. https://doi.org/10.3389/feart.2018.00215

Rizzo, A.L., Caracausi, A., Chavagnac, V., Nomikou, P., Polymenakou, P.N., Mandalakis, M., Kotoulas, G., Magoulas, A., Castillo, A., Lampridou, D., Marusczak, N., Sonke, J.E., 2019. Geochemistry of CO2-rich gases venting from submarine volcanism: the case of Kolumbo (Hellenic Volcanic Arc, Greece). Front. Earth Sci. 7, 1–20. https://doi.org/10.3389/feart.2019.00060.

Rolfo F., Groppo C., Mosca P.; Metamorphic CO_2 production in calc-silicate rocks from the eastern Himalaya. *Italian Journal of Geosciences* 2017; 136 (1): 28–38. doi: https://doi.org/10.3301/IJG.2015.36

Rossetti, F., Faccenna, C., Goffe, B., Monie, P., Argentieri, A., Funiciello, R., & Mattei, M. (2001). Alpine structural and metamorphic signature of the Sila Piccola Massif nappe stack (Calabria, Italy): Insights for the tectonic evolution of the Calabrian Arc. *Tectonics*, *20*(1), 112–133.

Rossetti, F., Goffe, B., Monie, P., Faccenna, C., & Vignaroli, G. (2004). Alpine orogenic P-T-t-deformation history of the Catena Costiera area and surrounding regions (Calabrian Arc, southern Italy): The nappe edifice of north Calabria revised with insights on the Tyrrhenian-Apennine system formation. *Tectonics*, *23*(6), 1–26. https://doi.org/10.1029/2003T C001560

Rovida, A., Locati, M., Camassi, R., Lolli, B. & Gasperini, P. (eds) CPTI15, the 2015 version of the Parametric Catalogue of Italian Earthquakes. Istituto Nazionale di Geofisica e Vulcanologia, https://doi.org/10.6092/INGV.IT-CPTI15 (2016).

Rovida, A., Locati, M., Camassi, R., Lolli, B., and Gasperini, P. (2019). Catalogo parametrico dei terremoti Italiani (CPTI15), versione 2.0 (Rome: Istituto Nazionale di Geofisica e Vulcanologia (INGV)). Available at: https://emidius.mi.ingv.it/CPTI15-DBMI15/.

Rovida, A., Locati, M., Camassi, R., Lolli, B., and Gasperini, P. (2020). The Italian earthquake catalogue CPTI15. Bull. Earthq. Eng. 18 (7), 2953–2984. doi:10.1007/s10518-020-00818-y

Sano, Y., & Wakita, H. (1985). Geographical distribution of $^{3}He/^{4}He$ ratios in Japan: Implications for arc tectonics and incipient magmatism. *Journal of Geophysical Research*, *90*(B10), 8729–8741. https://doi.org/10.1029/JB090iB10p08729

Sano, Y., Y. Nakamura, and H. Wakita, Areal distribution of $^{3}He/^{4}He$ ratios in the Tohoku district, north eastern Japan, Chem. Geol. Isot. Geosci. Sect., 52, 1-8, 1985.

Sano, Y., & Marty, B. (1995). Origin of carbon in fumarolic gas from island arcs. *Chemical Geology*, *119*, 265–274. https://doi.org/10.1016/0009-2541(94)00097-R

Sano, Y., Tominaga, T., & Williams, S. N. (1997). Secular variations of helium and carbon isotopes at Galeras volcano, Colombia. *Journal of Volcanology and Geothermal Research*, *77*(1–4), 255–265. https://doi.org/10.1016/S0377-0273(96)00098-4

Scarfì, L., Barberi, G., Barreca, G. *et al*. Slab narrowing in the Central Mediterranean: the Calabro-Ionian subduction zone as imaged by high resolution seismic tomography. *Sci Rep* **8,** 5178 (2018). https://doi.org/10.1038/s41598-018-23543-8

Schenk, V. (1980), U-Pb and Rb-Sr radiometric dates and their correlation with metamorphic events in the granulite facies basement of the Serre, southern Calabria (Italy), Contrib. Mineral. Petrol., 73, 23 – 38.

Schenk V., 1981. Synchronous uplift of the lower crust of the Ivrea Zone and of southern Calabria and its possible consequences for the Hercynian orogeny in southern Europe. *Earth and Planetary Sc. Lett.*, 56: 305-320.

Shimabukuro, D. H., Wakabayashi, J., Alvarez, W., & Chang, S.-C. (2012). Cold and old: The rock record of subduction initiation beneath a continental margin, Calabria, southern Italy. *Lithosphere*, *4*(6), 524–532. https://doi.org/10.1130/l222.1

Sizova E., Hauzenberger C., Fritz H., Faryad S. W. and Gerya T. (2019) Late orogenic heating of (ultra)high pressure rocks: Slab rollback vs. slab breakoff. Geosciences 9(12), 499.

Skelton, A., 2011, Flux rates for water and carbon during greenschist facies metamorphism: Geology, v. 39, p. 43–46, doi:10.1130/G31328.1.

Sketsiou P., De Siena L., Gabrielli S., Napolitano F., 3-D attenuation image of fluid storage and tectonic interactions across the Pollino fault network, *Geophysical Journal International*, Volume 226, Issue 1, July 2021, Pages 536–547, https://doi.org/10.1093/gji/ggab109

Spakman, W., and Wortel, R. (2004). "A tomographic view on western Mediterranean geodynamics," in The TRANSMED Atlas. The Mediterranean region from crust to mantle. Editors W. Cavazza, F. Roure, W. Spakman, G. M. Stampfli, and P. A. Ziegler (Heidelberg, Germany: Springer-Verlag), 31–52.

Stampfli, G. M., & Borel, G. D. (2002). A plate tectonic model for the Paleozoic and Mesozoic constrained by dynamic plate boundaries and restored synthetic oceanic isochrons. *Earth and Planetary Science Letters*, *196*(1–2), 17–33.

Tamburello, G., Pondrelli, S., Chiodini, G. *et al.* Global-scale control of extensional tectonics on CO_2 earth degassing. *Nat Commun* **9,** 4608 (2018). https://doi.org/10.1038/s41467-018-07087-z

Tansi, C., Tallarico, A., Iovine, G., Gallo, M.F., Falcone, G., 2005. Interpretation of radon anomalies in seismotectonic and tectonic-gravitational settings: the south-eastern Crati graben (Northern Calabria, Italy). Tectonophysics 396, 181–193.

Thomson, S. N. (1994), Fission track analysis of the crystalline basement rocks of the Calabrian Arc, southern Italy: Evidence of Oligo-Miocene late orogenic extension and erosion, Tectonophysics, 238, 331 – 352.

Thomson, S. N. (1998), Assessing the nature of tectonic contacts using fission-track thermochronology: An example from the Calabrian Arc, southern Italy,Terra Nova, 10, 32 – 36

Tiberti, M. M., Vannoli, P., Fracassi, U., Burrato, P., Kastelic, V., & Valensise, G. (2017). Understanding seismogenic processes in the Southern Calabrian Arc:A geodynamic perspective. *Italian Journal of Geosciences*, **136**(3), 365–388. https://doi.org/10.3301/IJG.2016.12

Tortorici, G., Bianca, M., De Guidi, G., Monaco, C., Tortorici, L., 2003. Fault activity and marine terracing in the Capo Vaticano area (southern Calabria) during the Middle-Late Quaternary. Quatern. Int., 269–278.

Tortorici, L., Monaco, C., Tansi, C., Cocina, O., 1995. Recent and active tectonics in the Calabrian Arc (Southern Italy). Tectonophysics 243, 37–55.

Tortorici, L., 1981. Analisi delle deformazioni fragili postorogene della Calabria settentrionale. Boll. Soc. Geol. It. 100, 291–308.

Tortorici L. (1982a) -Analisi delle deformazioni fragili dei sedimenti postorogeni della calabria Settentrionale.Boll. Soc. Geol.It., 100(3), 291-380.

Tortorici L. (1982b) - Lineamenti geologico strutturalidell'Arco Calabro-Peloritano. Rend. Soc. It. Mineral. e Petrol., 38(3), 927-940.

Tursi, F., Bianco, C., Brogi, A., Caggianelli, A., Prosser, G., Ruggieri, G., & Braschi, E. (2020). Cold subduction zone in northern Calabria (Italy) revealed by lawsonite–clinopyroxene blueschists. *Journal of Metamorphic Geology*, *38*(5), 451–469. https://doi.org/10.1111/jmg.12528

Tursi, F, Acquafredda, P, Festa, V, et al. What can high-*P* sheared orthogneisses tell us? An example from the Curinga–Girifalco Line (Calabria, southern Italy). *J Metamorph Geol*. 2021; 39: 919– 944. https://doi.org/10.1111/jmg.12596

Valensise, G., & Guidoboni, E. (2000). Towards new research strategies: silent seismogenic areas or silent sources? *Annali di Geofisica*, Vol. 43.

Valley J. W., Cole D.R., (2019). Stable Isotope Geochemistry. 1st ed. De Gruyter. https://www.perlego.com/book/864975/stable-isotope-geochemistry-pdf.

Vespasiano, G., Muto, F., Apollaro, C., De Rosa, R., 2012. Preliminary hydrogeochemical and geological characterization of the thermal aquifer in the Guardia Piemontese area (Calabria, south Italy). Rend. Online Soc. Geol. It. 21, 841–842.

Vespasiano, G., Apollaro, C., Muto, F., Dotsika, E., De Rosa, R., Marini, L., 2014. Chemical and isotopic characteristics of the warm and cold waters of the Luigiane Spa near Guardia Piemontese (Calabria, Italy) in a complex faulted geological framework. Appl. Geochem. 41, 73–88.

Vespasiano, G., Apollaro, C., Muto, F., De Rosa, R., Critelli, T., 2015a. Preliminary geochemical and geological characterization of the thermal site of Spezzano Albanese (Calabria, South Italy). . Rend. Online Soc. Geol. It. 33, 108–110.

Vespasiano, G., Apollaro, C., Muto, F., De Rosa, R., Dotsika, E., Marini, L., 2015b. Preliminary geochemical characterization of the warm waters of the Grotta delle Ninfe near Cerchiara di Calabria (South Italy). Rend. Online Soc. Geol. It. 39, 130–133.

Vespasiano G., Marini L., Muto F., Auqué L. F., Cipriani M., De Rosa R., Critelli S., Gimeno M. J., Blasco M., Dotsika E., Apollaro C.-Chemical, isotopic and geotectonic relations of the warm and cold waters of the Cotronei (Ponte Coniglio), Bruciarello and Repole thermal areas, (Calabria - Southern Italy), Geothermics, Volume 96, 2021, 102228, ISSN 0375-6505, https://doi.org/10.1016/j.geothermics.2021.102228.

Vitale, S., Ciarcia, S., Fedele, L., & Tramparulo, F. D. A. (2019). The Ligurian oceanic successions in southern Italy: The key to decrypting the first orogenic stages of the southern Apennines-Calabria chain system. *Tectonophysics*, *750*, 243–261. https://doi.org/10.1016/j.tecto.2018.11.010

Vogel, J.C., Grootes, P.M., Mook, W.G., 1970. Isotopic fractionation between gaseous and dissolved carbon dioxide. Zeitschrift für Physik A Hadrons and nuclei 230 (3), 225–238.

Von Blanckenburg F. and Davies J. H. (1995) Slab breakoff – a model for syncollisional magmatism and tectonics in the alps. Tectonics 14, 120–131.

Westaway, R., 1993. Quaternary uplift of Southern Italy. J. Geophys. Res. 98, 21741–21772.

Zanettin Lorenzoni E., 1982. Relationships of main structural elements of Calabria (southern Italy). *Nues Jabh. Geol. Paläont. Mh*., 7: 403-418.

Zarlenga, F., 2011. Le possibilit`a di utilizzo della risorsa geotermica a bassa e media entalpia per la sostenibilit`a della produzione energetica. Energia. Ambiente e Innovazione 3, 31–40.

Zhang M., Zhang L., Zhao W., Guo Z., Xu S., Sano Y., Lang Y., Liu C., Li Y.- Metamorphic CO2 emissions from the southern Yadong-Gulu rift, Tibetan Plateau: Insights into deep carbon cycle in the India-Asia continental collision zone, Chemical Geology, Volume 584, 2021, 120534, ISSN 0009-2541, https://doi.org/10.1016/j.chemgeo.2021.120534

Zeck S.E., 1990. The exhumation and preservation of deep continental crust in the northwestern Calabrian arc, southern Italy. University of California, Santa Barbara [PhD Thesis], 277 pp.

CHAPTER III

Active Degassing of Deeply Sourced Fluids in Central Europe: New Evidence From a Geochemical Study in Serbia

III.1. Introduction

Recognizing and identifying the transfer of mantle-derived fluids (e.g., CO_2, N_2, noble gases) in continental regions is critical for investigating the processes that shape the deep and shallow Earth's evolution, such as subduction, volcanism, natural degassing, active tectonics, and earthquakes (e.g., Ballentine et al., 2001; Broadley et al., 2020; Caracausi & Sulli, 2019; Caracausi et al., 2013; Chiodini et al., 2020; Holland & Gilfillan, 2013; Kennedy & Van Soest, 2007; Labidi et al., 2020; Lowenstern et al., 2014; O'Nions & Oxburgh, 1988; Torgersen, 1993). During the last four decades, the migration and surface discharge of deep-mantle volatiles has been verified in many crustal segments, including western-central Europe (e.g., Brauer et al., 2013; Carreira et al., 2009; Mamyrin & Tolstikhin, 1984; Minissale, 2000). New efforts are currently undertaken to extend such studies in central-eastern Europe, in the attempt to (a) understand natural degassing in active tectonic regions (e.g., Etiope et al., 2003, 2004; Frunzeti, 2013; Ionescu et al., 2017; Italiano et al., 2017; Kis et al., 2017; Sarbu et al., 2018; Vaselli et al., 2002), (b) investigate the possible presence of magma at depth below “quiescent” volcanoes (e.g., Kis et al., 2019), and (c) assess the role of fluids in seismogenetic processes (e.g., Baciu et al., 2007; Bräuer et al., 2004, 2005, 2008). Large-scale outgassing of mantle-derived fluids has been recognized in different European volcanic regions that last erupted thousands of years ago (e.g., Eger rift, Czech Republic; Eifel, Germany; Carpathians, Romania; Pannonian basin; Aeschbach-Hertig et al., 1996; Ballentine et al., 1991; Bräuer et al., 2013, 2016; Kis et al., 2017, 2019; Palcsu et al., 2014; Sherwood Lollar et al., 1997; Szöcs et al., 2013). Further to the south, in Greece and Turkey, a link between fluid release (with mantle-derived components), tectonic setting, and seismicity has been demonstrated, in both volcanic and nonvolcanic areas (e.g., D'Alessandro et al., 2020; Daskalopoulou et al., 2019; De Leeuw et al., 2010; Dogan et al., 2009; Italiano et al., 2013; Mutlu et al., 2008; Rizzo et al., 2018; Shimizu et al., 2005). The Serbian segment of the seismically active central-western Balkan Peninsula (Marović et al., 2002) is sited at the suture zone between African (Adria) and European

plate. The area is characterized by delamination and sinking of the Adria mantle lithosphere under the north-western and southern Dinarides, with hotter mantle materials filling the space left by the sinking slabs (e.g., Belinić et al., 2021). Serbia also exhibits high regional heat flow (up to 130 mW/m^2) and geothermal energy potential (Doljak & Glavonjić, 2016; Horwarth et al., 2015). Previous work in the central-western Balkan Peninsula has found several natural gas manifestations and gas-rich thermal waters (e.g., Burić et al., 2016; Rosca et al., 2016; Todorović et al., 2016). However, the source of these gases, and the geological/tectonic controls on their migration through the crust, remain uncharacterized. Here, we report on the results of a geochemical survey (carried out in autumn 2019) aimed at investigating the origin (e.g., atmospheric versus crustal versus mantle-sourced) of the volatiles outgassed in Serbia. We also attempt at a better characterization of the processes that control the chemistry of the fluids during their storage in, and transit through, the crust. Our study contributes to filling a knowledge gap on the nature of fluids circulating in this sector of Europe, and helps better reconstructing the complex geodynamic of the area.

III.2. Geological Setting

The sector of the Vardar zone in Serbia (south eastern Europe, SEE) is part of the mega-suture stretching along the entire Balkan Peninsula (e.g., Cvetković et al., 2016). Its present-day geological setting is the result of a complex geodynamic and tectonic evolution over the last ~200 Ma (from the middle Mesozoic to the present) that progressively involved subduction, continental collision, and finally lithospheric extension (e.g., Belinic et al., 2021; Cvetković et al., 2004). The engine of the regional geodynamic evolution is the interaction between Eurasian (Europe) and Gondwana (Africa) continental plates (Cvetković et al., 2016). More in detail, Serbia is part of the orogenic system composed by the Alpine, Carpathian, and Dinaride belts (e.g., Marović et al., 2007; Schmidt et al., 2008, 2019) and its territory can be divided into distinct tectonic units: (a) the Pannonian

basin (northern part), (b) the Dinaric Alps (central-western part), (c) the Vardar zone, divided in East and West zones (the study area, Fig. III.1), (d) the Serbian-Macedonian Massif, a belt stretching in north-south direction into north-western Macedonia and northern Greece, (e) the Carpatho-Balkan Region (eastern part), and (f) the Dacia basin (Bazylev et al., 2009; Cvetković et al., 2004; Jelenković et al., 2008; Moores & Fairbridge, 1997). In the study area, volcanism has recurrently insisted over the last ~200 Ma (e.g., Cvetković et al., 2016; Zelić et al., 2010), and includes alkaline magmatism during the middle to late Triassic rifting stage (Bortolotti et al., 2008), intrusive magmatic activity with calk-alkaline granitoids in the Late Jurassic-Miocene, and granitoid products in the early Eocene-late Oligocene (Pamić et al., 2002; Saric et al., 2009).

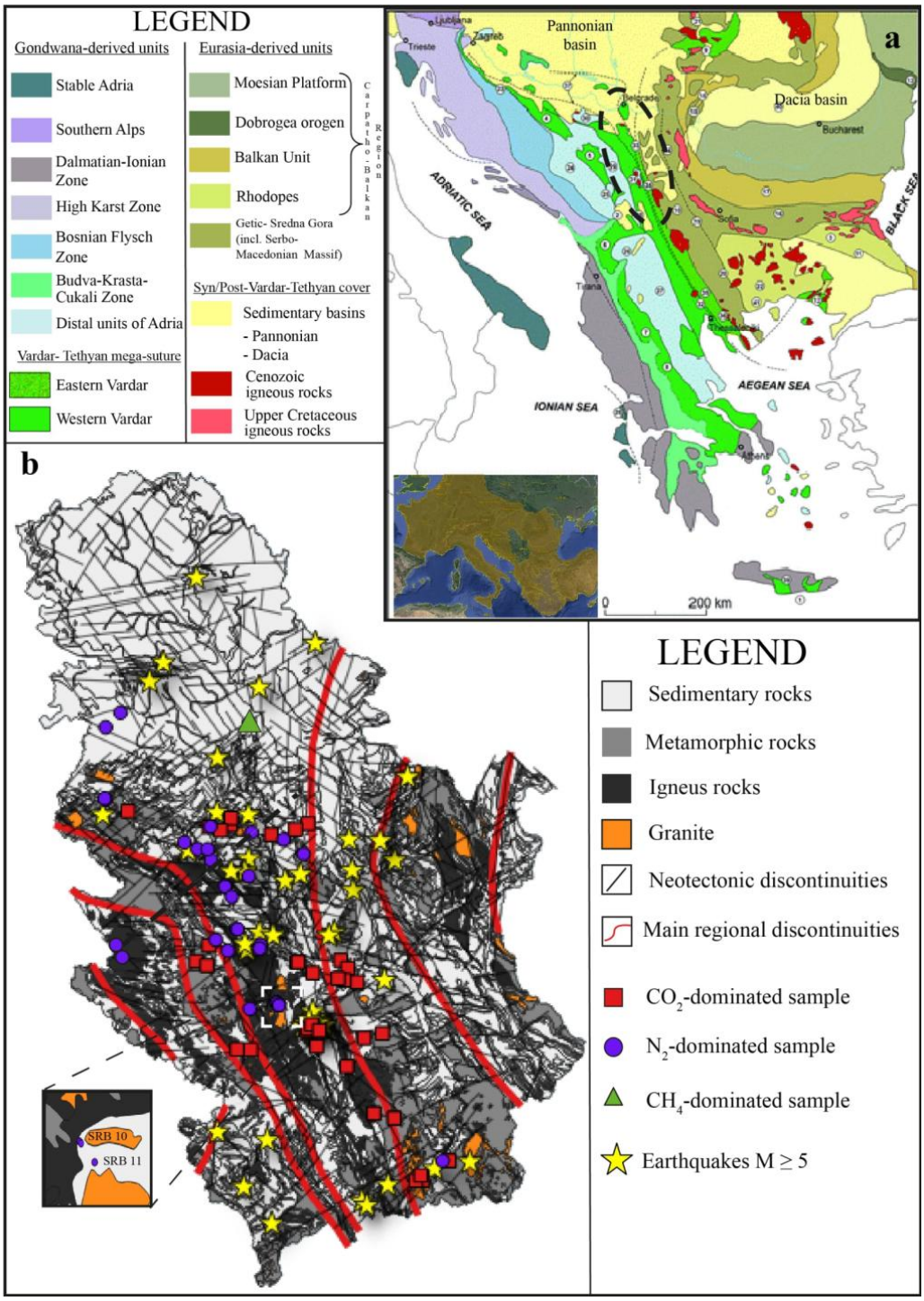

Figure III.1 | Geology of Serbia and sampling location. **a**) Simplified geological sketch map of south eastern Europe with the main tectonic units (for detailed information see Cvetkovic et al. 2016). The studied area is highlighted by the dashed ellipse on the map. Small inset at the bottom left indicates the European areas in which geochemical studies on natural degassing have been conducted (shaded yellow area); **b**) geological map of Serbia with sample locations, main regional faults (red), and neotectonic faults (black). The small inset is a zoom on the area in which a sample with lowest R/Ra has been collected in correspondence to a granitoid intrusion.

Since the Oligocene, widespread volcanism occurred throughout SEE, associated to the formation of a variety of volcanic landforms. Volcanism in Serbia concentrated along an NW-SE-trending belt (Cvetković et al., 2016), with the youngest volcanic activity pulse dating 16.8-8.6 Ma (Zelić et al., 2010, and reference therein). Currently, in the region, there are widespread outcrops of volcanic rocks, ranging in composition from andesites to basanites (upper Cretaceous-middle Paleogene), shoshonites and high-K calc-alkaline series with occurrence of lamproites (Cvetković et al., 2000; Djordjević, 2005; Pamić, 1997; Prelević et al., 2005; Zelić et al., 2010). The final stage of the regional geodynamic evolution involved an extensional phase of lithospheric thinning (Cvetković et al., 2016) that culminates in the Pannonian Basin and the Serbian-Macedonian Massif (40– 50 km of lithospheric crust) and is associated to an asthenosphere up-rise (Cvetković et al., 2016; Milivojević, 1993). The heat flow distribution in the Pannonian basin is consequently high (from 50 to 130 mW/m^2), and the highest values are observed in the Great Hungarian Plain, the Pannonian part of Serbia (Vojvodina) including its continuation into the Vardar zone (Horvath et al., 2015; Lenkey et al., 2002). The region is characterized by active seismicity with earthquake magnitudes up to 6.5 and hypocenters down to 20–30-km depth (http://www.seismo.gov.rs/Seizmicnost/Katalog-zemljotresa.pdf) and this depth coincides with the regional crust-mantle boundary (Marović et al., 2007; Metois et al., 2015).

III.3. Materials and Methods

Thirty-one bubbling gas samples were collected from north to south in the central and western sectors of Serbia (Fig. III.1b). The bubbling gases were sampled by using an inverted funnel that was positioned above the bubbles, so the gases fluxed through a two valves glass or steel bottle to avoid air contamination (Fig. III.2). Once the bottles had been flushed with an amount of gas at least tens of times the volume of the bottles (20–30 cc) the valves were closed to trap the gases into the bottles. All chemical and isotopic analyses were carried out at the laboratories of the INGV-

Palermo within 1 month from the sampling in order to prevent isotopic fractionation due to storage of gases.

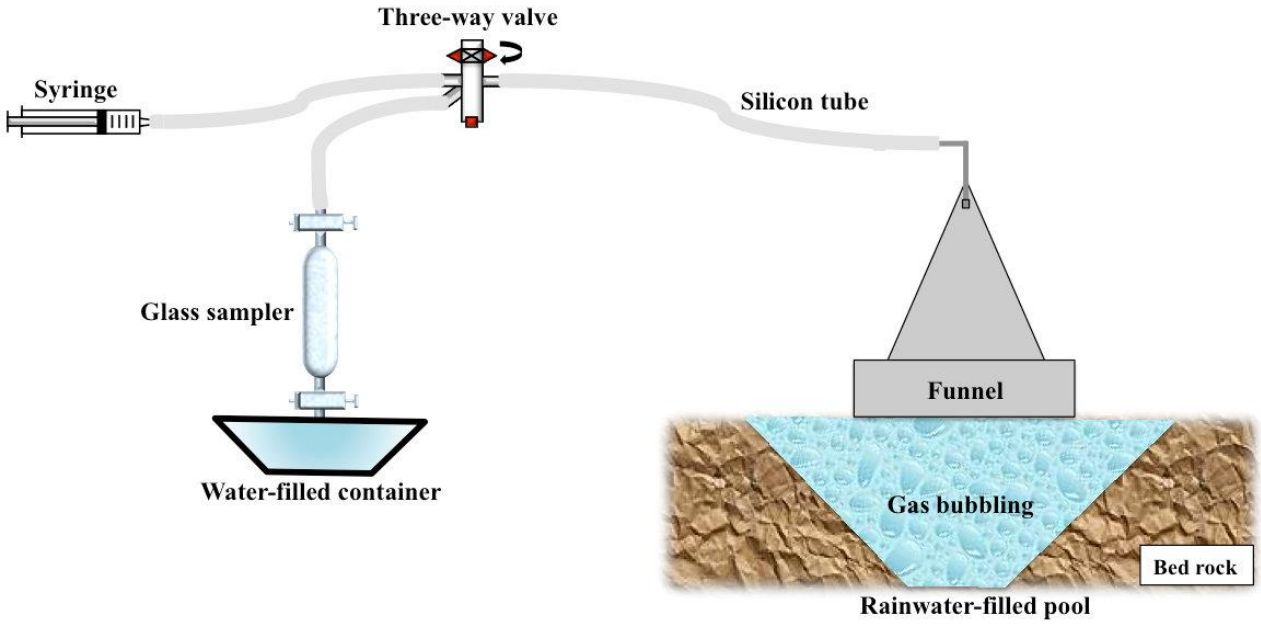

Figure III.2 | Sampling gas system**.** Schematic illustration showing the sampling system used for collecting the gaseous manifestations.The sampling system adopted for collecting the gaseous manifestations consists of three different components (a funnel, a sampler and a syringe) connected by silicone tubes through a three-way pyrex valve. The free gases were sampled following a cleaning procedure which allows to purge the glass bottle of air. The released gas is conveyed to the silicon tube through the funnel. The gas is slowly withdrawn by the syringe and then pushed hardly to the glass sampler for several times producing water bubbling in the container (the induced bubbling serves to test out the effective functioning of the sampling system).

Water temperature and pH were measured in the field by using a portable multiparameter instrument (WTW Multi 350i), which was previously calibrated using standard solutions (Table III.1). The chemical composition of the gases was analyzed by an Agilent 7890B gas chromatograph using Ar as carrier gas, and equipped with 4-m Carbosieve S II and PoraPlot-U columns. A thermal conductivity detector (TCD) was used to measure the concentrations of O_2, N_2, and CO_2, while a flame ionization detector (FID) was used for CH_4. Analytical errors of the measured concentrations are always within 5%. The $^{13}C/^{12}C$ ratios of CO_2 (expressed as $\delta^{13}C\text{-}CO_2$

in ‰ versus the V-PDB standard) were measured with a Finnigan Delta S mass spectrometer after purification of the gas mixture by standard procedures using cryogenic traps with precision of ±0.1‰. He isotopes were analyzed using a static vacuum mass spectrometer (GVI Helix SFT), using a double collector in order to detect ^{3}He and ^{4}He ion beams simultaneously (precision for isotopic ratio within ±0.5%). The $^{3}He/^{4}He$ ratio was determined by measuring ^{3}He in an electron multiplier detector and ^{4}He in an axial Faraday detector. ^{20}Ne was measured with a multicollector Thermo-Helix MC Plus mass spectrometer. Helium isotope compositions are expressed as R/Ra, normalizing the $^{3}He/^{4}He$ ratio of the sample against the atmospheric $^{3}He/^{4}He$ ratio ($Ra= 1.386\times10^{-6}$; Ozima & Podosek, 2002). The Ar concentrations and its isotope compositions (^{40}Ar, ^{38}Ar, and ^{36}Ar) were analyzed by multicollector Helix MC-GVI mass spectrometer with analytical uncertainty ($1\ \sigma$) for single $^{40}Ar/^{36}Ar$ measurements of <0.1%.

III.4. Results

The chemical composition of the sampled gases, together with the isotopic composition of He, Ar, and C(CO_2), are presented in Table III.1. On the base of their chemical compositions, the studied gases are subdivided into three different groups: CO_2-dominated (CO_2 > 50%), N_2-dominated (N_2 > 50%), and CH_4-dominated (this includes only sample SRB31, being methane-rich: 87%). CO_2-dominated and N_2-dominated samples have CH_4 concentrations ranging from 0.02% to 19%. Ar and O_2 concentrations are typically ≤1% (Table III.1), He and Ne are present in trace amounts (ppmv). The CH_4-dominated sample has a CO_2 concentration of 0.51% and N_2 of 11%. Also, for this sample, the O_2 and Ar concentration are very low (<1%) with He and Ne present in trace (37.3 and 0.24 ppmv). CO_2 and N_2 exhibit a negative correlation, as implied by their being the two dominant gas species (Fig. III.3).

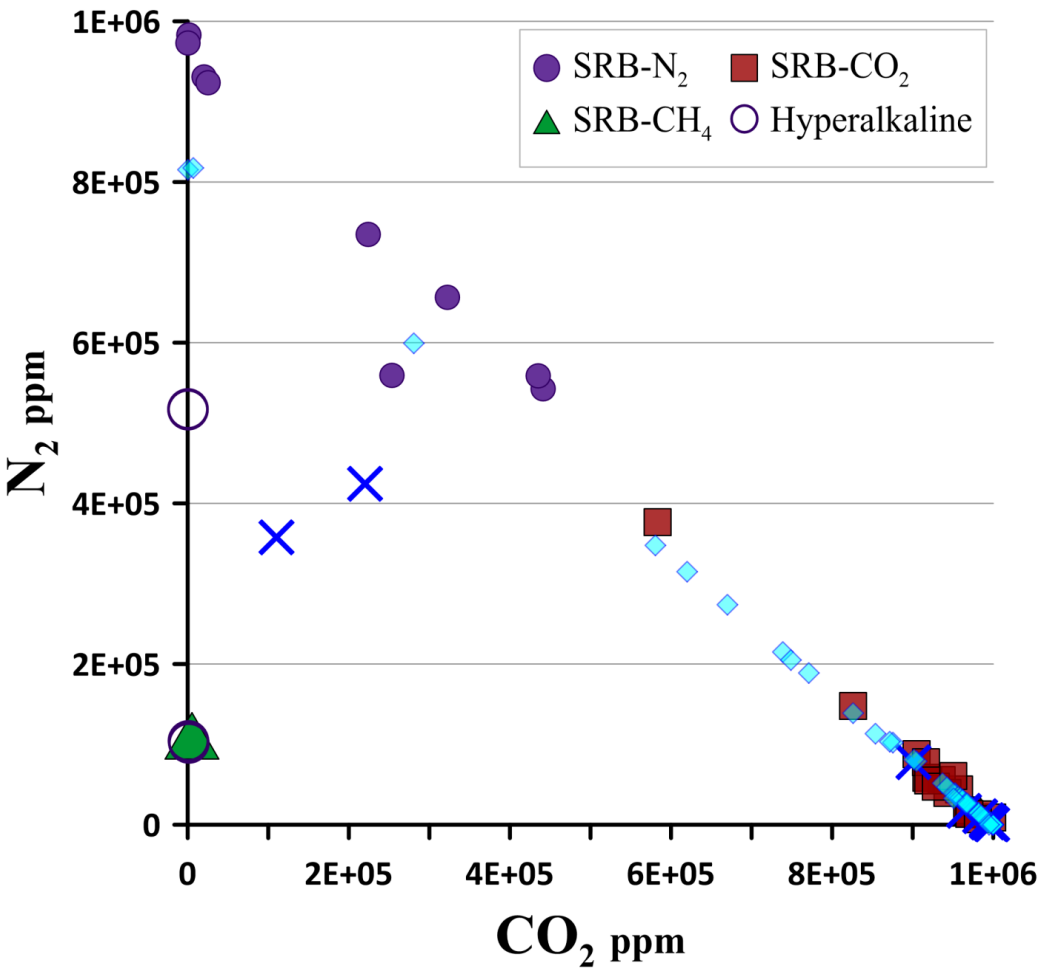

Figure III.3 | N_2 versus CO_2 concentrations in Serbian gases. See legend for symbols of three groups of fluids in the studied area. Purple open circles that along the *y* axis are two samples of bubbling gases in hyperalkaline water. The light blue diamonds and the dark blue crosses depict data from some central and eastern Europe areas (Eger rift; Weinlich et al., 1999) and from the Austria/Slovenia border, Pannonian basin (Bräuer et al., 2016).

Only the CH_4-rich sample, and two other N_2-dominated samples (10.1–51.6% of N_2) that are bubbling gases from hyperalkaline waters (pH from 11.6 to 12.2) depart from a pure CO_2-pure N_2 mixing line. Gases in hyperalkaline waters have high amount of H_2 (85% and 34%) and very low CO_2 amounts (<0.15%). The $\delta^{13}C_{CO2}$ values vary from −20.2‰ to −0.1‰ (Table III.1). The N_2-dominated gases exhibit the lowest $\delta^{13}C_{CO2}$ values, especially those with CO_2 <3% that plot in the field of biogenic CO_2 (Fig. III.4). The CO_2-C isotopic compositions of bubbling gases in hyperalkaline waters also plot in the same biogenic field (Fig. III.4). The He isotopic ratios, expressed as R/Ra, vary from 0.08 to 1.2 Ra, and the N_2-dominated gases have the lowest He

isotopic ratios (Fig. III.5). The $^{4}He/^{20}Ne$ ratios mostly range from 13 to 1,300, and are much higher than the atmospheric ratio (0.318; Ozima & Podosek, 2002), indicating a low air He contribution to the sampled gases. On the contrary, the two hyperalkaline samples have $^{4}He/^{20}Ne$ values of 0.53 and 0.59 indicating a dominant atmospheric component.

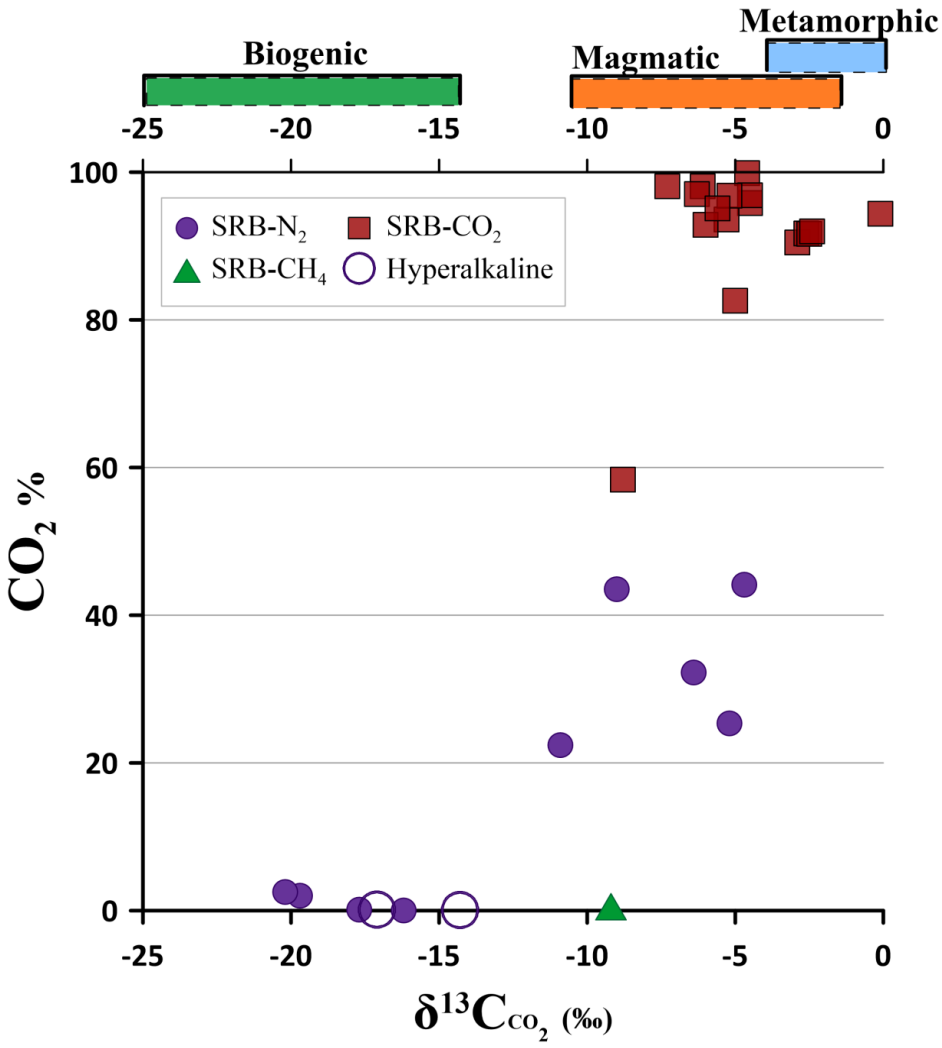

Figure III.4 | CO_2 concentrations versus $\delta^{13}C_{CO2}$. N_2-dominated gases (especially those with CO_2 <3%) exhibit the lowest $\delta^{13}C_{CO2}$ values, falling in the field of the biogenic CO_2 (green bar). Gases from hyperalkaline waters also plot in the same field of biogenic CO_2. CO_2-rich samples have more positive carbon isotopic compositions, falling within the magmatic (orange) and metamorphic (blue) fields. The three colored boxes indicate the typical $\delta^{13}C$ ranges for the three different sources: green = biogenic, orange = magmatic, blue = metamorphic. Note the overlap between the two field (magmatic-metamorphic) at -4‰ (from Holland and Gilfillan, 2013).

Table III.1 | Location, chemical and isotopic composition of serbian natural gases.

Name	Code	Coordinates		Date	pH	T	CO2	N2	O2	CH4	H2	He	Ne	Ar	R/Ra	He/Ne	∂13C(CO2)	CO2/3He	40Ar/36Ar	Atm	Mantle
		E	**N**			˚C	%	%	%	%	ppm	ppm	ppm	ppm			‰ (vs V-PDB)			%	%
Vranjska Banja	SRB1	42.5452	22.0064	06/11/2019	6.5	90	44.14	54.27	0.26	1.72	802	1013	8.81	6120	0.31	115	-4.7	1.00.E+09	298.6	0.25	5.04
Suva Cesma	SRB5	43.2345	21.5144	07/11/2019	6.36	21.1	43.52	55.90	0.06	0.13	-	1068	9.36	6150	0.30	114	-9.0	9.80.E+08	297.4	0.26	4.88
Vica	SRB6	43.2094	21.3810	07/11/2019	7.4	14.6	22.40	73.45	0.39	2.31	-	5819	4.38	5617	0.28	1329	-10.9	9.76.E+07	307.5	0	4.59
Josaniska Banja	SRB10	43.4001	20.7353	08/11/2019	8.3	73.1	0.13	98.28	0.11	0.19	11	862	12.68	13500	0.10	68.0	-17.7	1.10.E+07	296.9	0.45	1.57
Josaniska Banja	SRB11	43.3869	20.7528	08/11/2019	8.3	71.5	0.02	97.30	0.32	0.39	6	360	11.83	15800	0.08	30.4	-16.2	5.89.E+06	297.1	1.02	1.14
Mokra Gora	SRB16/A	43.7936	19.5253	10/11/2019	12.23	-	0.10	10.43	0.09	7.14	816200	-	-	2350	-	-	-14.3				
Mokra Gora	SRB16/B	43.7936	19.5253	10/11/2019	12.23	15.9	0.15	10.16	0.08	5.21	854100	0.95	1.79	2190	0.70	0.53	-17.1	1.61.E+09	295.2	59.98	1.64
Ribnica	SRB17/A	43.7035	19.5788	10/11/2019	11.66	15.1	0.003	51.63	0.06	14.68	340500	4.32	7.32	7280	0.57	0.59	-	9.31.E+06	296.7	53.88	0.51
Ribnica	SRB17/B	43.7033	19.5790	10/11/2019	11.66	-	0.003	51.79	0.19	15.73	323600	-	-	6300	-	-	-				
Petnica	SRB21	44.2454	19.9357	11/11/2019	7.11	14.9	2.03	93.07	3.76	0.02	-	7	-	8640	-	-	-19.7				
Bogatic	SRB29	44.8709	19.4803	13/11/2019	6.3	78	25.34	55.93	0.29	19.06	65	401	6.85	10800	0.24	58.5	-5.2	1.91.E+09	295.1	0.52	3.85
Savinac 2	SRB30	44.0257	20.3856	13/11/2019	7.1	19.4	2.53	92.38	0.0004	0.04	-	194	-	9860	-	-	-20.2				
Mataruska Banja	SRB12	43.6901	20.6113	09/11/2019	6.3	50	32.25	65.65	0.67	1.56	-	1066	6.37	7970	0.91	167	-6.4	2.37.E+08	298.0	0.17	14.89
Ovca	SRB31	44.8908	20.5349	13/11/2019	7.57	19.4	0.51	11.07	0.07	87.66	3	37.3	0.24	509	0.89	154	-9.2	1.10.E+08	348.8	0.18	14.56
Tulare	SRB3	42.8019	21.4518	06/11/2019	6.8	34.5	95.78	4.37	0.45	0.01	-	62.8	0.13	231	0.57	466	-4.5	1.90.E+10	305.5	0.05	9.34
Sijarinska Banja	SRB4	42.7764	21.6008	06/11/2019	6.43	58	99.88	0.89	0.22	0.03	-	2.34	0.06	32	0.80	38.7	-4.6	3.83.E+11	299.1	0.8	12.98
Kursumlijska Banja	SRB7	43.0570	21.2528	07/11/2019	6.56	68	93.59	5.58	0.18	0.41	-	66.0	0.41	594	0.28	161	-5.3	3.63.E+10	298.7	0.18	4.56
Lukoska Banja	SRB8/A	43.1645	21.0307	08/11/2019	6.7	41.7	90.50	8.79	0.3	0.13	-	59	-	-	-	-	-2.9				
Lukoska Banja	SRB8/B	43.1645	21.0307	08/11/2019	6.09	54	91.71	5.82	0.18	0.08	-	72.6	0.51	873	0.73	142	-2.6	1.24.E+10	297.1	0.2	11.93
Lukoska Banja	SRB8/C	43.1644	21.0323	08/11/2019	6.23	70	91.63	7.77	0.37	0.28	-	85	-	846	-	-	-2.5				
Zarevo	SRB9	43.2824	20.9938	08/11/2019	5.88	12.9	94.34	3.93	0.07	1.23	-	50.9	0.39	652	0.53	130	-0.1	2.50.E+10	303.3	0.22	8.65
Vrnjacka Banja	SRB13	43.6176	20.8863	09/11/2019	6.2	34.5	91.95	5.51	0.10	1.60	-	106	0.38	619	1.00	278	-2.4	6.19.E+09	300.3	0.09	16.38
Lomnicki Kiseljak	SRB14	43.5110	21.3281	09/11/2019	6.5	16.8	82.59	14.77	1.89	0.02	-	318	1.10	1280	0.53	290	-5.0	3.51.E+09	306.4	0.09	8.67
Cibutkovica	SRB23	44.3380	20.2381	12/11/2019	6.1	20.7	96.85	1.52	0.07	1.47	14	29.8	0.18	181	0.85	161	-4.5	2.74.E+10	300.9	0.18	13.91

Krusevica	SRB24	44.3473	20.3960	12/11/2019	6.3	21.4	96.79	1.78	0.35	0.90	1.7	2.92	0.23	250	0.95	12.7	-5.2	2.49.E+11	295.1	2.48	15.17
Rudovci	SRB25	44.3835	20.4000	12/11/2019	6.5	17.2	92.89	4.72	0.22	2.52	-	181	0.23	354	1.19	779	-6.0	3.07.E+09	312.1	0.02	19.51
Rudovci	SRB25/A	44.3835	20.4000	12/11/2019	-	-	98.08	1.31	0.07	1.08	-	-	-	-	-	-	-6.1				
Vozd Voda	SRB26	44.2963	20.6955	12/11/2019	6.6	19.8	58.35	37.67	0.06	3.95	-	586	1.37	1830	0.56	427	-8.8	1.28.E+09	308.7	0.05	9.17
Cerovac	SRB27	44.3244	20.8747	12/11/2019	6.3	19.5	97.04	1.35	0.06	0.80	-	6.50	0.20	180	0.51	33.0	-6.3	2.08.E+11	301.5	0.94	8.21
Smederevska Palanka	SRB28	44.3542	20.9674	12/11/2019	6.2	20.7	98.10	0.70	0.07	2.56	-	2.56	0.08	116	0.52	31.4	-7.3	5.26.E+11	296.8	0.99	8.36
Ljiljance/Bujanovac	SRB2	42.4387	21.8119	06/11/2019	6.47	18.7	95.06	6.08	0.08	0.003	-	108	0.42	680	0.34	259	-5.6	1.87.E+10	298.6	0.1	5.56

III.5. Discussion

He in natural fluids from tectonically active regions is typically interpreted as originating from three distinct sources: the mantle, the crust, and air (e.g., Burnard et al., 2013; O'Nions & Oxburgh, 1988; Sano et al., 1997). These three sources are characterized by distinct He isotopic signatures: (a) 6.1 ± 0.9 Ra, for the European Subcontinental Lithospheric Mantle, ESCLM (Gautheron & Moreira, 2002); (b) 0.01–0.02 Ra, for pure crustal fluids dominated by radiogenic ^{4}He produced by U and Th decay (Ballentine & Burnard, 2002); (c) 1 Ra, for air (Ozima & Podosek, 2002). ^{4}He/^{20}Ne ratios are >1,000 for crust and mantle and 0.318 for air respectively (Sano et al., 1985). Because of these different end-member compositions, He isotopes in natural fluids, coupled with their ^{4}He/^{20}Ne ratios, can be used to resolve the relative He contributions from the three sources (e.g., Caracausi & Sulli, 2019; Sano & Wakita, 1985; Sano et al., 1997, and references therein). Using the approach proposed in Sano et al. (1997), and assuming that all ^{20}Ne is atmospheric, we estimate low atmospheric contributions (<3%, Table III.1) for all samples, except those collected from the hyperalkaline waters, and mantle helium fractions of 1% to ~20%, with the highest fractions calculated for the CO_2-dominated samples (Fig. III.5). It is interesting to note that the two N_2-rich samples (SRB10 and SRB11) with the lowest He isotopic signatures (R/Ra < 0.1; mantle component ~1%) have been collected nearby two large granite intrusions (see inset in Fig. III.1) that are characterized by high U and Th concentrations (of, respectively, 563 and 270 ppm) (Schefer et al., 2011). Hence, it is reasonable that these low He isotopic ratios reflect the high radiogenic ^{4}He production in the U-Th-rich lithologies.

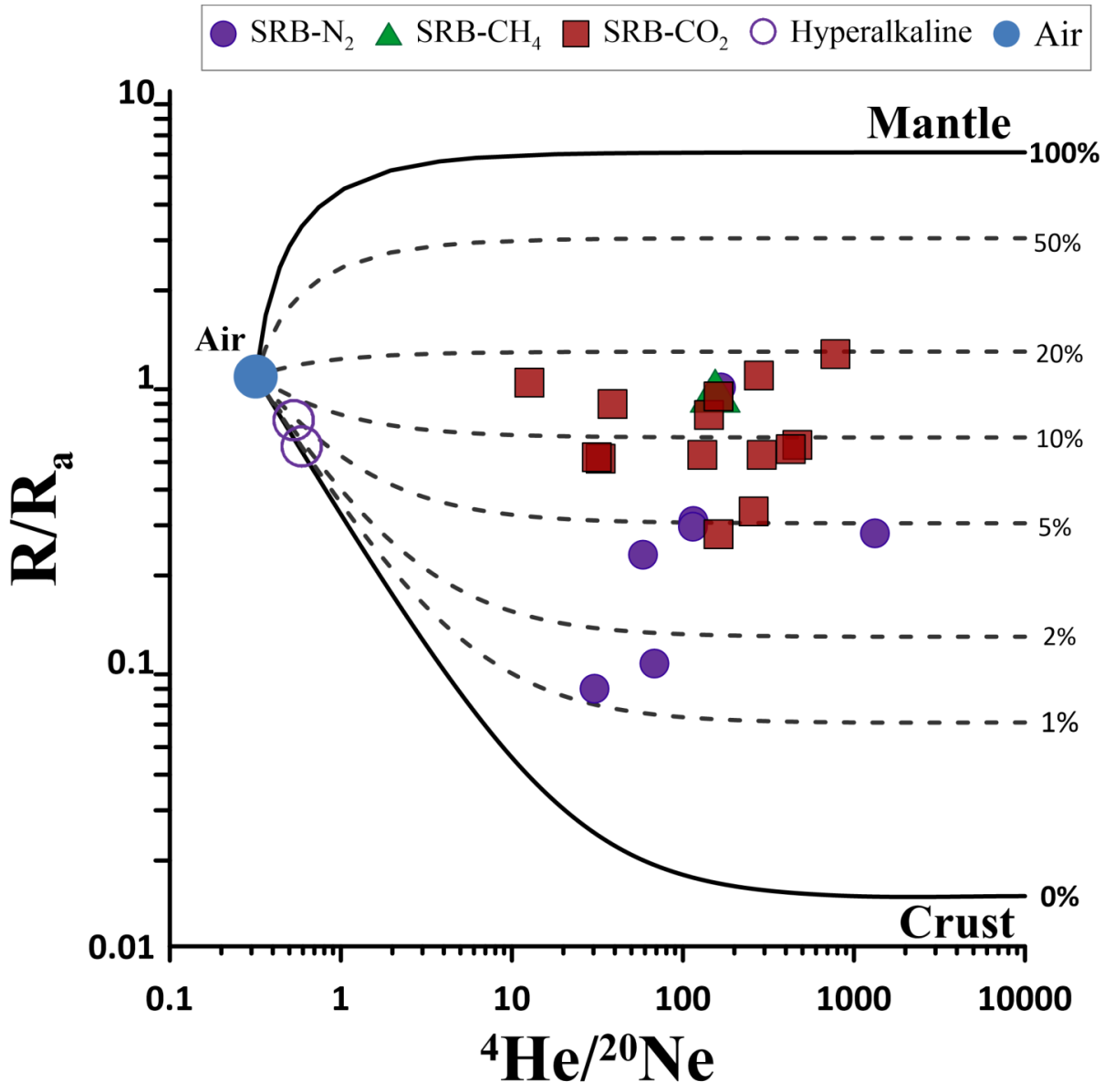

Figure III.5 | $^{3}He/^{4}He$ ratios (as R/Ra) versus $^{4}He/^{20}Ne$ ratios. CO_2-dominated samples (red squares) exhibit the ^{3}He-richest isotope signatures (corresponding to mantle He contributions of 5–20%), whereas N_2-dominated gases (purple circles) extend to more radiogenic values (i.e., crustal) with mantle He contributions up to 5%. For these samples only SRB12 show higher mantle He contribution like CO_2-dominated samples. Samples from the hyperalkaline waters have the lowest $^{4}He/^{20}Ne$ ratios, reflecting an atmospheric derivation.

III.5.1. Insights from $CO_2/^3He$ ratios

Additional insights into volatile sources and sinks, and into the processes occurring during (a) the migration of fluids through the crust and (b) their storage in shallow crustal layers can be derived from a joint analysis and interpretation of He and carbon isotopic signatures (e.g., Barry et al., 2020; Holland & Gilfillan, 2013). Our study highlights that natural gases in the Vardar zone of Serbia are dominated by either CO_2 or N_2 (Fig. III.3) and are characterized by a significant spread of $\delta^{13}C$ compositions (Fig. III.4) and R/Ra ratios (Fig. III.5) that could reflect a multiplicity of gas sources involved. ^3He in natural fluids is mainly primordial and sourced from the mantle. Thus, combining CO_2 and ^3He (into the $CO_2/^3He$ ratio) allows evaluating enrichments or depletions relative to a mantle-like signature (Fig. III.6). However, in continental environments, the lithospheric mantle often brings record of heterogeneities caused by metasomatizing events (Rizzo et al., 2018) that can lead to C enrichment ($CO_2/^3He$ ratio of 7×10^9) with respect to the MORB ($1.5–2\times10^9$; Marty et al., 2020). The European Subcontinental Lithospheric Mantle (ESCLM) is thought to be also isotopically heavier than the MORB ($\delta^{13}C_{CO2}$ of MORB from −8‰ to −4‰; Bräuer et al., 2016; Rizzo et al., 2018, and reference therein), so that we assume here a $CO_2/^3He$ ratio of $2–7\times10^9$ and $\delta^{13}C$ of −3.5‰ (Bräuer et al., 2016) for the local mantle source. Our CO_2-rich and N_2-rich fluids are characterized by distinct $CO_2/^3He$ ratios that are, respectively, higher (up to 5.26×10^{11}) and lower (as low as 5.89×10^6) than the above defined mantle range (Fig. III.6).

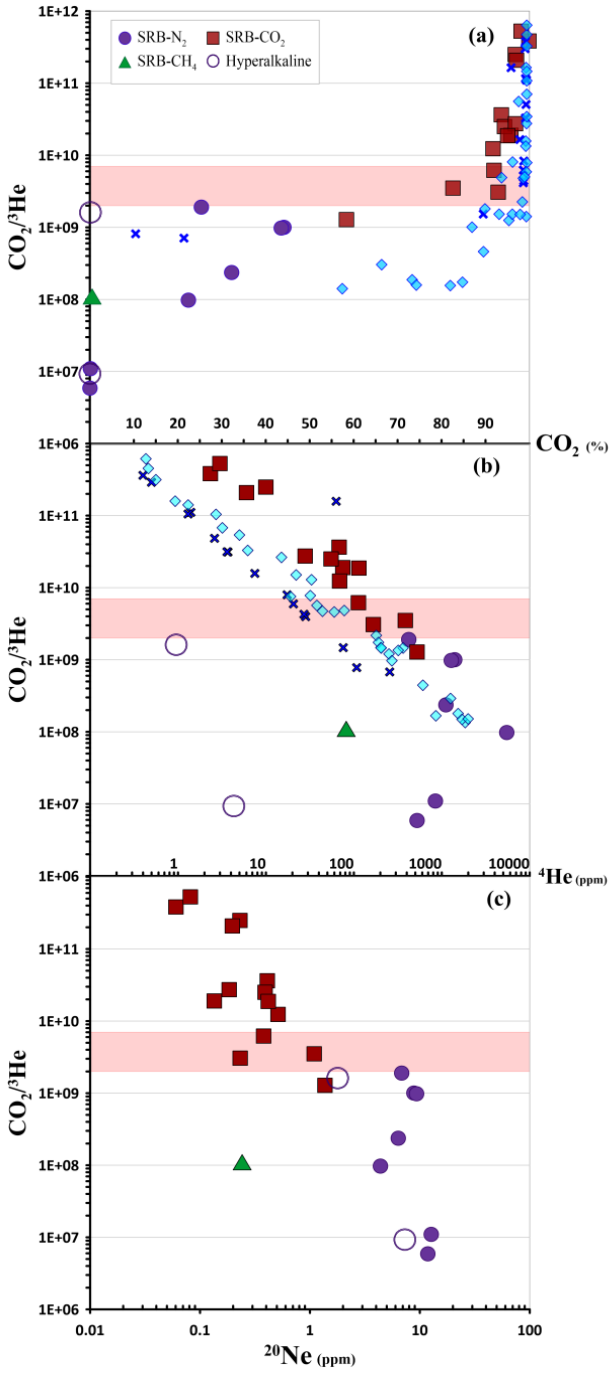

Figure III.6 | $CO_2/^3He$ ratios versus (**a**) CO_2, (**b**) ^4He, and (**c**) ^{20}Ne concentrations. The panel shows a trend from CO_2-rich, high $CO_2/^3He$ (low in He and Ne) samples to He-Ne-rich, low $CO_2/^3He$ ratio samples. The SCLM range is given by the shaded area ($CO_2/^3He$ = 2–7×10^9; Bräuer et al., 2016; Marty et al., 2020). Data for other central and eastern Europe areas follow the same trend (dark blue crosses, Bräuer et al., 2016; light blue diamonds, Weinlich et al., 1999).

In tandem with gas samples from nearby regions (Eger rift, Weinlich et al., 1999; Austria/Slovenia border region, Pannonian basin; Bräuer et al., 2016), our samples identify a continuous trend from (a) a CO_2-rich, high $CO_2/^3He$ ratio end-member, and (b) a ^4He-^{20}Ne-rich, low $CO_2/^3He$ ratio end-

member (Fig. III.6a–c). The high $CO_2/^3He$ ratios (10^{12}–10^{14}) of most CO_2-rich crustal continental gases are commonly interpreted (Sano & Marty, 1995; Sherwood Lollar et al., 1997) to result from decarbonation reaction and biological processes in the crust that produce a CO_2-rich, ^3He-free gas. We thus propose that the CO_2-dominated gases are mixtures of CO_2-rich crustal gas with a 5–20% mantle-derived component (Fig. III.5). This is additionally supported by Figure III.7, in which the CO_2-rich samples fall along hypothetical mixing curves between a SCLM pole and a set of hypothetical crustal end-members with same radiogenic R/Ra ratio but different $CO_2/^3He$ ratios. Moreover, a crustal (limestone + organic-biogenic) carbon addition to a SCLM-like gas is suggested by the $\delta^{13}C$ versus $CO_2/^3He$ ratio plot of Figure 8. Solid gray lines show mixing between three end-member: mantle ($CO_2/^3He$ = 2–7×10^9, $\delta^{13}C$ = −3.5‰; Bräuer et al., 2016; Rizzo et al., 2018), limestone ($CO_2/^3He$ = 10^{13}, $\delta^{13}C$ = 0‰), and sediment ($CO_2/^3He$ = 10^{13}, $\delta^{13}C$ = −30‰) after Sano and Marty (1995). Interpreting the N_2-dominated samples is less straightforward. However, except for sample SRB12, He in all the investigated N_2-dominated gases is minimally contributed by the mantle (<5%; Fig. III.5) and by atmosphere. Furthermore, these samples exhibit the highest ^4He and ^{20}Ne contents (Fig. III.6b-c), and the lowest $CO_2/^3He$ ratios and He isotopic signatures (Fig. III.7). Although there is no a priori reason to expect a correlation between ^4He and ^{20}Ne with the $CO_2/^3He$ ratio, such a correlation has been found regionally in natural gases (Ballentine et al., 2002; Gilfillan et al., 2009). ^4He is constantly produced in the subsurface by the radiogenic decay of U, Th, while ^{20}Ne enters subsurface groundwater systems as a component of air-saturated meteoric water (Ballentine & Sherwood Lollar, 2002). This atmospheric component can then be transferred to natural fluids in crustal layers, interacting with the groundwater that are able to trap the air component together with large amount of radiogenic volatiles (e.g., ^4He) produced over time into the crust and degassing through it (e.g., Ballentine et al., 2002). Previous studies indicated that such correlations are the result of ^4He accumulating in the groundwater which also contains atmospheric-derived ^{20}Ne, and subsequent quantitative partitioning of both ^4He and ^{20}Ne into the gas phase due to fractionation events, probably in the groundwater (e.g., Gilfillan et al., 2008). It is worth noting

that gases from gas-fields from central and eastern Europe (e.g., Eger rift, Austria/Slovenia border region, Pannonian basin) fit with similar CO_2-N_2-He concentration arrays (e.g., Bräuer et al., 2016; Weinlich et al., 1999), supporting the recurrence of solubility-dependent volatile fractionation. The low CO_2 concentrations and low $CO_2/^3He$ ratios in the N_2-dominated gases (Fig. III.5 and Fig. III.7), combined with their more negative 13C-compositions (Fig. III.8), imply some mechanism of CO_2 removal during gas-water-rock interactions. During their migration through the crust, volatiles can interact with groundwater and, due to its high solubility, CO_2 dissolves preferentially in water relative to He (in the range of temperature up to 90 °C: CO_2 solubility > He solubility; Ballentine et al., 2002; Clever et al., 1979; Gilfillan et al., 2009; Scharlin et al., 1996). Furthermore, groundwater can also precipitate carbonate minerals, additionally modifying the dissolved carbonate equilibria (Barry et al., 2020; Gillfillan et al., 2009). In both cases, CO_2 is retained either in form of carbonate minerals (mineral trapping) or dissolved in solution (solubility trapping) (e.g., Baines et al., 2004; Bradshaw et al., 2005) leading to decreased $CO_2/^3He$ ratios and more negative $\delta^{13}C$ in the residual gases.

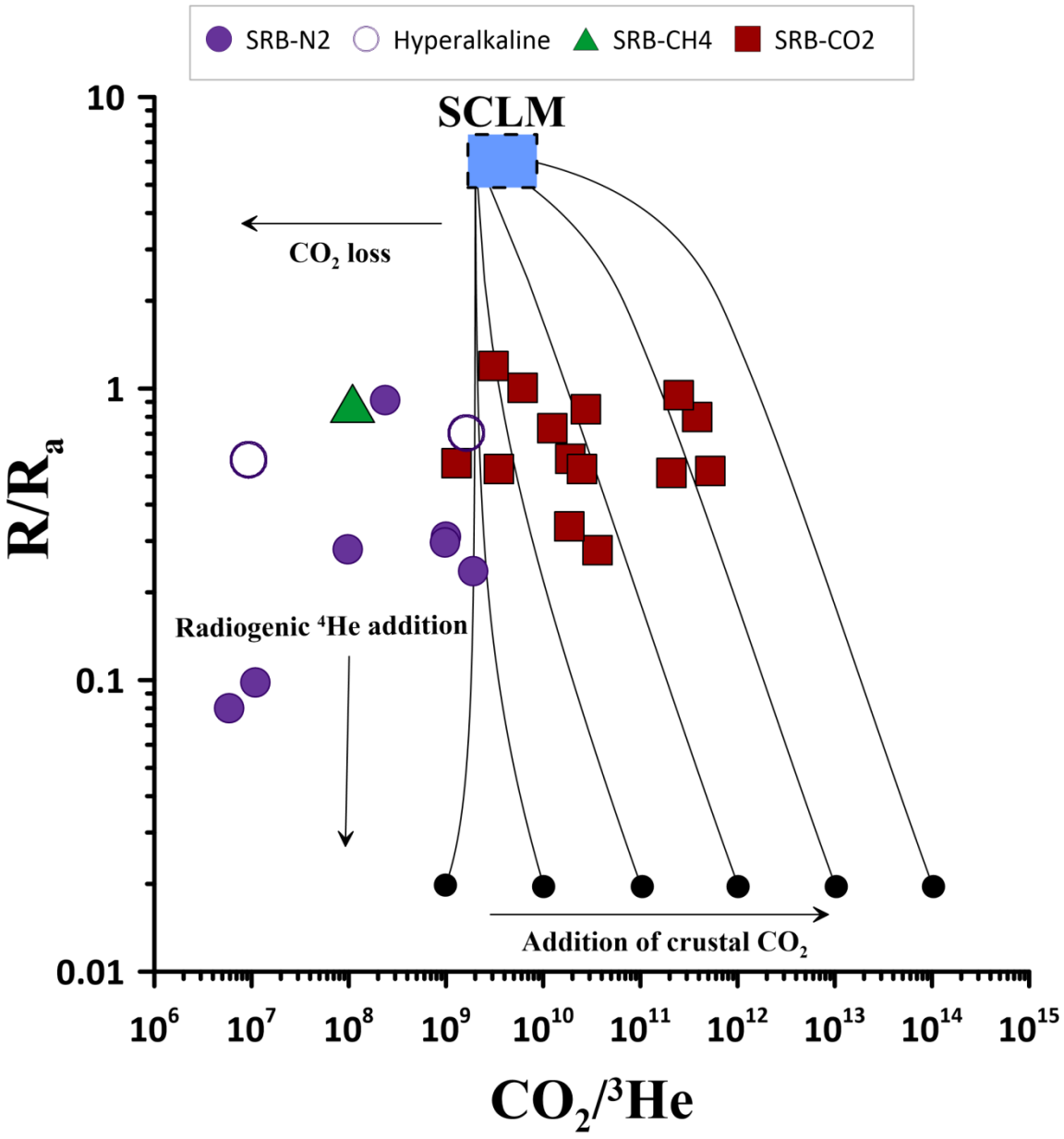

Figure III.7 | R/Ra versus $CO_2/^3He$ ratio plot of Serbian gases. Binary mixing curves are shown between the SCLM (6.1 ± 0.9 Ra and $CO_2/^3He$ of 7×10^9; Bräuer et al., 2016; Gautheron & Moreira, 2002) and different hypothetical crustal end-members with same helium isotopic composition (0.02 Ra) but variable $CO_2/^3He$ ratios. N_2-dominated, CH_4-dominated, and alkaline springs require CO_2 loss via gas-water-rock interactions.

In order to interpret the variability of $CO_2/^3He$ ratios coupled to that of $\delta^{13}C$ that we recognized in the Vardar zone samples, we investigate the processes of CO_2 partial dissolution in water, and calcite precipitation, by modeling (see Gillfillan et al., 2009) their potential control on $CO_2/^3He$ ratios and CO_2 carbon isotopic compositions ($\delta^{13}C$) (Fig. III.8). According to Gillfilan et al. (2009), the process can be modeled as (a) an open-system degassing (Rayleigh type) at isotopic equilibrium

(between phases) and (b) calcite precipitation (Fig. III.8). We model the progressive variation of the $CO_2/^3He$ ratio in the residual gas assuming that the $CO_2/^3He$ ratio and the $\delta^{13}C_{CO2}$ of the pristine gas are of mantle-type ($CO_2/^3He$ range = $2–7\times10^9$, $\delta^{13}C = -3.5‰$; Bräuer et al., 2016; Marty et al., 2020; Rizzo et al., 2018). We stress that here we consider the case of a pristine gas as the mantle end-member, but the choice of a different end-member, resulting from the mixing between crustal (limestone + organic-biogenic) and mantle-derived fluids, would lead to similar (but shifted) model curves. Our model curves, obtained over a range of pH values for increasing extents of gas dissolution, are plotted in Figure III.8. Overall, we find the model CO_2 dissolution lines at pH between 5.6 and 7 fit the data set nicely. This comparison demonstrates the N_2-dominated samples can be interpreted as due to different degrees of CO_2 loss by dissolution, from about 50% (for samples SRB 14, SRB 25, SRB 26) to about 99% for more fractionated samples. These gas/water fractionations ultimately result in 13C-depleted compositions and $CO_2/^3He$ spanning over 3 orders of magnitude. We caution that, for a thick crustal sector with a potentially high number of stratified aquifer such as in Serbia, a simple open-system degassing (Rayleigh type) model approach is evidently a simplified approach. In fact, it is possible that more complex gas-aquifer interactions, such as complete gas dissolution in deep aquifer, followed by multistep degassing upon groundwater upward migration (Chiodini et al., 2011), could have taken place instead. Also, we cannot exclude the lowest $\delta^{13}C_{CO2}$ values are not at least partially reflecting a biogenic origin, and carbonate precipitation (together with CO_2 dissolution at a lower pH than 5.6–7; Gillfillan et al., 2009) has not taken a role. This notwithstanding, although simplified, our model clearly highlights the role played by gas-water interaction in determining the composition of Serbian gas manifestations.

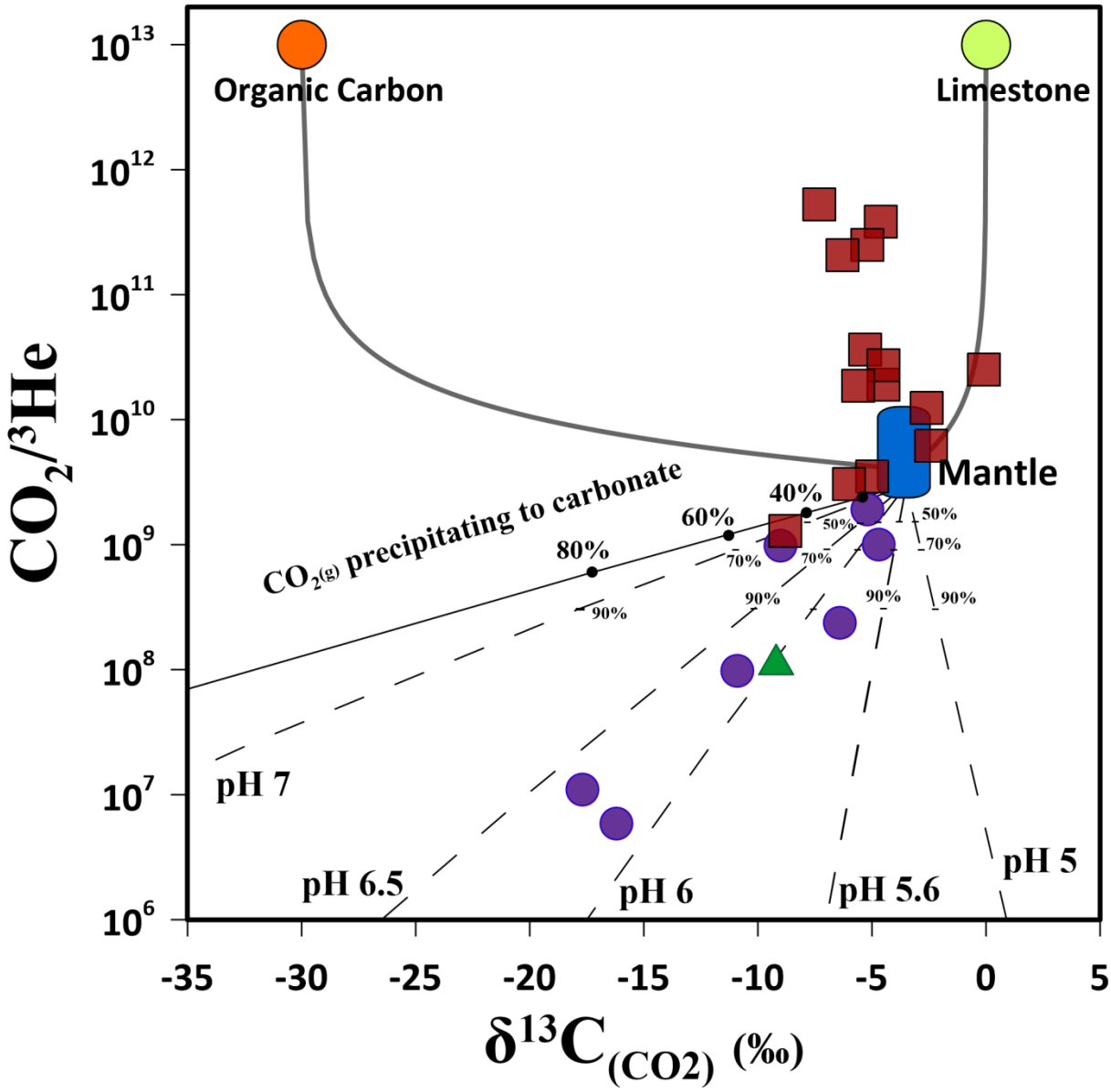

Figure III.8 | $\delta^{13}C(CO_2)$ versus $CO_2/^3He$ plot. The predicted model lines for Rayleigh-type gas dissolution at different pHs are shown as broken lines, while the solid lines are the predicted trend for carbonate mineral precipitation. Changes in $\delta^{13}C(CO_2)$ are calculated following the method from Gillfillan et al. (2009) using the Rayleigh fractionation equation either for precipitation or for dissolution. In the case of precipitation there is zero ^3He loss from the CO_2 phase and $CO_2/^3He$ changes in proportion to the fraction of the remaining CO_2 phase while for CO_2 dissolution, the change in $CO_2/^3He$ ratio is calculated following the Rayleigh equation.

III.5.2. Mantle Helium Source and Tectonic Implications

The chemistry of both CO_2-dominated and N_2-dominated gas samples unravels the active outgassing of mantle-derived volatiles (He and, to a lesser extent, CO_2) in Serbia. In continental areas far from any evidence of active volcanism, the possible main sources of mantle-derived volatiles are (a) reservoirs of fossil mantle-derived volatiles (e.g., Ballentine et al., 2001), (b) the presence of magmatic intrusions into the crust, and (c) the transfer of mantle He through lithospheric faults (e.g., Burnard et al., 2013; Caracausi & Sulli, 2019; Kennedy et al., 2007; Lee et al., 2019). A reservoir of fossil mantle-derived volatiles as a source of the mantle He should not be associated to a heat-excess, as presently observed at regional scale in Serbia (up to 130 mW/m^2). Magmatic intrusions in the crust could in principle supply both mantle-derived heat and fluids toward the surface. However, at a regional scale, a magmatic intrusion can be considered as a localized source of both volatiles and heat. In spite of some possible long-range transport through groundwaters, the He isotopic ratio and heat flux anomaly should thus decrease upon increasing distance from the position of the source at depth. In the study area, in contrast, we recognize a fairly homogeneous and generalized outgassing of mantle-derived He (Fig. III.1) and high regional heat flow. Therefore, it is unlikely that isolated magmatic intrusions in the crust are involved. Volatiles (i.e., CO_2, He) can reach the surface directly from the mantle through lithospheric faults (e.g., Burnard et al., 2012; Caracausi & Sulli, 2019; Lee et al., 2019), acting as a network of pathways of high permeability enhancing the transfer of deep fluids and heat through the crust. The study area is strongly affected by active tectonics as indicated by seismicity (http://www.seismo.gov.rs/Seizmicnost/Katalog-zemljotresa.pdf.). All the investigated emissions are located along tectonic discontinuities, even if all of them are not in correspondence of the main regional faults (Fig. III.1). Hence, a system of well-connected faults with roots down to the mantle, through which the fluids and heat from the mantle can cross the crust and reach the surface, seems the most plausible mechanism to explain the combined high heat flux and regional-scale outgassing

of mantle He in the study area. In Serbia, crustal thickness progressively increases in ~260 km, from about 25 km in the north up to 35 km in the south (Horváth et al., 2015; Marovic et al., 2007). The greater thickness in the south of Serbia could lead to a higher production of ^{4}He by the U and Th decay if we assume a homogeneous and constant distribution of U and Th concentrations in the crust below the study area. However, we find no geographical control on He isotopic signature, and a large He isotope variability occurs sometimes over short distances (e.g., 1 order of magnitude change in only 27 km; Fig. III.9). Therefore, the variability of the He isotopic signature does not appear to correlate with crustal thickness. Moreover, we highlight that the lowest He isotopic signatures (SRB10 site, 0.08 Ra; SRB11 site, 0.10 Ra) have been measured in fluids that circulate in U-rich and Th-rich granitic rocks. Thus, it is reasonable that the lowest He isotopic signatures could be due to local high production of ^{4}He (Fig. III.9, Section b) from granitoid lithologies.

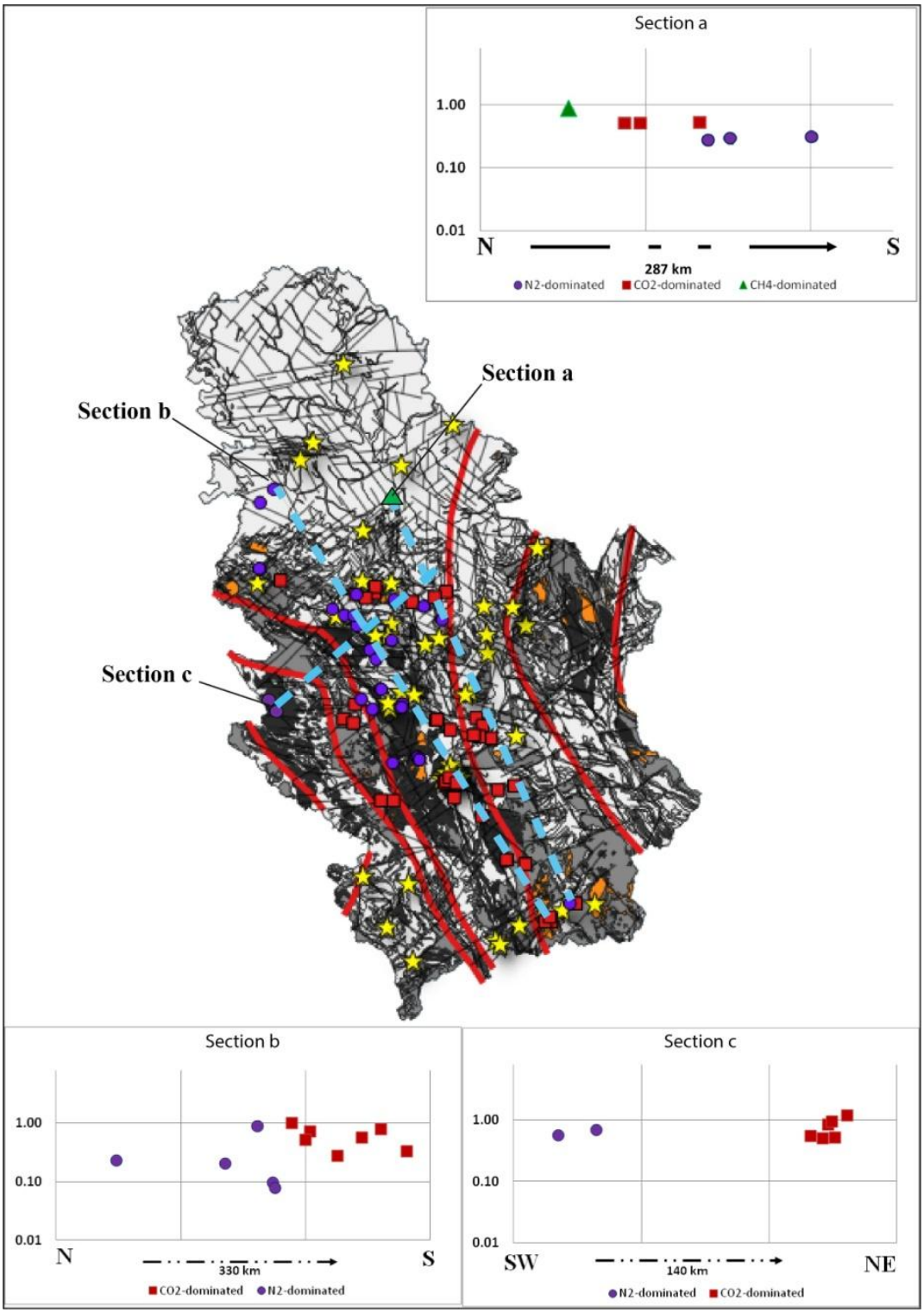

177

178 **Figure III.9** | R/Ra distribution on Serbia region. Geological map with samples location, faults and three section
179 respectively named a,b and c. The three graphs show the R/Ra trend vs. distance referred to th three sections on the
180 map.

181

182

A quantitative He flux estimate can provide insights into the transfer of volatiles through the crust. Estimates of the ^{4}He flux in continental regions are mainly based on calculations of in-situ production and steady-state degassing through the continental crust, and these calculations yield a crustal ^{4}He degassing flux of ~3.3 ± 0.5×10^{10} atoms m^{-2} s^{-1} (Buttitta et al., 2020, and references therein). However, experimental work highlights that the release of volatiles from rock increases in an active stress field, which implies that ^{4}He degassing through the crust can be episodic in active tectonic areas (e.g., Bräuer et al., 2016; Honda et al., 1982; Torgersen & O'Donnell, 1991). It is worthy of note that deformation and failure of rocks crack mineral grains, causing pervasive microfracturing. Consequently, the rocks can increase their porosities from 20% to as high as 400% prior to failure, opening new microfracture surfaces, and eventually causing macroscopic failure and fracture of rocks (Bräuer et al., 2016). These processes lead to a higher release of volatiles (e.g., He) previously trapped within mineral grains along fracture networks and the pore fluids transport these volatiles through the crust. Considering that, during the transfer of mantle-derived fluids through the crust, the addition of crustal radiogenic ^{4}He produces a decrease of the pristine mantle He isotopic ratio, it is possible to assess the flux of mantle-derived He by using the approach proposed by O'Nions and Oxburgh (1988) and making a guess for the crustal He flux range. This method is based on the assumption that, if the degassing of He occurs at steady state, then it is possible to estimate the mantle He flux from the helium isotope composition of the system. This principle is illustrated in Figure 8 that shows the dependence of R/Ra in the surface gas on mantle He flux (for a crustal ^{4}He flux of 3.3 ± 0.5×10^{10} atoms m^{-2} s^{-1}). The three curves have been made following the equation:

$$\frac{R/R_{a_M}\cdot F_M + R/R_{a_C}\cdot F_C}{F_T} \qquad \text{Eq.1}$$

where R/Ra_M and R/Ra_C are the Helium isotopic compositions of mantle and crustal end members, F_M and F_C are the fluxes values for mantle and crust in atoms m^{-2} s^{-1} and F_T is the total flux. The solid curve refers to an average continental crust ^{4}He steady-state flux of $3.3 \pm 0.5 \times 10^{10}$ atoms m^{-2} s^{-1} (Buttitta et al., 2020) while the dotted curves refer to 10× and 100× the average continental crust steady-state He flux.

From this, we estimate a mantle-derived He flux in the study area of ~2.1×10^8 to ~9.0×10^9 atoms m^{-2} s^{-1}, up to 2 orders of magnitude higher than normally found in stable continental areas (<<10^8; e.g., O'Nions & Oxburgh, 1988).

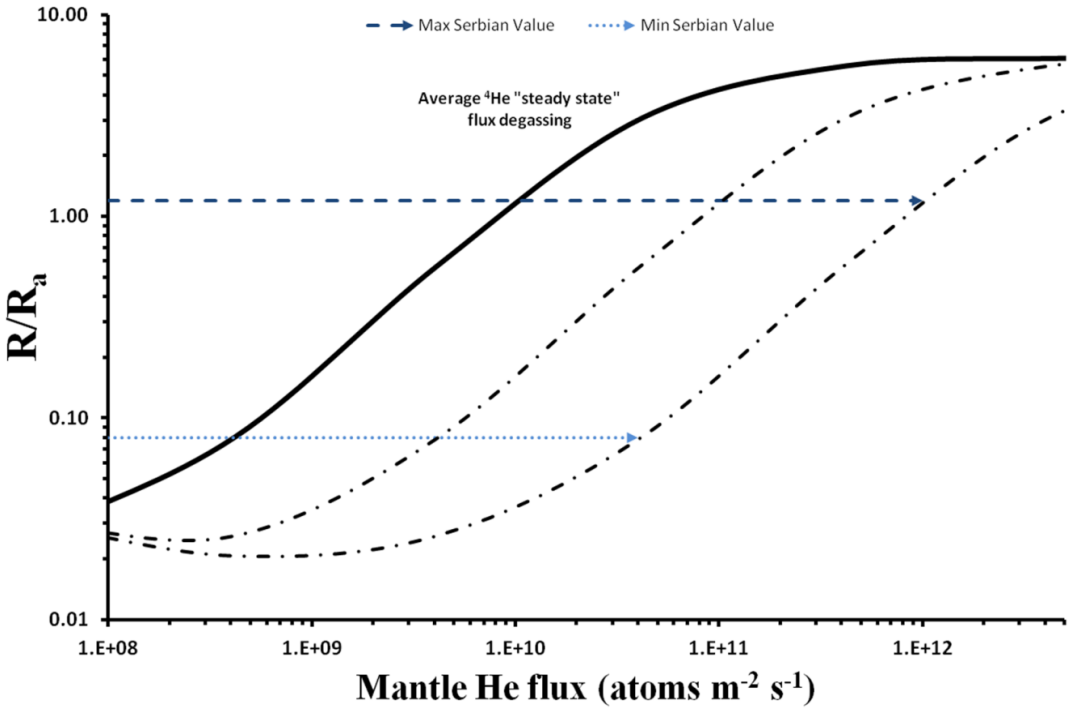

Figure III.10 | Helium isotope composition versus mantle-derived He flux. The lines are computed by using the approach proposed by O'Nions and Oxburgh (1988) that is based on the progressive addition (as a mixing) of a crustal He component that dilute the mantle He component producing a decrease of the He isotopic signature from the typical mantle derived component (6.1 Ra; Gautheron & Moreira, 2002) to the radiogenic signature (0.02 Ra; Ballentine & Burnard, 2002). The solid curve refers to an average continental crust ^{4}He steady-state flux of $3.3 \pm 0.5 \times 10^{10}$ atoms m^{-2} s^{-1} (Buttitta et al., 2020). The dotted curves refer to 10× and 100× the average continental crust steady-state He

flux. The blue dotted line corresponds to minimum and dark blue dashed line to maximum R/Ra values in our samples, and are used to infer the mantle He flux range in Serbia region.

However, in active tectonic regions an enhanced release of He from rocks occurs that is up to 10^4 times higher the steady-state values. Therefore, assuming a ^{4}He crustal flux of 10–10^4 times the average "steady-state" value, the mantle He fluxes increase to between 10^{11} and 10^{14} atoms m^{-2} s^{-1} (Fig. III.10). These are typical He fluxes encountered in active tectonic regions and/or in volcanic systems (Fig. III.11; Torgersen, 2010). Active fault zones are regions of advanced permeability that permit a fast transfer of volatiles through the crust, and seismicity is a strong evidence of the capacity of faults to transfer fluids through the crust. However, the mechanisms that control the migration of fluids in the deep crust (e.g., ductile layers) are still not well recognized (e.g., Caracausi & Sulli, 2019; Kulongoski et al., 2005). In active tectonic regions, fluids can move via developing fault-fracture meshes with a mechanism analogous to the fault valve model that drives flow by fluid over-pressurization and stress switching (compression to extension) (Newell et al., 2015; Sibson, 2013, 2020), or by creep cavitation that can establish a dynamic granular fluid pump in ductile shear zones (i.e., Fusseis et al., 2009). Therefore, considering: (a) that the study area is affected by extensional tectonics and active seismicity down to the crust-mantle boundary (Faccenna et al., 2014; Marović et al., 2007; Metois et al., 2015); (b) the high regional heat flow (up to 130 mW/m^2) due to the up-rise of the asthenosphere up to 50–60-km depth at regional scale (Horváth et al., 2015), (c) the presence of inherited lithospheric tectonic discontinues that allowed the up-rise of magmas since the Jurassic (Zelić et al., 2010), and that can still work today as pathways for the transfer of deep volatiles through the crust, (d) the computed high fluxes of mantled derived He, we conclude that the mantle below Serbia is the most obvious source of the surface-released heat and fluids.

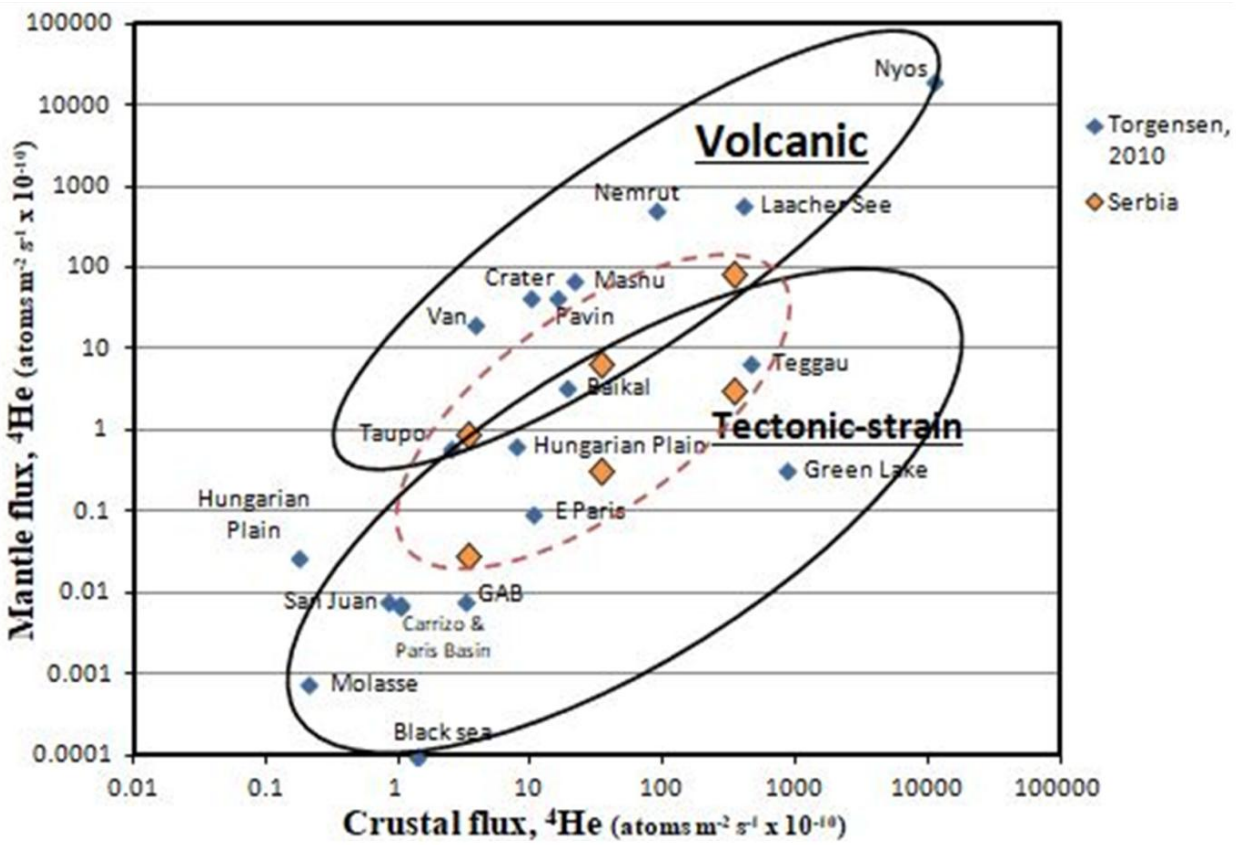

Figure III.11 | Crustal vs. Mantle derived He fluxes. Crustal-derived He fluxes in Serbia compared with mantle-derived He fluxes estimated by using the approach proposed by O'Nions and Oxburgh (1988). The assessed mantle-derived He flux for the Serbian gases (orange diamonds), using the highest R/Ra value, is ~9.0×10^{9} atoms m^{-2} s^{-1} while for the lowest R/Ra value the mantle derived He flux is ~3×10^{9} atoms m^{-2} s^{-1}. For crustal-derived ^{4}He fluxes being 10–10^{4} times higher than the "steady state" crust, the mantle helium fluxes would also be in the order of magnitude of values characteristic of "Volcanic field" and/or "Tectonic-strain field" (red dotted ellipse area; modified after Torgensen [2010]). The six orange diamonds (Serbian point) represent, respectively, the mantle ^{4}He flux values for maximum and minimum R/Ra calculated on the base of continental crust ^{4}He production ($3.3 \pm 0.5 \times10^{10}$ atoms m^{-2} s^{-1}; Buttitta et al., 2020) and for 10 times and 100 times this value.

III.6. Conclusions

We investigated the chemical and isotopic composition of natural gas manifestations along the Serbian Vardar zone, a mega-suture zone between the Eurasia and the African plate. Gas compositions are very heterogeneous and cluster into the groups of CO_2-dominated, N_2-dominated, and CH_4-dominated gases. Based on their He isotope compositions (<1.19 Ra), the CO_2-rich samples are interpreted as mixtures of crustal CO_2-rich gas (from limestones and organic matter) and mantle-derived components. The latter accounts for up to 20% of He (Fig. III.10). N_2-dominated samples are more atmospheric/crustal in nature (mantle He, <5%), and are inferred to have experienced extensive chemical and isotopic fractionations during water-gas-rock interactions in shallow crustal layers (Fig. III.12). We estimate a mantle-derived He flux of ~2.1×10^8 to ~9.0×10^9 atoms m^{-2} s^{-1}, or 2 orders of magnitude higher than normally found in stable continental areas. This elevated transport of mantle-derived volatiles in the Serbian crustal sector is interpreted to occur through lithospheric faults that work as regions of enhanced permeability and favor the migration of fluids throught the whole crust (Fig. III.12). Our study thus confirms that elevated outgassing of mantle-derived fluids can occurs in tectonically active continental regions, even far from active volcanism (e.g., Caracausi & Sulli, 2019; Chiodini et al., 2004; Lee et al., 2019; Tamburello et al., 2018). Finally, we recognize that at regional scale the mantle volatiles are sourced directly from the mantle together with heat and this scenario supports the asthenosphere up-rise and delamination processes at the mantle-crust boundary recognized by recent regional geophysical investigations (Belinić et al., 2021).

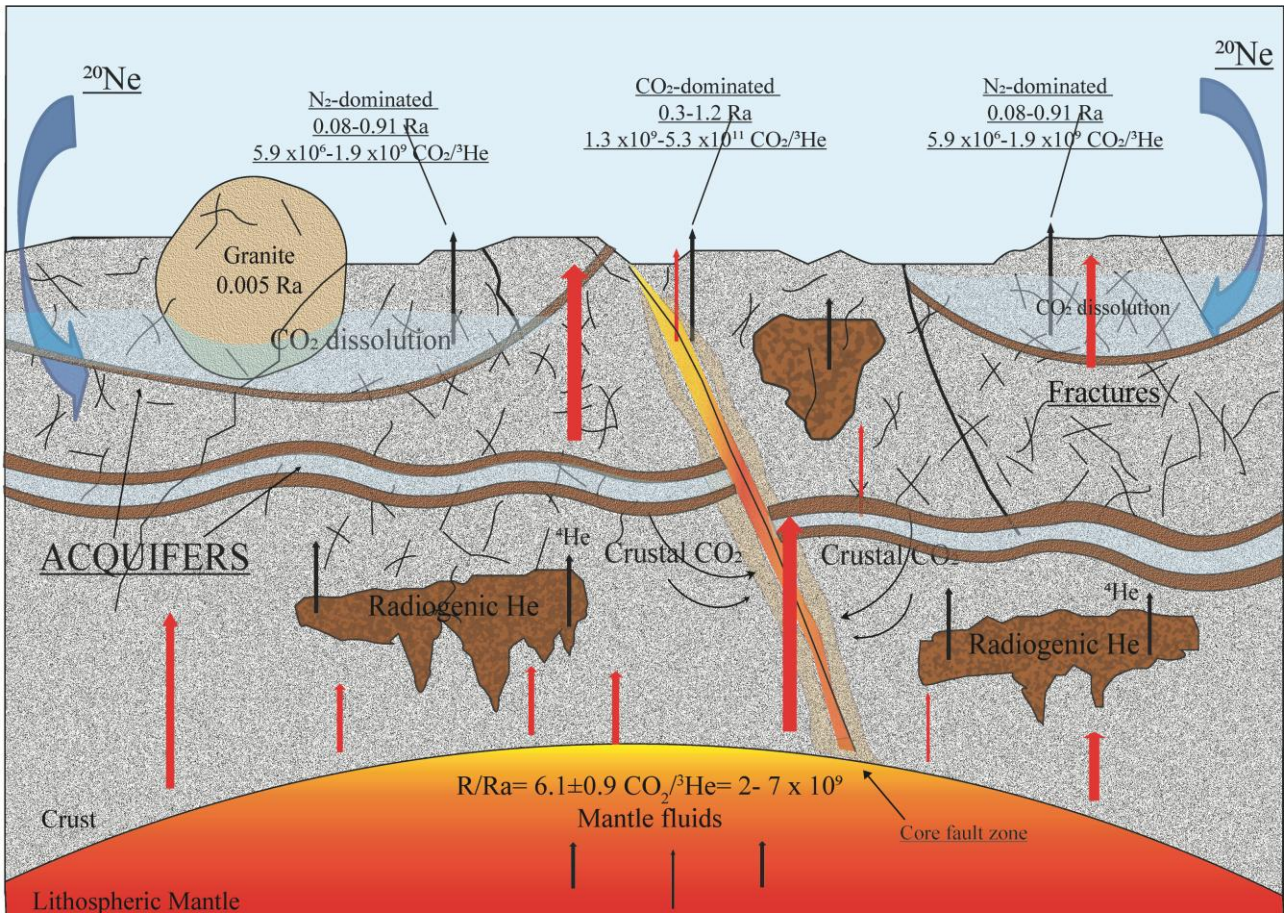

Figure III.12 | Possible source/s, pathways and processes for Serbian volatiles. Cross section cartoon showing the scenario proposed for the possible source, volatile pathways, and secondary processes (dissolution, radiogenic addition). Not to scale. Brown bodies are fossil intrusions which could be present deep under the surface. Red arrows indicate the heat flux.

References

Aeschbach-Hertig, W., Kipfer, R., Hofer, M., Imboden, D. M., Wieler, R., & Signer, P. (1996). Quantification of gas fluxes from the subcontinental mantle: The example of Laacher See, a Maar lake in Germany. *Geochimica et Cosmochimica Acta*, *60*, 31–41. https://doi.org/10.1016/0016-7037(95)00370-3

Baciu, C., Caracausi, A., Etiope, G., & Italiano, F. (2007). Mud volcanoes and methane seeps in Romania: Main features and gas flux. *Annals of Geophysics*, *50*(4), 501–511.

Baines Shelagh, J., & Worden Richard, H. (2004). The long-term fate of CO_2 in the subsurface: Natural analogues for CO2 storage. *Geological Society, London, Special Publications*, *233*(1), 59–85. https://doi.org/10.1144/GSL.SP.2004.233.01.06

Ballentine, C. J., Burgess, R., & Marty, B. (2002). Tracing fluid origin, transport and interaction in the crust. In D. R. Porcelli, C. J. Ballentine, & R. Weiler (Eds.), *Noble gases in geochemistry and cosmochemistry* (pp. 539–614). Geochemical Society and Mineralogical Society of America. https://doi.org/10.1515/9781501509056-015

Ballentine, C. J., & Burnard, P. (2002). Production, release and transport of noble gases in the continental crust. *Reviews in Mineralogy and Geochemistry*, *47*(1), 481–538. https://doi.org/10.2138/rmg.2002.47.12

Ballentine, C. J., O'Nions, R. K., Oxburgh, E. R., Horvath, E., & Deak, J. (1991). Rare gas constraints on hydrocarbon accumulation, crustal degassing and groundwater flow in the Pannonian Basin. *Earth and Planetary Science Letters*, *105*, 229–246. https://doi.org/10.1016/0012-821X(91)90133-3

Ballentine, C. J., Schoell, M., Coleman, D., & Cain, B. A. (2001). 300-Myr-old magmatic CO_2 in natural gas reservoir of the west Texas Permian basin. *Nature*, *409*(6818), 327–331. https://doi.org/10.1038/35053046

Ballentine, C. J., & Sherwood Lollar, B. (2002). Regional groundwater focusing of nitrogen and noble gases into the Hugoton-Panhandle giant gas field, USA. *Geochimica et Cosmochimica Acta*, *66*, 2483–2497. https://doi.org/10.1016/S0016-7037(02)00850-5

Barry, P. H., Negrete-Aranda, R., Spelz, R. M., Seltzer, A. M., Bekaert, D. V., Virrueta, C., & Kulongoski, J. T. (2020). Volatile sources, sinks and pathways: A helium-carbon isotope study of Baja California fluids and gases. *Chemical Geology*, *550*(2020), 119722. https://doi. org/10.1016/j.chemgeo.2020.119722

Bazylev, B., Popević, A., Karamata, S., Kononkova, N. N., Simakin, S. G., Olujić, J., et al. (2009). Mantle peridotites from the Dinaridic ophiolite belt and the Vardar zone western belt, central Balkan: A petrological comparison. *Lithos*, *108*, 37–71. https://doi.org/10.1016/j.lithos.2008.09.011

Belinić, T., Kolínský, P., & Stipčević, J. (2021). Shear-wave velocity structure beneath the Dinarides from the inversion of Rayleigh-wave dispersion. *Earth and Planetary Science Letters*, *555*, 116686. https://doi.org/10.1016/j.epsl.2020.116686

Bortolotti, V., Chiari, M., Marcucci, M., Photiades, P., Principi, G. & Saccani, E. (2008). New geochemical and age data on the ophiolites from the Othrys area (Greece): Implication for the Triassic evolution of the Vardar Ocean. *Ofioliti*, *33*, 135–151.

Bradshaw, J., Boreham, C., & La Pedalina, F. (2005). Storage retention time of CO_2 in sedimentary basins: Examples from petroleum systems. In E. Rubin, D. Keith, & C. Gilboy (Eds.), *Proceedings of the 7th International Conference on Greenhouse Gas Control Technologies* (pp. 541–549). Elsevier Science. https://doi.org/10.1016/b978-008044704-9/50055-0

Bräuer, K., Geissler, W. H., Kämpf, H., Niedermann, S., & Rman, N. (2016). Helium and carbon isotope signatures of gas exhalations in the westernmost part of the Pannonian Basin (SE Austria/NE Slovenia): Evidence for active lithospheric mantle degassing. *Chemical Geology*, *422*, 60–70. https://doi.org/10.1016/j.chemgeo.2015.12.016

Bräuer, K., Kämpf, H., Niedermann, S., & Strauch, G. (2005). Evidence for ascending upper mantle-derived melt beneath the Cheb basin, central Europe. *Geophysical Research Letters*, *32*, L08303. https://doi.org/10.1029/2004GL022205

Bräuer, K., Kämpf, H., Niedermann, S., & Strauch, G. (2013). Indications for the existence of different magmatic reservoirs beneath the Eifel area (Germany): A multi-isotope (C, N, He, Ne, Ar) approach. *Chemical Geology*, *356*, 193–208. https://doi.org/10.1016/j.chemgeo.2013.08.013

Bräuer, K., Kämpf, H., Niedermann, S., Strauch, G., & Tesar, J. (2008). Natural laboratory NW Bohemia: Comprehensive fluid studies between 1992 and 2005 used to trace geodynamic processes. *Geochemistry, Geophysics, Geosystems*, *9*, Q04018. https://doi.org/10.1029/2007GC001921

Bräuer, K., Kämpf, H., Niedermann, S., Strauch, G., & Weise, S. M. (2004). Evidence for a nitrogen flux directly derived from the European Subcontinental Mantle in the western Eger Rift, central Europe. *Geochimica et Cosmochimica Acta*, *68*, 4935–4947. https://doi.org/10.1016/j.gca.2004.05.032

Broadley, M. W., Bekaert, D. V., Marty, B., Yamaguchi, A., & Barrat, J. A. (2020). Noble gas variations in ureilites and their implications for ureilite parent body formation. *Geochimica et Cosmochimica Acta*, *270*, 325–337. https://doi.org/10.1016/j.gca.2019.11.032

Burić, M., Nikić, Z., & Papić, P. (2016). Mineral waters of Montenegro. In P. Papic (Ed.), *Mineral and thermal waters of southeastern Europe. Environmental Earth Sciences* (pp. 65–79). Springer. https://doi.org/10.1007/978-3-319-25379-4_4

Burnard, P., Bourlange, S., Blard, P. H., Geli, L., Tryon, M. D., Natal'in, B., et al. (2012). Constraints on fluid origins and migration velocities along the Marmara main fault (Sea of Marmara, Turkey) using helium isotopes. *Earth and Planetary Science Letters*, *341–344*, 68–78. https://doi.org/10.1016/j.epsl.2012.05.042

Burnard, P., Zimmermann, L., & Sano, Y. (2013). The noble gases as geochemical tracers: History and background. In P. Burnard (Ed.), *The noble gases as geochemical tracers. Advances in isotope geochemistry* (pp. 1–15). Springer. https://doi.org/10.1007/978-3-642-28836-4_1

Buttitta, D., Caracausi, A., Chiaraluce, L., Favara, R., Gasparo Morticelli, M., & Sulli, A. (2020). Continental degassing of helium in an active tectonic setting (northern Italy): The role of seismicity. *Nature Scientific Reports*, *10*, 162. https://doi.org/10.1038/s41598-019-55678-7

Caracausi, A., Martelli, M., Nuccio, M., Paternoster, M., & Stuart, F. M. (2013). Active degassing of mantle-derived fluids; a geochemical study along the Vulture Line, Southern Appennines. *Journal of Volcanology and Geothermal Research*, *253*, 65–74. https://doi.org/10.1016/j.jvolgeores.2012.12.005

Caracausi, A., & Sulli, A. (2019). Outgassing of mantle volatiles in compressional tectonic regime away from volcanism: The role of continental delamination. *Geochemistry, Geophysics, Geosystems*, *20*, 2007–2020. https://doi.org/10.1029/2018GC008046

Carreira, P. M., Marques, J. M., Carvalho, M. R., Capasso, G., & Grassa, F. (2009). Mantle-derived carbon in Hercynian granites. Stable isotopes signatures and C/He associations in the thermomineral waters, N-Portugal. *Journal of Volcanology and Geothermal Research*, *189*(1–2), 49–56. https://doi.org/10.1016/j.jvolgeores.2009.10.008

Chiodini, G., Caliro, S., Cardellini, C., Frondini, F., Inguaggiato, S., & Matteucci, F. (2011). Geochemical evidence for and characterization of CO_2 rich gas sources in the epicentral area of the Abruzzo 2009 earthquakes. *Earth and Planetary Science Letters*, *304*(3–4), 389–398. https://doi.org/10.1016/j.epsl.2011.02.016

Chiodini, G., Cardellini, C., Amato, A., Boschi, E., Caliro, S., Frondini, F., & Ventura, G. (2004). Carbon dioxide degassing and seismogenesis in central southern Italy. *Geophysical Research Letter*, *31*, L07615. https://doi.org/10.1029/2004GL019480

Chiodini, G., Cardellini, C., Di Luccio, F., Selva, J., Frondini, F., Caliro, S., et al. (2020). Correlation between tectonic CO2 Earth degassing and seismicity is revealed by a 10-year record in the Apennines, Italy. *Science Advances*, *6*(35), eabc2938. https://doi.org/10.1126/sciadv. abc2938

Clever, H. L. (1979). Helium and neon-International Union of Pure and Applied Chemistry. *IUPAC Solubility Data Series* (Vol. *1*).

Cvetković, V., Prelević, D., Downes, H., Jovanović, M., Vaselli, O., & Pecskay, Z. (2004). Origin and geodynamic significance of Tertiary post-collisional basaltic magmatism in Serbia

(central Balkan Peninsula). *Lithos*, *73*(3–4), 161–186. https://doi.org/10.1016/j.lithos.2003.12.004

Cvetković, V., Prelević, D., & Pécskay, Z. (2000). Lamprophyric rocks of the Miocene Borac eruptive complex (Central Serbia, Yugoslavia). *Acta Geologica Hungarica*, *43*(1), 25–41.

Cvetković, V., Prelević, D., & Schmid, S. (2016). Geology of south-eastern Europe. In P. Papic (Ed.), *Mineral and thermal waters of southeastern Europe* (pp. 1–29). Springer International Publishing. https://doi.org/10.1007/978-3-319-25379-4_1

D'Alessandro, W., Li Vigni, L., Gagliano, A. L., Calabrese, S., Kyriakopoulos, K., & Daskalopoulou, K. (2020). CO_2 release to the atmosphere from thermal springs of Sperchios Basin and northern Euboea (Greece): The contribution of "hidden" degassing. *Applied Geochemistry*, *119*, 104660. https://doi.org/10.1016/j.apgeochem.2020.104660

Daskalopoulou, K., Gagliano, A. L., Calabrese, S., & D'Alessandro, W. (2019). Estimation of the geogenic carbon degassing of Greece. *Applied Geochemistry*, *106*, 60–74. https://doi.org/10.1016/j.apgeochem.2019.04.018

De Leeuw, G. A. M., Hilton, D. R., Güleç, N., & Mutlu, H. (2010). Regional and temporal variations in $CO_2/^3He$, $^3He/^4He$ and δ13C along the North Anatolian Fault Zone, Turkey. *Applied Geochemistry*, *25*, 524–539. https://doi.org/10.1016/j.apgeochem.2010.01.010

Djordjević, M. (2005). Volcanogenic Turonian and epiclastics of Senonian in the Timok Magmatic Complex between Bor and the Tupižnica Mountain (eastern Serbia). *Annales Geologiques de la Peninsula Balkanique*, *66*, 63–71. https://doi.org/10.2298/gabp0566063d

Dogan, T., Sumino, H., Nagao, K., Notsu, K., Tuncer, M. K., & Celik, C. (2009). Adjacent releases of mantle helium and soil CO_2 from active faults: Observations from the Marmara region of the North Anatolian Fault zone, Turkey. *Geochemistry, Geophysics, Geosystems*, *10*, Q11009. https://doi.org/10.1029/2009GC002745

Doljak, D., & Jojić Glavonjić, T. (2016). State and prospects of geothermal energy usage in Serbia. *Journal of Geographical Institute "Jovan Cvijic"*, *66*(2), 221–236. https://doi.org/10.2298/IJGI1602221D

Etiope, G., Caracausi, A., Favara, R., Italiano, F., & Baciu, C. (2003). Reply to comment by A. Kopf on "Methane emission from the mud volcanoes of Sicily (Italy)", and notice on CH_4 flux data from European mud volcanoes. *Geophysical Research Letters*, *30*, 1094. https://doi.org/10.1029/2002GL016287

Etiope, G., Caracausi, A., Italiano, F., Baciu, C., & Cosma, C. (2004). Gas flux to the atmosphere from mud volcanoes in eastern Romania. *Terra Nova*, *16*, 179–184. https://doi.org/10.1111/j.1365-3121.2004.00542.x

Faccenna, C., Becker, T. W., Auer, L., Billi, A., Boschi, L., Brun, J. P., et al. (2014). Mantle dynamics in the Mediterranean. *Reviews of Geophysics*, *52*, 283–332. https://doi.org/10.1002/2013RG000444

Frunzeti, N. (2013). *Geogenic emissions of greenhouse gases in the Southern part of the Eastern Carpathians* (doctoral dissertation). Babes-Bolyai University, Faculty of Environmental Science and Engineering. (in Romanian).

Fusseis, F., Regenauer-Lieb, K., Liu, J., Hough, R. M., & De Carlo, F. (2009). Creep cavitation can establish a dynamic granular fluid pump in ductile shear zones. *Nature*, *459*, 974–977. https://doi.org/10.1038/nature08051

Gautheron, C., & Moreira, M. (2002). Helium signature of the subcontinental lithospheric mantle. *Earth and Planetary Science Letters*, *199*(1–2), 39–47. https://doi.org/10.1016/S0012-821X(02)00563-0

Gilfillan, S. M. V., Ballentine, C. J., Holland, G., Blagburn, D., Sherwood Lollar, B., Stevens, S., et al. (2008). The noble gas geochemistry of natural CO_2 gas reservoirs from the Colorado Plateau and Rocky Mountain provinces, USA. *Geochimica et Cosmochimica Acta*, *72*, 1174–1198. https://doi.org/10.1016/j.gca.2007.10.009

Gilfillan, S. M. V., Lollar, B. S., Holland, G., Blagburn, D., Stevens, S., Schoell, M., et al. (2009). Solubility trapping in formation water as dominant CO_2 sink in natural gas fields. *Nature*, *458*(7238), 614–618. https://doi.org/10.1038/nature07852

Holland, G., & Gilfillan, S. (2013). Application of noble gases to the viability of CO_2 storage. In P. Burnard (Ed.), *The noble gases as geochemical tracers. Advances in isotope geochemistry* (pp. 177–223). Springer. https://doi.org/10.1007/978-3-642-28836-4_8

Honda, M., Kurita, K., Hamano, Y., & Ozima, M. (1982). Experimental studies of He and Ar degassing during rock fracturing. *Earth and Planetary Science Letters*, *59*(2), 429–436. https://doi.org/10.1016/0012-821X(82)90144-3

Horváth, F., Musitz, B., Balázs, A., Végh, A., Uhrin, A., Nádor, A., et al. (2015). Evolution of the Pannonian basin and its geothermal resources. *Geothermics*, *53*, 328–352. https://doi.org/10.1016/j.geothermics.2014.07.009

Ionescu, A., Baciu, C., Kis, B.-M., & Sauer, P. E. (2017). Evaluation of dissolved light hydrocarbons in different geological settings in Romania. *Chemical Geology*, *469*, 230–245. https://doi.org/10.1016/j.chemgeo.2017.04.017

Italiano, F., Kis, B. M., Baciu, C., Ionescu, A., Harangi, S., & Palcsu, L. (2017). Geochemistry of dissolved gases from the eastern Carpathians- Transylvanian Basin boundary. *Chemical Geology*, *469*, 117–128. https://doi.org/10.1016/j.chemgeo.2016.12.019

Italiano, F., Sasmaz, A., Yuce, G., & Okan, O. (2013). Thermal fluids along the East Anatolian Fault Zone (EAFZ): Geochemical features and relationships with the tectonic setting. *Chemical Geology*, *339*, 103–114. https://doi.org/10.1016/j.chemgeo.2012.07.027

Jelenković, R., Kostić, A., Životić, D., & Ercegovac, M. (2008). Mineral resources of Serbia. *Geologica Carpatica*, *59*(4), 345–361.

Kennedy, B. M., & Van Soest, M. C. (2007). Flow of mantle fluids through the ductile lower crust: Helium isotope trends. *Science*, *318*(5855), 1433–1436. https://doi.org/10.1126/science.1147537

Kis, B. M., Caracausi, A., Palcsu, L., Baciu, C., Ionescu, A., Futó, I., et al. (2019). Noble gas and carbon isotope systematics at the seemingly inactive Ciomadul volcano (Eastern-Central Europe, Romania): Evidence for volcanic degassing. *Geochemistry, Geophysics, Geosystems*, *20*, 3019–3043. https://doi.org/10.1029/2018GC008153

Kis, B. M., Ionescu, A., Cardellini, C., Harangi, S., Baciu, C., Caracausi, C., & Viveiros, F. (2017). Quantification of carbon dioxide emissions of Ciomadul, the youngest volcano of the Carpathian-Pannonian Region (Eastern-Central Europe, Romania). *Journal of Volcanology and Geothermal Research*, *341*, 119–130. https://doi.org/10.1016/j.jvolgeores.2017.05.025

Kulongoski, J. T., Hilton, D. R., & Izbicki, J. A. (2005). Source and movement of helium in the eastern Morongo groundwater basin: The influence of regional tectonics on crustal and mantle helium fluxes. *Geochimica et Cosmochimica Acta*, *69*, 3857–3872. https://doi.org/10.1016/j.gca.2005.03.001

Labidi, J., Barry, P. H., Bekaert, D. V., Broadley, M. W., Marty, B., Giunta, T., et al. (2020). Hydrothermal 15N15N abundances constrain the origins of mantle nitrogen. *Nature*, *580*, 367–371. https://doi.org/10.1038/s41586-020-2173-4

Lee, H., Kim, H., Kagoshima, T., Park, J., Takahata, N., & Sano, Y. (2019). Mantle degassing along strike-slip faults in the Southeastern Korean Peninsula. *Nature Scientific Report*, *9*, 15334. https://doi.org/10.1038/s41598-019-51719-3

Lenkey, L., Dövényi, P., Horváth, F., & Cloetingh, S. A. P. L. (2002). *Geothermics of the Pan-Nonian Basin and its bearing on the neotectonics* (Vol. *3*, pp. 1–12). EGU Stephan Mueller Special Publication Series. https://doi.org/10.5194/smsps-3-29-2002

Lowenstern, J. B., Evans, W. C., Bergfeld, D., & Hunt, A. G. (2014). Prodigious degassing of a billion years of accumulated radiogenic helium at Yellowstone. *Nature*, *506*, 355–358. https://doi.org/10.1038/nature12992

Mamyrin, B. A., & Tolstikhin, I. N. (1984). Helium isotopes in nature. In *Developments in geochemistry*. Elsevier Science Ltd.

Marović, M., Djoković, I., Pešić, L., Radovanović, S., Toljić, M., & Gerzina, N. (2002). Neotectonics and seismicity of the southern margin of the Pannonian Basin in Serbia. *EGU Stephan Mueller Special Publication Series*, *3*, 277–295.

Marović, M., Toljić, M., Rundić, L., & Milivojević, J. (2007). *Neoalpine tectonics of Serbia* (p. 87 and map). Serbian Geological Society, Ser. Monographie.

Marty, B., Almayrac, M., Barry, P. H., Bekaert, D. V., Broadley, M. W., Byrne, D. J., et al. (2020). An evaluation of the C/N ratio of the mantle from natural CO2-rich gas analysis: Geochemical and cosmochemical implications. *Earth and Planetary Science Letters*, *551*(2020), 116574. https://doi.org/10.1016/j.epsl.2020.116574

Métois, M., D'Agostino, N., Avallone, A., Chamot-Rooke, N., Rabaute, A., Duni, L., et al. (2015). Insights on continental collisional processes from GPS data: Dynamics of the peri-Adriatic belts. *Journal of Geophysical Research: Solid Earth*, *120*, 8701–8719. https://doi. org/10.1002/2015JB012023

Milivojević, M. (1993). Geothermal model of Earth's crust and lithosphere for the territory of Yugoslavia: Some tectonic implications. *Studia Geophysica et Geodaetica*, *37*, 265–278. https://doi.org/10.1007/BF01624600

Minissale, A., Magro, G., Martinelli, G., Vaselli, O., & Tassi, F. (2000). Fluid geochemical transect in the Northern Apennines (central- northern Italy): Fluid genesis and migration and tectonic implications. *Tectonophysics*, *319*, 199–222. https://doi.org/10.1016/ S0040-1951(00)00031-7

Moores, E. M., & Fairbridge, R. W. (Eds.). (1997). *Encyclopedia of European and Asian regional geology* (p. 804). Chapman and Hall.

Mutlu, H., Güleç, N., & Hilton, D. R. (2008). Helium–carbon relationships in geothermal fluids of western Anatolia, Turkey. *Chemical Geology*, *247*(1–2), 305–321. https://doi.org/10.1016/j.chemgeo.2007.10.021

Newell, D. L., Jessup, M. J., Hilton, D. R., Shaw, C. A., & Hughes, C. A. (2015). Mantle-derived helium in hot springs of the Cordillera Blanca, Peru: Implications for mantle-to-crust fluid transfer in a flat-slab subduction setting. Chemical Geology, 417, 200–209. https:// doi.org/10.1016/j.chemgeo.2015.10.003

602 O'Nions, R. K., & Oxburgh, E. R. (1988). Helium, volatile fluxes and the development of
603 continental crust. Earth and Planetary Science Letters, 90(3), 331–334.
604 https://doi.org/10.1016/0012-821X(88)90134-3
605
606 Ozima, M., & Podosek, F. A. (2002). Noble gas geochemistry (p. 286). Cambridge University
607 Press.
608
609 Palcsu, L., Vetö, I., Futó, I., Vodila, G., Papp, L., & Majo, Z. (2014). In-reservoir mixing of mantle-
610 derived CO_2 and metasedimentary CH4-N2 fluids—Noble gas and stable isotope study of
611 two multistacked fields (Pannonian Basin System, W-Hungary). Marine and Petroleum
612 Geology, 54, 216–227. https://doi.org/10.1016/j.marpetgeo.2014.03.013
613
614 Pamic, J. (1997). Volcanic rocks from the Sava-Drava interfluve and Baranja in the South
615 Pannonian Basin (Croatia) (p. 192). Nafta J. Special Publications, Monograph. (in Croatian
616 with English summary).
617
618 Pamić, J., Tomljenović, B., & Balen, D. (2002). Geodynamic and petrogenetic evolution of Alpine
619 ophiolites from the central and NW Dinarides: An overview. Lithos, 65, 113–142.
620 https://doi.org/10.1016/S0024-4937(02)00162-7
621
622 Prelevic, D., Foley, S. F., Rome, R. L., Cvetkovic, V., & Downes, H. (2005). Tertiary ultrapotassic
623 volcanism in Serbia: Constraints on petrogenesis and mantle source characteristics. Journal
624 of Petrology, 46, 1443–1487. https://doi.org/10.1093/petrology/egi022
625
626 Randazzo, P., Caracausi, A., Aiuppa, A., Cardellini, C., Chiodini, G., D'Alessandro, W., et al.
627 (2021). Location, chemical and isotopic composition of bubbling gases collected in the
628 central west Serbia, Version 1.0. Interdisciplinary Earth Data Alliance (IEDA). https://doi.
629 org/10.26022/IEDA/112164
630
631 Rizzo, A. L., Pelorosso, B., Coltorti, M., Ntaflos, T., Bonadiman, C., Matusiak-Małek, M., et al.
632 (2018). Geochemistry of noble gases and CO2 in fluid inclusions from lithospheric mantle
633 beneath Wilcza Góra (Lower Silesia, Southwest Poland). Frontiers in Earth Science, 6, 215.
634 https://doi.org/10.3389/feart.2018.00215
635

636 Rosca, M., Bendea, C., & Vîjdea, A. M. (2016). Mineral and thermal waters of Romania. In P.
637 Papic (Ed.), Mineral and thermal waters of southeastern Europe. Environmental Earth
638 Sciences (pp. 97–114). Springer. https://doi.org/10.1007/978-3-319-25379-4_6
639
640 Sano, Y., & Marty, B. (1995). Origin of carbon in fumarolic gas from island arcs. Chemical
641 Geology, 119, 265–274. https://doi. org/10.1016/0009-2541(94)00097-R
642
643 Sano, Y., Tominaga, T., & Williams, S. N. (1997). Secular variations of helium and carbon isotopes
644 at Galeras volcano, Colombia. Journal of Volcanology and Geothermal Research, 77(1–4),
645 255–265. https://doi.org/10.1016/S0377-0273(96)00098-4
646
647 Sano, Y., & Wakita, H. (1985). Geographical distribution of $^{3}He/^{4}He$ ratios in Japan: Implications
648 for arc tectonics and incipient magmatism. Journal of Geophysical Research, 90(B10),
649 8729–8741. https://doi.org/10.1029/JB090iB10p08729
650
651 Sarbu, S., Aerts, J. W., Flot, J. F., Van Spanning, R. J. M., Baciu, C., Ionescu, A., et al. (2018).
652 Sulfur Cave (Romania), an extreme environment with microbial mats in a CO_2-H_2S/O gas
653 chemocline dominated by mycobacteria. International Journal of Speleology, 47(2), 173–
654 187. https://doi.org/10.5038/1827-806x.47.2.2164
655
656 Šarić, K., Cvetković, V., Romer, R. L., Christofides, G., & Koroneos, A. (2009). Granitoids
657 associated with East Vardar ophiolites (Serbia, F.Z.R. of Macedonia and northern Greece):
658 Origin, evolution and geodynamic significance inferred from major and trace element data
659 and Sr–Nd–Pb isotopes. Lithos, 108(1–4), 131–150.
660 https://doi.org/10.1016/j.lithos.2008.06.001
661
662 Scharlin, P., & Cargill, R. W. (1996). Carbon dioxide in water and aqueous electrolyte solutions. In
663 Solubility data series (Vol. 62, p. 1996). IUPAC.
664
665 Schefer, S., Cvetkovic, V., Fügenschuh, B., Kounov, A., Ovtcharova, M., Schaltegger, U., &
666 Schmid, S. M. (2011). Cenozoic granitoids in the Dinarides of southern Serbia: Age of
667 intrusion, isotope geochemistry, exhumation history and significance for the geodynamic
668 evolution of the Balkan Peninsula. International Journal of Earth Sciences, 100, 1181–1206.
669 https://doi.org/10.1007/s00531-010-0599-x

Schmid, S. M., Bernoulli, D., Fügenschuh, B., Mațenco, L., Schefer, S., Schuster, R., et al. (2008). The Alpine-Carpathian-Dinaridic orogenic system: Correlation and evolution of tectonic units. Swiss Journal of Geosciences, 101, 139–183. https://doi.org/10.1007/ s00015-008-1247-3

Schmid, S. M., Fügenschuh, B., Kounov, A., Matenco, L., Nievergelt, P., Oberhänsli, R., et al. (2019). Tectonic units of the Alpine collision zone between Eastern Alps and Western Turkey. Gondwana Research, 78, 308–374. https://doi.org/10.1016/j.gr.2019.07.005

Sherwood Lollar, B., Ballentine, C. J., & O'Nions, R. K. (1997). The fate of mantle-derived carbon in a continental sedimentary basin: Integration of C/He relationships and stable isotope signatures. Geochimica et Cosmochimica Acta, 61, 2295–2307. https://doi.org/10.1016/ S0016-7037(97)00083-5

Shimizu, A., Sumino, H., Nagao, K., Notsu, K., & Mitropoulos, P. (2005). Variation in noble gas isotopic composition of gas samples from the Aegean arc, Greece. Journal of Volcanology and Geothermal Research, 140(4), 321–339. https://doi.org/10.1016/j.jvolgeores.2004.08.016

Sibson, R. H. (2013). Stress switching in subduction forearcs: Implications for overpressure containment and strength cycling on megathrusts. Tectonophysics, 600, 142–152. https://doi.org/10.1016/j.tecto.2013.02.035

Sibson, R. H. (2020). Dual-driven fault failure in the lower seismogenic zone. Bulletin of the Seismological Society of America, 110, 850–862. https://doi.org/10.1785/0120190190

Szocs, T., Rman, N., Suveges, M., Palcsu, L., Toth, G., & Lapanje, A. (2013). The application of isotope and chemical analyses in managing transboundary groundwater resources. Applied Geochemistry, 32, 95–107. https://doi.org/10.1016/j.apgeochem.2012.10.006

Tamburello, G., Pondrelli, S., Chiodini, G., & Rouwet, D. (2018). Global-scale control of extensional tectonics on CO_2 earth degassing. Nature Communication, 9, 4608. https://doi.org/10.1038/s41467-018-07087-z

Todorović, M., Štrbački, J., Ćuk, M., Andrijašević, J., Šišović, J., & Papić, P. (2016). Mineral and thermal waters of Serbia: Multivariate statistical approach to hydrochemical characterization. In P. Papic (Ed.), Mineral and thermal waters of southeastern Europe. Environmental Earth Sciences (pp. 81–95). Springer. https://doi.org/10.1007/978-3-319-25379-4_5

Torgersen, T. (1993). 3He fluxes in extensional basins: Limits on the role of magmatism in extensional basins. Journal of Geophysical Research, 98(B9), 16257–16269. https://doi.org/10.1029/93JB00891

Torgersen, T. (2010). Continental degassing flux of ^{4}He and its variability. Geochemistry, Geophysics, Geosystems, 11, Q06002. https://doi. org/10.1029/2009GC002930

Torgersen, T., & O'Donnell, J. (1991). The degassing flux from the solid Earth-release by fracturing. Geophysical Research Letters, 18, 951–954. https://doi.org/10.1029/91GL00915

Vaselli, O., Minissale, A., Tassi, F., Magro, G., Seghedi, I., Ioane, D., & Szakács, A. (2002). Ageochemical traverse across the Eastern Carpathians (Romania): Constraints on the origin and evolution of the mineral waters and gas discharge. Chemical Geology, 182(2–4), 637–654. https://doi.org/10.1016/S0009-2541(01)00348-5

Weinlich, F. H., Bräuer, K., Kämpf, H., Strauch, G., Tesař, J., & Weise, S. M. (1999). An active subcontinental mantle volatile system in the western Eger rift, central Europe: Gas flux, isotopic (He, C, and N) and compositional fingerprints. *Geochimica et Cosmochimica Acta*, *63*, 3653–3671. https://doi.org/10.1016/S0016-7037(99)00187-8

Zelić, M., Agostini, S., Marroni, M., Pandolfi, L., & Tonarini, S. (2010). Geological and geochemical features of the Kopaonik intrusive complex (Vardar zone, Serbia). *Ofioliti*, *35*, 33–47

CHAPTER IV

Deep sourced fluids in the Croatian part of the Pannonian Basin: new insights from Carbon and Helium isotopic systematic

IV.1. Introduction

Over the past few decades, the degassing of natural fluids in both volcanically (e.g., Alonso et al., 2022; Kimani et al., 2021; Werner et al. 2019; Chiodini et al. 2008) and tectonically-active (e.g., Rufino et al., 2021; Zhang et al., 2021; Buttitta et al. 2020) regions has received increasing attention. Identifying the transfer of deep-derived fluids (e.g., CO_2, N_2, noble gases) in continental regions, in particular, is critical for investigating the processes that shape the deep and shallow evolution of our planet (e.g., subduction, volcanism, metamorphic processes, natural degassing, active tectonics, and earthquakes; Barry et al., 2021; Broadley et al., 2020; Labidi et al., 2020; Chiodini et al., 2020; Caracausi & Sulli, 2019; Newell et al., 2008; Ballentine et al., 2001). In the last years, extensive work has been carried out in central-eastern Europe with the aim to understand natural degassing processes in active tectonic regions (e.g., Randazzo et al., 2021; Sarbu et al., 2018; Ionescu et al., 2017, Italiano et al., 2017; Frunzeti, 2013; Bräuer et al.,2008).

Croatia, in the Balkan peninsula in Central–SE Europe, has inherited its present geological setting from the collision processes between the Eurasian (Europe) and Gondwana (Africa) continental plates (Cvetkovic et al. 2016). In particular, the North-Eastern region of Croatia represents the south-western margin of the Pannonian Basin System (PBS). The latter represents a back-arc basin formed due to Oligocene–Miocene diachronous extension as result of subduction roll-back in the Carpathians and Dinarides regions, combined with asthenospheric mantle flow and/or lithospheric delamination processes (Brlek et al., 2020 and reference therein). The area is characterized by high regional heat flow (up to 130 mW/m^2) and geothermal energy potential (Borović et al., 2016; Horwarth et al., 2015). Previous work in the Croatian part of the PBS has identified several natural gas manifestations and gas-rich thermal waters (e.g., Fiket et al., 2015; Borovic et al., 2016). However, unlike other regions of the PBS, where a large-scale outgassing of mantle-derived fluids has been clearly identified (e.g., Brauer et al., 2016, Sherwood Lollar et al., 1994, 1997; Ballentine et al., 1991, O'Nions & Oxburgh, 1988), much less is known for Croatia, where the process that

control the chemical and isotopic composition of the gas manifestations, and the tectonic control on gas migration through the crust, remain uncharacterized. This work, through the use of specific geochemical tools, attempts to identify the sources of fluids released in Croatia, and the processes that control the chemical and isotopic composition during their storage in, and transit through, the crust. Our study contributes to fill a gap of knowledge on the nature of fluids circulating in this sector of the PBS, and helps better understanding and reconstructing the complex geodynamic of the area.

IV.2. Geological setting

Croatia is a part of Central – SE Europe, and is located in the Balkan peninsula between Slovenia (North), the Adriatic Sea (West), Bosnia and Erzegovina (South), Ungary and Serbia (East) (Fig. IV.1a). The on- and offshore territory can be divided into the NW-SE trending Dinaric thrust belt and the Adriatic Basin to NE and the Neogene Pannonian Basin to the north (Fig. IV.1b-c ; Velic et al., 2015). The tectonic and geodynamic history of the area is very complex and reflects the combination of the subduction, collision and extension processes that developed from middle Mesozoic until present (Schmid et al., 2019; Horvath et al., 2015; Cvetkovic et al., 2004). The Dinarides belt formation is attributable to the collision of the north-eastern parts of the Apulian with the southern boundary of the Eurasian plates (Tari et al., 1998).

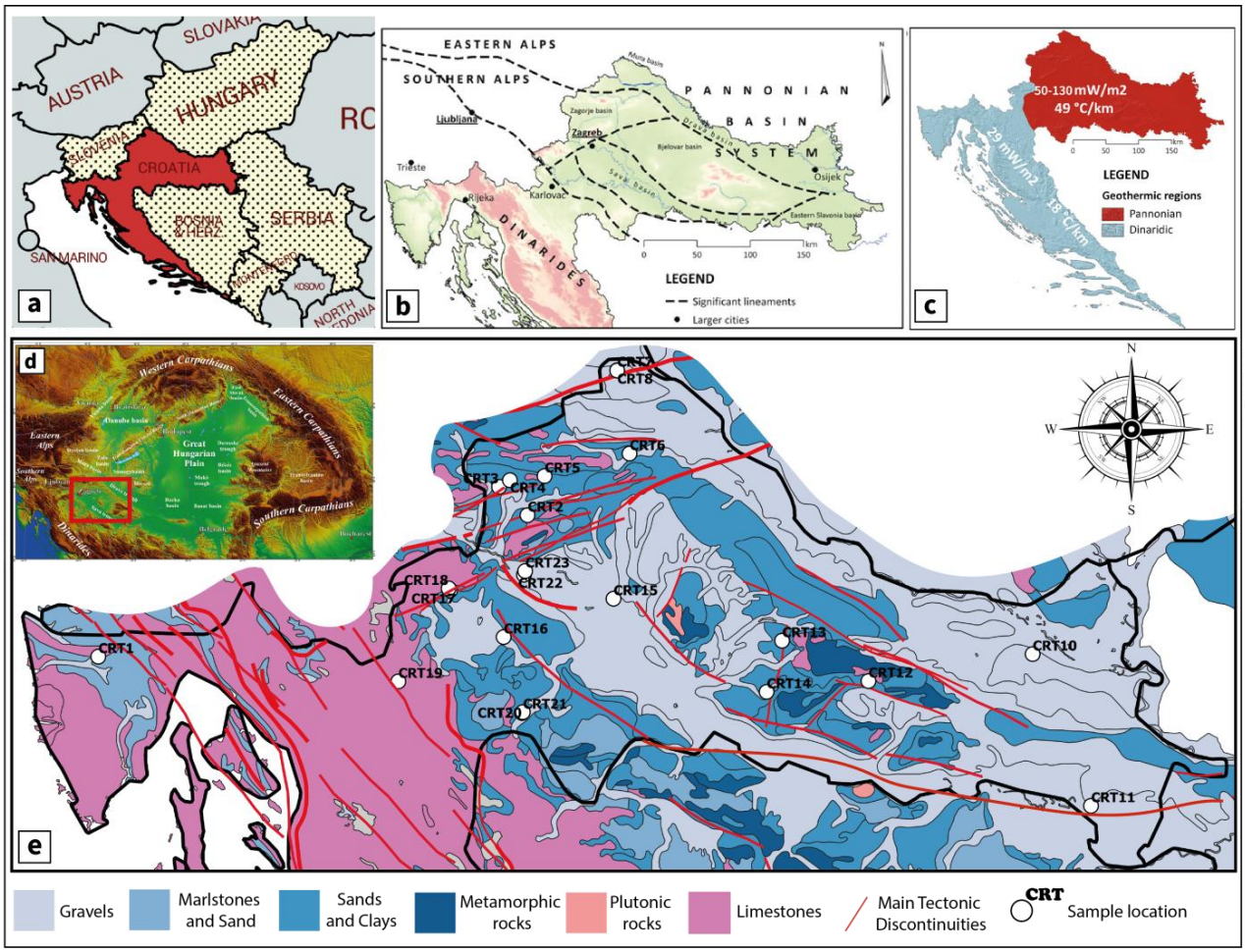

804

805 **Figure IV.1** | Simplified Geological Map of the Croatian segment of the Pannonian basin. **a**) Location of Croatia **b**)
806 major European tectonic units (according to Tari and Pamić 1998; Lučić et al. 2001; Velić et al. 2012); **c**) heat flow
807 density and geothermal gradient in geothermically different Croatian regions; **d**) digital terrain model of the Pannonian
808 basin to show its position within the Alpine mountain belt (Horwarth et al., 2015); **e**) the location of different subunits
809 and of the sampling sites (white circles).

810

811 This convergence led to the formation of a suture zone, named the Sava zone (Fig. IV.1b; Pamic
812 1993; Schmid et al. 2008), from the Late Cretaceous to the Early Paleogene until the final collision
813 between the Dinarides and Tisia Mega-Unit (Pamic 2002). This zone extends from Zagreb toward
814 the south-east of Belgrade, and further to the south through the Vardar Zone into southern Serbia,
815 North Macedonia and Greece (Balen et al., 2020; Schmid et al. 2008). To the north-west, close to
816 Zagreb, the Sava Zone is buried below the cenozoic sediments of the Pannonian Basin (Schmid et
817 al. 2020). The latter represents a back-arc basin formed due to Oligocene–Miocene diachronous

818 extension in the Tisza–Dacia and AlCaPa tectonic mega-units. Extension in these continental units
819 resulted from subduction roll-back in the Carpathians and Dinarides, combined with asthenospheric
820 mantle flow and/or litospheric delamination (Fig. IV.2; Brlek et al., 2020 and reference therein).
821 Magmatism in Croatia started in the mid-triassic, when it was spatially and genetically linked to the
822 onset of the formation of the Tethyan Mesozoic Adriatic–Dinaridic carbonate platforms and their
823 later disintegration (Slovenec et al., 2020). Neogene to quaternary volcanism, in particular in the
824 Carpathian-Pannonian Region, was related to the youngest evolutionary stage of the Carpathian arc
825 and the intra-Carpathian area, with subduction, extension and asthenospheric upwelling as the main
826 driving mechanisms (Pekskay et al., 2006, Pamic et al., 1998). The erupted magmas, including
827 those emplaced in the most recent magmatic events (during the last ~20 Ma), exhibit a spread of
828 compositions (Horváth et al. 2015; Balázs et al. 2016; Brlek et al, 2020). Regional asthenospheric
829 upwelling produced an overall thinning of the lithosphere, with the Mohorovicic seismic
830 discontinuity relatively shallow at around 50 km under the External Dinarides (Borovic et al.,
831 2016), and at around 28 km in the Pannonian basin (Cvetkovic et al 2016; Markusic et al., 2008;
832 Milivojević, 1993). The majority of Croatia's geothermal manifestations is thus concentrated in the
833 Pannonian basin area, where the average geothermal gradient (49 °C/km) is high and surface heat
834 flow ranges from 50 to 130 mW/m^2. For comparison, the external Dinarides are characterized by
835 average geothermal gradient of 18 °C/km and by a surface heat flow of about 30 mW/m^2 (Horvath
836 et al., 2015; Lenkey et al., 2002; EIHP 1998).

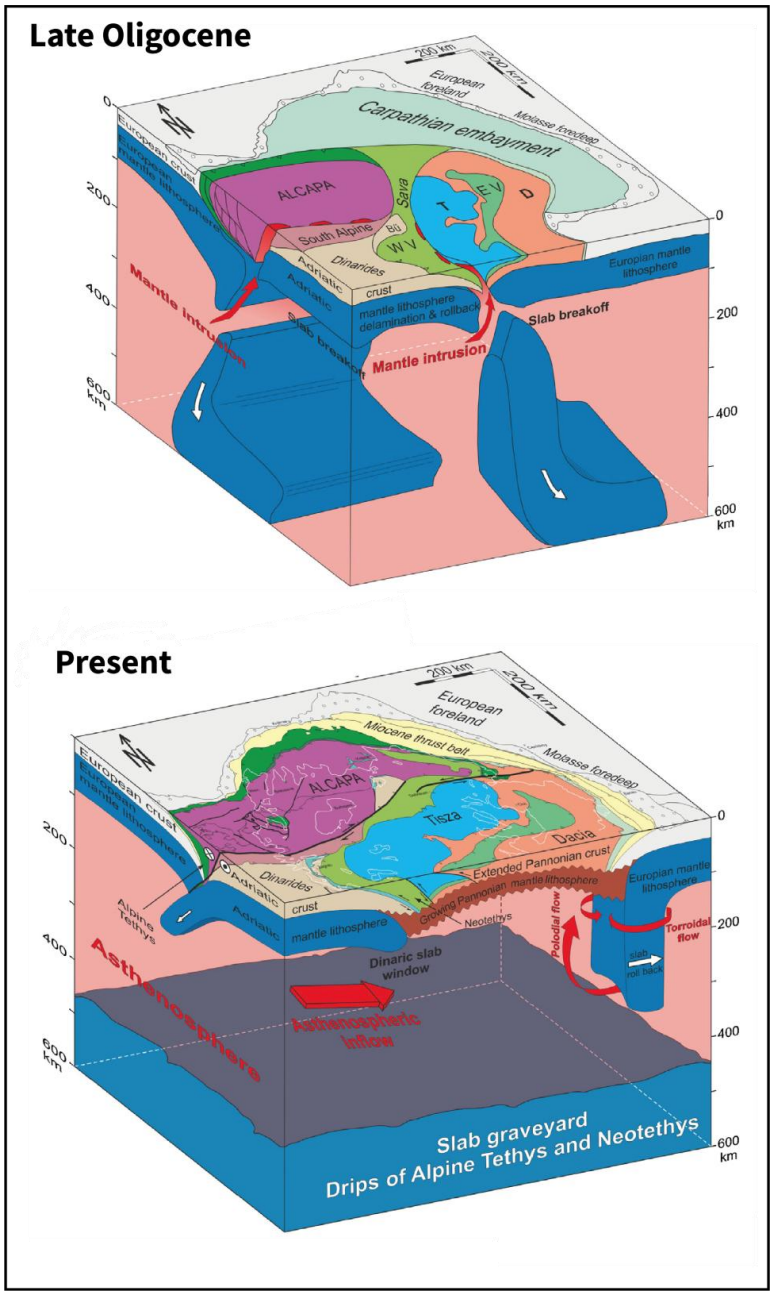

Figure IV.2 | Pannonian Basin evolution. Block model showing the Late Oligocene position of the Alcapa and Tisza-Dacia terranes in the Carpathian embayment and the present position of the Alcapa and Tisza-Dacia terranes. The figure also show the associated lithospheric and asthenospheric processes down to the upper mantle transition zone (Modified after Horwarth et al., 2015).

The seismicity of Croatia is unevenly distributed, albeit most earthquakes occur in the coastal area of the country (the Dinarides), with the Dubrovnik area being the most seismically active part of Croatia (e.g., Dubrovnik earthquake of 1667; Markusic et al., 2008). This is commonly explained by the ongoing collision between the Adriatic Platform and the Dinarides (Kotzev et al., 2008).

Some historical earthquakes took place along the Croatia–Slovenia border and the Zagreb metropolitan area (e.g., November 9, 1880, with magnitude $M \approx 6.3$; Kozák and Čermák, 2010). Seismicity in the Dinarides is concentrated at upper crustal depth, between 3-11 km while the lower crust is nearly aseismic (Markusic et al., 2008). In continental Croatia the interaction between the Adriatic microplate, the Dinarides, the Alps and the Pannonian basin have led to a complex tectonic and structural setting, with the most seismically active area in the north-western part of Croatia and the Pannonian basin exhibiting intraplate seismicity characterized by rare large events (Pribicevic et al., 2002). Despite this, historical seismicity shows that seismic potential of this area is considerable (e.g., Kupa Valley earthquake, M 5.8 event, 8 October 1909; Herak et al., 2009; Fig. IV.3) with most earthquakes occurring deeper in the Pannonian Basin than in the Dinarides (between 6 and 18 km; Ivancic et al., 2018; Markusic et al., 2008). Recently, the area has been hit by a strong earthquake of Mw 6.4 with epicentre in Petrinja town (December 29, 2020; Markusic et al., 2021) preceded by a series of earthquakes that began with the M5 foreshock and considered the largest onshore earthquake rupture in Central Europe since the M 6.5 Norcia earthquake occurred in 2016 (e.g., Scognamiglio et al.,2018), and the largest earthquake in Croatia since instrumental records began in 1908 (Markušić et al., 2020; ISC and USGS catalogue). The earthquake was caused by a well-known active fault zones in this region (Basili et al., 2013).

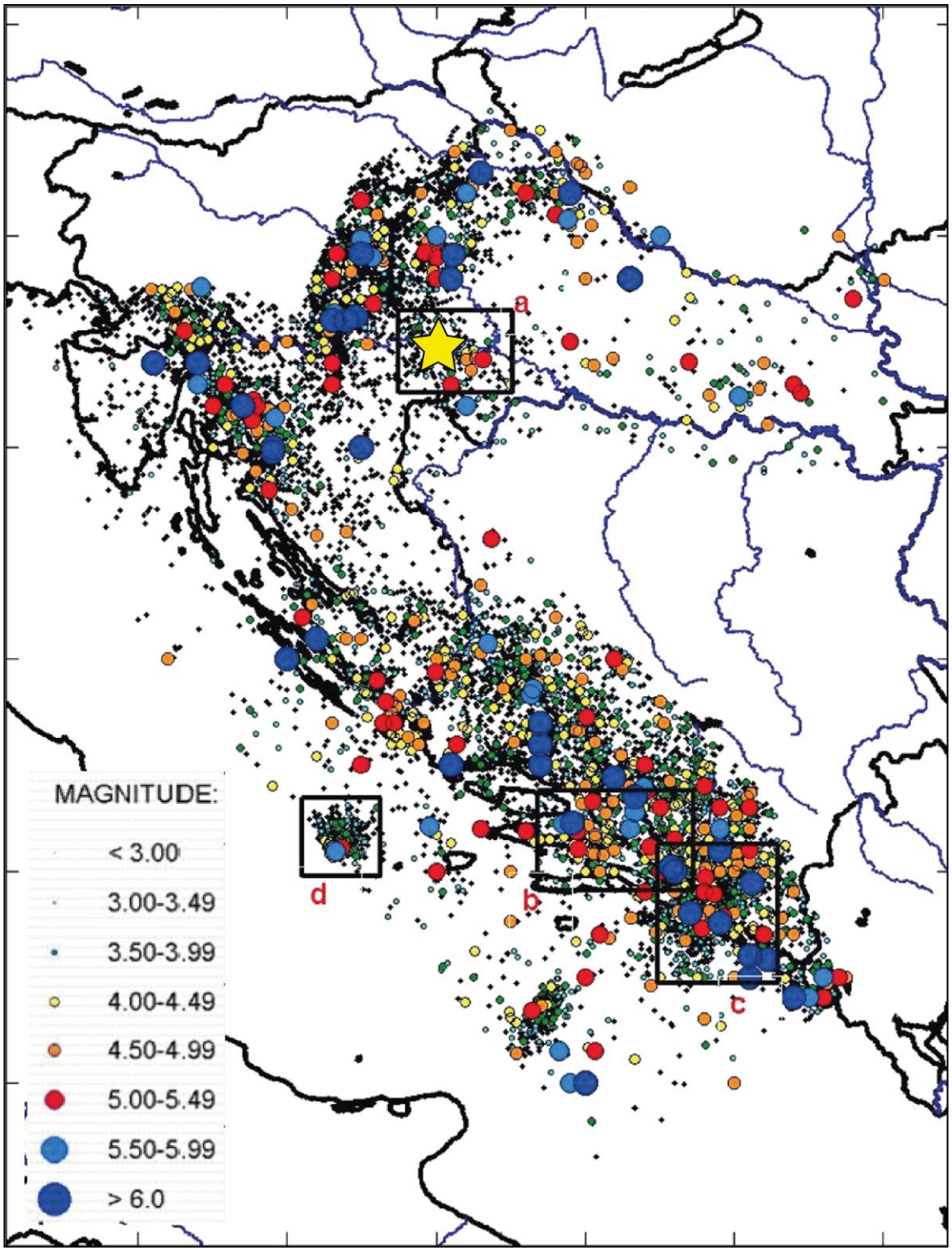

Figure IV.3 | Croatia seismicity map. Croatia seismicity with positions (black boxes) of the strongest earthquake sequences in Croatia: (**a)** Kupa Valley (north), 1909–1910; (**b**) Biokovo Mt., 1962; (**c**) Ston-Slano (south), 1996; (**d**) Jabuka Island (off coast), 2003. Yellow star: Petrinja earthquake (December 29, 2020; Markusic et al., 2021). Modified after Markusic et al., 2008.

IV.3. Methods and Materials

Twenty-three gas samples were collected in the Sava zone and in the Croatian part of Pannonian basin (Fig. IV.1). Eighteen samples are bubbling gases and five are dissolved gases. Temperature, pH, Eh, and electrical conductivity (EC) were measured in situ by means of a multiparametric probe (WTW Multi 350i), which was previously calibrated using standard solutions (Table IV.1). Total alkalinity was measured in situ by acidimetric titration with 0.05N HCl using methyl-orange as indicator. Dissolved gases were sampled and analyzed according to the method described by Capasso and Inguaggiato (1998) which is based on the equilibrium partition of gas species between a liquid and a gas phase after the introduction of a host gas (Ar) into the sample. The bubbling gases were sampled by using an inverted funnel that was positioned above the bubbles, so the gases fluxed through a two valves glass or steel bottle to avoid air contamination. Once the bottles had been flushed with an amount of gas at least tens of times the volume of the bottles (20–30 cc), the valves were closed to trap the gases into the bottles. All chemical and isotopic analyses were carried out at the laboratories of the INGV-Palermo within one month from the sampling in order to prevent isotopic fractionation due to storage of gases. The chemical composition of the gases was determined with an Agilent 7890B gas chromatograph using Ar as carrier gas, and equipped with 4-m Carbosieve S II and PoraPlot-U columns. A thermal conductivity detector (TCD) was used to measure the concentrations of O_2, N_2, and CO_2, while a flame ionization detector (FID) was used for CH_4. Analytical errors of the measured concentrations are always within 5%. The $^{13}C/^{12}C$ ratios of CO_2 (expressed as $\delta^{13}C\text{-}CO_2$ in ‰ versus the V-PDB standard) were measured with a Finnigan Delta S mass spectrometer after purification of the gas mixture by standard procedures using cryogenic traps with precision of ±0.1‰. The carbon isotopic composition of total dissolved inorganic carbon ($\delta^{13}C_{TDIC}$) has been determined by acid extraction following the method proposed by Capasso et al. (2005). All $\delta^{13}C_{TDIC}$ values were reported relative to Vienna Pee Dee Belemnite

(VPDB), the international reference standard for carbon isotopes, and the analytical precision was ±0.15‰.

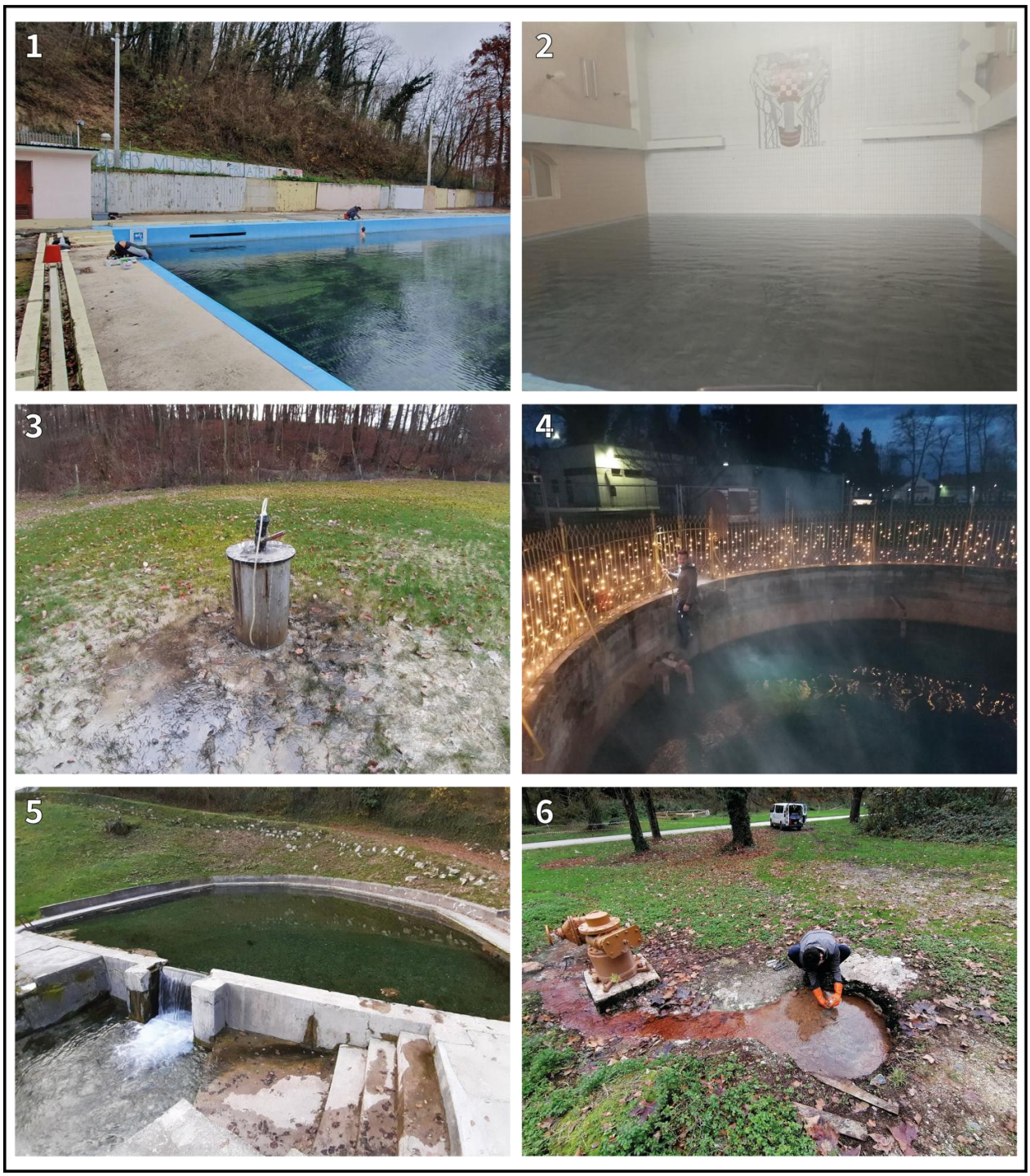

Figure IV.4 | Sampling natural gases location. **1**) CRT3- Tuherljske toplice - Stari bazen; **2**) CRT4-Krapinske Tolpice-SBKT (Secijalna bolnica Kr.T.); **3**) CRT8-Toplice Sveti Martin; **4**) CRT13-Daruvarske toplice-Ivanovo vrelo; **5**) CRT18-Toplica Svetojanska; **6**) CRT21-Topusko Bristo vrelo (Spiegelbad).

Analyses of the dissolved and free noble gases (Ne and Ar) and He isotopic composition were performed using the methodology proposed by Inguaggiato and Rizzo (2004), which is based on isotope equilibrium between liquid and host gas phases. He isotopes were analyzed using a static vacuum mass spectrometer (GVI Helix SFT), using a double collector in order to detect the ^{3}He and ^{4}He ion beams simultaneously (precision for isotopic ratio within ±0.5%). The $^{3}He/^{4}He$ ratio was determined by measuring ^{3}He in an electron multiplier detector and ^{4}He in an axial Faraday detector. ^{20}Ne was measured with a multicollector Thermo-Helix MC Plus mass spectrometer. Helium isotope compositions are expressed as R/Ra, normalizing the $^{3}He/^{4}He$ ratio of the sample against the atmospheric $^{3}He/^{4}He$ ratio ($Ra=1.386\times10^{-6}$; Ozima & Podosek, 2002). The Ar concentrations and its isotope compositions (^{40}Ar, ^{38}Ar, and ^{36}Ar) were analyzed by multicollector Helix MC-GVI mass spectrometer with analytical uncertainty (1σ) for single $^{40}Ar/^{36}Ar$ measurements of <0.1%.

IV.4. Results

The location of the sampled manifestations, their physico-chemical properties, and chemical and isotopic compositions (He, Ne, Ar , $\delta^{13}C_{CO2}$) of the 18 bubbling gases and 5 dissolved gases, are listed in Table IV.1.

Based on their chemical composition, the sampled gases are subdivided in three different families: CO_2-dominated (CRT-CO_2), with CO_2 concentrations ranging from 59% to 98.7%; N_2-dominated (CRT-N_2), with N_2 concentrations from 51.2% to 95%; and CH_4-dominated (CRT-CH_4), with CH_4 concentrations from 73.4% to 97%. CRT-CO_2 and CRT-N_2 have CH_4 concentrations ranging from 0.02% to 40% and O_2 from 0.1% to 9.8%. Argon (Ar) is present in low amounts (<2%). He concentrations are up to 939 ppmv, while Ne are up to 15 ppmv with the highest values found in CRT-N_2 samples

The CRT-CH_4 samples have CO_2 concentrations from 1.9% to 10.3% and N_2 from 0.6% to 17.9%. These samples also exhibit low O_2 (from 0.04% to 5%) and the lowest Ar values (< 0.2%). He ranges from 12 to 166 ppmv, while Ne concentrations are up to 6 ppmv. H_2 reaches 19% in CH_4-rich samples, while in CRT-CO_2 and CRT-N_2 samples is ≤ 0.1%. The CRT-CH_4 samples also show the highest concentrations of the hydrocarbon species C_2H_6 (up to 6800 ppmv) and C_3H_8 (up to 3000 ppmv).

CO_2 and N_2 concentrations exhibit a negative correlation in CRT-CO_2 and CRT-N_2 samples, except for one sample (CRT7) having very low N_2 (0.6%) but CH_4 at up to 40% (Fig. IV.5). CH_4-rich samples depart from a pure CO_2-pure N_2 mixing trend, likewise other CH_4-rich samples from other Pannonian basin areas (orange diamonds in Fig. IV.5; Ballentine et al., 1991).

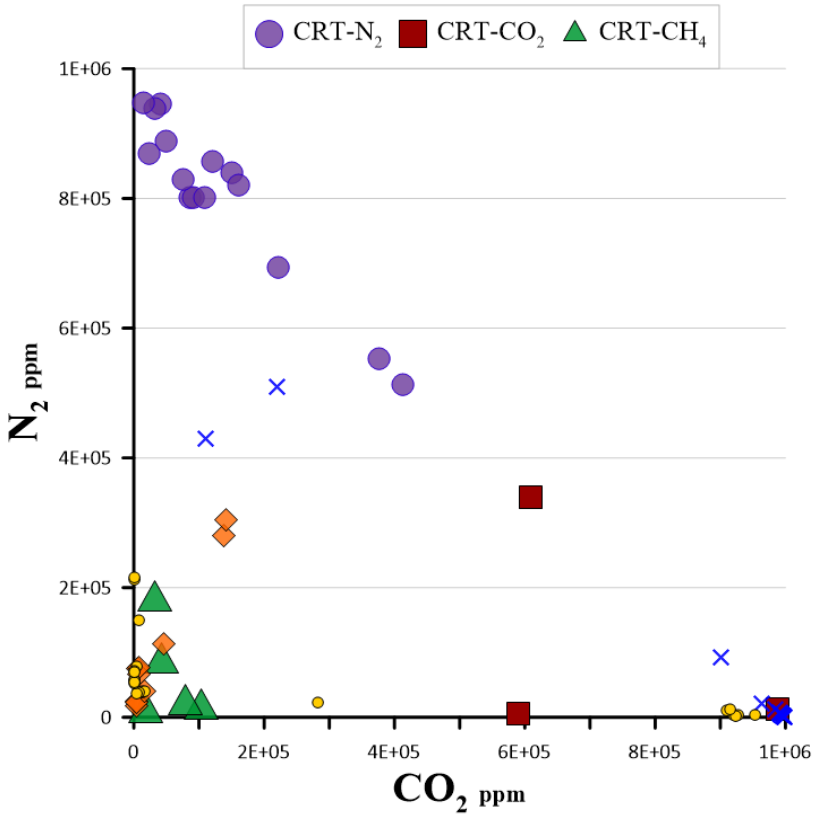

Figure IV.5 | N_2 vs. CO_2 concentration plot for natural gases. N_2 and CO_2 concentrations exhibit a negative correlation except for the CH_4-rich samples that depart from the main trend (likewise CH_4-rich sample from other Pannonian basin

areas. Blue cross: data from Brauer et al., 2016, Yellow circles from Sherwood Lollar et al., 1997 and Orange diamonds from Ballentine et al., 1991).

The $\delta^{13}C_{CO2}$ values vary from −19.3‰ to 12.8‰ (Table IV.1) with most N_2-dominated gases exhibiting the lowest values, plotting in the field of biogenic CO_2 (Fig. IV.6). The highest $\delta^{13}C_{CO2}$ (+10.6‰ and +12.8‰) values, found in samples CRT7 and CRT8, likely reflect the presence of hydrocarbons and to biodegradation processes (Fig. IV.6). For the five dissolved gas samples, we computed the theoretical equilibrium $\delta^{13}C$ of gaseous CO_2 (Table IV.1) from the following equation (Zhang et al., 1995):

$$\delta^{13}C_{(CO_2)g}=\delta^{13}C_{(TDIC)}-[(H_2CO_3/TDIC)*\varepsilon_{(H_2CO_3-CO_2)}]-[(HCO_3^-/TDIC)*\varepsilon_{(HCO_3^--CO_2)}]-[(CO_3^{2-}/TDIC)*\varepsilon_{(CO_3^{2-}-CO_2)}] \quad \textbf{(1)}$$

Eqn. 1 takes into account the measured $\delta^{13}C$ of TDC, the equilibrium molar ratios of aqueous carbon species at sampling temperature and pH, computed with the PHREEQC code (Parkhurst & Appelo, 1999), and the isotope enrichment factors (Ɛ) between dissolved carbon species and gaseous CO_2 under the same conditions (Zhang et al., 1995). The He isotopic ratios, expressed as R/Ra, vary from 0.02 to 2.2 Ra, where Ra is the atmospheric values ($1.39x10^{-6}$ Ozima & Podosek, 2002). The N_2-rich samples span a wide range (Fig. IV.7). The $^4He/^{20}Ne$ ratios mostly range from 2 to 2766, and are therefore higher than atmospheric ratio (0.318;Ozima & Podosek, 2002), indicating a low air He contribution (≤15%) to the sampled gases.

Table IV.1 | *Location, Geochemical and Isotopic Composition of Croatian Samples.* *Recalculated chemical and isotopic composition ($\delta^{13}C$) at equilibrium with free gas phase following Capasso & Inguaggiato 1998 and Federico et al., 2002.)

D-Dissolved; F-Free

Name	ID	Type	pH	T	N_2	CO_2	CH_4	O_2	H_2	C_2H_6	C_3H_8	Ar	Ne	He	$\delta^{13}C(CO_2)$	R/Ra	$^4He/^{20}Ne$	$CO_2/^3He$
				˚C	%	%	%	%	ppm	ppm	ppm	%	ppm	ppm	‰ (vs V-PDB)			
Istarske Toplice - Bagni S. Stefano*	CRT1	D	7.3	23.2	82.0	16.0	0.1	0.3	b.d.l.	b.d.l.	b.d.l.	1.7	9.10	300	-18.1	0.02	33	1.6E+10
Stubicke Toplice B-1 SBST	CRT2	F	6.8	52.0	84.0	15.0	0.5	0.7	b.d.l.	b.d.l.	b.d.l.	-	-	-	-	-	-	-
Tuherljske toplice - Stari bazen	CRT3	F	7.4	30.5	94.5	4.0	0.5	0.1	b.d.l.	b.d.l.	b.d.l.	0.99	14.95	106	-16.1	1.20	7	2.3E+08
Krapinske Tolpice - SBKT (Secijalna bolnica Kr.T.)	CRT4	F	7.1	40.9	94.0	3.2	0.7	0.9	1402	b.d.l.	b.d.l.	1.10	13.78	43	-15.8	0.86	3	6.3E+08
Sutinske Toplice*	CRT5	D	7.4	32.5	87.0	2.3	1.2	7.3	b.d.l.	b.d.l.	b.d.l.	1.8	11.92	56	-16.8	0.44	5	6.7E+08
Varazdinske Toplice	CRT6	F	6.4	57.2	55.3	37.6	6.4	0.2	b.d.l.	3300	b.d.l.	-	-	-	-	-	-	-
Toplice Sveti Martin - thermal	CRT7	F	6.9	29.2	0.6	59.0	40.0	0.1	b.d.l.	1200	b.d.l.	0.01	0.22	54	12.8	0.14	251	5.7E+10
Toplice Sveti Martin - subthermal	CRT8	F	7.7	13.8	1.2	10.3	88.0	0.04	12	3200	1100	0.23	5.86	12	10.6	0.17	2	3.5E+10
Draskovec - DR-2	CRT9	F	-	-	8.3	4.2	86.4	0.1	189000	6800	3000	0.004	0.04	113	-	0.31	2766	8.5E+08
Bizovacke toplice - BH Slavonka-1 (Slk-1)	CRT10	F	7.8	75.3	2.0	7.9	89.4	0.1	42	2900	447	0.02	0.17	69	-4.5	0.92	395	9.0E+08
Bosnjaci	CRT11	F	7.7	56.9	17.9	3.2	73.4	5.0	11	677	b.d.l.	0.04	0.32	166	-10.6	1.40	524	9.9E+07
Velika*	CRT12	D	7.3	28.5	80.1	10.9	0.5	6.9	b.d.l.	b.d.l.	b.d.l.	1.6	13.05	47	-16.5	0.20	4	8.2E+09
Daruvarske toplice - Ivanovo vrelo spring	CRT13	F	7.1	48.6	94.7	1.5	1.00	1.0	b.d.l.	b.d.l.	b.d.l.	1.11	13.19	84	-14.7	0.15	6	8.7E+08
Lipik B-4a*	CRT14	D	6.8	58.4	69.3	22.1	1.2	7.1	b.d.l.	b.d.l.	b.d.l.	0.3	2.43	132	-5.4	2.21	54	5.4E+08
Naftalan	CRT15	F	8.8	22.4	0.7	1.9	96.9	0.04	70	b.d.l.	b.d.l.	-	-	-	-	-	-	-
Jamnica B-6	CRT16	F	6.6	22.7	1.2	98.7	0.02	0.1	b.d.l.	b.d.l.	b.d.l.	-	-	-	-	-	-	-
Jana-2	CRT17	F	7.4	24.0	80.2	8.6	1.3	9.8	b.d.l.	b.d.l.	b.d.l.	-	-	-	-	-	-	-
Toplica Svetojanska	CRT18	F	7.2	28.7	80.1	9.2	1.1	8.7	b.d.l.	b.d.l.	b.d.l.	0.90	14.70	44	-19.3	0.14	3	1.1E+10
Lesce toplice	CRT19	F	7.3	36.9	83.0	7.6	1.7	6.7	b.d.l.	b.d.l.	b.d.l.	0.97	14.27	140	-17.9	0.05	10	8.5E+09
Topusko TEB-4	CRT20	F	6.6	55.8	88.8	4.9	3.9	1.0	21	b.d.l.	b.d.l.	1.08	13.58	61	-5.8	0.23	5	2.5E+09
Topusko Bristo vrelo (Spiegelbad)*	CRT21	D	6.7	43.6	85.7	12.1	0.6	9.8	b.d.l.	b.d.l.	b.d.l.	1.2	9.85	55	-	0.10	6	1.6E+10
KBNZ-1b	CRT22	F	6.7	67.0	34.0	61.0	4.0	0.2	3.3	469	b.d.l.	0.61	3.51	895	-6.3	0.72	255	6.8E+08
Maldost-3 (Mla-3)	CRT23	F	-	-	51.2	41.3	6.9	0.2	11	884	b.d.l.	0.83	7.02	939	-6.9	0.69	134	4.6E+08

IV.5. Discussion

Different processes can affect the He-CO_2 characteristics and the regional helium isotopic signature values. Our intent in this work is to identify volatile sources, and characterise possible secondary processes that act to modify the pristine chemical and isotopic volatiles signature upon crustal storage and migration (e.g., carbon addition/loss, fractionation processes, addition of radiogenic components, etc.). We attempt at using helium isotopic signature, He-C systematics, and its relationships with noble gas and $\delta^{13}C$ compositions of fluids to understand volatile source features (i.e., mantle vs. crustal), sinks, and volatile pathways from source to the surface, as well as connections to larger tectonic processes.

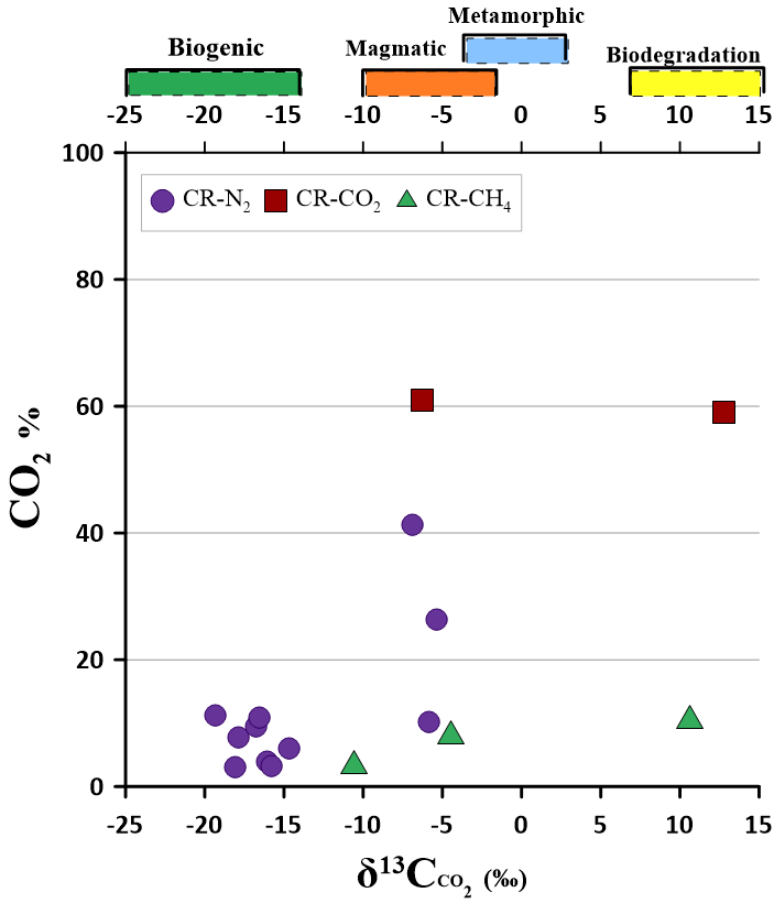

Figure IV.6 | CO_2 concentrations versus its carbon isotopic composition ($\delta^{13}C$). The most of N_2-dominated samples exhibit low $\delta^{13}C$ values, plotting in the field of biogenic CO_2. The highest $\delta^{13}C_{CO2}$ showed by CRT7 and CRT8 are related to the presence of hydrocarbon and to biodegradation processes. Green box= biogenic; Orange box=magmatic; Blue box= metamorphic; Yellow box=biodegradation (Holland & Gilfillan, 2013; Milkov,2010).

IV.5.1. Helium source/s

The He isotopic composition represents an useful tool to investigate the source/s of volatiles. In fact, He in natural fluids is typically interpreted as deriving from three distinct sources with well distinct isotopic signatures: the mantle ($^3He/^4He=10^{-5}$), the crust ($^3He/^4He=10^{-8}$) and the atmosphere ($^3He/^4He=10^{-6}$) (e.g., Burnard et al., 2013; O'Nions & Oxburgh, 1988; Sano et al., 1997). While ^3He is of primordial origin (i.e., linked to earth formation) and released from mantle, He within the crust is predominantly of radiogenic origin (^4He), as produced by the $^{235,238}U$ and ^{232}Th α-decay in the crust (Ballentine & Burnard, 2002; O'Nions & Oxburgh, 1988). Thermal neutrons produced from spontaneous fission of U and Th in crustal rocks can potentially generate nucleogenic ^3He through different reactions (e.g., $^6Li(n, \alpha) \rightarrow {}^3H(\beta) \rightarrow {}^3He$; Tolstikhin et al., 2016; Dunai et al., 2007; Tolstikhin et al., 1996; Mamyrin & Tolstikhin, 1984), but this effect is typically negligible (Barry et al., 2020; Kulongosky et al., 2005; Ballentine & Burnard, 2002). As a consequence, the He isotopic signatures of the sources, normalized to atmospheric (Ra) values, are: (a) 6.1 ± 0.9 Ra, for the European Subcontinental Lithospheric Mantle, ESCLM (Gautheron & Moreira, 2002); (b) 0.01–0.02 Ra, for pure crustal fluids dominated by radiogenic ^4He (Ballentine & Burnard, 2002); (c) 1 Ra, for air (Ozima & Podosek, 2002). $^4He/^{20}Ne$ ratios are >1,000 for crust and mantle, and 0.318 for air (Sano et al., 1985). Because of these different end-member compositions, coupling He isotopes in natural fluids with their $^4He/^{20}Ne$ ratios helps resolving the relative He contributions from the three sources (e.g., Caracausi & Sulli, 2019; Sano et al., 1997).

Using the approach proposed by Sano et al. (1997), assuming that all ^{20}Ne is of atmospheric origin, we estimate low atmospheric contributions (≤15%) for all samples and mantle helium fractions up to ~40%. These values are lower than those found by Brauer et al. (2016) for free gas sample in the westernmost part of the Pannonian Basin, near the Austria/Slovenia borderline (Blue crosses in Fig. IV.7) but higher than those observed in a series of commercial gas reservoirs in the Hungarian part of the Pannonian basin (Fig. IV.7; Sherwood Lollar et al.,1997; Ballentine et al., 1991) and for free

gases from nearby region (Serbia, Randazzo et al., 2021, see Chapter II). Noteworthy, the two N_2-rich samples with the lowest He isotopic signatures (CRT1 and CRT19, 0.02 and 0.05 Ra respectively) have been collected outside the Pannonian basin region (Fig. IV.1).

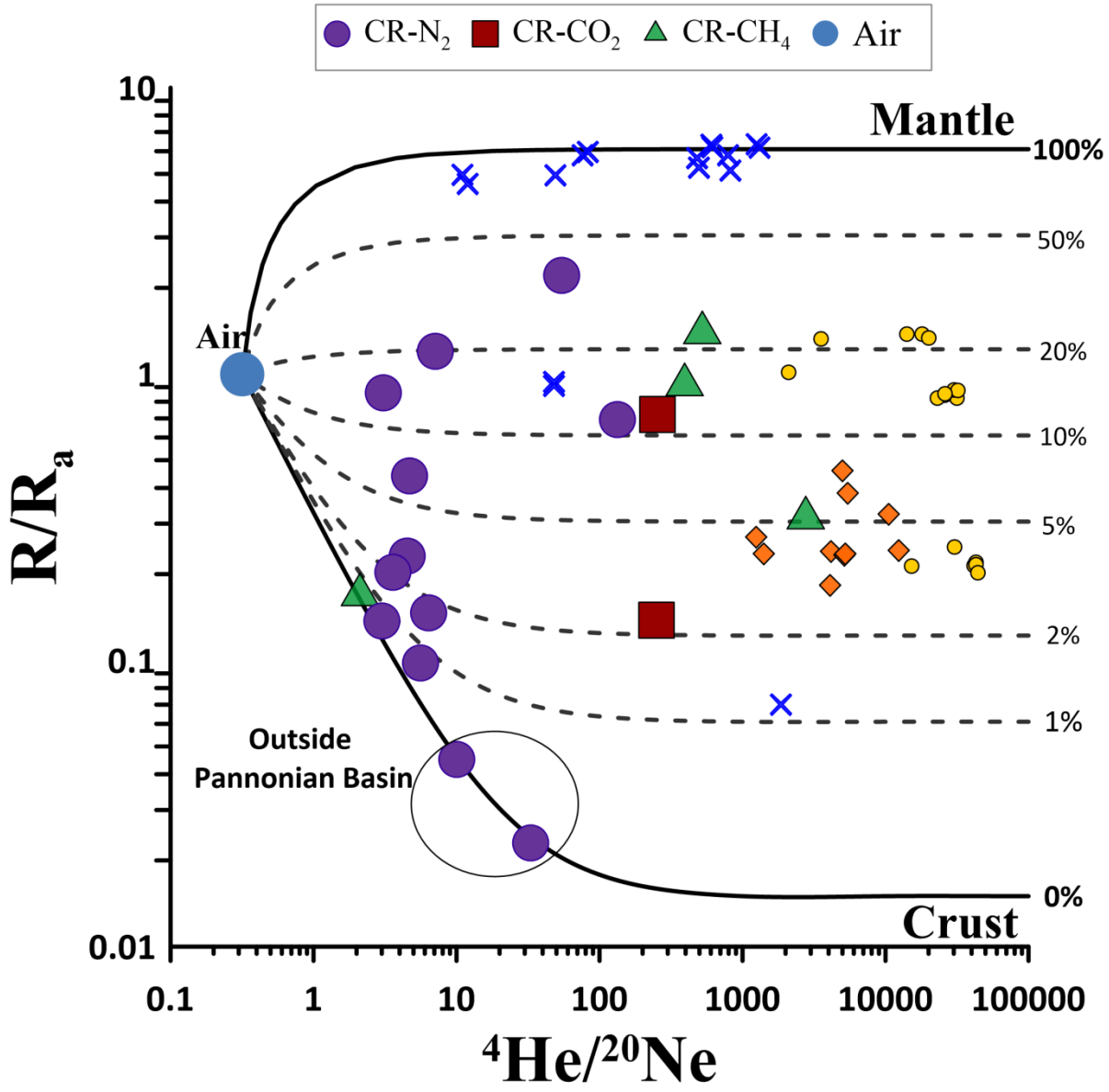

Figure IV.7 | He isotopic composition versus $^4He/^{20}Ne$ ratios. Low atmospheric contributions (up to 15%) are showed from all samples. Mantle helium fractions are up to ~40%. These value are lower than those found for gas samples of the westernmost part of the Pannonian Basin (blue crosses), but higher than in reservoir gas samples from the Hungarian part of the Pannonian basin (yellow circles and orange diamonds; Sherwood Lollar et al.,1997; Ballentine et al., 1991). The two N_2-rich samples with typical crustal values (0.02 and 0.05 Ra) have been collected outside the Pannonian basin region.

IV.5.2. He-C relationship

During the migration through the crust and storage in crustal layers, fluids can undergo different processes that may act to modify their pristine chemical and isotopic composition. Additional insights into volatile sources, sinks and processes can be derived from a joint analysis and interpretation of He and carbon isotopic signatures (e.g., Randazzo et al., 2021; Barry et al., 2020; Holland & Gilfillan, 2013).

Our results indicate that natural gases in the Croatian part of Pannonian basin are mainly dominated by N_2 and CH_4, with only two samples being CO_2-dominated (Fig. IV.5). There is also a significant spread of $\delta^{13}C$ compositions (Fig. IV.6) and R/Ra ratios (Fig. IV.7) that could reflect a multiplicity of processes and gas sources involved. In natural fluids ^3He is mainly primordial and sourced from the mantle. We therefore combine CO_2 with ^3He (into the $CO_2/^3He$ ratio) to evaluate any volatile enrichment or depletion relative to a mantle-like signature. For the local mantle source, we assume a $CO_2/^3He$ ratio of $2–7\times10^9$ and $\delta^{13}C$ of −3.5‰ (Bräuer et al., 2016). These values differ from typical MORB composition (e.g., $1.5–2\times10^9$; Marty et al., 2020) because, in continental environments, the lithospheric mantle often brings record of heterogeneities caused by metasomatizing events that can lead to carbon enrichment (Rizzo et al., 2018). Moreover, Brauer et al., (2016), by comparing free gas sample results for different locations in Europe, suggested that the European SCLM reservoir may be characterized by $\delta^{13}C$ values slightly higher than those of MORB.

Our samples show distinct $CO_2/^3He$ ratios that are, respectively, higher (up to 5.7×10^{10}) and lower (as low as 9.9×10^7) than the defined mantle range ($CO_2/^3He$ ratio of $2–7\times10^9$ and $\delta^{13}C$ of −3.5‰; Bräuer et al., 2016; Fig. IV.8). In tandem with gas samples from other Pannonian basin areas (Austria/Slovenia, Bräuer et al., 2016; Hungary, Sherwood Lollar et al., 1997; Ballentine et al., 1991), our samples define array of decreasing $CO_2/^3He$ ratios (and CO_2 concentrations) upon increasing ^4He concentrations (Fig. IV.8).

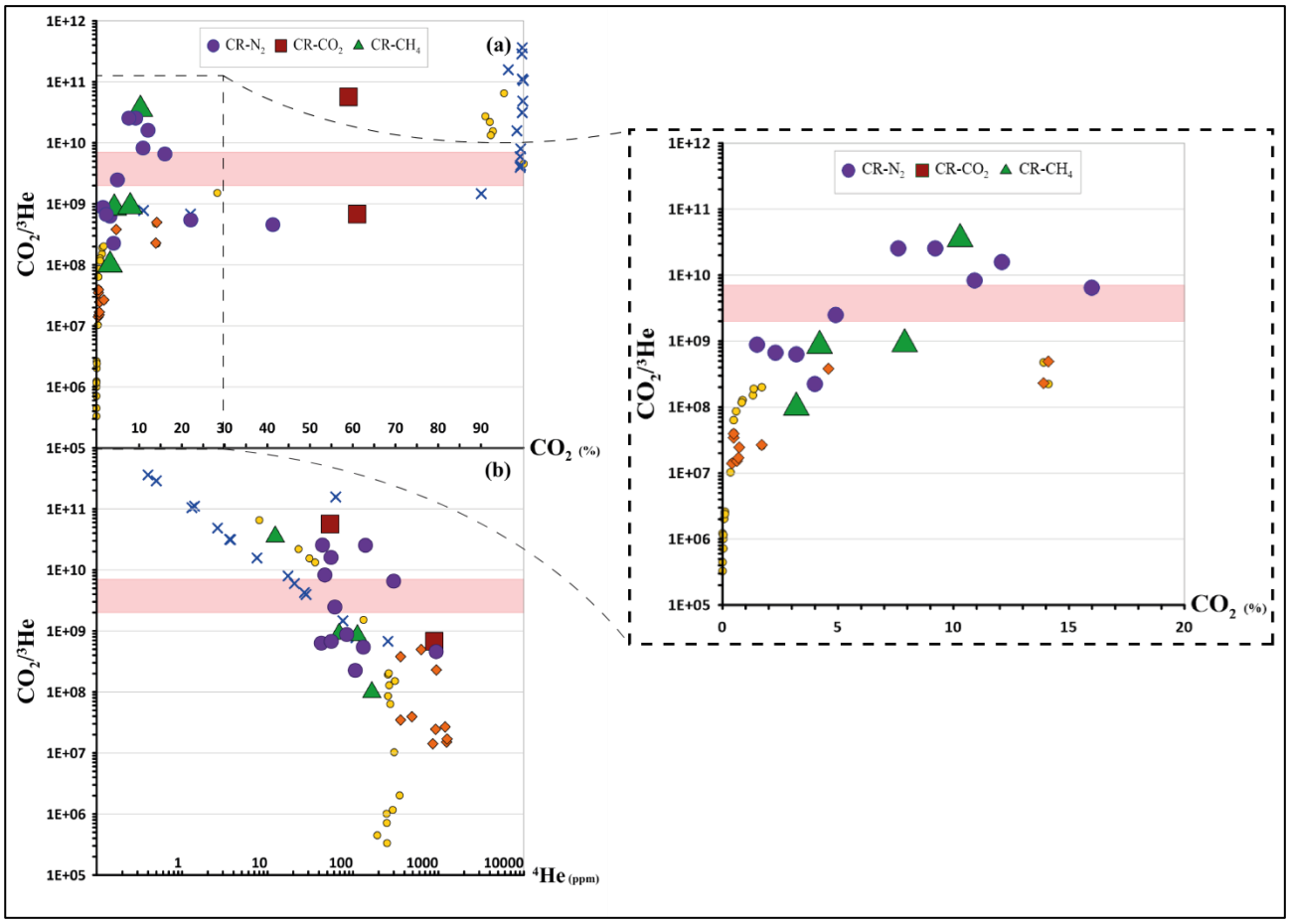

Figure IV.8 | $CO_2/^3He$ ratios versus (**a**) CO_2, (**b**) ^4He. The panels show a decreasing $CO_2/^3He$ (and CO_2) trend with increasing ^4He. The inset to the right is a zoom on low CO_2 concentration (<20%) samples. Shaded area= SCLM range ($2–7\times10^9$; Bräuer et al., 2016; Marty et al., 2020). Data for other Pannonians basin areas follow the same trend (Dark blue crosses, Bräuer et al., 2016; Orange diamonds, Ballentine et al., 1991;Yellow circles Sherwood Lollar et al., 1997).

The high $CO_2/^3He$ ratios of most CO_2-rich crustal continental gases are commonly interpreted (Sano & Marty, 1995; Sherwood Lollar et al., 1997) to result from decarbonation reaction and biological processes in the crust that produce a CO_2-rich, ^3He-free gas. We thus propose that the samples with highest $CO_2/^3He$ ratio are mixtures of CO_2-rich crustal, with different percentages of mantle-derived component. This is additionally supported by Figure IV.9, in which the aforementioned samples fall along hypothetical mixing curves between a SCLM pole and a set of hypothetical crustal end-members with same He isotopic ratio but different $CO_2/^3He$ ratios. Moreover, addition to a SCLM-like gas of a crustal carbon component, of organic-biogenic derivation, is suggested by the $\delta^{13}C$ versus $CO_2/^3He$ ratio plot of Figure IV.10. Solid gray lines show mixing between four end-member:

limestones ($CO_2/^3He$ = 10^{13}, $\delta^{13}C$ = 0‰), sediments ($CO_2/^3He$ = 10^{13}, $\delta^{13}C$ = −30‰), gases from hydrocarbon biodegradation ($CO_2/^3He$ = 10^{13}, $\delta^{13}C$ = 20‰; Milkov, 2010) and mantle ($CO_2/^3He$ = 2–7×10^9, $\delta^{13}C$ = −3.5‰; Bräuer et al., 2016; Rizzo et al., 2018). In particular, samples CRT7 and CRT8 exhibit the most positive carbon isotopic compositions ($\delta^{13}C_{CO2}$ of +12.8‰ and +10.6‰; Table IV.1) that are characteristic of oil biodegradation processes in which $\delta^{13}C_{CO2}$ enrichment could result from partial conversion of oil-derived CO_2 into secondary microbial methane (Milkov, 2010 and reference therein).

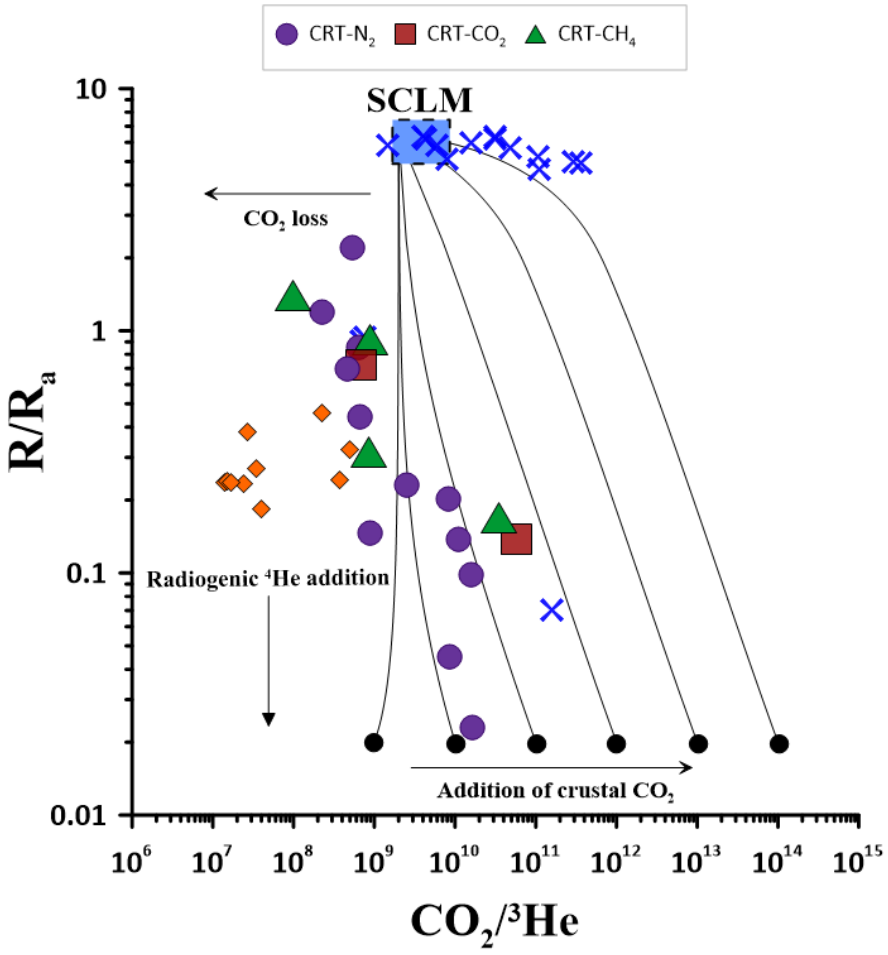

Figure IV.9 | $^3He/^4He$ (expressed as R/Ra) versus $CO_2/^3He$ ratio plot. Binary mixing curves are shown between the SCLM (6.1 ± 0.9 Ra and $CO_2/^3He$ of 7×10^9; Bräuer et al., 2016; Gautheron & Moreira, 2002) and different hypothetical crustal end-members with same helium isotopic composition (0.02 Ra) but variable $CO_2/^3He$ ratios. The samples with highest $CO_2/^3He$ ratio are mixtures of CO_2-rich crustal gas linked to biological processes with different percentages of mantle-derived component. The other samples require CO_2 loss via gas-water-rock interactions and/or addition of radiogenic He to explain their compositions.

The interpretation of samples with lower-than-SCLM $CO_2/^3He$ ratios is less straightforward. These samples exhibit the highest ^4He contents (Fig. IV.8b), and yet an He isotopic composition that implies a non-negligible mantle contribution (some of the highest R/Ra values in the entire dataset; e.g., CRT14 2.2 Ra, CRT3 1.2 Ra, CRT11 1.4 Ra; Fig. IV.7). Although there is no a priori reason to expect a correlation between ^4He with the $CO_2/^3He$ ratio, such a correlation has been found regionally in natural gases (Ballentine et al., 2002; Gilfillan et al., 2009). Radiogenic volatiles (e.g., ^4He) produced over time in the crust and degassing through it (e.g., Ballentine et al., 2002) can be transferred to natural fluids during their transit and storage in crustal layers. Previous studies indicated that such correlations are the result of ^4He accumulating in the groundwater (e.g., Gilfillan et al., 2008). Moreover, the low CO_2 concentrations and low $CO_2/^3He$ ratios, combined with more negative ^{13}C-compositions (Fig. IV.10), imply some mechanism of CO_2 removal during gas-water-rock interactions. In fact, during their migration through the crust, volatiles can interact with groundwater and, due to different solubilities, CO_2 dissolves preferentially in water relative to He (in the range of temperature up to 90 °C: CO_2 solubility > He solubility; Ballentine et al., 2002; Clever et al., 1979; Gilfillan et al., 2009; Scharlin et al., 1996). Furthermore, groundwater can also precipitate carbonate minerals, additionally modifying the dissolved carbonate equilibria (Randazzo et al., 2021; Barry et al., 2020; Gillfillan et al., 2009). In both cases, CO_2 is retained either in form of carbonate minerals (mineral trapping) or dissolved in solution (solubility trapping) (e.g., Baines et al., 2004; Bradshaw et al., 2005) leading to decreased $CO_2/^3He$ ratios and more negative $\delta^{13}C$ in the residual gases.

In order to interpret the variability of $CO_2/^3He$ ratios coupled to that of $\delta^{13}C$, we investigate the processes of CO_2 partial dissolution in water, and calcite precipitation, by modeling (see Gillfillan et al., 2009) their potential control on $CO_2/^3He$ ratios and CO_2 carbon isotopic compositions ($\delta^{13}C_{CO2}$) (Fig. IV.10). The process can be modeled as (i) an open-system degassing (Rayleigh type) at isotopic equilibrium (between phases) and (ii) calcite precipitation (Fig. IV.10). Assuming a

mantle-like composition for the pristine gas ($CO_2/^3He$= 2–7×10^9, $\delta^{13}C$ = −3.5‰; Bräuer et al., 2016; Marty et al., 2020; Rizzo et al., 2018) we model the progressive variation of the $CO_2/^3He$ ratio in the residual gas.

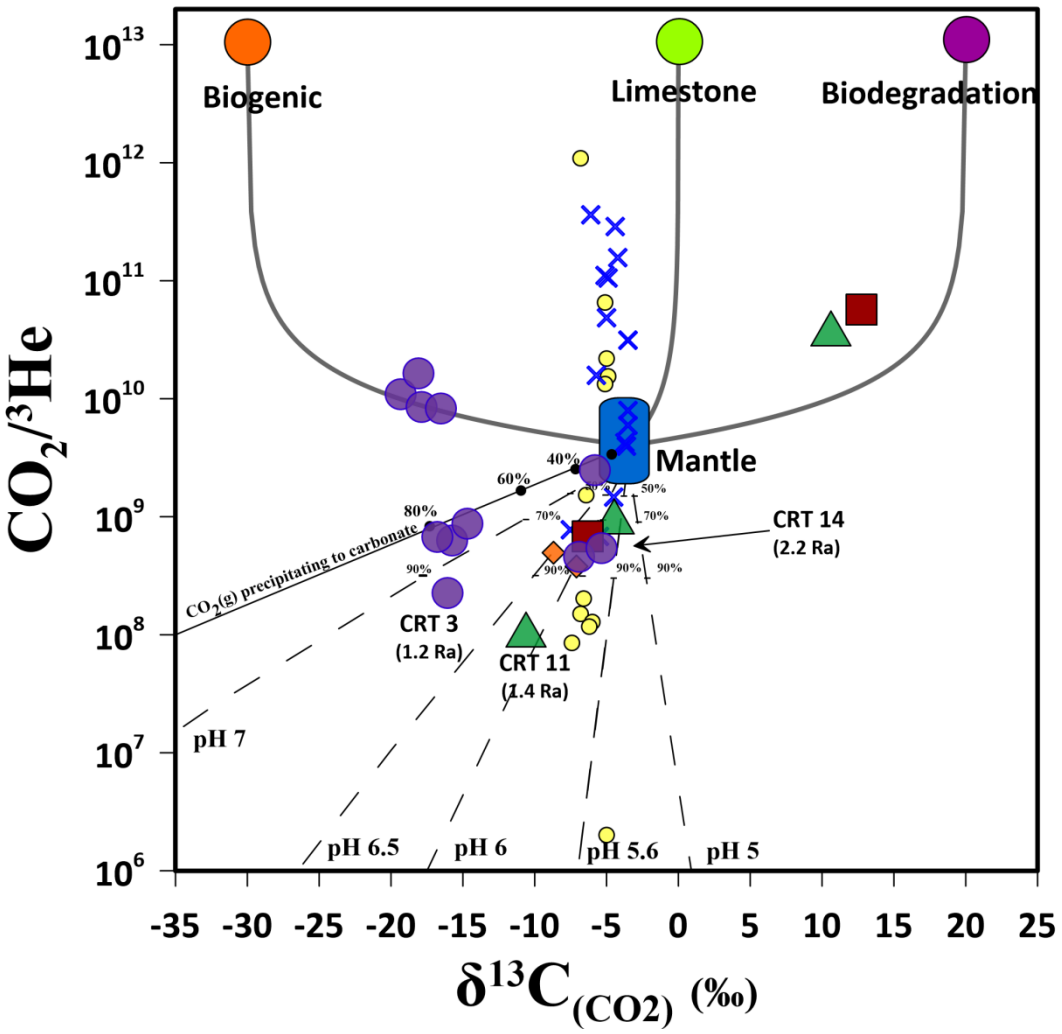

Figure IV.10 | $CO_2/^3He$ versus $\delta^{13}C(CO_2)$ Plot. Broken lines show the predicted model for Rayleigh-type gas dissolution at different pHs, black solid line represents the predicted trend for carbonate mineral precipitation. In the case of precipitation there is zero ^3He loss from the CO_2 phase and $CO_2/^3He$ changes in proportion to the fraction of the remaining CO_2 phase while for CO_2 dissolution, the change in $CO_2/^3He$ ratio is calculated following the Rayleigh equation. The samples with the highest He isotopic composition are labelled.

We stress that here we consider the case of a pristine gas as the mantle end-member, but the choice of a different end-member, resulting from the mixing between crustal (limestone+organic/biogenic) and mantle-derived fluids, would lead to similar (but shifted) model curves. Our model curves,

obtained over a range of pH values for increasing extents of gas dissolution (dotted lines) and for calcite precipitation (solid line), are plotted in Figure IV.10. Overall, we find the model CO_2 dissolution lines at pH between 5.6 and 7 nicely fit the data set. This comparison demonstrates that most samples can be interpreted as due to different degrees of CO_2 loss by dissolution (from about 40% to over 90% for the most fractionated samples), in line with gas samples from the Hungarian part of the Pannonian basin for which evidence of interaction processes with groundwater have been identified (Sherwood Lollar et al., 1997; Ballentine et al., 1991). Some samples (CRT4, CRT5 and CRT13) also show evidence of calcite precipitation up to 80% (Fig. IV.10). These gas/water fractionations ultimately result in ^{13}C-depleted compositions and $CO_2/^3He$ spanning over 2 orders of magnitude. We stress that, for a crustal sector with a potentially high number of stratified aquifer such as in Croatian Pannonian Basin, a simple open-system degassing (Rayleigh type) model approach is evidently a simplified approach. In fact, it cannot be ruled out that more complex gas-aquifer interactions, such as complete gas dissolution in deep aquifer, followed by multistep degassing upon groundwater upward migration (Chiodini et al., 2011), could have taken place. This notwithstanding, our model clearly highlights the role played by gas-water interaction in determining the composition of studied gas manifestations.

IV.5.3. Helium Fluxes and Tectonic Implications

Although the processes described in the previous paragraps are likely to have strongly modified the chemical and isotopic composition of the emitted fluids, an active outgassing of mantle-derived components is suggested from the He isotopic compositions of samples. Mantle-derived volatiles in continental areas far from any evidence of active volcanism can be sourced from i) reservoirs of fossil mantle-derived volatiles (e.g., Ballentine et al., 2001), ii) magmatic intrusions into the crust, and iii) by the transfer through lithospheric faults (e.g., Burnard et al., 2013; Kennedy et al., 2007; Lee et al., 2019). For Croatia, the Pannonian Basin area is characterized by an average geothermal

gradient of 49 °C/km, with values up to 70 °C/km in some places, and the terrestrial heat-flow ranges between 50 and 130 mW/m^2 (Hurter and Haenel, 2002; Lenkey et al., 2002; Horwath et al., 2015; Živković et al., 2016). A reservoir of fossil mantle-derived volatiles as a source of mantle He should not be associated to an heat-excess, as presently observed at regional scale in the study area. On the other hand, magmatic intrusions in the crust could in principle supply both mantle-derived heat and fluids toward the surface but, at a regional scale, a magmatic intrusion can be considered as a localized source of both volatiles and heat. In spite of some possible long-range transport through groundwaters, the He isotopic ratio and heat flux anomaly should thus decrease upon increasing distance from the position of the source at depth. In the study area, in contrast, we recognize a fairly homogeneous and generalized outgassing of mantle-derived He and high regional heat flow (Borovic et al., 2016; Horwath et al., 2015). In light of this, we feel justified to exclude the first two options.

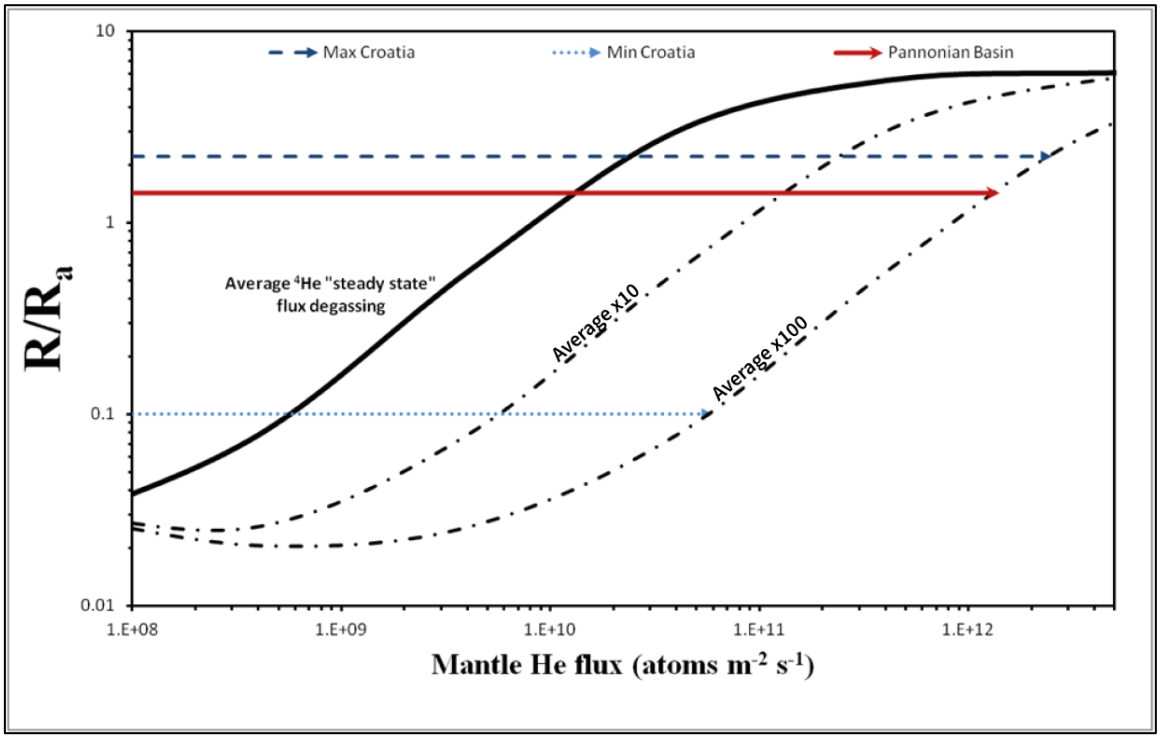

Figure IV.11 | Helium isotope composition vs. mantle-derived He flux. The mixing curves are computed by using the approach proposed by O'Nions and Oxburgh (1988) based on the progressive addition of a crustal He component that dilute the mantle He component producing a decrease of the He isotopic signature from the typical mantle-derived

component (6.1 Ra; Gautheron & Moreira, 2002) to the radiogenic signature (0.02 Ra; Ballentine & Burnard, 2002). The solid curve refers to an average continental crust ^{4}He steady-state flux of $3.3 \pm 0.5 \times 10^{10}$ atoms m^{-2} s^{-1} (Buttitta et al., 2020). The dotted curves refer to 10 times and 100 times the average continental crust steady-state He flux. Red line refers to average flux calculated on the average R/Ra values of samples from different part of Pannonian basin.

Volatiles (i.e., CO_2, He) can reach the surface directly from the mantle through lithospheric faults (e.g., Burnard et al., 2012; Caracausi & Sulli, 2019; Lee et al., 2019). Active fault zones are regions of advanced permeability that permit a fast transfer of volatiles through the crust, and seismicity is a strong evidence of the capacity of faults to transfer fluids through the crust. However, the mechanisms that control the migration of fluids in the deep crust (e.g., ductile layers) are still not well recognized (e.g., Caracausi & Sulli, 2019; Kulongoski et al., 2005). In active tectonic regions, fluids can move via developing fault-fracture meshes with a mechanism analogous to the fault valve model that drives flow by fluid over-pressurization and stress switching (compression to extension) (Sibson, 2013, 2020), or by creep cavitation that can establish a dynamic granular fluid pump in ductile shear zones (i.e., Fusseis et al., 2009). The study area is strongly affected by active tectonics as indicated by seismicity (Fig. IV.3). The Pannonian basin area exhibits intraplate seismicity characterized by rare occurrences of large events (Pribicevic et al., 2002). Despite this, historical and recent (e.g., Petrinja earthquake, Mw 6.4, 29 December 2020) seismicity shows the considerable seismic potential for this area (Markušić et al., 2020; Herak et al., 2009). Most earthquakes occur at depth between 6 and 18 km (crustal depths; Ivancic et al., 2018; Markusic et al., 2008) with lithospheric thickness of 40–50 km (Moho around 28 km; Cvetkovic et al 2016; Markusic et al., 2008; Milivojević, 1993). In addition, all the investigated emissions are located on well-known active fault zones (Fig. IV.1; Basili et al., 2013; Bruckl et al., 2011). Hence, a system of well-connected faults with roots down to the mantle, through which the fluids and heat from the mantle can cross the crust and reach the surface, seems the most plausible mechanism to explain the combined high heat flux and regional-scale outgassing of mantle He in the study area.

Quantitative He flux estimates provide insights into the rate of volatile transfer through the crust. Estimates of the ^{4}He flux in continental regions are mainly based on calculations of in-situ production and steady-state degassing, and these calculations yield a typical crustal ^{4}He degassing flux of $\sim 3.3 \pm 0.5 \times 10^{10}$ atoms m^{-2} s^{-1} (Buttitta et al., 2020, and references therein). Moreover, the release of volatiles from rock increases in an active stress field, which implies that ^{4}He degassing through the crust can be episodic in active tectonic areas (e.g., Bräuer et al., 2016; Honda et al., 1982; Torgersen & O'Donnell, 1991). Deformation and failure of rocks crack mineral grains causes pervasive micro-fracturing, leading to an increase of rocks porosities from 20% to as high as 400% prior to failure with the opening of new micro-fracture surfaces, and eventually causing macroscopic failure and fracture of rocks (Bräuer et al., 2016). These processes lead to higher release of volatiles (e.g., He) previously trapped within mineral grains along fracture networks, and pore fluids can transport these volatiles through the crust.

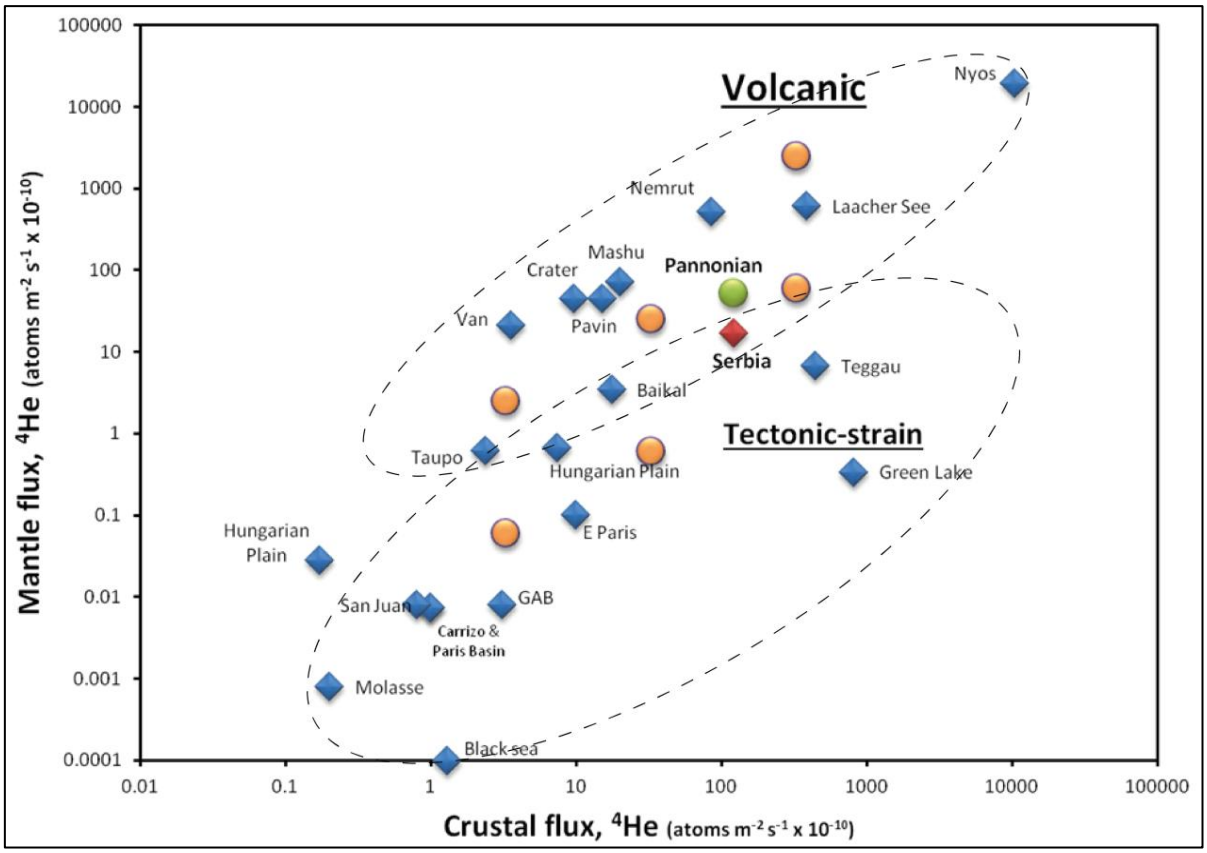

Figure IV.12 | Crustal-derived He fluxes compared to mantle-derived He fluxes. The assessed mantle-derived He flux for the Croatian samples (orange circles) is $6x10^{8}$ atoms m^{-2} s^{-1} using the lowest R/Ra value and $2.5x10^{10}$ atoms m^{-2} s^{-1} for the highest R/Ra value. For crustal-derived ^{4}He fluxes being $10–10^{4}$ times higher than the "steadystate" crustal flux, the mantle helium fluxes would also be in the order of magnitude of values characteristic of "Volcanic field" and/or "Tectonic-strain field" (black dotted ellipse areas; modified after Torgensen, 2010). The six orange circles (croatian point) represent, respectively, the mantle ^{4}He flux values for maximum and minimum R/Ra calculated on the base of continental crust ^{4}He production ($3.3 \pm 0.5\times10^{10}$ atoms m^{-2} s^{-1}; Buttitta et al., 2020) and for 10 times and 100 times this value. Green circe is the average value for Pannonian basin region achieved by the average of He isotope composition (R/Ra) of gas from different Pannonian basin areas.

Using the approach proposed by O'Nions and Oxburgh (1988), it is possible to assess the flux of mantle-derived He, making guess for the crustal He flux range. Considering that, during the transfer of mantle-derived fluids through the crust, the addition of crustal radiogenic ^{4}He produces a decrease of the pristine mantle He isotopic ratio, this method is based on the assumption that, if He degassing occurs at steady state, then it is possible to estimate the mantle He flux from the helium

isotope composition of the system. Figure IV.11 shows the dependence of R/Ra in the surface gas on mantle He flux (for average crustal ^{4}He flux of 3.3 ± 0.5 × 10^{10} atoms m^{-2} s^{-1}). From this, we estimate a mantle-derived He flux in the study area of ~6×10^8 to ~2.5 × 10^{10} atoms m^{-2} s^{-1}. These values are up to three orders of magnitude higher than normally found in stable continental areas (~ 10^7; O'Nions & Oxburgh, 1988). Considering the He isotopic composition of gases from different areas of the Pannonian basin, it is possible to obtain an average mantle He flow for the whole Pannonian basin. Excluding the two samples (CRT1 and CRT19) out of the croatian pannonian area, we estimate an He flux of ~ 1.4x10^{10} atoms m^{-2} s^{-1}, one order of magnitude higher than estimated by O'Nions and Oxburg (1988) (4x10^9 atoms m^{-2} s^{-1}). However, an enhanced release of He from rocks, up to 10^4 times the steady-state values, may occur in active tectonic regions (Buttitta et al., 2020; Torgersen, 2010). Therefore, assuming a ^{4}He crustal flux from 10 to 10^4 times the average "steady-state" value, the mantle He fluxes increase to between 10^{11} and 10^{14} atoms m^{-2} s^{-1}. These He flux values are encountered in active tectonic regions and/or in volcanic systems (Fig. IV. 12; Torgersen, 2010). Our results together with i) extensional tectonic regime (Faccenna et al., 2014) and active seismicity (Markovic et al., 2020) characterizing the whole area, ii) the evidence of high regional heat flow (up to 130 mW/m^2), linked to asthenosphere up-rise at regional scale (up to 50–60-km depth, Horváth et al., 2015), and iii) the presence of lithospheric discontinuity zones on a regional scale (Bruckl et al., 2011) that can still work today as pathways for the transfer of deep volatiles through the crust, all conduct to indicate that the released fluids in the study area are sourced, together with heat, by the underlying mantle.

IV.6. Conclusions

We investigated the chemical and isotopic composition of natural gas from the Croatian part of the Pannonian basin. Gas compositions are very heterogeneous and cluster into three groups: N_2-dominated, CH_4-dominated and CO_2-dominated gases with the prevalence of the former. For the first time the He isotopic composition in sample from the Croatian part of the Pannonian basin was analysed, allowing to identify a mantle He fraction of up to 40%. Based on their He and C isotope compositions, the samples with high $CO_2/^3He$ ratio (respect to mantle value) are interpreted as mixtures of crustal CO_2-rich gas (from organic-biogenic sources) and mantle-derived components. Two samples show mixing between mantle components and ^{13}C-enriched CO_2 linked to oil biodegradation processes, in which partial conversion of oil-derived CO_2 into secondary microbial methane occurs (Milkov, 2010). Most of the samples are found to have experienced extensive chemical and isotopic fractionations due to water-gas-rock interactions during storage in shallow crustal layers and transfer through the crust. Using the He isotopic composition, the mantle-derived He flux is estimated to range from $\sim 6 \times 10^8$ to $\sim 2.5 \times 10^{10}$ atoms m^{-2} s^{-1}, or 3 orders of magnitude higher than normally found in stable continental areas. Averaging the He isotopic compositions of gas samples taken in other areas of the Pannonian basin, an average mantle He flux of $1.4x10^{10}$ atoms m^{-2} s^{-1} is estimated. This value is one order of magnitude greater than found by O'Nions & Oxburgh, (1988), and places the Pannonian basin among the areas affected by strong tectonic stress and/or active volcanism, in ligh with what found in neighboring areas such as Serbia (Randazzo et al., 2021; Fig. IV.12). In addition to asthenospheric uprise (Horwath et al., 2015), the active seismicity and high heat flux characterizing the whole area (up to 130 mW/m^2) support the conclusion of a direct volatiles/heat derivation from the mantle. This elevated transport of mantle-derived volatiles is interpreted to occur through lithospheric faults that operate as regions of enhanced permeability, promoting the migration of fluids through the whole crust. As already discussed elsewhere (e.g., Caracausi & Sulli, 2019; Chiodini et al., 2004; Lee et al., 2019), our

study confirms that an elevated outgassing of mantle-derived fluids can occur in tectonically active continental regions, even far from active volcanism.

References

Alonso M., Pérez N. M., Hernández P.A., Padrón E., Melián G., Rodríguez F., Padilla G., Barrancos J., Asensio-Ramos M., Fridriksson T., Sumino H., Thermal energy and diffuse 4He and 3He degassing released in volcanic-geothermal systems, Renewable Energy, Volume 182, 2022, Pages 17-31, ISSN 0960-1481, https://doi.org/10.1016/j.renene.2021.10.016.

Brlek, M., Kutterolf, S., Gaynor, S. *et al.* Miocene syn-rift evolution of the North Croatian Basin (Carpathian–Pannonian Region): new constraints from Mts. Kalnik and Požeška gora volcaniclastic record with regional implications. *Int J Earth Sci (Geol Rundsch)* **109,** 2775–2800 (2020). https://doi.org/10.1007/s00531-020-01927-4

Balázs, A., Matenco, L., Magyar, I., Horváth, F., and Cloetingh, S. (2016), The link between tectonics and sedimentation in back-arc basins: New genetic constraints from the analysis of the Pannonian Basin, *Tectonics*, 35, 1526– 1559, doi:10.1002/2015TC004109.

Balen D., Schneider P., Massonne H., Opitz J., Luptáková J., Putiš M. and Petrinec Z.-The Late Cretaceous A-type alkali-feldspar granite from Mt. Požeška Gora (N Croatia): Potential marker of fast magma ascent in the Europe–Adria suture zone. *GEOLOGICA CARPATHICA*, AUGUST 2020, 71, 4, 361–381 https://doi.org/10.31577/GeolCarp.71.4.5

Ballentine C. J., O'Nions R. K., Oxburgh E. R., Horvath F., and Deak J. (1991) Rare gas constraints on hydrocarbon accumulation, crustal degassing, and groundwater flow in the Pannonian Basin, *Earth Planet. Sci. Lett.* 105, 229-246.

Ballentine, C. J., Schoell, M., Coleman, D., & Cain, B. A. (2001). 300-Myr-old magmatic CO_2 in natural gas reservoir of the west Texas Permian basin. *Nature*, *409*(6818), 327–331. https://doi.org/10.1038/35053046

Ballentine, C. J., & Burnard, P. (2002). Production, release and transport of noble gases in the continental crust. *Reviews in Mineralogy and Geochemistry*, *47*(1), 481–538. https://doi.org/10.2138/rmg.2002.47.12

Ballentine, C. J., & Sherwood Lollar, B. (2002). Regional groundwater focusing of nitrogen and noble gases into the Hugoton-Panhandle giant gas field, USA. *Geochimica et Cosmochimica Acta*, *66*, 2483–2497. https://doi.org/10.1016/S0016-7037(02)00850-5

Barry, P. H., Negrete-Aranda, R., Spelz, R. M., Seltzer, A. M., Bekaert, D. V., Virrueta, C., & Kulongoski, J. T. (2020). Volatile sources, sinks and pathways: A helium-carbon isotope study of Baja California fluids and gases. *Chemical Geology*, *550*(2020), 119722. https://doi. org/10.1016/j.chemgeo.2020.119722

Barry P. H., Bekaer D. V. t, Krantz J. A., Halldórsson S. A., de Moor J.M., Fischer T. P., Werner C., Kelly P. J., Seltzer A. M., Franz B. P., Kulongoski J. T., Helium-carbon systematics of groundwaters in the Lassen Peak Region, Chemical Geology, Volume 584, 2021, 120535, ISSN 0009-2541, https://doi.org/10.1016/j.chemgeo.2021.120535

Basili R., Kastelic V., Demircioglu M. B., Garcia Moreno D., Nemser E. S., Petricca P., Sboras S. P., Besana-Ostman G. M., Cabral J., Camelbeeck T., Caputo R., Danciu L., Domac H., Fonseca J., García-Mayordomo J., Giardini D., Glavatovic B., Gulen L., Ince Y., Pavlides S., Sesetyan K., Tarabusi G., Tiberti M. M., Utkucu M., Valensise G., Vanneste K., Vilanova S., Wössner J. (2013). The European Database of Seismogenic Faults (EDSF) compiled in the framework of the Project SHARE. Istituto Nazionale di Geofisica e Vulcanologia (INGV). https://doi.org/10.6092/ingv.it-share-edsf

Borović, S., Marković, T., Larva, O., Brkić, Ž. and Mraz, V. (2016): Mineral and Thermal Waters in the Croatian Part of the Pannonian 395 Basin. In: Papić, P. (ed.): Mineral and Thermal Waters of Southeastern Europe - Springer, 31-45, 174 p.

Bräuer, K., Kämpf, H., Niedermann, S., Strauch, G., & Tesar, J. (2008). Natural laboratory NW Bohemia: Comprehensive fluid studies between 1992 and 2005 used to trace geodynamic processes. *Geochemistry, Geophysics, Geosystems*, *9*, Q04018. https://doi.org/10.1029/2007GC001921

Bräuer, K., Geissler, W. H., Kämpf, H., Niedermann, S., & Rman, N. (2016). Helium and carbon isotope signatures of gas exhalations in the westernmost part of the Pannonian Basin (SE Austria/NE Slovenia): Evidence for active lithospheric mantle degassing. *Chemical Geology*, *422*, 60–70. https://doi.org/10.1016/j.chemgeo.2015.12.016

Brlek, M., Kutterolf, S., Gaynor, S. *et al.* Miocene syn-rift evolution of the North Croatian Basin (Carpathian–Pannonian Region): new constraints from Mts. Kalnik and Požeška gora volcaniclastic record with regional implications. *Int J Earth Sci (Geol Rundsch)* **109,** 2775–2800 (2020). https://doi.org/10.1007/s00531-020-01927-4

Broadley, M. W., Bekaert, D. V., Marty, B., Yamaguchi, A., & Barrat, J. A. (2020). Noble gas variations in ureilites and their implications for ureilite parent body formation. *Geochimica et Cosmochimica Acta, 270*, 325–337. https://doi.org/10.1016/j.gca.2019.11.032

Burnard, P., Zimmermann, L., & Sano, Y. (2013). The noble gases as geochemical tracers: History and background. In P. Burnard (Ed.), *The noble gases as geochemical tracers. Advances in isotope geochemistry* (pp. 1–15). Springer. https://doi.org/10.1007/978-3-642-28836-4_1

Buttitta, D., Caracausi, A., Chiaraluce, L., Favara, R., Gasparo Morticelli, M., & Sulli, A. (2020). Continental degassing of helium in an active tectonic setting (northern Italy): The role of seismicity. Nature Scientific Reports, 10, 162. https://doi.org/10.1038/s41598-019-55678-7

Capasso, G., and S. Inguaggiato (1998), A simple method for the determination of dissolved gases in natural waters: An application to the thermal waters from Volcano Island, Appl. Geochem., 13, 631– 642.

Capasso, G., Favara, R., Grassa, F., Inguaggiato, S., Longo, M., 2005. On-line technique for preparing and measuring stable carbon isotope of total dissolved inorganic carbon in water samples ($\delta^{13}C_{TDIC}$). Ann. Geophys. 48, 159–166. https://doi.org/10.4401/ag-3190.

Caracausi, A., & Sulli, A. (2019). Outgassing of mantle volatiles in compressional tectonic regime away from volcanism: The role of continental delamination. *Geochemistry, Geophysics, Geosystems, 20*, 2007–2020. https://doi.org/10.1029/2018GC008046

Chiodini G., Valenza M., Cardellini C. & Frigeri A. (2008) - A new web-based catalogue of Earth degassing sites in Italy. Eos, Vol. 89, N. 37, 341342.

Chiodini G., Cardellini C., Di Luccio F., Selva J., Frondini F., Caliro S., Rosiello A., Beddini G., Ventura G., Correlation between tectonic CO_2 Earth degassing and seismicity is revealed by a 10-year record in the Apennines, Italy. *Sci. Adv.* **6**, eabc2938 (2020).

Cvetković, V., Prelević, D., Downes, H., Jovanović, M., Vaselli, O., & Pecskay, Z. (2004). Origin and geodynamic significance of Tertiary post-collisional basaltic magmatism in Serbia (central Balkan Peninsula). *Lithos*, *73*(3–4), 161–186. https://doi.org/10.1016/j.lithos.2003.12.004

Cvetković, V., Prelević, D., & Schmid, S. (2016). Geology of south-eastern Europe. In P. Papic (Ed.), *Mineral and thermal waters of southeastern Europe* (pp. 1–29). Springer International Publishing. https://doi.org/10.1007/978-3-319-25379-4_1

Dunai, T.J., Stuart, F.M., Pik, R., Burnard, P., Gayer, E., 2007. Production of ^{3}He in crustal rocks by cosmogenic thermal neutrons. Earth Planet. Sci. Lett. 258 (1–2), 228–236.

Fiket, Ž., Rožmarić, M., Krmpotić, M. and Petrinec,B.(2015). Trace and Rare Earth Element Geochemistry of Croatian ThermalWaters. *International Journal of Environmental Research*, 9(2), 595-604. doi: 10.22059/ijer.2015.934

Frunzeti, N. (2013). *Geogenic emissions of greenhouse gases in the Southern part of the Eastern Carpathians* (doctoral dissertation). Babes-Bolyai University, Faculty of Environmental Science and Engineering. (in Romanian).

Gautheron, C., & Moreira, M. (2002). Helium signature of the subcontinental lithospheric mantle. *Earth and Planetary Science Letters*, *199*(1–2), 39–47. https://doi.org/10.1016/S0012-821X(02)00563-0

Herak, D., M. Herak, and B. Tomljenović (2009). Seismicity of North-Western Croatia. Tectonophysics 465, 212–220

Holland, G., & Gilfillan, S. (2013). Application of noble gases to the viability of CO_2 storage. In P. Burnard (Ed.), *The noble gases as geochemical tracers. Advances in isotope geochemistry* (pp. 177–223). Springer. https://doi.org/10.1007/978-3-642-28836-4_8

Horváth, F., Musitz, B., Balázs, A., Végh, A., Uhrin, A., Nádor, A., et al. (2015). Evolution of the Pannonian basin and its geothermal resources. *Geothermics*, *53*, 328–352. https://doi.org/10.1016/j.geothermics.2014.07.009

Hurter, S., Haenel, R., Atlas of Geothermal Resources in Europe. Office for Official Publications of the European Communities, Luxembourg. 2002.

Inguaggiato S., Rizzo A., Dissolved helium isotope ratios in ground-waters: a new technique based on gas–water re-equilibration and its application to Stromboli volcanic system, Applied Geochemistry, Volume 19, Issue 5, 2004, Pages 665-673, ISSN 0883-2927, https://doi.org/10.1016/j.apgeochem.2003.10.009.

Ionescu, A., Baciu, C., Kis, B.-M., & Sauer, P. E. (2017). Evaluation of dissolved light hydrocarbons in different geological settings in Romania. *Chemical Geology*, *469*, 230–245. https://doi.org/10.1016/j.chemgeo.2017.04.017

Italiano, F., Kis, B. M., Baciu, C., Ionescu, A., Harangi, S., & Palcsu, L. (2017). Geochemistry of dissolved gases from the eastern Carpathians- Transylvanian Basin boundary. *Chemical Geology*, *469*, 117–128. https://doi.org/10.1016/j.chemgeo.2016.12.019

Ivančić I., Herak D., Herak M., Allegretti I., Fiket T., Kuk K., Markušić S., Prevolnik S., Sović I., Dasović I. and Stipčević J.- Seismicity of Croatia in the period 2006–2015. Geofizika, Vol.35, 2018. DOI: 10.15233/gfz.2018.35.2

Kimani C.N., Kasanzu C.H., Tyne R.L., Mtili K.M., Byrne D.J., Kazimoto E.O., Hillegonds D.J., Ballentine C.J., Barry P.H., He, Ne, Ar and CO_2 systematics of the Rungwe Volcanic Province, Tanzania: Implications for fluid source and dynamics, Chemical Geology, Volume 586, 2021, 120584, ISSN 0009-2541, https://doi.org/10.1016/j.chemgeo.2021.120584

Kotzev, V., King, R.W., Burchfiel, B.C., Todosov, A., Nurce, B., Nakov, R., 2008. Crustal motion and strain accumulation in the South Balkan region inferred from GPS measurements. In E.S. Husebye (ed). Earthquake Monitoring and Seismic Hazard in Balkan Countries. Springer Publishing, Berlin, 19-43

Kozak J. and Cermak V. The illustrated history of natural disasters. Heidelberg, Germany: Springer, 2010. 203 pp.

Kulongoski, J. T., Hilton, D. R., & Izbicki, J. A. (2005). Source and movement of helium in the eastern Morongo groundwater basin: The influence of regional tectonics on crustal and mantle helium fluxes. Geochimica et Cosmochimica Acta, 69, 3857–3872. https://doi.org/10.1016/j.gca.2005.03.001

Labidi, J., Barry, P. H., Bekaert, D. V., Broadley, M. W., Marty, B., Giunta, T., et al. (2020). Hydrothermal 15N15N abundances constrain the origins of mantle nitrogen. Nature, 580, 367–371. https://doi.org/10.1038/s41586-020-2173-4

Lenkey, L., Dövényi, P., Horváth, F., & Cloetingh, S. A. P. L. (2002). *Geothermics of the Pan-Nonian Basin and its bearing on the neotectonics* (Vol. *3*, pp. 1–12). EGU Stephan Mueller Special Publication Series. https://doi.org/10.5194/smsps-3-29-2002

Lučić D, Saftić B, Krizmanić K et al (2001) The Neogene evolution and hydrocarbon potential of the Pannonian Basin in Croatia. Mar Pet Geol 18:133–147

Mamyrin, B. A. & Tolstikhin, I. N. Helium isotopes in nature. Developments in Geochemistry (Elsevier Science Ltd, 1984).

Markušić S. (2008) Seismicity of Croatia. In: Husebye E.S. (eds) Earthquake Monitoring and Seismic Hazard Mitigation in Balkan Countries. NATO Science Series: IV: Earth and Environmental Sciences, vol 81. Springer, Dordrecht. https://doi.org/10.1007/978-1-4020-6815-7_5

Markušić S, Stanko D, Korbar T, Belić N, Penava D, Kordić B. The Zagreb (Croatia) M5.5 Earthquake on 22 March 2020. *Geosciences*. 2020; 10(7):252. https://doi.org/10.3390/geosciences10070252

Markušić S, Stanko D, Penava D, Ivančić I, Bjelotomić Oršulić O, Korbar T, Sarhosis V. Destructive M6.2 Petrinja Earthquake (Croatia) in 2020—Preliminary Multidisciplinary Research. *Remote Sensing*. 2021; 13(6):1095. https://doi.org/10.3390/rs13061095

Marty, B., Almayrac, M., Barry, P. H., Bekaert, D. V., Broadley, M. W., Byrne, D. J., et al. (2020). An evaluation of the C/N ratio of the mantle from natural CO_2-rich gas analysis: Geochemical and cosmochemical implications. *Earth and Planetary Science Letters*, *551*(2020), 116574. https://doi.org/10.1016/j.epsl.2020.116574

Milivojević, M. (1993). Geothermal model of Earth's crust and lithosphere for the territory of Yugoslavia: Some tectonic implications. *Studia Geophysica et Geodaetica*, *37*, 265–278. https://doi.org/10.1007/BF01624600

Newell, D. L., M. J. Jessup, J. M. Cottle, D. R. Hilton, Z. D. Sharp, and T. P. Fischer (2008), Aqueous and isotope geochemistry of mineral springs along the southern margin of the Tibetan plateau: Implications for fluid sources and regional degassing of CO_2, Geochem. Geophys. Geosyst., 9, Q08014, doi:10.1029/2008GC002021.

O'Nions, R. K., & Oxburgh, E. R. (1988). Helium, volatile fluxes and the development of continental crust. *Earth and Planetary Science Letters*, *90*(3), 331–334. https://doi.org/10.1016/0012-821X(88)90134-3

Ozima, M., & Podosek, F. A. (2002). *Noble gas geochemistry* (p. 286). Cambridge University Press.

Pamic J. (1993) Eoalpine to Neoalpine magmatic and metamorphic processes in the northwestern Vardar zone, the easternmost Periadriatic zone and the southwestern Pannonian Basin. Tectonophysics 225: 503-518

PamicÂ J, Lanphere M, McKee E (1988) Radiometric ages of metamorphic and associated igneous rocks of the Slavonian mountains in the southern part of the Pannonian Basin, Yugoslavia. Acta geol 18/2: 13-39

Pamić, J., Tomljenović, B., & Balen, D. (2002). Geodynamic and petrogenetic evolution of Alpine ophiolites from the central and NW Dinarides: An overview. *Lithos*, *65*, 113–142. https://doi.org/10.1016/S0024-4937(02)00162-7

Parkhurst, D.L., Appelo, C.A.J., 1999. User's guide to PHREEQC a computer program for speciation, reaction-path, 1D-transport, and inverse geochemical calculations (Version 2). Technical Report 99-4259. U. S. Geological Survey, USA.

Pécskay Z., Lexa J., Szakács A., Seghedi I., Balogh K., Konečný V., Zelenka T., Kovacs M., Póka T., Fülöp A., Márton E., Panaiotu P. and Cvetkovic V.- Geochronology of Neogene magmatism in the Carpathian arc and intra-Carpathian area. GEOLOGICA CARPATHICA, DECEMBER 2006, 57, 6, 511—530

Pribičevic´, B., Medak, D., Prelogovic´, E., 2002. Determination of the recent structural fabric in the Alps-Dinarides area by combination of geodetic and geologic methods, *Raziskave s področja geodezije in geofizike 2002*, Kuhar, M. Brilly, M. (eds.), Ljubljana: Fakulteta za gradbeništvo in geodezijo, Univerza v Ljubljani, 57–65 (international peer-review).

Randazzo, P., Caracausi, A., Aiuppa, A., Cardellini, C., Chiodini, G., D'Alessandro, W., et al. (2021). Active degassing of deeply sourced fluids in central Europe: New evidences from a geochemical study in Serbia. *Geochemistry, Geophysics, Geosystems*, *22*, e2021GC010017. https://doi.org/10.1029/2021GC010017

Rizzo, A. L., Pelorosso, B., Coltorti, M., Ntaflos, T., Bonadiman, C., Matusiak-Małek, M., et al. (2018). Geochemistry of noble gases and CO_2 in fluid inclusions from lithospheric mantle beneath Wilcza Góra (Lower Silesia, Southwest Poland). *Frontiers in Earth Science*, *6*, 215. https://doi.org/10.3389/feart.2018.00215

Rufino, F., Cuoco, E., Busico, G. *et al.* Deep carbon degassing in the Matese massif chain (Southern Italy) inferred by geochemical and isotopic data. *Environ Sci Pollut Res* **28,** 46614–46626 (2021). https://doi.org/10.1007/s11356-020-11107-1

Sano, Y., Tominaga, T., & Williams, S. N. (1997). Secular variations of helium and carbon isotopes at Galeras volcano, Colombia. *Journal of Volcanology and Geothermal Research*, *77*(1–4), 255–265. https://doi.org/10.1016/S0377-0273(96)00098-4

Sano, Y., & Wakita, H. (1985). Geographical distribution of $^{3}He/^{4}He$ ratios in Japan: Implications for arc tectonics and incipient magmatism. Journal of Geophysical Research, 90(B10), 8729–8741. https://doi.org/10.1029/JB090iB10p08729

Sano, Y., & Marty, B. (1995). Origin of carbon in fumarolic gas from island arcs. Chemical Geology, 119, 265–274. https://doi.org/10.1016/0009-2541(94)00097-R

Sarbu, S., Aerts, J. W., Flot, J. F., Van Spanning, R. J. M., Baciu, C., Ionescu, A., et al. (2018). Sulfur Cave (Romania), an extreme environment with microbial mats in a CO_2-H_2S/O gas chemocline dominated by mycobacteria. International Journal of Speleology, 47(2), 173–187. https://doi.org/10.5038/1827-806x.47.2.2164

Schmid, S. M., Bernoulli, D., Fügenschuh, B., Maţenco, L., Schefer, S., Schuster, R., et al. (2008). The Alpine-Carpathian-Dinaridic orogenic system: Correlation and evolution of tectonic units. *Swiss Journal of Geosciences*, *101*, 139–183. https://doi.org/10.1007/s00015-008-1247-3

Schmid, S. M., Fügenschuh, B., Kounov, A., Matenco, L., Nievergelt, P., Oberhänsli, R., et al. (2019). Tectonic units of the Alpine collision zone between Eastern Alps and Western Turkey. *Gondwana Research*, *78*, 308–374. https://doi.org/10.1016/j.gr.2019.07.005

Scognamiglio, L., Tinti, E., Casarotti, E., Pucci, S., Villani, F., Cocco, M., et al. (2018). Complex fault geometry and rupture dynamics of the M_W 6.5, 30 October 2016, central Italy earthquake. *Journal of Geophysical Research: Solid Earth*, 123, 2943–2964. https://doi.org/10.1002/2018JB015603

Sherwood Lollar B., O'Nions R. K., and Ballentine C. J. (1994) Helium and neon isotope systematics in carbon dioxide-rich and hydrocarbon-rich gas reservoirs. *Geochim. Cosmochim. Actu 58, 5279-5290.*

Sherwood Lollar, B., Ballentine, C. J., & O'Nions, R. K. (1997). The fate of mantle-derived carbon in a continental sedimentary basin: Integration of C/He relationships and stable isotope signatures. *Geochimica et Cosmochimica Acta*, *61*, 2295–2307. https://doi.org/10.1016/S0016-7037(97)00083-5

Slovenec, D, Šegvić, B, Halamić, J, Goričan, Š, Zanoni, G. An ensialic volcanic arc along the northwestern edge of Palaeotethys—Insights from the Mid-Triassic volcano-sedimentary succession of Ivanščica Mt. (northwestern Croatia). *Geological Journal*. 2020; 55: 4324 4351. https://doi.org/10.1002/gj.3664

Tari V, Pamić J (1998) Geodynamic evolution of the northern Dinarides and the southern part of the Pannonian basin. Tectonophysics 297:269–281

Tari G., Dövényi P., Dunkl I., Horváth F., Lenkey L., Stefanescu M., Szafián P. and Tóth T.- Lithospheric structure of the Pannonian basin derived from seismic, gravity and geothermal data. Geological Society, London, Special Publications, 156, 215-250, 1 January 1999, https://doi.org/10.1144/GSL.SP.1999.156.01.12

Tolstikhin I.N. , O'Nions R.K. Some comments on isotopic structure of terrestrial xenon Chem. Geol., 129 (1996), pp. 185-199

Tolstikhin I., . Verchovsky A, Kamensky I., Skiba V., Gannibal M., Vetrin V., Tarakanov S. Amphibole: a major carrier of helium isotopes in crustal rocks Chem. Geol., 444 (2016), pp. 187-198

Velić J, Malvić T, Cvetković M (2012) Reservoir geology, hydrocarbon reserves and production in the Croatian part of the Pannonian Basin System. Geologia Croat 65(1):91–101

Velić, J., Malvić, T., Cvetković, M. and Velić, I. (2015), Stratigraphy and petroleum geology of the croatian part of the adriatic basin. Journal of Petroleum Geology, 38: 281-300. https://doi.org/10.1111/jpg.12611

Živković, S., Kolbah, S., Škrlec, M., 2016: Croatia Country Update. European Geothermal Congress 2016, Strasbourg, France, 19-24 Sept 2016

Zhang J., Quay P. D., and Wilbur D. O. (1995) Carbon isotope fractionation during gas-water exchange and dissolution of CO_2. *Geochim. Cosmochim. Acta* **59,** 107–114.

Zhang M., Xu S., Zhou X., Caracausi A., Sano Y., Guo Z., Zheng G., Lang Y., Liu C., Deciphering a mantle degassing transect related with India-Asia continental convergence from the perspective of volatile origin and outgassing, Geochimica et Cosmochimica Acta, Volume 310, 2021, Pages 61-78, ISSN 0016-7037, https://doi.org/10.1016/j.gca.2021.07.010.

CHAPTER V

V. General discussion and conclusions

This PhD dissertation has provided novel constraints on Earth degassing in active tectonic regions, by using CO_2 and light noble gases as tracers of volatiles origin, and of the processes that occur during storage and transfer of fluids through the crust. The acquired results contribute to an improved understanding of the source/s and behaviour of natural fluids in active tectonic areas in continental environment. Although three regions with distinct geological and tectonic features have been investigated, one general conclusion we can derive is that of a widespread circulation of deeply rising fluids of mixed mantle-crustal origin in tectonically active, seismogenetic crustal segments.

In particular, for the first investigated area, the Calabrian arc, which represents an accretionary wedge, caused by the collision of Eurasian and African plates and also one of the strongest seismic areas in Italy was possible to estimate, for the first time, a deep-derived CO_2 flux on the base of field sampling and modelling of secondary processes. The joint analysis of C and noble gases data allowed to identify two totally different domains, one characterized by gas components of atmospheric signature (He) and biogenic origin (C) and the other one in which crustal fluids (CO_2, He) are dominant. For the last one a deep CO_2 (i.e. crustal/metamorphic) component associated to the fluids released in the hydrothermal basins was identified and the secondary process (dissolution/precipitation) that modify the pristine chemical and isotopic composition of fluids leading to a CO_2 loss of over 90% have been defined. This lost CO_2 fraction will remain trapped at deep aquifer conditions in either dissolved or mineral form. The obtained deep-carbon flux is in the order of $2.1x10^5$ mol CO_2 km^{-2} yr^{-1}, and is comparable to the carbon budgets inferred for the Central Appenine in Italy and for the Himalayan orogen corroborate earlier findings that globally

significant carbon amount can be transported and degassed in continental crustal segments. The conclusions is that collisional crustal sectors, both hot and cold orogens, can represent a substantial but poorly quantified fraction of the global carbon budget. Additional studies are urgently required to better characterize this previously overlooked piece in the puzzle of the global CO_2 budget.

The south eastern Europe (SEE) is the second area studied and described in this work whit a focus in Chapter III on the Serbian sector of the Vardar zone, a mega-suture stretching along the entire Balkan Peninsula whose present-day geological setting is the result of a complex geodynamic and tectonic evolution over the last ~200 Ma that progressively involved subduction, continental collision, and finally lithospheric extension. This PhD thesis reports the first comprehensively geochemical dataset on gas manifestations for the Serbian Vardar zone identifying three different group of fluids on the base of their chemical composition: CO_2-dominated, N_2-dominated, and CH_4-dominated. Based on He and C isotope data, the CO_2-rich samples are interpreted as mixtures of crustal CO_2-rich gas and mantle-derived fluids, while N_2-dominated are inferred to have experienced extensive chemical and isotopic fractionations during water-gas-rock interactions in shallow crustal layers. A mantle-derived He flux of two orders of magnitude higher than normally found in stable continental areas is estimated, confirming that elevated outgassing of mantle-derived fluids can occur in tectonically active continental regions, even far from active volcanism. The elevated transport of mantle-derived volatiles is interpreted at regional scale to originate directly from the mantle with lithospheric faults that work as regions of enhanced permeability favouring the migration of fluids through the whole crust.

The third area treated in this thesis (Chapter IV) was a Croatian sector of Pannonian basin, a back-arc basin formed due to Oligocene–Miocene diachronous extension of continental units resulted from subduction roll-back in the Carpathians and Dinarides, combined with asthenospheric mantle flow and/or litospheric delamination. For the first time, the He isotopic composition of fluids from the Croatian segment of the Pannonian basin was analysed allowing to identify a mantle component

contributing up to 40% of the total degassed He budget. The presence of a crustal fluid component, characterized by prevalent biogenic C signature, with some additional C contributions being derived from oil biodegradation (in which light C is preferentially incorporated into secondary microbial methane) was established from the He and C isotopes joint analysis. A model of gas-water-rock interaction is developed, in which most of the samples show signs of extensive chemical and isotopic fractionations taking place during storage/transit in shallow crustal layers. Finally, a value one order of magnitude greater than previous thoughts (O'Nions & Oxburgh, 1988) was estimated for the average mantle-derived He flux in the Pannonian basin.

Ultimately, results presented here (chapters III and IV) offer additional validation to the combined use of noble gases (He, Ne, and Ar) and major volatiles (CO_2) for understanding fluid sources and pathways in different geodynamic contexts. The obtained results contribute to shed light into the geochemical features of volatiles released in the Serbian Vardar zone, and in Croatian part of the Pannonian basin, and its relationships with the underlying mantle and crustal structure. These results thus fill a knowledge gap on the nature of fluids circulating in this sector of Europe, and contribute to a more comprehensive reconstruction of the complex geodynamic evolution and structure of the area.

V.4. Broader impact and future research lines

The outcomes of this PhD research offer some broader implications and perspectives that help raising some fundamental questions to answer in future lines of investigation. A conclusion common to the three areas is that thorough characterization of the processes that occur during storage of fluids in the crust, and during their transfer through the different crustal layers, is the key to identifying fluid sources and to obtain more accurate volatile budgets. Carbon isotope compositions, if combined with noble gas results, constitute a very powerful tool for understanding

these processes. This thesis clearly shows that the knowledge on the behavior of gases, estimation of fluxes, and relation with tectonic settings is still limited and certainly will open new opportunities to continue this work on other settings with the methods used in this doctoral dissertation, with a focus on Helium and Carbon, that can be applied in other parts of the world. The study of carbon isotopic composition, with a focus on ^{14}C, can will improve our knowledge on the source/s of carbon, on carbon cycles from different settings and will could to allow better estimation for the global carbon budget. Furthermore, beyond the CO_2 which is the major species on which this work has focused it is clear that other major volatile species are present in some of the studied areas, such as N_2 and CH_4. Isotopic studies of these two gases may help to improve our knowledge on the source/s of this species and on the processes that could take place inside the crust integrating nicely what show in this work.

A further contribution to the knowledge on these processes could and should be given by the study of chemical and isotopic composition of all noble gases, including therefore Ar and also heavy noble gases (e.g. Kr, Xe) not only for fluids released but also for rocks with which gas and water interact. In this way it would be possible to better understand the processes that occur inside the crust and the links between the different reservoirs such as atmosphere, crust and mantle, defining better interaction models that give more strict information on the relationship between degassing and tectonic and allow accurate quantification of different flows (CO_2, He).